

Arbeitsbericht NAB 22-04

**TBO Bachs-1-1:
Data Report
Dossier V
Structural Geology**

August 2023

A. Ebert, E. Hägerstedt, S. Cioldi,
L. Gregorczyk & F.Casanova

**National Cooperative
for the Disposal of
Radioactive Waste**

Hardstrasse 73
P.O. Box
5430 Wettingen
Switzerland
Tel. +41 56 437 11 11

nagra.ch

Arbeitsbericht NAB 22-04

**TBO Bachs-1-1:
Data Report
Dossier V
Structural Geology**

August 2023

A. Ebert¹, E. Hägerstedt¹, S. Cioldi¹,
L. Gregorczyk² & F. Casanova³

¹Geologiegemeinschaft Strukturgeologie-Experten
Nagra Tiefbohrungen

²G-Geologie GmbH

³Nagra

Keywords:

BAC1-1, Nördlich Lägern, TBO, deep drilling campaign,
structural geology, goniometry, drill cores

**National Cooperative
for the Disposal of
Radioactive Waste**

Hardstrasse 73
P.O. Box
5430 Wettingen
Switzerland
Tel. +41 56 437 11 11

nagra.ch

Nagra Arbeitsberichte ("Working Reports") present the results of work in progress that have not necessarily been subject to a comprehensive review. They are intended to provide rapid dissemination of current information.

This NAB aims at reporting drilling results at an early stage. Additional borehole-specific data will be published elsewhere.

In the event of inconsistencies between dossiers of this NAB, the dossier addressing the specific topic takes priority. In the event of discrepancies between Nagra reports, the chronologically later report is generally considered to be correct. Data sets and interpretations laid out in this NAB may be revised in subsequent reports. The reasoning leading to these revisions will be detailed there.

This Dossier was prepared by a project team consisting of:

- A. Ebert (core description, core photograph picking, core goniometry, writing and QC)
- S. Cioldi (core description, core photograph picking and core goniometry)
- E. Hägerstedt (core description, core photograph picking and core goniometry)
- L. Gregorczyk (project management and QC)
- F. Casanova (Head Deep Drilling Campaign)

Editorial work: Geomecon, P. Blaser and M. Unger

The Dossier has greatly benefitted from technical discussions with, and reviews by, external and internal experts. Their input and work are very much appreciated.

Copyright © 2023 by Nagra, Wettingen (Switzerland) / All rights reserved.

All parts of this work are protected by copyright. Any utilisation outwith the remit of the copyright law is unlawful and liable to prosecution. This applies in particular to translations, storage and processing in electronic systems and programs, microfilms, reproductions, etc.

Table of Contents

Table of Contents	I	
List of Tables.....	III	
List of Figures	IV	
List of Appendices	X	
1	Introduction	1
1.1	Context.....	1
1.2	Location and specifications of the borehole	2
1.3	Documentation structure for the BAC1-1 borehole.....	6
1.4	Scope and objectives of this dossier	7
1.5	Petrophysical logs and preliminary log analysis available	7
1.6	Borehole deviation.....	8
2	Methodology.....	9
2.1	Core goniometry	9
2.1.1	Introduction	9
2.1.2	Workflow.....	9
2.1.3	Dip picking and dip type classification	12
2.1.4	Dip data for non-oriented and missing cores.....	13
2.1.5	Goniometry confidence assessment and uncertainties.....	16
2.2	Structural work	19
2.3	Geo-statistical evaluation.....	26
3	Inventory of structure types	27
3.1	Examples of fault planes.....	27
3.2	Example of fault zone.....	34
3.3	Examples of joints	35
3.4	Examples of veins / tension gashes.....	36
3.5	Examples of stylolites.....	38
3.6	Examples of open pores.....	40
3.7	Examples of drilling-induced fractures.....	42
3.7.1	General examples.....	42
3.7.2	Subvertical fracture at approx. 808 to 811 m MD (core depth).....	45
4	Geo-statistical evaluation: results	48
4.1	Entire cored borehole section (517.58 m to 1'306.77 m MD log depth)	48
4.1.1	Basic structural dip evaluation.....	48
4.1.2	Natural structural discontinuities.....	52
4.1.3	Fracture density (P10 and P32) and distribution	62
4.1.4	Kinematic indicators.....	62

4.2	Malm.....	67
4.2.1	«Felsenkalke» + «Massenkalk».....	68
4.2.2	Schwarzbach Formation.....	75
4.2.3	Villigen Formation.....	82
4.2.4	Wildeggen Formation.....	89
4.3	Dogger.....	96
4.3.1	«Brauner Dogger» (Wutach Formation to «Murchisonae-Oolith Formation»).....	96
4.3.2	Opalinus Clay.....	101
4.4	Lias (Staffellegg Formation).....	106
4.5	Keuper.....	111
5.5.1	Klettgau Formation.....	111
4.5.2	Bänkerjoch Formation.....	116
4.6	Muschelkalk.....	121
4.6.1	Schinznach Formation.....	121
4.6.2	Zeglingen Formation.....	127
4.6.3	Kaiseraugst Formation.....	134
4.7	Dinkelberg and Weitenau Formations.....	139
5	Main structural findings.....	143
5.1	Deformation zone in the Opalinus Clay between 911.63 m and 912.16 m MD (log depth).....	143
5.2	Fractures in the Staffellegg Formation at 940.58 m, 941.62 m and 942.78 m MD (log depth).....	146
5.3	Joint in the Schinznach Formation at 1'060.82 m MD (log depth).....	146
5.4	Joints in the Schinznach Formation from 1'099.40 m to 1'103.98 m MD (log depth).....	148
6	References.....	151

List of Tables

Tab. 1-1:	General information about the BAC1-1 borehole.....	2
Tab. 1-2:	Core and log depth for the main lithostratigraphic boundaries in the BAC1-1 borehole.....	5
Tab. 1-3:	List of dossiers included in NAB 22-04	6
Tab. 2-1:	Core goniometry confidence assessment of the analysed interval.....	16
Tab. 2-2:	Types of structural discontinuities identified in this study	20
Tab. 2-3:	Systematically recorded parameters for the investigated structures	23
Tab. 4-1:	Vector means of orientation for bedding planes and structural discontinuities.....	48
Tab. 4-2:	List of interpreted fault zones, mirror-like fault plane (MirFP) zones, salt SB (shear band) zones and the associated FDC.....	54
Tab. 4-3:	List of all kinematic indicators in oriented and non-oriented cores.....	63
Tab. 5-1:	Orientation of the three main fault planes and associated striations and shear senses.....	143

List of Figures

Fig. 1-1:	Tectonic overview map with the three siting regions under investigation	1
Fig. 1-2:	Overview map of the investigation area in the Nördlich Lägern siting region with the location of the BAC1-1 borehole in relation to the boreholes Weiach-1, BUL1-1, STA3-1 and STA2-1	3
Fig. 1-3:	Lithostratigraphic profile and casing scheme for the BAC1-1 borehole	4
Fig. 1-4:	Borehole deviation within the cored section.....	8
Fig. 2-1:	Using a goniometer to determine kinematic indicators along fault planes	11
Fig. 2-2:	Symbols for dip types, fracture density classes and kinematic data used for this study.....	12
Fig. 2-3:	Fault planes identified within the drill core at 538.10 m and 538.26 m MD (log depth) («Felsenkalke» + «Massenkalk»).....	13
Fig. 2-4:	Example of dip data in a non-oriented core interval.....	14
Fig. 2-5:	Interval without 360° core photographs from 1'129.50 m to 1'130.15 m MD (log depth) in the Zeglingen Formation.....	15
Fig. 2-6:	Core – FMI / UBI correlation for a fault plane at 564.14 m MD (log depth) in the Schwarzbach Formation	17
Fig. 2-7:	Core – FMI / UBI correlation from 917.79 m to 918.62 m MD (log depth) in the Staffelegg Formation	17
Fig. 2-8:	Core – FMI / UBI correlation for subhorizontal to shallow dipping bedding	18
Fig. 2-9:	The five main groups of structural discontinuities	20
Fig. 2-10:	Completed DIN A3 sheet of primary record of the detailed structural core analysis	25
Fig. 3-1:	Fault plane	27
Fig. 3-2:	Fault plane	28
Fig. 3-3:	Fault plane	29
Fig. 3-4:	Mirror-like fault plane	30
Fig. 3-5:	Mirror-like fault plane	31
Fig. 3-6:	Stylolitic fault plane.....	32
Fig. 3-7:	Stylolitic fault plane.....	33
Fig. 3-8:	Fault zone	34
Fig. 3-9:	Fault zone	34
Fig. 3-10:	Joint	35
Fig. 3-11:	Joint	35
Fig. 3-12:	Vein / tension gash.....	36
Fig. 3-13:	Vein / tension gash.....	36
Fig. 3-14:	Vein / tension gash.....	37

Fig. 3-15:	Vein / tension gash.....	37
Fig. 3-16:	Stylolite.....	38
Fig. 3-17:	Stylolite.....	38
Fig. 3-18:	Stylolite.....	39
Fig. 3-19:	Open pore	40
Fig. 3-20:	Open pores.....	41
Fig. 3-21:	Petal fractures	42
Fig. 3-22:	Petal and centreline fractures.....	42
Fig. 3-23:	Discing.....	43
Fig. 3-24:	Discing.....	44
Fig. 3-25:	Morphology of the subvertical fracture in drill core section (CS) number 99.....	46
Fig. 3-26:	Appearance of the vertical fracture in FMI borehole image and in the drill cores	47
Fig. 4-1:	Stereogram and depth plot for bedding planes (n = 629) in oriented cores.....	49
Fig. 4-2:	Dip azimuth rose diagram, dip histogram and depth plot for bedding planes (n = 629) in oriented cores.....	50
Fig. 4-3:	Vector azimuth (or walkout) plot with bedding dips (n = 782) in oriented cores picked on oriented 360° core photographs.....	51
Fig. 4-4:	Overview plot showing P32 densities for fractures and stylolites along the BAC1-1 borehole.....	53
Fig. 4-5:	Stereogram and depth plot of fault planes for the entire cored interval.....	55
Fig. 4-6:	Dip azimuth rose diagram, dip histogram and depth plot for fault planes in the entire cored interval	56
Fig. 4-7:	Stereogram and depth plot for tension gashes / veins, unassigned fractures and joints in the entire cored interval	58
Fig. 4-8:	Dip azimuth rose diagram of tension gashes / veins, unassigned fractures and joints in the entire cored interval.....	59
Fig. 4-9:	Stereogram and depth plot for stylolites (n = 630) recorded in oriented cores of the BAC1-1 borehole.....	60
Fig. 4-10:	Dip azimuth rose diagram and depth plot for stylolites (n = 630) recorded in oriented cores.....	61
Fig. 4-11:	Plunge azimuth of striations along fault planes in the entire cored interval.....	63
Fig. 4-12:	Stereogram of striations on all oriented fault planes (including multiple lineations on a single fault plane) and associated kinematic data.....	64
Fig. 4-13:	Stereogram of all striations of oriented thrust / reverse fault planes (including multiple lineations on a single fault plane).....	64
Fig. 4-14:	Stereogram of striations on all oriented normal fault planes (including multiple lineations on a single fault plane).....	65
Fig. 4-15:	Stereogram of striations on all oriented strike-slip fault planes (including multiple lineations on a single fault plane).....	65

Fig. 4-16:	Stereogram of striations on all oriented fault planes with unknown shear sense (including multiple lineations on a single fault plane).....	66
Fig. 4-17:	Stereogram and depth plot of fault planes («Felsenkalke» + «Massenkalk»)	68
Fig. 4-18:	Dip azimuth rose diagram, dip histogram and depth plot of fault planes («Felsenkalke» + «Massenkalk»)	69
Fig. 4-19:	Stereogram and depth plot of tension gashes / veins and unassigned fractures («Felsenkalke» + «Massenkalk»)	70
Fig. 4-20:	Dip azimuth rose diagram, dip histogram and depth plot of tension gashes / veins, joints and unassigned fractures («Felsenkalke» + «Massenkalk»).....	71
Fig. 4-21:	Stereogram and depth plot of stylolites («Felsenkalke» + «Massenkalk», n = 54).....	72
Fig. 4-22:	Dip azimuth rose diagram, dip histogram and depth plot of stylolites («Felsenkalke» + «Massenkalk», n = 54).....	73
Fig. 4-23:	Stereogram of striations on fault planes (including multiple lineations on a single fault plane) («Felsenkalke» + «Massenkalk», n = 69)	74
Fig. 4-24:	Stereogram and depth plot of fault planes (Schwarzbach Formation).....	75
Fig. 4-25:	Dip azimuth rose diagram, dip histogram and depth plot of fault planes (Schwarzbach Formation).....	76
Fig. 4-26:	Stereogram and depth plot of tension gashes / veins and unassigned fractures (Schwarzbach Formation).....	77
Fig. 4-27:	Dip azimuth rose diagram, dip histogram and depth plot of tension gashes / veins, joints and unassigned fractures (Schwarzbach Formation)	78
Fig. 4-28:	Stereogram and depth plot of stylolites (Schwarzbach Formation, n = 18).....	79
Fig. 4-29:	Dip azimuth rose diagram, dip histogram and depth plot of stylolites (Schwarzbach Formation, n = 18)	80
Fig. 4-30:	Stereogram of striations on fault planes (including multiple lineations on a single fault plane) (Schwarzbach Formation, n = 30).....	81
Fig. 4-31:	Stereogram and depth plot of fault planes (Villigen Formation).....	82
Fig. 4-32:	Dip azimuth rose diagram, dip histogram and depth plot of fault planes (Villigen Formation).....	83
Fig. 4-33:	Stereogram and depth plot of tension gashes / veins and unassigned fractures (Villigen Formation).....	84
Fig. 4-34:	Dip azimuth rose diagram, dip histogram and depth plot of tension gashes / veins, joints and unassigned fractures (Villigen Formation)	85
Fig. 4-35:	Stereogram and depth plot of stylolites (Villigen Formation, n = 276).....	86
Fig. 4-36:	Dip azimuth rose diagram, dip histogram and depth plot of stylolites (Villigen Formation, n = 276).....	87
Fig. 4-37:	Stereogram of striations on fault planes (including multiple lineations on a single fault plane) (Villigen Formation, n = 112).....	88
Fig. 4-38:	Stereogram and depth plot of fault planes (Wildegge Formation)	89

Fig. 4-39:	Dip azimuth rose diagram, dip histogram and depth plot of fault planes (Wildegge Formation)	90
Fig. 4-40:	Stereogram and depth plot of tension gashes / veins and unassigned fractures (Wildegge Formation)	91
Fig. 4-41:	Dip azimuth rose diagram, dip histogram and depth plot of tension gashes / veins, joints and unassigned fractures (Wildegge Formation).....	92
Fig. 4-42:	Stereogram and depth plot of stylolites (Wildegge Formation, n = 52)	93
Fig. 4-43:	Dip azimuth rose diagram, dip histogram and depth plot of stylolites (Wildegge Formation, n = 52)	94
Fig. 4-44:	Stereogram of striations on fault planes (including multiple lineations on a single fault plane) (Wildegge Formation, n = 39)	95
Fig. 4-45:	Stereogram and depth plot of fault planes («Brauner Dogger»).....	96
Fig. 4-46:	Dip azimuth rose diagram, dip histogram and depth plot of fault planes («Brauner Dogger»).....	97
Fig. 4-47:	Stereogram and depth plot of tension gashes / veins, joints and unassigned fractures («Brauner Dogger»).....	98
Fig. 4-48:	Stereogram and depth plot of stylolites («Brauner Dogger», n = 4).....	99
Fig. 4-49:	Stereogram of striations on fault planes (including multiple lineations on a single fault plane) («Brauner Dogger», n = 20).....	100
Fig. 4-50:	Stereogram and depth plot of fault planes (Opalinus Clay).....	101
Fig. 4-51:	Dip azimuth rose diagram, dip histogram and depth plot of fault planes (Opalinus Clay).....	102
Fig. 4-52:	Stereogram and depth plot of tension gashes / veins, joints and unassigned fractures (Opalinus Clay).....	103
Fig. 4-53:	Dip azimuth rose diagram, dip histogram and depth plot of tension gashes / veins, joints and unassigned fractures (Opalinus Clay)	104
Fig. 4-54:	Stereogram of striations on fault planes (including multiple lineations on a single fault plane) (Opalinus Clay, n = 41).....	105
Fig. 4-55:	Stereogram and depth plot of fault planes (Lias).....	106
Fig. 4-56:	Stereogram and depth plot of tension gashes / veins, joints and unassigned fractures (Lias).....	107
Fig. 4-57:	Dip azimuth rose diagram, dip histogram and depth plot of tension gashes / veins, joints and unassigned fractures (Lias).....	108
Fig. 4-58:	Stereogram and depth plot of stylolites (Lias, n = 1).....	109
Fig. 4-59:	Stereogram of striation on a single (n = 1) fault plane in the Lias.....	110
Fig. 4-60:	Stereogram and depth plot of fault planes (Klettgau Formation)	111
Fig. 4-61:	Dip azimuth rose diagram, dip histogram and depth plot of faults (Klettgau Formation)	112
Fig. 4-62:	Stereogram and depth plot of tension gashes / veins, joints and unassigned fractures (Klettgau Formation)	113

Fig. 4-63:	Dip azimuth rose diagram, dip histogram and depth plot of tension gashes / veins, joints and unassigned fractures (Klettgau Formation).....	114
Fig. 4-64:	Stereogram of striations on fault planes (including multiple lineations on a single fault plane) (Klettgau Formation, n = 50)	115
Fig. 4-65:	Stereogram and depth plot of fault planes (Bänkerjoch Formation).....	116
Fig. 4-66:	Dip azimuth rose diagram, dip histogram and depth plot of faults (Bänkerjoch Formation).....	117
Fig. 4-67:	Stereogram and depth plot of tension gashes / veins, joints and unassigned fractures (Bänkerjoch Formation).....	118
Fig. 4-68:	Dip azimuth rose diagram, dip histogram and depth plot of tension gashes / veins, joints and unassigned fractures (Bänkerjoch Formation).....	119
Fig. 4-69:	Stereogram of striations on fault planes (including multiple lineations on a single fault plane) (Bänkerjoch Formation, n = 88).....	120
Fig. 4-70:	Stereogram and depth plot of fault planes (Schinznach Formation).....	121
Fig. 4-71:	Stereogram and depth plot of tension gashes / veins, joints and unassigned fractures (Schinznach Formation).....	122
Fig. 4-72:	Dip azimuth rose diagram, dip histogram and depth plot of tension gashes / veins, joints and unassigned fractures (Schinznach Formation).....	123
Fig. 4-73:	Stereogram and depth plot of stylolites (Schinznach Formation, n = 221)	124
Fig. 4-74:	Dip azimuth rose diagram, dip histogram and depth plot of stylolites (Schinznach Formation, n = 221)	125
Fig. 4-75:	Stereogram of striations on fault planes (including multiple lineations on a single fault plane) (Schinznach Formation, n = 3).....	126
Fig. 4-76:	Stereogram and depth plot of fault planes (Zeglingen Formation).....	128
Fig. 4-77:	Dip azimuth rose diagram, dip histogram and depth plot of fault planes (Zeglingen Formation).....	129
Fig. 4-78:	Stereogram and depth plot of tension gashes / veins, joints and unassigned fractures (Zeglingen Formation).....	130
Fig. 4-79:	Dip azimuth rose diagram, dip histogram and depth plot of tension gashes / veins, joints and unassigned fractures (Zeglingen Formation).....	131
Fig. 4-80:	Stereogram and depth plot of stylolites (Zeglingen Formation, n = 4).....	132
Fig. 4-81:	Stereogram of striations on fault planes (including multiple lineations on a single fault plane) (Zeglingen Formation, n = 24).....	133
Fig. 4-82:	Stereogram and depth plot of fault planes (Kaiseraugst Formation)	134
Fig. 4-83:	Dip azimuth rose diagram, dip histogram and depth plot of fault planes (Kaiseraugst Formation)	135
Fig. 4-84:	Stereogram and depth plot of tension gashes / veins, joints and unassigned fractures (Kaiseraugst Formation)	136
Fig. 4-85:	Dip azimuth rose diagram, dip histogram and depth plot of tension gashes / veins, joints and unassigned fractures (Kaiseraugst Formation)	137

Fig. 4-86:	Stereogram of striations on fault planes (including multiple lineations on a single fault plane) (Kaiseraugst Formation, n = 18).....	138
Fig. 4-87:	Stereogram and depth plot of fault planes (Dinkelberg Formation and Weitenau Formation).....	139
Fig. 4-88:	Stereogram and depth plot of tension gashes / veins, joints and unassigned fractures (Dinkelberg Formation and Weitenau Formation)	140
Fig. 4-89:	Stereogram of striation on a single fault plane within the Dinkelberg and Weitenau Formations (n = 1).....	141
Fig. 5-1:	Overview plot of the Opalinus Clay from 910.00 m to 914.00 m MD (log depth).....	144
Fig. 5-2:	Stereogram and depth plot of structures from 910.00 m to 915.00 m MD (log depth).....	145
Fig. 5-3:	Stereogram of striations on fault planes from 910.00 m to 915.00 m MD (log depth).....	146
Fig. 5-4:	Partly open fractures within the Staffegg Formation from 940.30 m to 943.10 m MD (log depth)	147
Fig. 5-5:	Joint within the Schinznach Formation from 1'059.15 m to 1'059.55 m MD (log depth).....	147
Fig. 5-6:	Overview plot of the joints in the Schinznach Formation (interval from 1'099.00 m to 1'105.00 m MD log depth).....	148
Fig. 5-7:	Stereogram and depth plot of structures within the interval 1'099.00 m to 1'105.00 m MD (log depth)	149
Fig. 5-8:	Examples of joints in the Schinznach Formation	150

List of Appendices

- App. A: Lithostratigraphy profile Bachs-1-1, 1:2'500, 0.0 m to 1'306.26 m MD core depth
- App. B: Structural geology profile Bachs-1-1, 1:1'000, 500.00 m to 1'306.77 m MD log depth
- App. C-1: Structural geology profile Bachs-1-1, 1:100, 510.00 m to 750.00 m MD log depth
- App. C-2: Structural geology profile Bachs-1-1, 1:100, 725.00 m to 1'000.00 m MD log depth
- App. C-3: Structural geology profile Bachs-1-1, 1:100, 975.00 m to 1'306.77 m MD log depth
- App. D-1: Overview plot of stereograms and rose diagrams: «Felsenkalke» + «Massenkalk» to Staffelegg Fm.
- App. D-2: Overview plot of stereograms and rose diagrams: Klettgau to Weitenau Fm.
- App. E-1: Core goniometry depth shift table
- App. E-2: Core goniometry rotation angle table
- App. F: Lithostratigraphy patterns, colours, weathering index and symbols for lithostratigraphy

Note: The enclosures are included in the digital version of this report. In the printed version, the enclosures are on a flash drive included with the report.

1 Introduction

1.1 Context

To provide input for site selection and the safety case for deep geological repositories for radioactive waste, Nagra has drilled a series of deep boreholes ("Tiefbohrungen", TBO) in Northern Switzerland. The aim of the drilling campaign is to characterise the deep underground of the three remaining siting regions located at the edge of the Northern Alpine Molasse Basin (Fig. 1-1).

In this report, we present the results from the Bachs-1-1 borehole.

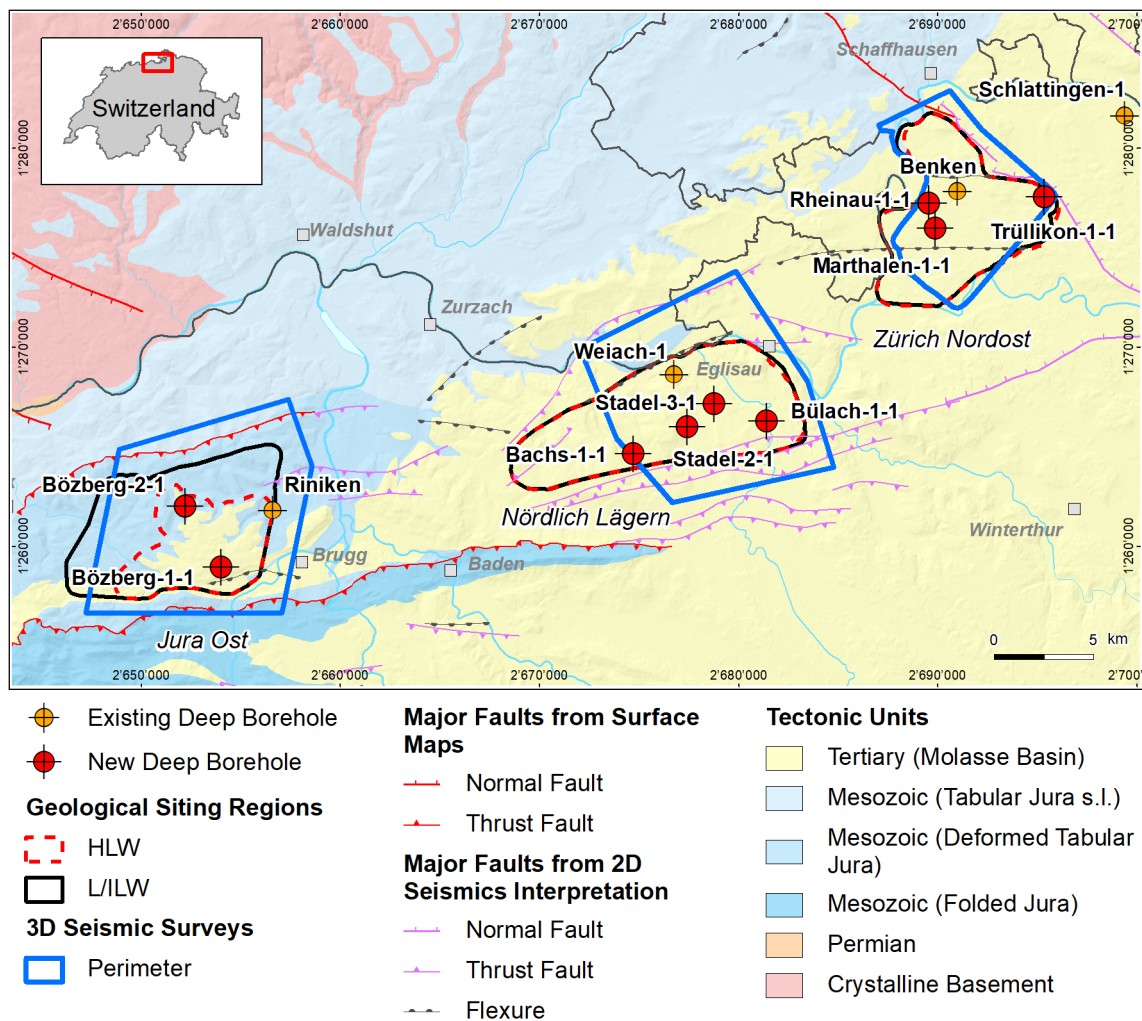


Fig. 1-1: Tectonic overview map with the three siting regions under investigation

1.2 Location and specifications of the borehole

The Bachs-1-1 (BAC1-1) exploratory borehole is the ninth (and last) borehole drilled within the framework of the TBO project. The drill site is located in the western part of the Nördlich Lägern siting region (Fig. 1-2). The vertical borehole reached a final depth of 1'306.26 m (MD)¹. The borehole specifications are provided in Tab. 1-1.

Due to a loss of a measurement tool (dilatometer), the borehole was cemented up to 500 m MD and a sidetrack was initiated with a kickoff point (KOP) at about 600 m MD. This sidetrack was labelled Bachs-1-1B (BAC1-1B). BAC1-1B reached a final depth of 952 m MD but was abandoned during borehole reaming operations due to entering the original borehole BAC1-1. Therefore, the vertical borehole BAC1-1 was used again for the remaining investigations. For easier communication and labelling, the name BAC1-1 is generally used for this borehole, including the sidetrack, unless stated otherwise. A detailed description of all technical details about the drilling process can be found in Dossier I.

Tab. 1-1: General information about the BAC1-1 borehole

Siting region	Nördlich Lägern
Municipality	Bachs (Canton Zürich / ZH), Switzerland
Drill site	Bachs-1 (BAC1)
Borehole	Bachs-1-1 (BAC1-1) including sidetrack Bachs-1-1B (BAC1-1B)
Coordinates	LV95: 2'674'769.089 / 1'264'600.698
Elevation	Ground level = top of rig cellar: 450.35 m above sea level (asl)
Borehole depth	1'306.26 m measured depth (MD) below ground level (bgl)
Drilling period	10th September 2021 – 23rd April 2022 (spud date to end of rig release)
Drilling company	Daldrup & Söhne AG
Drilling rig	Wirth B 152t
Drilling fluid	Water-based mud with various amounts of different components such as ² : 0 – 700 m: Bentonite & polymers 700 – 1'057 m: Potassium silicate & polymers ³ 1'057 – 1'129 m: Water & polymers 1'129 – 1'306.26 m: Sodium chloride brine & polymers

The lithostratigraphic profile and the casing scheme are shown in Fig. 1-3. The comparison of the core versus log depth⁴ of the main lithostratigraphic boundaries in the BAC1-1 borehole is shown in Tab. 1-2.

¹ Measured depth (MD) refers to the position along the borehole trajectory, starting at ground level, which for this borehole is the top of the rig cellar. For a perfectly vertical borehole, MD below ground level (bgl) and true vertical depth (TVD) are the same. In all Dossiers depth refers to MD unless stated otherwise.

² For detailed information see Dossier I.

³ Including sidetrack.

⁴ Core depth refers to the depth marked on the drill cores. Log depth results from the depth observed during geophysical wireline logging. Note that the petrophysical logs have not been shifted to core depth, hence log depth differs from core depth.

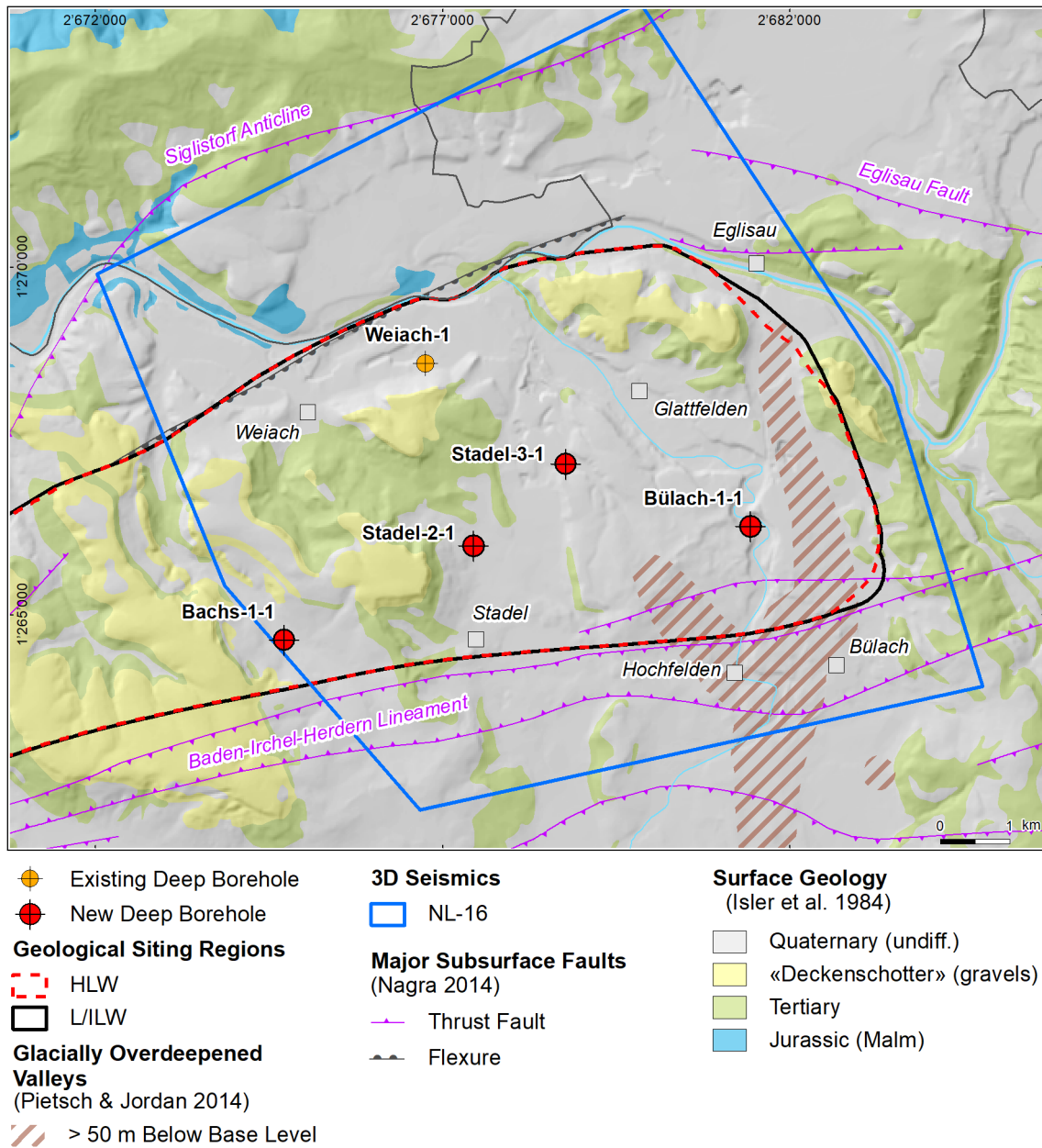


Fig. 1-2: Overview map of the investigation area in the Nördlich Lägern siting region with the location of the BAC1-1 borehole in relation to the boreholes Weiach-1, BUL1-1, STA3-1 and STA2-1

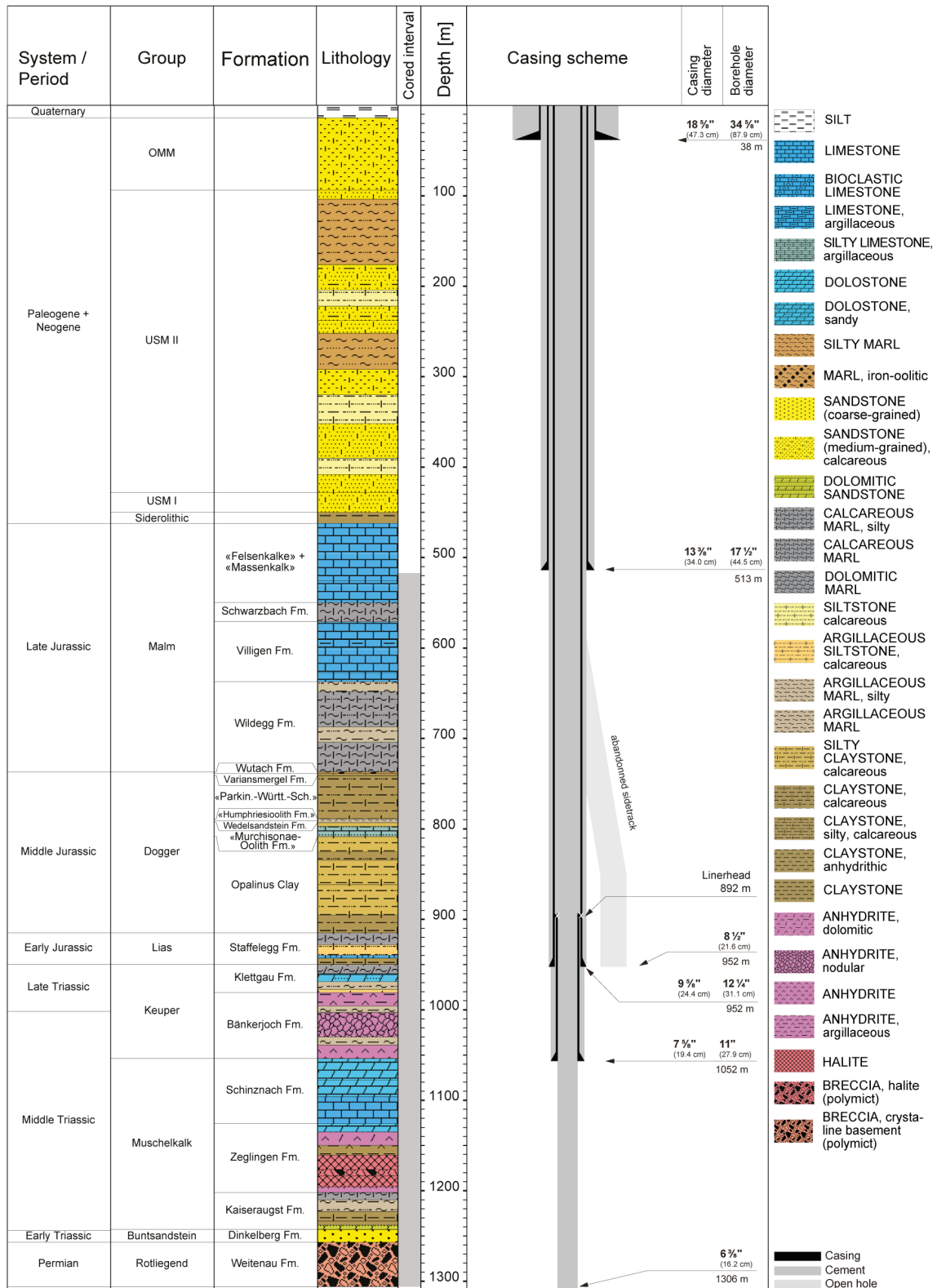


Fig. 1-3: Lithostratigraphic profile and casing scheme for the BAC1-1 borehole⁵

⁵ For detailed information see Dossier I and III.

Tab. 1-2: Core and log depth for the main lithostratigraphic boundaries in the BAC1-1 borehole⁶

System / Period	Group	Formation	Core top depth in m (MD)	Log
Quaternary			14	—
Paleogene + Neogene	OMM		94	—
	USM		450	—
	Siderolithic		462	—
Jurassic	Malm	«Felsenkalke» + «Massenkalk»		
		Schwarzbach Formation	549.69	550.03
		Villigen Formation	570.98	571.29
	Dogger	Wildeggen Formation	637.31	637.55
		Wutach Formation	737.05	737.32
		Variansmergel Formation	738.81	739.08
		«Parkinsoni-Württembergica-Schichten»	741.22	741.47
		«Humphriesiolith Formation»	788.92	789.12
		Wedelsandstein Formation	791.05	791.25
	Lias	«Murchisonae-Oolith Formation»	793.11	793.31
		Opalinus Clay	808.34	808.57
		Staffellegg Formation	914.91	915.30
			949.73	950.07
Triassic	Keuper	Klettgau Formation	980.93	981.27
		Bänkerjoch Formation	1053.90	1054.30
	Muschelkalk	Schinznach Formation	1125.75	1126.20
		Zeglingen Formation	1202.03	1202.43
	Buntsandstein	Kaiseraugst Formation	1242.82	1243.12
		Dinkelberg Formation	1256.86	1257.26
Permian	Rotliegend	Weitenau Formation	<small>final depth</small> 1306.26	1306.77

⁶ For details regarding lithostratigraphic boundaries see Dossier III and IV; for details about depth shifts (core goniometry) see Section 2.1.

1.3 Documentation structure for the BAC1-1 borehole

NAB 22-04 documents the majority of the investigations carried out in the BAC1-1 borehole, including laboratory investigations on core material. The NAB comprises a series of stand-alone dossiers addressing individual topics and a final dossier with a summary composite plot (Tab. 1-3).

This documentation aims at early publication of the data collected in the BAC1-1 borehole. It includes most of the data available approximately one year after completion of the borehole. Some analyses are still ongoing (e.g. diffusion experiments, analysis of veins, hydrochemical interpretation of water samples) and results will be published in separate reports.

The current borehole report will provide an important basis for the integration of datasets from different boreholes. The integration and interpretation of the results in the wider geological context will be documented later in separate geoscientific reports.

Tab. 1-3: List of dossiers included in NAB 22-04
Black indicates the dossier at hand.

Dossier	Title	Authors
I	TBO Bachs-1-1: Drilling	P. Hinterholzer-Reisegger
II	TBO Bachs-1-1: Core Photography	D. Kaehr, M. Stockhecke & Hp. Weber
III	TBO Bachs-1-1: Lithostratigraphy	P. Jordan, P. Schürch, M. Schwarz, R. Felber, H. Naef, T. Ibele & F. Casanova
IV	TBO Bachs-1-1: Microfacies, Bio- and Chemostratigraphic Analyses	S. Wohlwend, H.R. Bläsi, S. Feist-Burkhardt, B. Hostettler, U. Menkveld-Gfeller, V. Dietze & G. Deplazes
V	TBO Bachs-1-1: Structural Geology	A. Ebert, E. Hägerstedt, S. Cioldi, L. Gregorczyk & F. Casanova
VI	TBO Bachs-1-1: Wireline Logging, Micro-hydraulic Fracturing and Pressure-meter Testing	J. Gonus, E. Bailey, J. Desroches & R. Garrard
VII	TBO Bachs-1-1: Hydraulic Packer Testing	R. Schwarz, R. Beauheim, L. Schlickenrieder, E. Manukyan & A. Pechstein
VIII	TBO Bachs-1-1: Rock Properties, Porewater Characterisation and Natural Tracer Profiles	E. Gaucher, L. Aschwanden, T. Gimmi, A. Jenni, M. Kiczka, M. Mazurek, P. Wersin, C. Zwahlen, U. Mäder & D. Traber
IX	<i>The geomechanical campaign in BAC-1-1 was limited to two oedometric tests. Hence, no dedicated Dossier IX was produced for NAB 22-04. The hydraulic conductivity values derived from the oedometric tests are documented in the Summary Plot.</i>	
X	TBO Bachs-1-1: Petrophysical Log Analysis	S. Marnat & J.K. Becker
	TBO Bachs-1-1: Summary Plot	Nagra

1.4 Scope and objectives of this dossier

The dossier at hand (Dossier V) documents the work of the structural geology experts. The objectives of the report are:

- core goniometry to reset drill cores to the correct depth and original orientation based on high resolution borehole images and high resolution 360° core photographs (Appendices E-1 and E-2)
- structural discontinuities identification on high resolution 360° core photographs and drill cores
- true dip and dip azimuth analysis of structures and bedding planes on high resolution 360° photographs in TerraStation II and/or manual measurements with a geological compass on drill cores
- documentation of recorded structures and their relevant parameters
- visualisation of structural geology data as profiles and overview plots:
 - profile 1:1'000: Appendix B
 - profile 1:100: Appendices C-1 to C-3
 - overview plot of stereograms and rose diagrams: Appendices D-1 and D-2

The lithostratigraphic subdivision used in this report is in line with the finding in Dossier III.

1.5 Petrophysical logs and preliminary log analysis available

The petrophysical logs and preliminary log analysis listed below were available at the data-freeze and considered as a supplementary source of information for this report (for more details, see Dossier VI):

- total natural gamma ray borehole and potassium corrected (GR)
- caliper / radius (RD1 to RD6)
- near / array corrected limestone porosity (APLC)
- high resolution formation density (RHO8)
- high resolution formation photoelectric factor (PEF8)
- array laterolog apparent resistivity from computed focusing mode 0 to 5 (RLA1 to RLA5)
- formation micro imager (FMI)
- ultrasonic borehole image (UBI)
- borehole breakouts and centreline fractures analysis based on FMI and UBI images

1.6 Borehole deviation

The cored section of BAC1-1 is almost vertical, initially with a slight average deviation towards the NW followed by a deviation towards the SE. At 525.02 m TVD (true vertical depth) the maximal horizontal deviation of 1.35 m is reached, trending towards the NW (azimuth 286.5°). The deviation direction changes from NW to SE at this depth (Fig. 1-4).

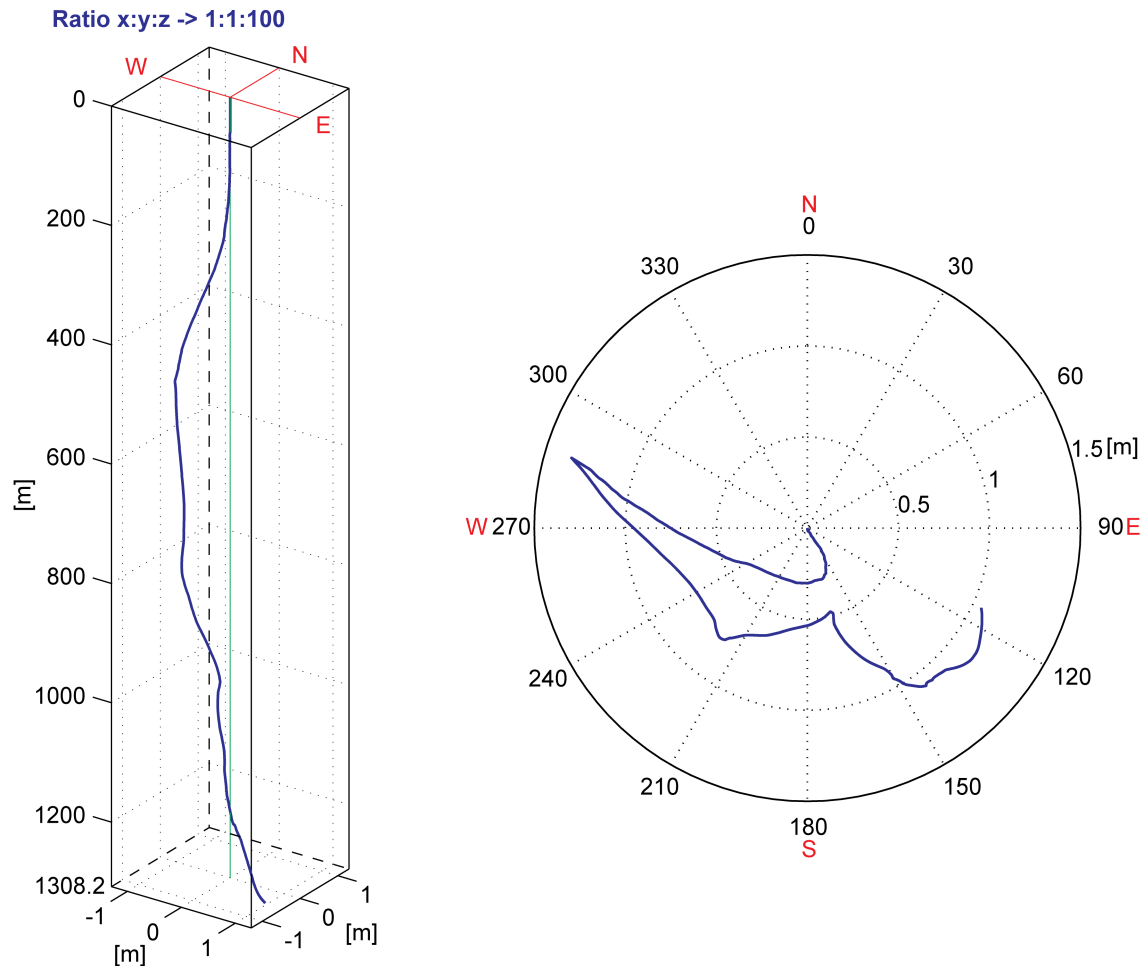


Fig. 1-4: Borehole deviation within the cored section
 The left image visualises the borehole path in 3D. Compared to the x- and y-axes, the z-axis is compressed. The borehole azimuth is shown on the right.

2 Methodology

2.1 Core goniometry

2.1.1 Introduction

A detailed structural analysis was performed on drill cores along with circumferential and planar drill core photographs. Using the reference line on the core surface positioned at an azimuth of 0° during core photography, most drill cores could be oriented using borehole image logs.

For this study, high-resolution 360° and planar photographs were available for most of the cored interval from 517.16 m to 1'306.26 m MD (core depth). The data were delivered as 1'215 circumferential and 1'269 planar photographs in TIF format. However, the original photographs with a resolution of 10 pixels/mm were too large to be handled with TerraStation II (TERRASCIENCES Inc.). Therefore, the original photographs were compressed by 25% and exported with a resolution of 300 dpi. In addition, FMI and UBI logs of good to excellent quality were also available. Further relevant data included auxiliary borehole data, core orientation line (COL) and core section listings, lithostratigraphic tops and petrophysical logs.

2.1.2 Workflow

This section describes the methodology used for extracting the directional information from 360° core photographs. The following steps were tailored for efficient core goniometry using the TerraStation II software:

1. Quality control of core photographs:

Prior to loading the data, it was ensured that the COL (red) on the 360° core photographs was set to 0°.

Note: the core orientation line (COL) represents a continuous reference line set to an azimuth of 0° to fix the relative orientation of drill cores. The COL was drawn on the core surface immediately after core retrieval at the drill site. The line lengths vary widely from a few centimetres up to several metres and therefore sometimes continue over several core sections, depending on whether each individual core section could be fitted together along the core edges or not. If core sections could not be merged, a new COL was determined. The coherent COL was then used to orient the drill core using borehole image logs.

2. Data loading:

All 360° core photographs were loaded as mirrored images in order to simulate the borehole image log as seen from the inside of the borehole. A constant value of 95 mm (3.74") was added as diameter.

The processed FMI and UBI logs as well as the auxiliary petrophysical logs were imported into TerraStation II. It was checked that the depth of the petrophysical logs, especially the first GR (gamma ray) run, matched the depth of the FMI data.

3. Depth shifting:

The 360° core photographs were shifted manually to FMI logs using distinct, correlated planar and/or non-planar features. For the purpose of simplicity and consistency, only one shift value was applied for each individual core section (generally 3 m per section). This resulted in minor data gaps and/or overlaps at core section boundaries of a few centimetres maximum. In total, 262 distinct depth shift values were applied for the entire cored borehole section; these varied from +0.06 m to +0.75 m. The defined values are listed in Appendix E-1.

4. Core orientation:

The core was oriented using correlated geological features (e.g. faults / fractures, inclined / deformed bedding, nodules, etc.) which were matched with the orientation on the FMI by rotating the 360° core photographs clockwise around the borehole axis.

The obtained angle of rotation was then applied to the entire core section with a continuous COL. Simultaneously, the validity across other geological features was checked. Note that the length of a linked COL segment was highly variable and could continue across several core sections. All COLs and the applied angles of rotation of the individual COLs are listed in Appendix E-2. To highlight the uncertainties related to core orientation, an uncertainty assessment was carried out and visualised using three confidence classes.

5. Quality control of core goniometry:

Prior to the structural recording of the drill cores, the depth shifts, the core correlation with the FMI / UBI image logs and the core orientations were reviewed.

The following steps do not belong to classical core goniometry. However, they played a key role in the coherent workflow of the structural core analysis and are thus mentioned here:

6. Dip picking on oriented 360° core photographs:

Bedding-related planes were picked manually for a structural dip evaluation. Structural elements on drill cores were picked manually and characterised in detail with respect to relevant parameters.

7. Recording of kinematic features:

Kinematic shear sense indicators along fault surfaces such as e.g. slickensides, striations and (fault) offsets were identified and measured on the cores. To determine the lineation azimuth and plunge and/or planes not visible in the photographs, a goniometer was used. The drill core was placed in the goniometer facing up-hole and rotated around the vertical axis by the angle of rotation determined from the core orientation line. Subsequently, the azimuth and plunge of the striation were measured using a geological compass (see Fig. 2-1).

8. Examination of angular differences:

The angular differences between the striation azimuths / plunges and the orientation of associated fault planes were checked using the TectonicsFP software. If the angular offset exceeded 15°, the fault plane and lineation were remeasured.

9. Quality control:

A final quality control was performed, with the main focus on consistency (between TerraStation II, primary records of detailed structural core analysis and the structural inventory metadata), completeness of records and the accurate characterisation of the recorded tectonic features.

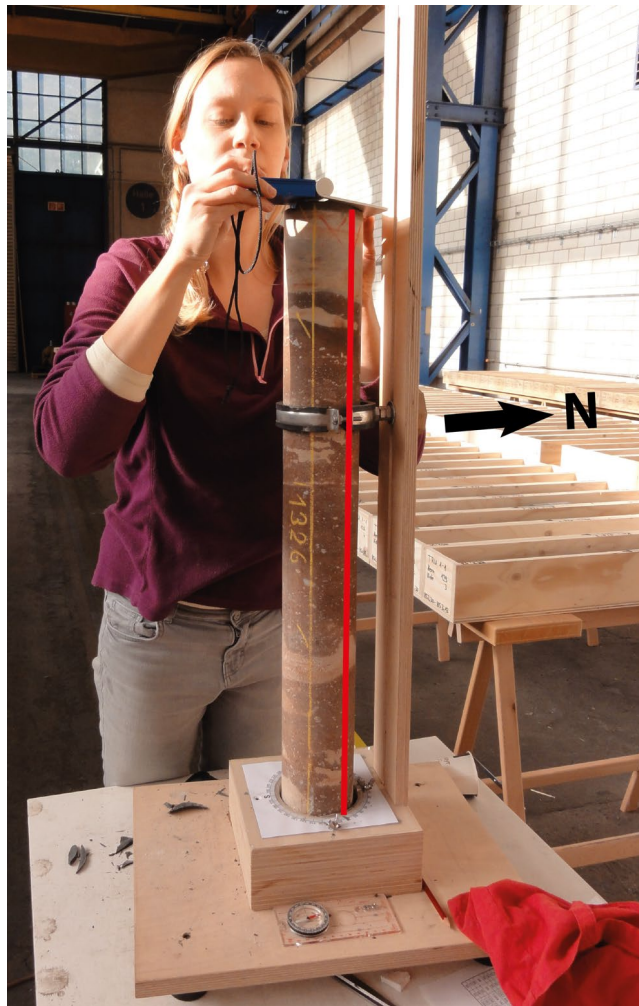

















Fig. 2-1: Using a goniometer to determine kinematic indicators along fault planes
Note the red COL on the core piece defining the position of the drill core in the goniometer.

2.1.3 Dip picking and dip type classification

Due to higher accuracy and reliability compared to automated methods, a manual sinusoid method and a point-to-point method were used to pick all relevant features on the 360° core photographs. In a cylindrical borehole, a perfect plane will appear as a sine wave on the circumferential core photograph and its amplitude reflects the dip relative to the borehole axis.

Different dip classes were defined for the different structure types. For this study, a total of 15 different dip types were defined in TerraStation II (Fig. 2-2).

Dip Types

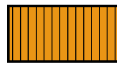
	Fault plane		Undifferentiated bedding		Drilling-induced fracture
	Mirror-like fault plane		Cross-bedding		Borehole breakout
	Stylolitic fault plane		Deformed bedding		Centreline fracture
	Unassigned fracture		Stylolite		
	Joint		Fold axis		
	Tension gash / vein		Open pore		

Fracture density classes

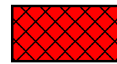
FDC2: 20 to 60 m²/m³



FDC3: 60 to 200 m²/m³




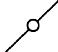


FDC4: > 200 m²/m³



TectonicsFP symbols

Shear sense:

	up / down - direction indicated by arrow in relation to fault plane
	dextral - direction indicated by arrows
	sinistral - direction indicated by arrows
	unknown

Shear sense quality:




good	
moderate	
poor	

Fig. 2-2: Symbols for dip types, fracture density classes and kinematic data used for this study

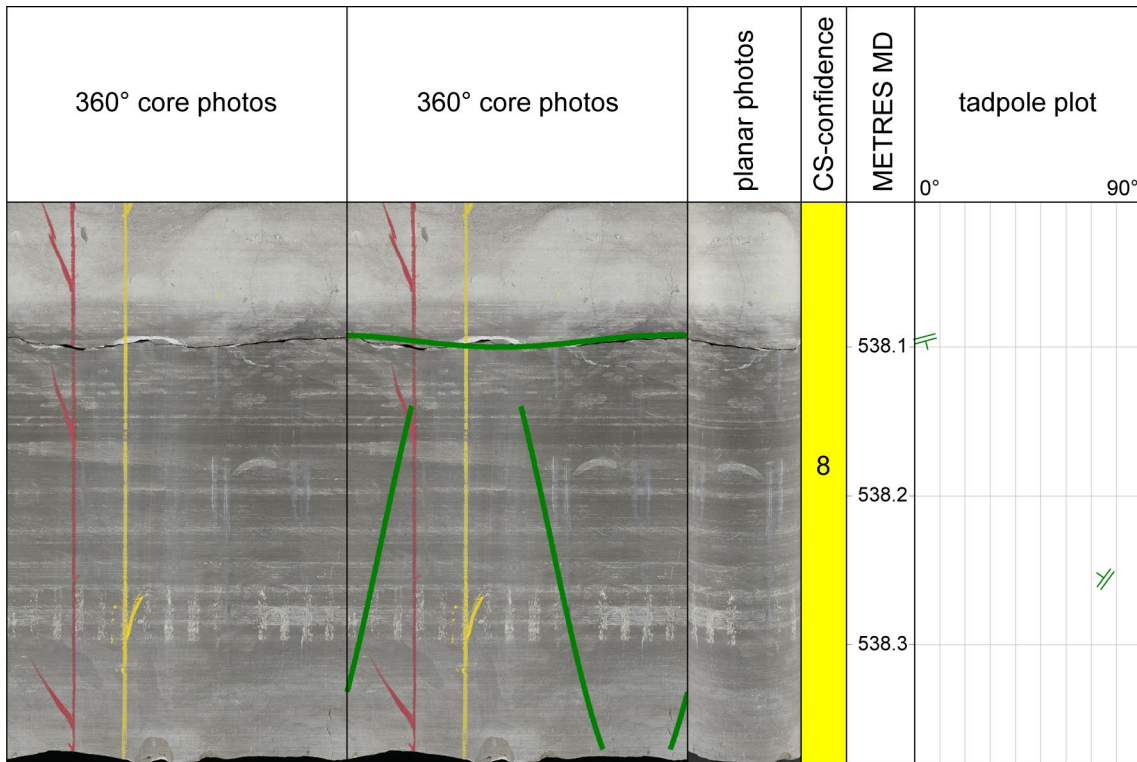


Fig. 2-3: Fault planes identified within the drill core at 538.10 m and 538.26 m MD (log depth) («Felsenkalke» + «Massenkalk») From left to right: shifted and oriented 360° core photograph without (left) and with (right) picked sine waves, followed by depth-shifted planar core photographs, core section numbering in the coloured bar displaying the goniometry confidence ranking, depth track showing the position and length of the currently displayed window and tadpole plot. Note that the displayed sine wave of the structure at 538.26 m MD (log depth) is not visible on the 360° core photograph. The fault plane was therefore implemented from the core analysis and the orientation was obtained by compass measurement.

Some structures were only visible on planes not outcropping at the rim of the core and were not visible on the 360° core photographs. The orientation of these structures was obtained with a geological compass, as described above, and the data were subsequently imported into the digital dip dataset. Consequently, the associated dip sine waves did not fit with any visible traces and/or were simply not visible at this depth level, as exemplified in Fig. 2-3.

2.1.4 Dip data for non-oriented and missing cores

Due to a lack of correlated features, poor data quality or missing image log data, 91.16 m of the available drill cores remained non-oriented. Within these non-oriented drill cores, a total of 6 bedding planes and 95 tectonic / drilling-induced discontinuities could be observed and picked. The structural planes were nevertheless measured manually with a geological compass and included in TerraStation II, or picked digitally on 360° core photographs. For non-oriented drill cores and core photographs, the red core orientation line was set to 0°. Because in a vertical borehole, the dip angle of these features are correct and only the dip azimuths are affected by the lack of orientation, the non-oriented dataset can only be used for fracture density calculations. To

highlight the incorrect dip azimuth measurements of these features, a quality indicator of 0 was assigned and open tadpoles were used for visualisation (Fig. 2-4). A quality indicator of 1 was assigned to all oriented features.

For intervals lacking 360° core photographs, short drill core sections could still be oriented using the coherent COL, which sometimes continued across several cores. The depth and orientation of the structures were then measured on the core, and the dip data were subsequently imported into the digital database of TerraStation II (see Fig. 2-5).

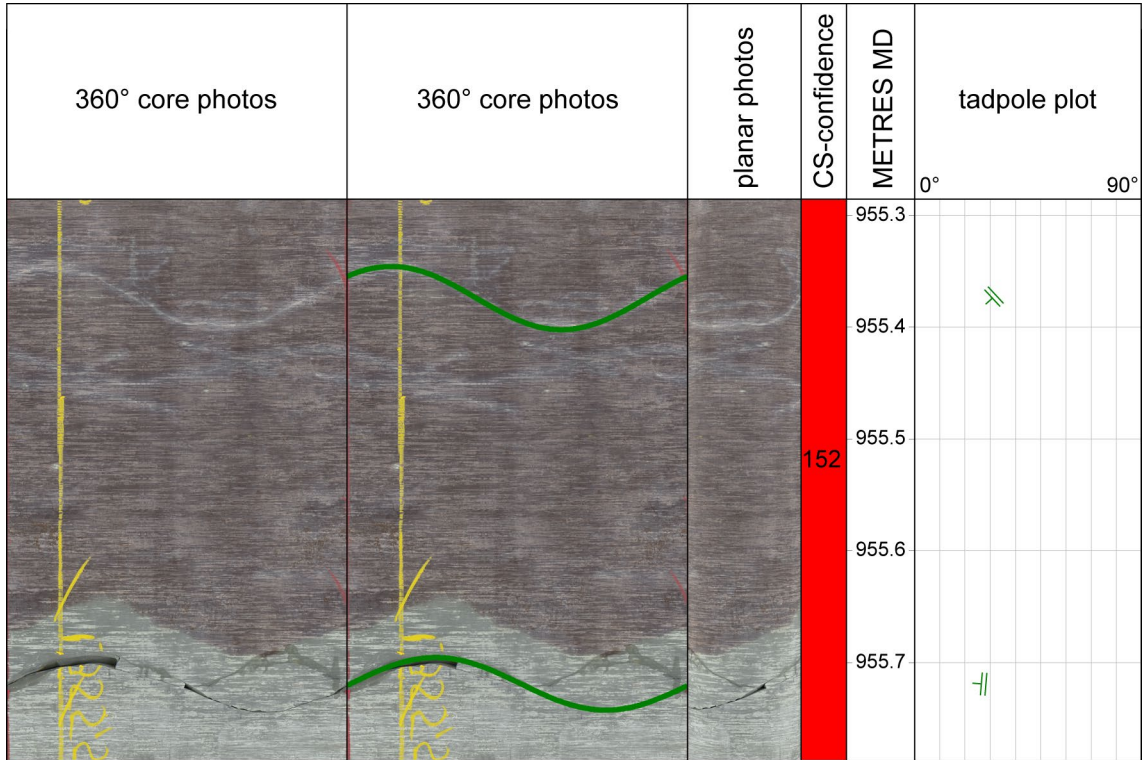


Fig. 2-4: Example of dip data in a non-oriented core interval
 The goniometry confidence is set to "core not oriented" (column "CS-confidence", red).
 Example from the Klettgau Formation from 955.29 m to 955.78 m MD (log depth).



Fig. 2-5: Interval without 360° core photographs from 1'129.50 m to 1'130.15 m MD (log depth) in the Zeglingen Formation

In this example, the core goniometry and structural analysis were performed on the drill core. The orientation data were determined with a geological compass and subsequently imported into the digital dip database of TerraStation II. The goniometry confidence for this core section is high (column "CS-confidence", green).

2.1.5 Goniometry confidence assessment and uncertainties

Goniometry confidence ranking

To visualise the uncertainties related to the core goniometry, the reliability of the core orientation was classified using a confidence ranking scheme. The assessment was carried out for each connected COL and depended particularly on the number of reliably correlated features within these intervals. Features with a moderate to steep (> 15°) dip generally provided a higher confidence and resulted in lower angular uncertainties than e.g. shallow structures (< 15°). The features used for the core goniometry are listed in Appendix E-1 and E-2 along with the coherent COLs. Examples of the correlated features between the FMI and the core are presented in Figs. 2-6, 2-7 and 2-8.

There are three confidence levels for the goniometry, illustrated as coloured fields in the structural composite plots (Appendix A). The confidence level depends on the number of evident structures found within each coherent COL:

- **high** is defined by three or more distinct, preferably moderately inclined to steep (> 15°) planar and/or non-planar features (Figs. 2-6 and 2-8), resulting in a high angular accuracy.
- **moderate** is associated with one or two correlated (non-)planar structures with shallow to moderate dip angles (< 15°; Fig. 2-7). Thus, the core orientation contains some uncertainty and is less accurate.
- **not oriented** is characterised by a lack of obvious indicators for the core orientation.

Tab. 2-1 gives an overview of the core goniometry confidence assessment. The procedure described in Section 2.1.2 resulted in the successful orientation of 697.94 m out of the total 789.10 m drill cores (92%).

Tab. 2-1: Core goniometry confidence assessment of the analysed interval

Borehole interval			Goniometry confidence								
Top	Bottom	Length	High			Moderate			Not oriented		
[m MD core depth]			[m]	[%]	No. of COLs	[m]	[%]	No. of COLs	[m]	[%]	No. of COLs
517.16	1'306.26	789.10	243.58	31	25	454.36	58	109	91.16	12	60

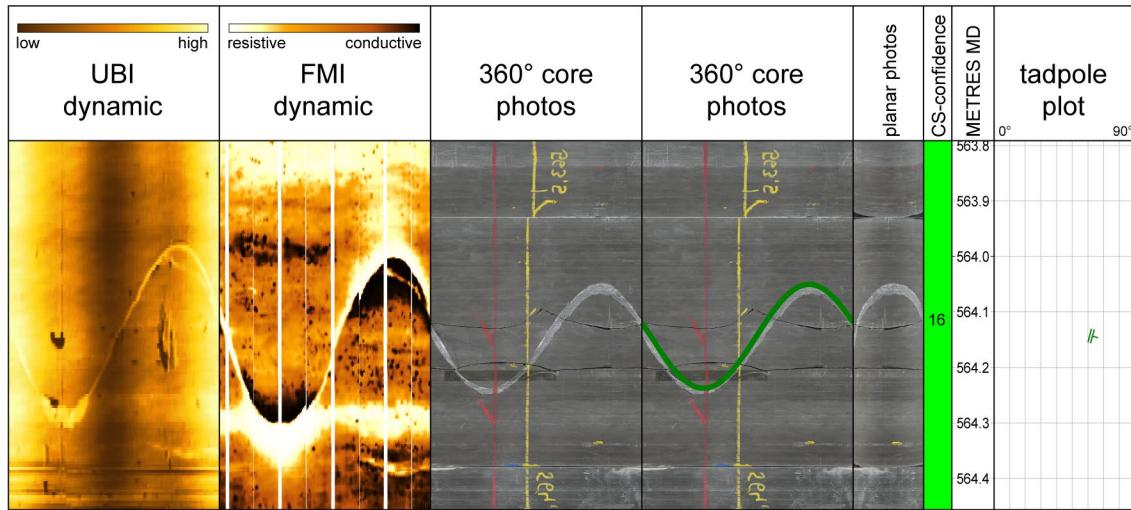


Fig. 2-6: Core – FMI / UBI correlation for a fault plane at 564.14 m MD (log depth) in the Schwarzbach Formation

This prominent ESE-dipping fault plane was unequivocally correlated across the UBI and FMI logs and the core photographs, and therefore represents a high-confidence indicator for the core orientation. From left to right: dynamically normalised UBI and FMI image logs, shifted and oriented 360° core photographs without (left) and with (right) sine wave, followed by shifted planar core photographs. The core section numbering is shown in the coloured bar displaying the goniometry confidence ranking (column "CS-confidence", high – green in this case). The depth track shows the position and length of the currently displayed window (about 65 cm). A tadpole plot with true orientation of the manually picked fault plane (shown in green) is also displayed.

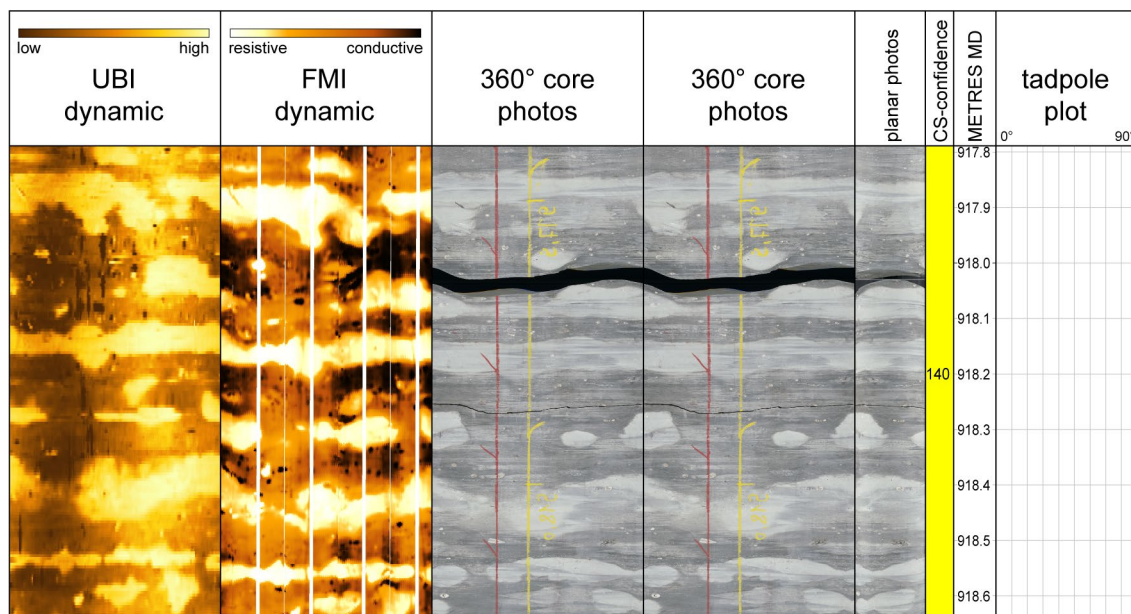


Fig. 2-7: Core – FMI / UBI correlation from 917.79 m to 918.62 m MD (log depth) in the Staffelegg Formation

These unique structures represent nodules which appear bright on the UBI (high amplitude) and on the FMI (high resistivity) images. They were used to shift and orient core section 140. Due to their heterogeneous nature, they are considered as indicators of limited quality for the core goniometry and assigned a moderate confidence level (column "CS-confidence", yellow).

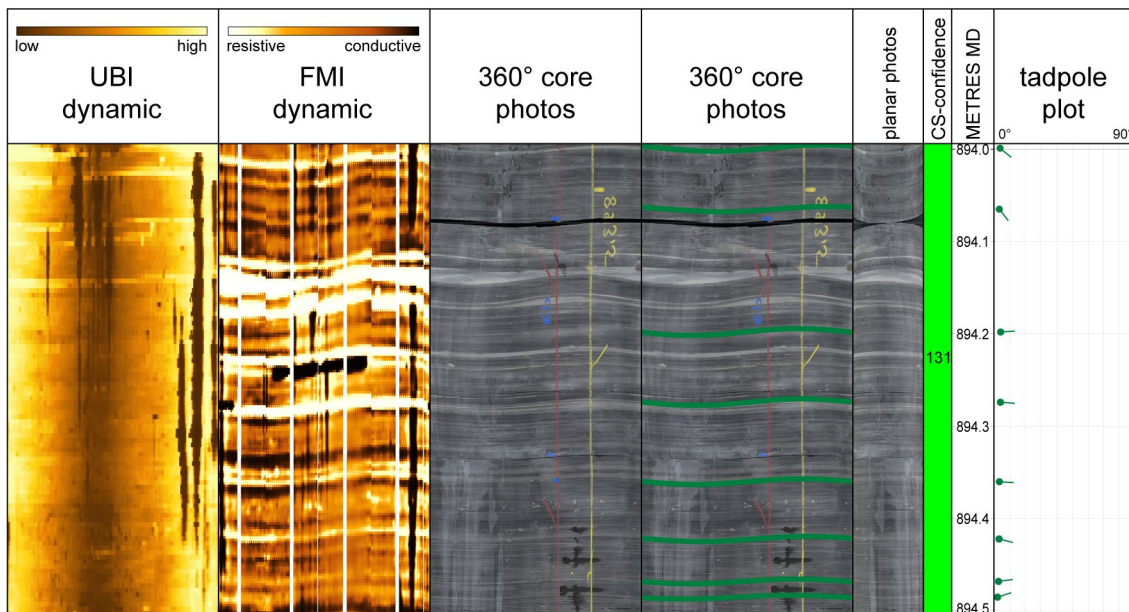


Fig. 2-8: Core – FMI / UBI correlation for subhorizontal to shallow dipping bedding

The FMI and the core photograph match within the well-bedded strata in the Opalinus Clay from 894 m to 894.5 m MD (log depth). Although the bedding planes match at relatively low dip angles ($< 10^\circ$), they are distinctive and are clearly visible on both the FMI and core photographs and are considered as robust indicators for core orientation (column "CS-confidence", green).

Project-specific uncertainties

A number of unavoidable limitations and uncertainties were associated with the work performed and may have affected the accuracy of the results. These factors are evaluated below:

- angular uncertainty: is associated with the core goniometry and is reflected by the confidence scheme. It implies, in particular, an angular error for the azimuth.
- Errors related to compass measurements on drill cores: to explore the measurement-related error, multiple measurements of the same structure were performed by different users. The reproducibility was 5° for the dip magnitudes and 5° to 10° for the dip azimuths. Considering that most geological compasses have an error margin within 2° for dip azimuth and dip magnitude, it can be concluded that the above-mentioned goniometer has an acceptable error margin and can safely be used for accurate structural core analysis.
- Dip picking on 360° photographs: the pixel resolution of the screen defines the angular uncertainty of the dip picks in 3D space and is 1° to 2° for the dip angle and 2° to 4° for the dip azimuth.
- Core photographs: although the derived 360° core photographs covered almost the entire studied interval (517.16 m to 1'306.26 m MD core depth), some data gaps occurred: from 517.16 m to 520.10 m MD (core depth), from 690.86 m to 720.98 m MD (core depth), from 747.93 m to 760.05 m MD (core depth), from 775.01 m to 778.10 m MD (core depth), from 832.01 m to 835.01 m MD (core depth), from 877.92 m to 881.64 m MD (core depth), from 882.30 m to 884.05 m MD (core depth), from 901.90 m to 910.87 m MD (core depth), from 940.76 m to 941.40 m MD (core depth), from 943.19 m to 945.68 m MD (core depth), from 949.15 m to 959.01 m MD (core depth), from 970.25 m to 973.14 m MD (core depth), from

975.79 m to 977.13 m MD (core depth), from 1'068.12 m to 1'068.89 m MD (core depth), from 1'110.02 m to 1'110.80 m MD (core depth), from 1'113.68 m to 1'115.67 m MD (core depth), from 1'212.65 m to 1'213.08 m MD (core depth) and from 1'218.53 m to 1'219.17 m MD (core depth). These gaps, all larger than 30 cm, are mainly related to dis-integrated and/or highly fractured drill cores, which were not suitable for circumferential photography, or to data gaps between core sections

- In some core intervals, the COL was discontinuous. This was mainly related to uncertainties in the fitting of individual core pieces / sections together at the drill site. In such cases, the non-coherent core sections were treated separately (see Appendix E-2).
- Due to the presence of steel in the Nagra core storage facility in Würenlingen, a site-specific magnetic field disturbance was recognised. Consequently, the goniometer needed to be carefully aligned towards relative north to obtain the correct orientations of the geological features (mainly lineations) measured with a compass. This always had to be kept in mind when moving the equipment across the core store.

2.2 Structural work

This section describes (A) how the structural recording and characterisation of drill cores were carried out, (B) which structure types were distinguished, and (C) which structure parameters were defined. Details with regard to the structural core analysis are given in the structural analysis manual and enclosed factsheets and templates (Ebert & Decker 2019).

- A) After the core goniometry was finalised, all deformation structures were recorded on the drill cores. The recording was usually finalised within a few weeks.

The overall core quality was excellent. Only cores from clay-rich lithologies (particularly the Dogger) were affected by progressive discing but were still suitable for structural analysis. Due to 351 samples with lengths of up to 50 cm being taken at the drill site (e.g. for porewater or geomechanical analyses), there were gaps within the core sections. Samplers were strictly advised not to sample core intervals containing tectonic structures. The completeness of the structural record is therefore not biased or limited by sampling. Furthermore, it can be assumed that the complete structural inventory was recorded because high-resolution core photographs were taken from all cores, including the sampled ones.

Most of the structural work was performed by two people. A structural geology expert defined all visible structure types along with their relevant parameters for each core section, which was usually 3 m long. At the same time, a colleague manually picked the structure on the 360° core photographs in TerraStation II. The structures and their parameters such as mineralisation, thickness or shear sense were documented on a DIN A3 template with its content previously defined in Ebert & Decker (2019). The log depth was determined in metres MD along with the true orientation of the structures on oriented 360° core photographs. The difference in depth between the core and log depth mostly varied by only a few centimetres and depended on the dynamic depth shift of the core photographs with regard to the FMI used as the main depth reference. Striations on slickensides recognised on surfaces of broken cores were measured with a geological compass (Fig. 2-1). As soon as a core section was completely analysed, all entries from the DIN A3 template were digitised and data QC was carried out.

- B) Depending on rock rheology and the type and degree of deformation, different types of structural discontinuities may develop. Based on this, the structures were subdivided into five main groups of discontinuities (Fig. 2-9). In total, 11 types of structures were distinguished in this study (Tab. 2-2) and are illustrated with numerous examples in Chapter 4. Detailed definitions and information on the origin of the structures can be found in the structural manual of Ebert & Decker (2019).
- C) Additionally, parameters such as mineralisation, shear sense and thickness (listed in Tab. 2-3) were determined and documented for each individual structure on the DIN A3 template (Fig. 2-10). In addition, each structure was sketched and labelled with a consecutive number on the designed grid with a scale of 1:10.


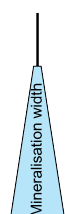
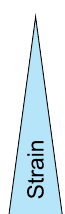
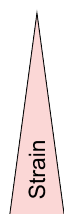
Mohr-Coulomb type brittle failure			Viscous (ductile) deformation	
Fractures			Without cohesion loss	
Drilling-induced	Extensional	Shear	Carbonate solution	Ductile shear
 <ul style="list-style-type: none"> Centreline fracture Petal fracture Core discing 	 <ul style="list-style-type: none"> Joint Vein (Tension gash) 	 <ul style="list-style-type: none"> Fault plane Fault zone 	<ul style="list-style-type: none"> Stylolite / Dissolution seam Stylobreccia 	 <ul style="list-style-type: none"> Shear band Mylonite

Fig. 2-9: The five main groups of structural discontinuities

Tab. 2-2: Types of structural discontinuities identified in this study
For more details, see Ebert & Decker (2019).

Discontinuity group	Structure type	Characteristics
Brittle structures with shear indications	Fault plane	A plane of shear failure, i.e. a plane along which there has been plane-parallel movement (Peacock et al. 2016). A single, thin, planar and sharp structural discontinuity with shear indications (e.g. striation or slickenfibres).
	Mirror-like fault plane	A fault plane with a smoothed, polished or shiny slip surface.
	Stylolitic fault plane	A fault plane with dissolution seams and stylolite-bearing columns which are oblique or parallel to the plane (modified from Hancock 1985).
	Fault zone	A zone with a volume which includes interacting and linked fault segments, densely fractured rock and/or fault rocks; zones are typically bounded by sub-parallel margins or fault planes (modified from Peacock et al. 2016).

Tab. 2-2: (continued)

Discontinuity group	Structure type	Characteristics
Brittle structures without shear or slip indications	Joint	A barren, closed fracture on which there is no measurable slip or dilatation at the scale of observation. If any mineral fill, including crystal growth fibres, is visible, the structure is better called a vein (Hancock 1985).
	Vein	Extensional fracture filled by secondary mineral crystallisation.
	Tension gash	Vein formed by dilatation; tension gashes may be fully cemented (vein), partly cemented (partly open) or open (Passchier & Trouw 1996).
Structure without preserved evidence for the mode of fracturing	Unassigned fracture	General term for a structure without preserved evidence for the mode of fracturing, i.e. it is applicable to structures formed by extension or shear; fractures can include close-to-planar discontinuities such as dykes, fault planes, joints and veins (Peacock et al. 2016).
Structures caused by dissolution	Stylolites	Irregular seams of insoluble residues with dark, "mountainous" rough teeth formed by pressure solution (Passchier & Trouw 1996).
	Open pores	Isolated open volumes in the rock mass, resulting e.g. from incomplete cementation of veins, dissolution or preserved cavities in fossils.
	Karst	Open networks resulting from dissolution of carbonates. These cm- to m-wide cavities may have been refilled later.
Fabrics without cohesion loss, e.g. caused by ductile deformation	Shear bands	Minor planar shear zones in which the progressive deformation is non-coaxial (Passchier & Trouw 1996).
	Mylonites	Strongly deformed rock from a ductile shear zone with a planar foliation and usually with a stretching lineation (Passchier & Trouw 1996).
	Schistosity	Secondary foliation defined by preferred orientation of equant fabric elements in a medium- to coarse-grained rock. Individual foliation-defining elements (e.g. micas) are visible with the naked eye (Passchier & Trouw 1996).
	Dynamic recrystallisation	Represented by small (mm-sized) and elongated rock salt (Zeglingen Formation) crystals.

Tab. 2-2: (continued)

Discontinuity group	Structure type	Characteristics
Drilling-induced fractures (DIF)	Drilling-induced fractures	Collective term for fractures created by forces associated with drilling and coring procedures. Depending on load on drill bit, mud weight and rock properties, drilling-induced fractures develop during drilling or shortly thereafter. Based on the aperture, fracture surface and geometric relationships, drilling-induced fractures can be distinguished from natural fractures. Drilling-induced fractures are always open and never mineralised.
	Petal fracture	Drilling-induced fracture with convex-up geometry cutting a core downwards starting from its perimeter. Petal fractures form immediately ahead of the drill bit as a result of excessive bit weight during coring. They propagate downhole.
	Centreline fracture	Drilling-induced fracture that typically splits a core approximately in half.
	Core discing	The formation of discs of relatively uniform thickness which fracture on surfaces approximately normal to the axis of the core.
Additional features / dip types	Undifferentiated bedding	Planar surface representing either the boundary between two different lithological units or internal bedding. Thought to reflect original horizontal and planar surfaces.
	Deformed bedding	Bedding planes occurring in narrow zones in any lithology with moderate to steep dip angles ($> 15^\circ$) which differ from the general structural dip. They have been subject to deformation due to faulting and/or folding.
	Cross-bedding	Inclined foreset surfaces in sandstone occurring in sets and bounded by set boundaries. These sedimentary features may be used as paleocurrent indicators. Upper truncation by the next set is diagnostic.
	Fold (axis)	One or a stack of originally flat and planar surfaces, such as sedimentary rocks, that are bent or curved due to applied external stress. Folds appear in various scales and shapes.

Tab. 2-3: Systematically recorded parameters for the investigated structures

Parameter	Definition of parameters and procedure for defining parameters
Depth	<p>All types of structures are recorded quantitatively along the scanline of the core axis. The depth of the structure is measured at the point where it cuts the core axis. For steeply dipping planes, the depth should be determined halfway between the top and the base of the intersection ellipse of the structure.</p> <p>If a zone is recorded (e.g. fault zone, shear band, fracture density class), the top (Top MD) and the base (Bottom MD) of the zone are specified in the corresponding columns.</p>
Core orientation line number	<p>After extraction of the core from the inner tube, the core pieces are juxtaposed whenever possible. Continuous sections without drilling breaks, demarcated by grinding, crushed or core loss zones, are marked with a COL and denoted with a consecutive number. This number enables linking of the recorded structure with the key structure of this orientation line section that was identified on the borehole image.</p>
Depth shift between core and FMI	<p>The depth shift is defined using correlated structures visible on both the FMI and core.</p>
Correlation with log	<p>Assessment of whether each individual structure can be clearly identified on FMI / UBI and core. “yes” indicates that the structure can be correlated with the image log and “no” indicates structures which cannot be correlated, or which are not shown by the image log. In addition, a correlation quality ranking is carried out (1 – good, 2 – moderate, 3 – no correlation).</p>
Dip direction and dip angle	<p>Measured dip direction and dip angle of the structure.</p>
Structure type	<p>The abbreviations for structure types according to Tab. 2-2 are entered into the paper template.</p>
Length of structure	<p>The length of the long axis of the intersection ellipse is measured for structures which cut the core axis at acute angles (dipping with more than about 70°) and structures which do not cut through the entire core diameter. The measured length will be used for the calculation of P32 fracture density. Measurements are required to reduce the inaccuracy resulting from calculating fracture areas solely from the angle between the structure and the core axis.</p>
Azimuth and plunge of lineations	<p>Measured dip azimuth and plunge of the lineation observed on the measured plane.</p>
Shear sense and quality	<p>Shear sense of fault planes and shear bands using up (reverse fault), down (normal fault), dex (dextral strike slip) or sin (sinistral strike slip), and reliability indicators (good, fair, poor) of the shear sense observation.</p>
Mineralisation / fault rock type	<p>Any type of filling, mineralisation or fault rock associated with the structure (e.g. CC for calcite of a vein filling, synCC for mineralisation of slickenfibres).</p>

Tab. 2-3: (continued)

Parameter	Definition of parameters and procedure for defining parameters
Open / closed and width / length of open structures	Information on whether a tension gash / vein is open (displaying a continuous aperture), partly open (displaying a discontinuous aperture) or closed at the observation scale (i.e. the naked eye), including the width of the aperture and the observed lengths of open streaks for partly open structures.
Roughness	Roughness classification of a structure using the joint roughness coefficient (JRC). The JRC gives a picture of the classification of fracture smoothness and waviness (planarity) along 10 cm length of the fracture (Barton 1976, Barton & Choubey 1977). The scale of the JRC is from 0 (very smooth and planar) to 20 (very rough and wavy).
Fracture condition	Specifies whether the core is broken naturally or artificially at the structure under consideration or intact. If it cannot be specified whether the break occurred naturally or artificially, it should be classified as broken.
Fracture density	Numerical value that reflects a quantitative measure of the abundance of fractures in a rock mass (e.g. fractures per metre, fracture area per rock volume).
Fracture density class (FDC)	In cases where cores or parts of a core are heavily disintegrated and order cannot be restored, the density of natural fractures cannot be assessed accurately. Fracture density should be estimated using the classification scheme of Bauer et al. (2016): fracture density class 2 (spacing of fractures = 5 cm to 10 cm), fracture density class 3 (spacing of fractures = 1 cm to 5 cm) or fracture density class 4 (spacing of fractures < 1 cm).
Additional remarks	Offsets or displacements as well as cross-cutting relations are documented under "remarks". Further remarks are e.g. karstification, the shape and length of the teeth of stylolites, alterations, recrystallisation phenomena or whether a structure could be of synsedimentary origin.

Detailed Structural Core Analysis

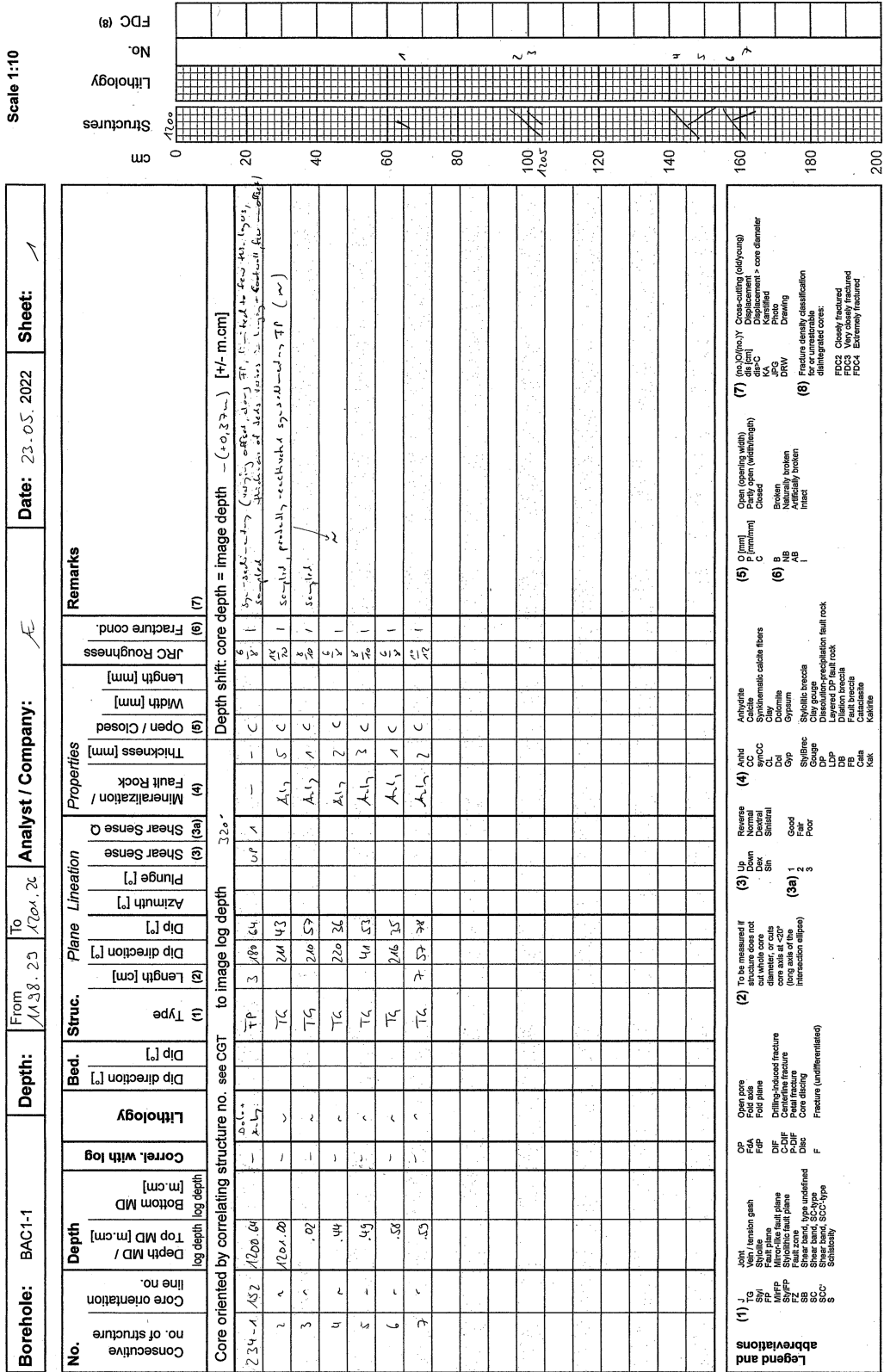


Fig. 2-10: Completed DIN A3 sheet of primary record of the detailed structural core analysis Example of core section 234 (1'198.29 m to 1'201.26 m MD core depth).

2.3 Geo-statistical evaluation

For the geo-statistical evaluation presented in Chapter 4, different structural tools and techniques were applied to analyse the available dip dataset. Most of the work was performed with TerraStation II, which provides several advanced modules for the import, processing, visualisation and analysis of all types of available borehole data such as petrophysical logs, borehole images, core data and stratigraphic information.

For the structural evaluation of the different lithostratigraphic units and the different types of structural discontinuities, a series of figures was compiled:

- Stereograms (Schmidt projection, lower hemisphere equal-area projections)
 - Poles of the planes were displayed to examine the spatial orientation of bedding and structural planes.
- Dip azimuth rose diagrams were compiled for planar features (bedding, fractures and stylolites). The diagrams show the dip azimuth of the planes under consideration. The rose diagram is a circular histogram summarising orientation measurements. The radius of each segment of a rose diagram is proportional to the number of observations that occur within the angular range of that segment. Dip azimuth rose diagrams are displayed with cumulative petals, resulting in staked petals for different dip categories. For the directional statistics in Chapter 4, a minimum threshold of ten structures was set for the rose diagrams.
- Dip histograms visualise the dip angle distribution and clustering for a given dip dataset.
- Vector means for representative clusters of the different structure types were calculated in stereograms.
- The dip vector azimuth plot (dip walkout plot) reflects the along-borehole dip azimuth variations and was compiled for bedding-related dips only (deformed dips and cross-bedding were excluded). Here, the azimuth of the bedding was plotted in a nose-to-tail fashion pointing in the direction of dip. The length of an interval is related to the number of dip picks and not to the thickness of lithostratigraphic units.
- Fracture density (P32 curves) reflects the fracture area per unit of rock volume (m^2/m^3). The algorithm computes the area of each fracture and creates a sum of the areas across the defined volume (window of 1 m core length and steps of 0.1524 m). The lengths of subvertical fractures are incorporated whereas truncated parts of fractures are discarded. The computation of the area accounts for borehole ellipticity. The total area of fractures is then divided by the borehole volume (or volume of the rock mass) of the selected window. See Ebert & Decker (2019) and the literature therein for a more detailed discussion on P32 fracture density calculation. For this study, P32 fracture densities were calculated for all structural discontinuities as well as for each individual group:
 - Fault planes, mirror-like fault planes and stylolitic fault planes
 - Unassigned fractures, joints and tension gashes / veins
 - Stylolites

The recorded kinematic indicators were analysed using the TectonicsFP software. The available fault and kinematic data were plotted in stereographic Angelier projection, with the symbols and colours reflecting the different shear senses (up, down, sinistral or dextral) and the observed shear sense reliability (good, moderate, poor). All Angelier plots in this report show corrected datasets in which the data points of the lineations are projected onto the great circle of the corresponding fault plane, even if they have an angular offset $< 15^\circ$.

3 Inventory of structure types

The different structure types identified in the drill cores from BAC1-1 and their relevant characteristics were described in Section 2.2. In this Chapter, these structures are visualised with examples. The diameter of the cores in the following figures (Figs. 3-1 to 3-24) is 95 mm.

3.1 Examples of fault planes



Fig. 3-1: Fault plane

Characteristics: Example of a fault plane with striation and mm-thick synkinematic calcite fibres. Shear sense is top up (reverse fault).

Formation: Wildegg Formation, depth: 665.79 m MD (core depth)



Fig. 3-2: Fault plane

Characteristics: Example of a strike-slip fault plane. The striation and synkinematic calcite fibres are subhorizontal.

Formation: Opalinus Clay, depth: 911.47 m MD (core depth)

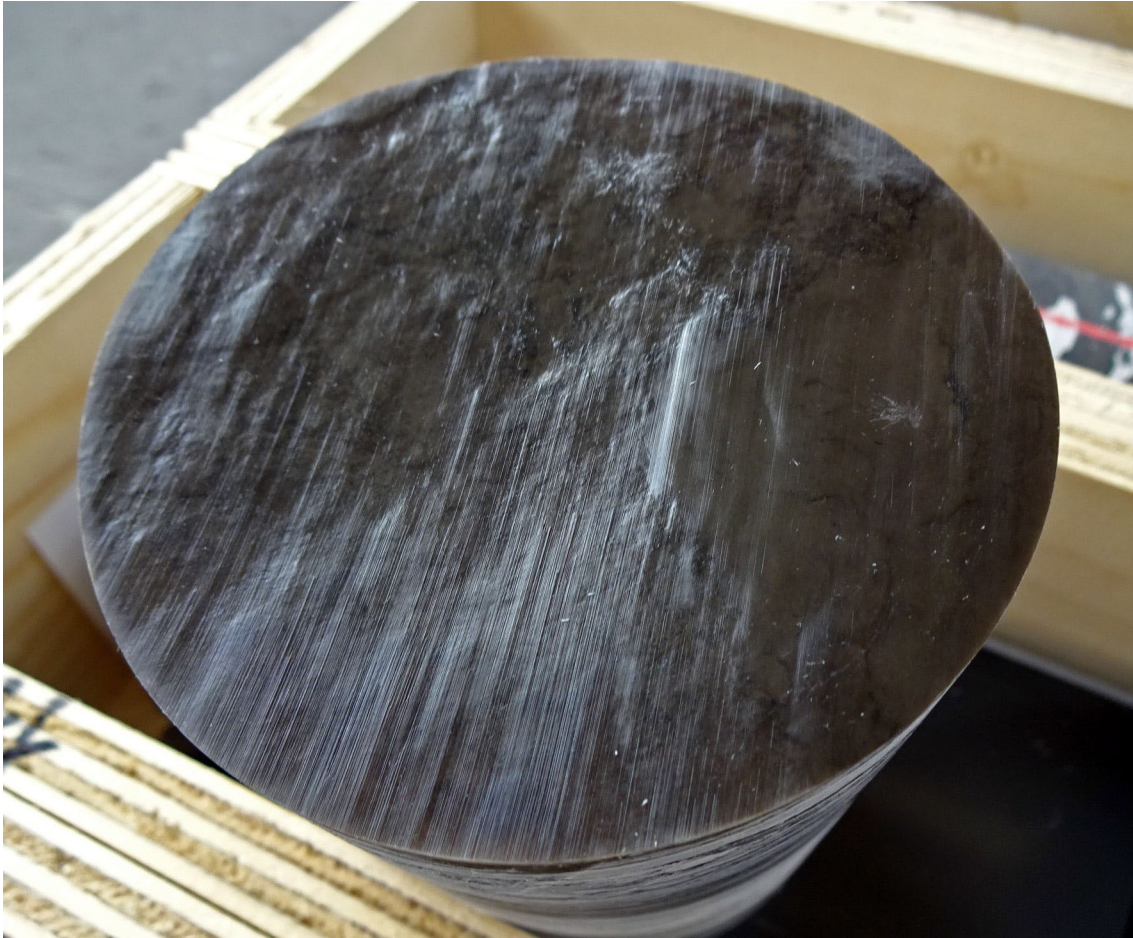


Fig. 3-3: Fault plane

Characteristics: Example of a subhorizontal fault plane with striation.

Formation: Zeglingen Formation, depth: 1'158.58 m MD (core depth)



Fig. 3-4: Mirror-like fault plane

Characteristics: Example of a fault plane with a smooth mirror-like slip surface and striation.

Formation : Villigen Formation, depth: 606.23 m MD (core depth)



Fig. 3-5: Mirror-like fault plane

Characteristics: A shallow-dipping, non-planar fault plane with a polished, mirror-like slip surface and striation.

Formation : Klettgau Formation, depth: 969.30 m MD (core depth)



Fig. 3-6: Stylolitic fault plane

Characteristics: Example of a stylolitic fault plane with striation generated by carbonate dissolution and displacement subparallel to the plane.

Formation: Wildegg Formation, depth: 666.28 m MD (core depth)

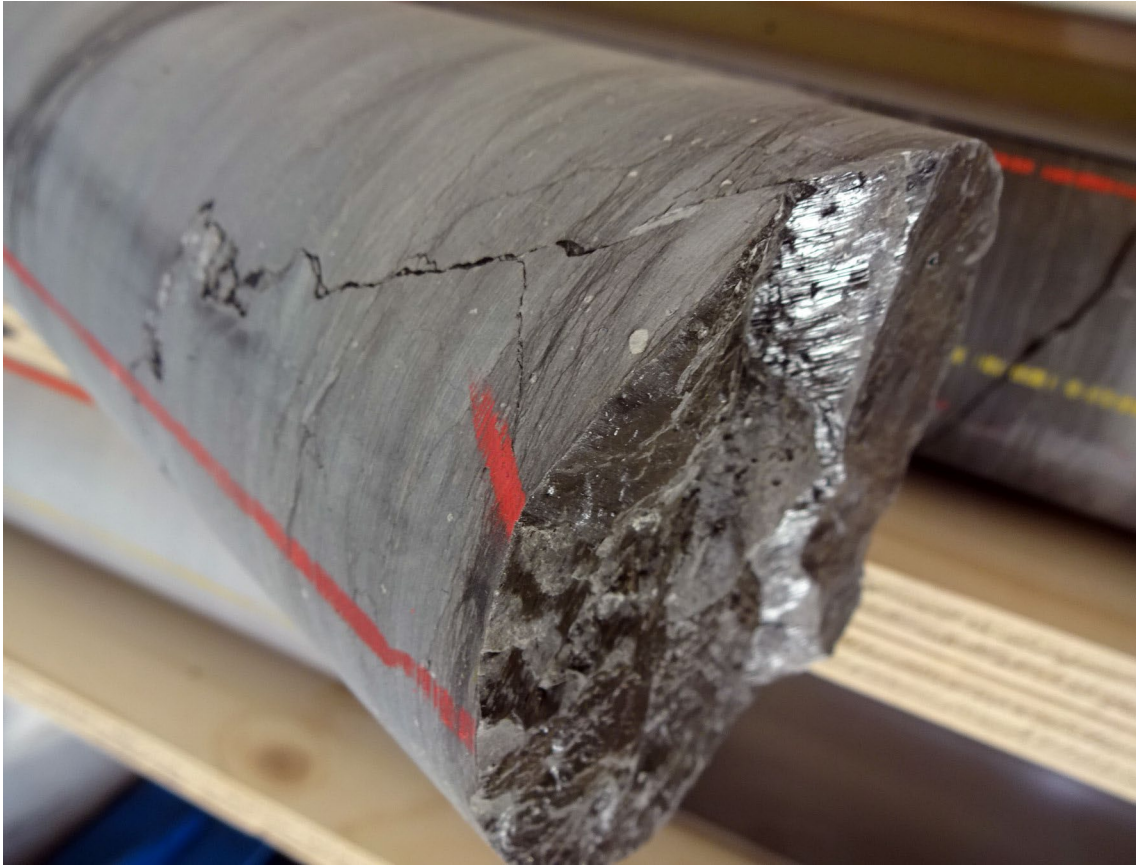


Fig. 3-7: Stylolitic fault plane

Characteristics: Example of a stylolitic fault plane with striation generated by carbonate dissolution and displacement subparallel to the fault plane.

Formation: Villigen Formation, depth: 613.95 m MD (core depth)

3.2 Example of fault zone

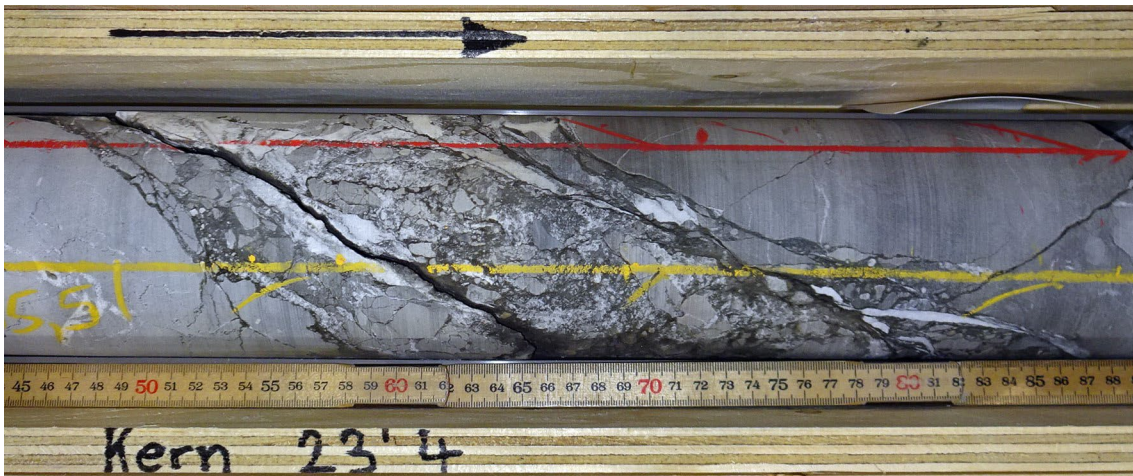


Fig. 3-8: Fault zone

Characteristics: Example of a fault zone with fault planes with synkinematic calcite mineralisation and fault breccia. The fault zone shows an orientation of 038/66.

Formation: Villigen Formation, depth: 585.56 m to 585.72 m MD (core depth)



Fig. 3-9: Fault zone

Characteristics: Example of a cm-thick fault zone with a dense network of mirror-like fault planes. The core disintegration level corresponds to fracture density class 4.

Formation: Klettgau Formation, depth: 976.88 m to 976.95 m MD (core depth)

3.3 Examples of joints



Fig. 3-10: Joint

Characteristics: Examples of three parallel and subvertical joints characterised by the absence of slip indications.

Formation: Schinznach Formation, depth: 1'125.35 m MD (core depth)

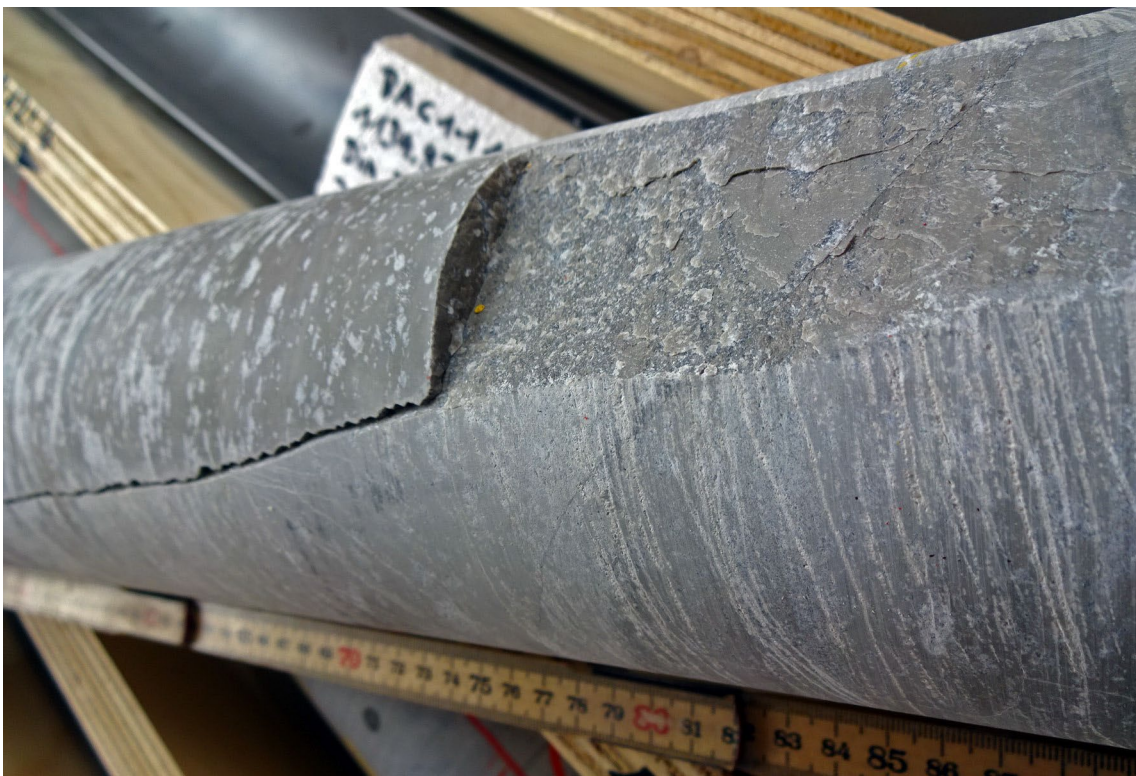


Fig. 3-11: Joint

Characteristics: A 60 cm-long, subvertical joint characterised by the absence of slip indications.

Formation: Zeglingen Formation, depth: 1'133.56 m MD (core depth)

3.4 Examples of veins / tension gashes

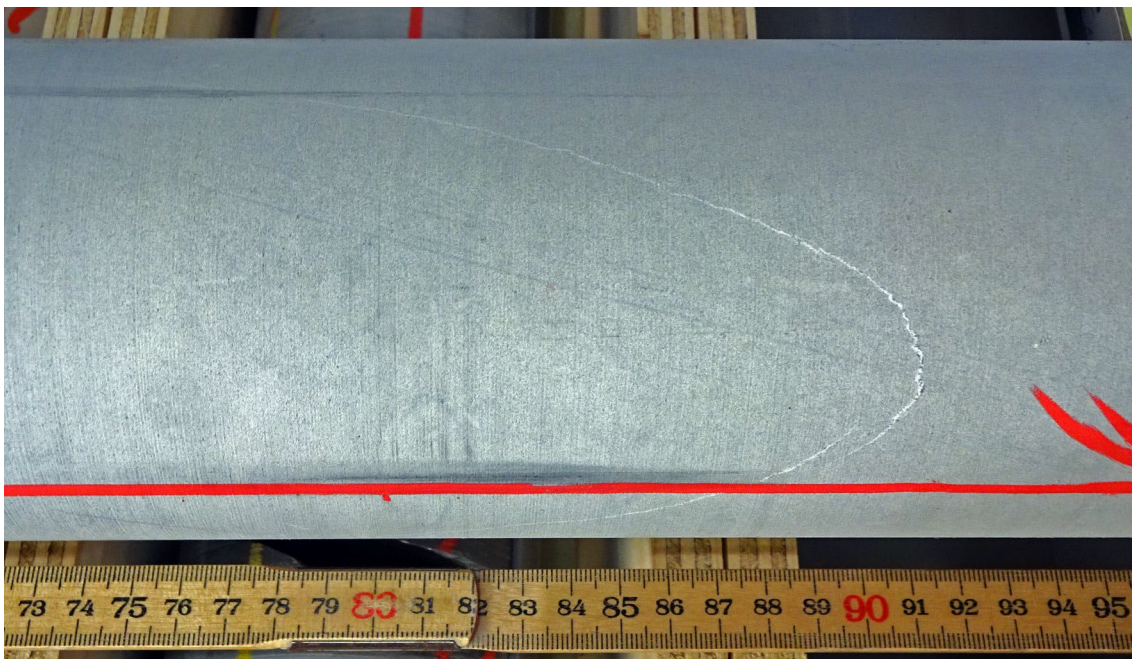


Fig. 3-12: Vein / tension gash
 Characteristics: Example of a thin, steeply-dipping calcite-filled tension gash.
 Formation: Villigen Formation, depth: 614.79 m MD (core depth)

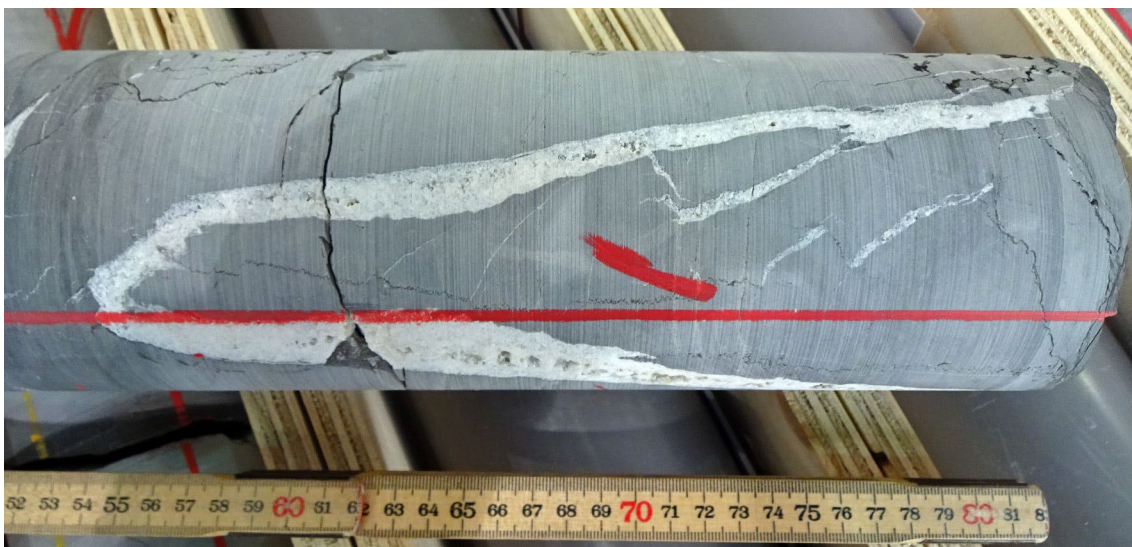


Fig. 3-13: Vein / tension gash
 Characteristics: Example of a cm-thick tension gash filled with calcite.
 Formation: Villigen Formation, depth: 620.68 m MD (core depth)

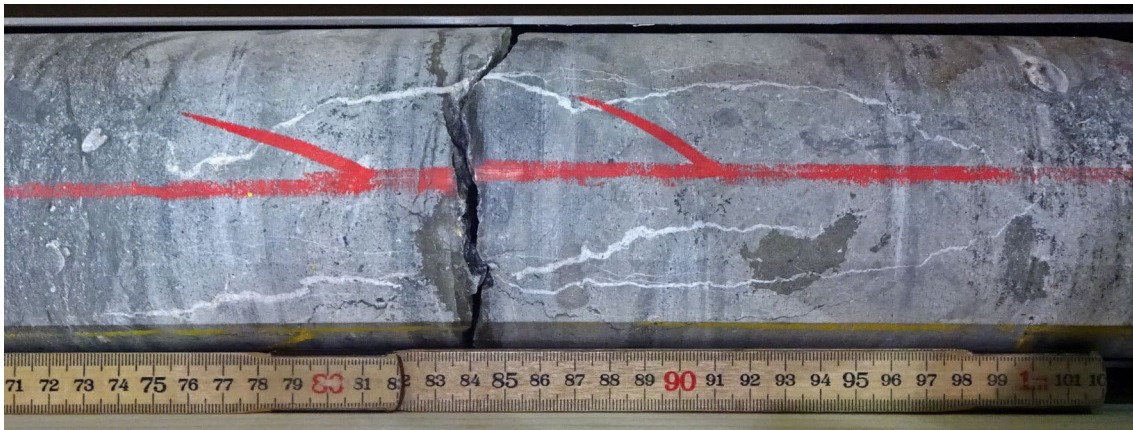


Fig. 3-14: Vein / tension gash

Characteristics: Example of a subvertical, several-mm-thick and undulating calcite-filled tension gash.

Formation: Staffelegg Formation, depth: 927.87 m MD (core depth)



Fig. 3-15: Vein / tension gash

Characteristics: Example of a subvertical, anhydrite-filled tension gash, typical for the Bänkerjoch Formation that often shows a gnarly structure.

Formation: Bänkerjoch Formation, depth: 1'001.83 m MD (core depth)

3.5 Examples of stylolites

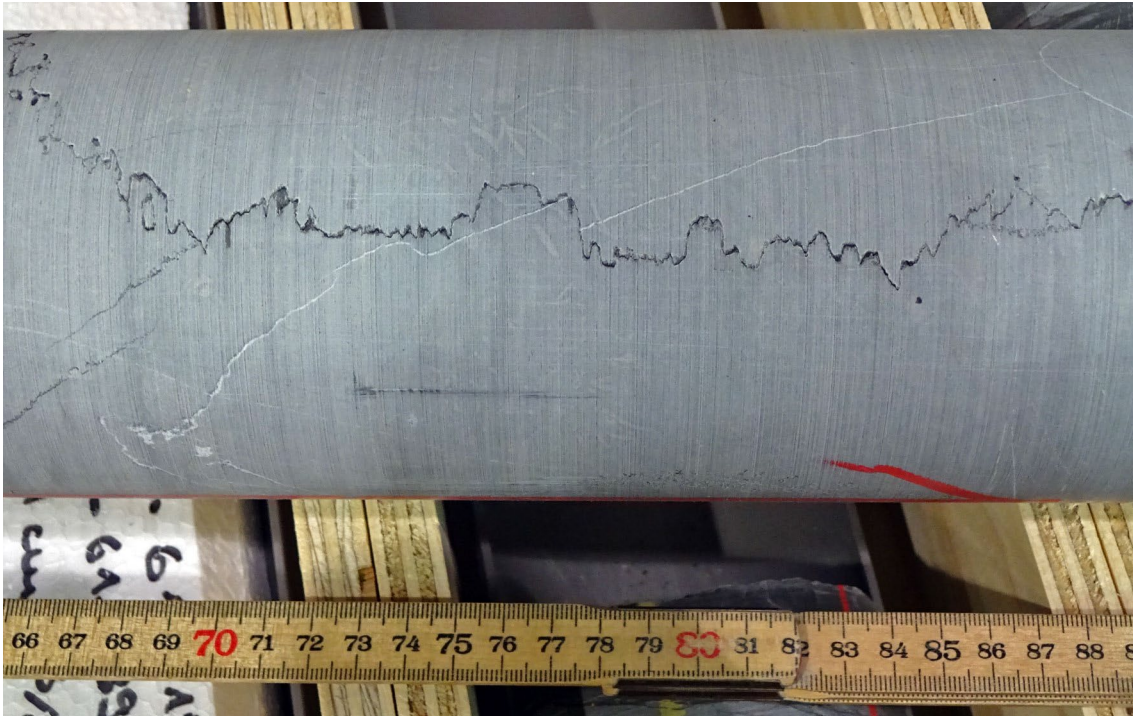


Fig. 3-16: Stylolite

Characteristics: Example of a subvertical stylolite with subhorizontal teeth. Note the older thin tension gash is displaced by the younger stylolite.

Formation: Villigen Formation, depth: 611.81 m MD (core depth)

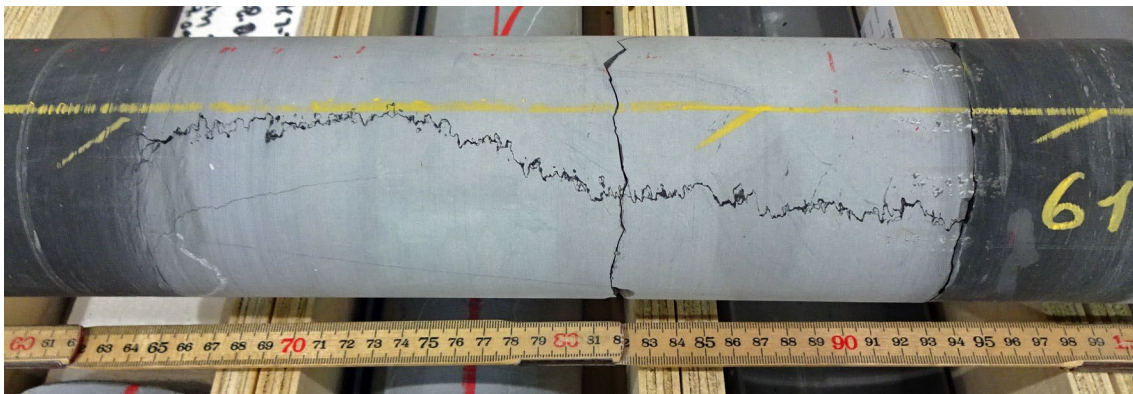


Fig. 3-17: Stylolite

Characteristics: Example of a subvertical and bedding-confined stylolite limited exclusively to the calcareous layer.

Formation: Villigen Formation, depth: 609.79 m MD (core depth)



Fig. 3-18: Stylolite

Characteristics: Example of two subhorizontal stylolites with cm-long, subvertical teeth.

Formation: Schinznach Formation, depth: 1'115.73 m MD (core depth)

3.6 Examples of open pores



Fig. 3-19: Open pore

Characteristics: Example of a large druse-like open pore with idiomorphic calcite crystals.

Formation: Schinznach Formation, depth: 1'089.30 m MD (core depth)



Fig. 3-20: Open pores

Characteristics: Example of open pores. Typical layer found in bioclastic-rich layers with a dense network of mm-sized open pores in the Schinznach Formation.

Formation: Schinznach Formation, depth: 1'089.59 m to 1'089.68 m MD (core depth)

3.7 Examples of drilling-induced fractures

3.7.1 General examples

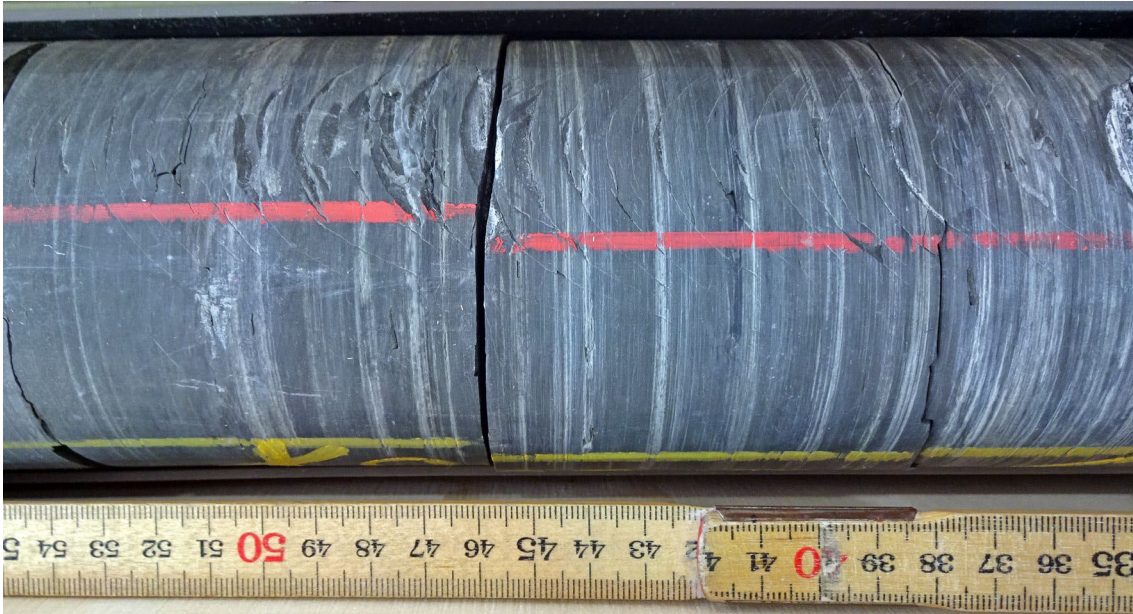


Fig. 3-21: Petal fractures

Characteristics: Example of a sequence of petal fractures with dip azimuth to the ENE. Similar ones were observed on the backside of the core with dip azimuth to the WSW.

Formation: Bänkerjoch Formation, depth: 982.46 m to 982.66 m MD (core depth)

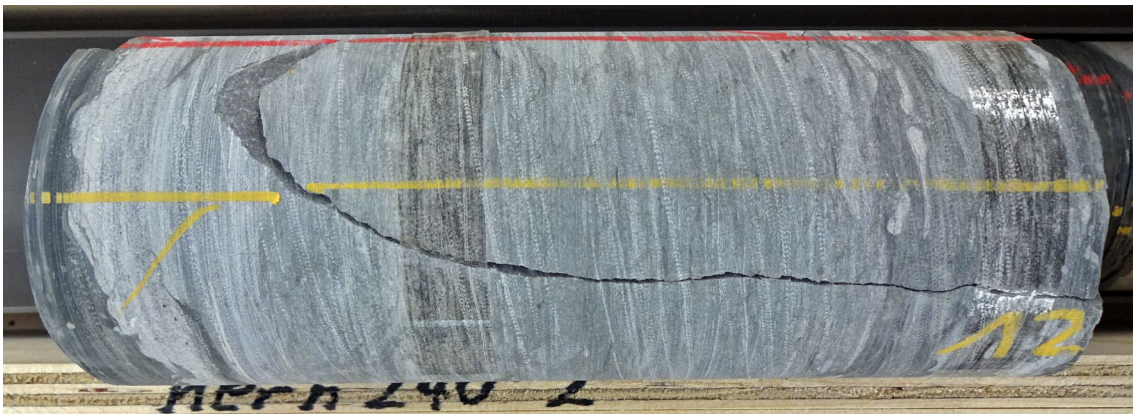


Fig. 3-22: Petal and centreline fractures

Characteristics: Example of a petal fracture descending into a subvertical centreline fracture with dip azimuth to the WSW.

Formation: Kaiseraugst Formation, depth: 1'217.32 m to 1'217.51 m MD (core depth)



Fig. 3-23: Discing

Characteristics: Example of discing in clay-rich sediments, splitting the core into discs with typical parallel fractures. Discs are oriented perpendicular to the core axis and (sub-) parallel to the bedding.

Formation: Opalinus Clay, depth: 897.48 m MD (core depth)



Fig. 3-24: Discing

Characteristics: Example of discing in a claystone, splitting the core into several discs with typical parallel fractures. Discs are oriented perpendicular to the core axis and (sub-) parallel to the bedding. Here, fracturing nucleated from the shell as indicated by the plumose structure.

Formation: Opalinus Clay, depth: 901.37 m MD (core depth)

3.7.2 Subvertical fracture at approx. 808 to 811 m MD (core depth)

In the drill cores (Fig. 3-25) a subvertical fracture starts abruptly at the top of core section number 99 at 808.09 m MD (core depth) within a sandy-limestone of the basal «Murchisonae-Oolith Formation», approx. 0.25 m above the top of the Opalinus Clay at 808.34 m MD (core depth). Until 810.72 m MD (core depth) this fracture gradually runs out of the core section 99, resulting in a total length of 2.63 m. The fracture is restricted to core section 99 only and is not seen in core section 98 (Fig. 3-25).

Drill core investigations (Fig. 3-25) revealed a gentle plumose structure (“hackles”) and some (a few millimetres high) steps on the generally smooth (not polished) and even surface of this fracture, without any indications neither for mineralisation nor tectonic shear/slip.

The UBI and FMI borehole images (Fig. 3-26) show a subvertical fracture extending from approx. 795 m to 813 m MD (log depth) along the borehole wall with an electrically conductive (dark) image response. It strikes NNW-SSE, parallel to drilling-induced (tensile) fractures detected within other sections of the BAC1-1 borehole (see Appendix C). The fact that such a subvertical fracture was not detected in the drill cores above 808.09 m implies the development of the fracture after drilling of section 98.

This drilling-induced fracture likely relates to drilling fluid losses that started on 14th Oktober 2021 after coring section 98. The total losses account to approx. 15 m³ (cf. Dossier I). The drilling fluid losses declined over time until they finally reached levels below detection limit when a depth of approx. 811 m MD was reached.

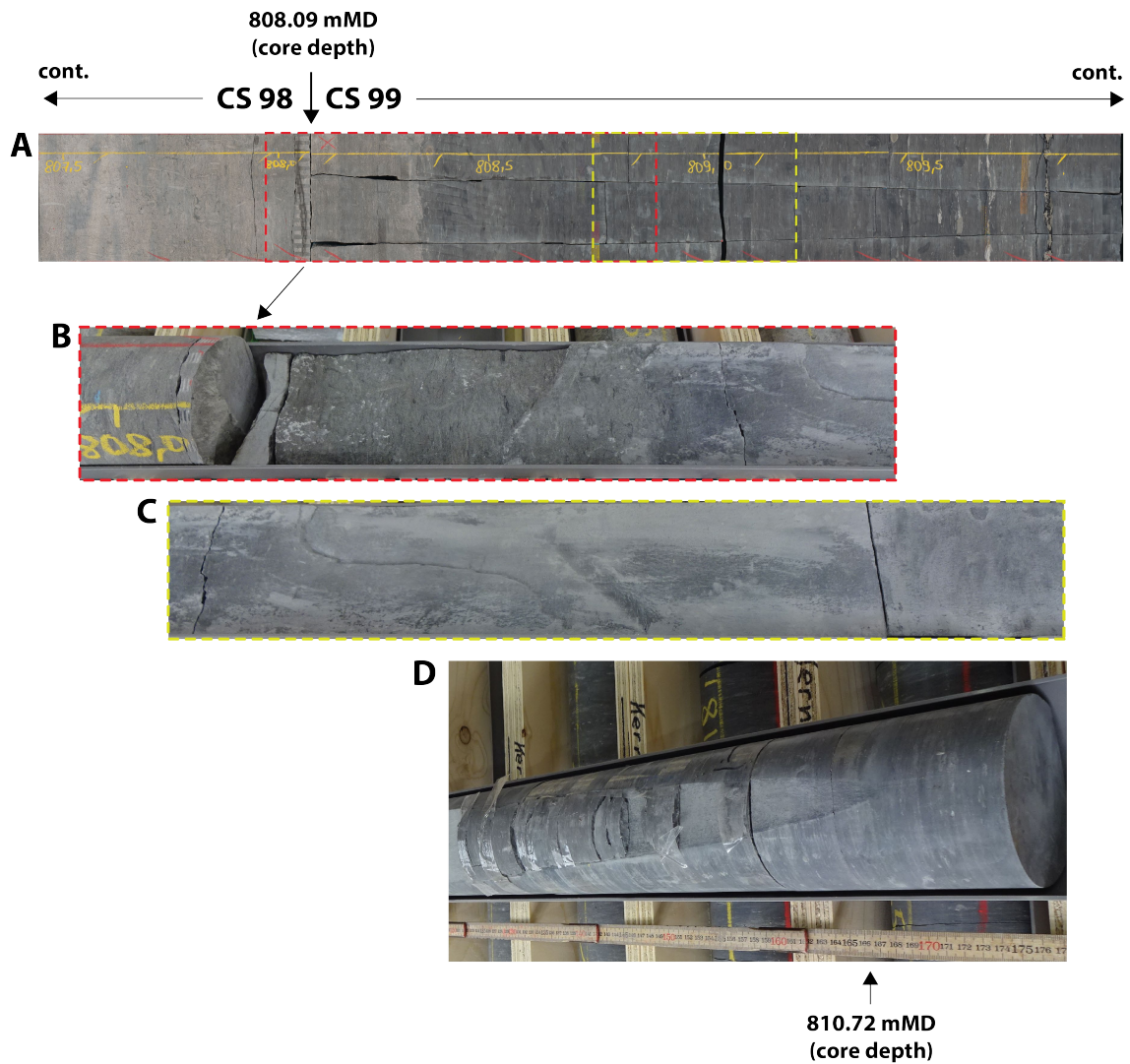


Fig. 3-25: Morphology of the subvertical fracture in drill core section (CS) number 99
 This 2.63 m long fracture occurs exclusively in core section 99 and as seen on the (a) 360° core scan, it starts abruptly at 808.09 m MD. The planar drill core photos (b and c) show the fracture surface without any indications for tectonic slip/shear nor mineralisation. This fracture runs gradually out of the drill core (d) at 810.72 m MD (core depth).

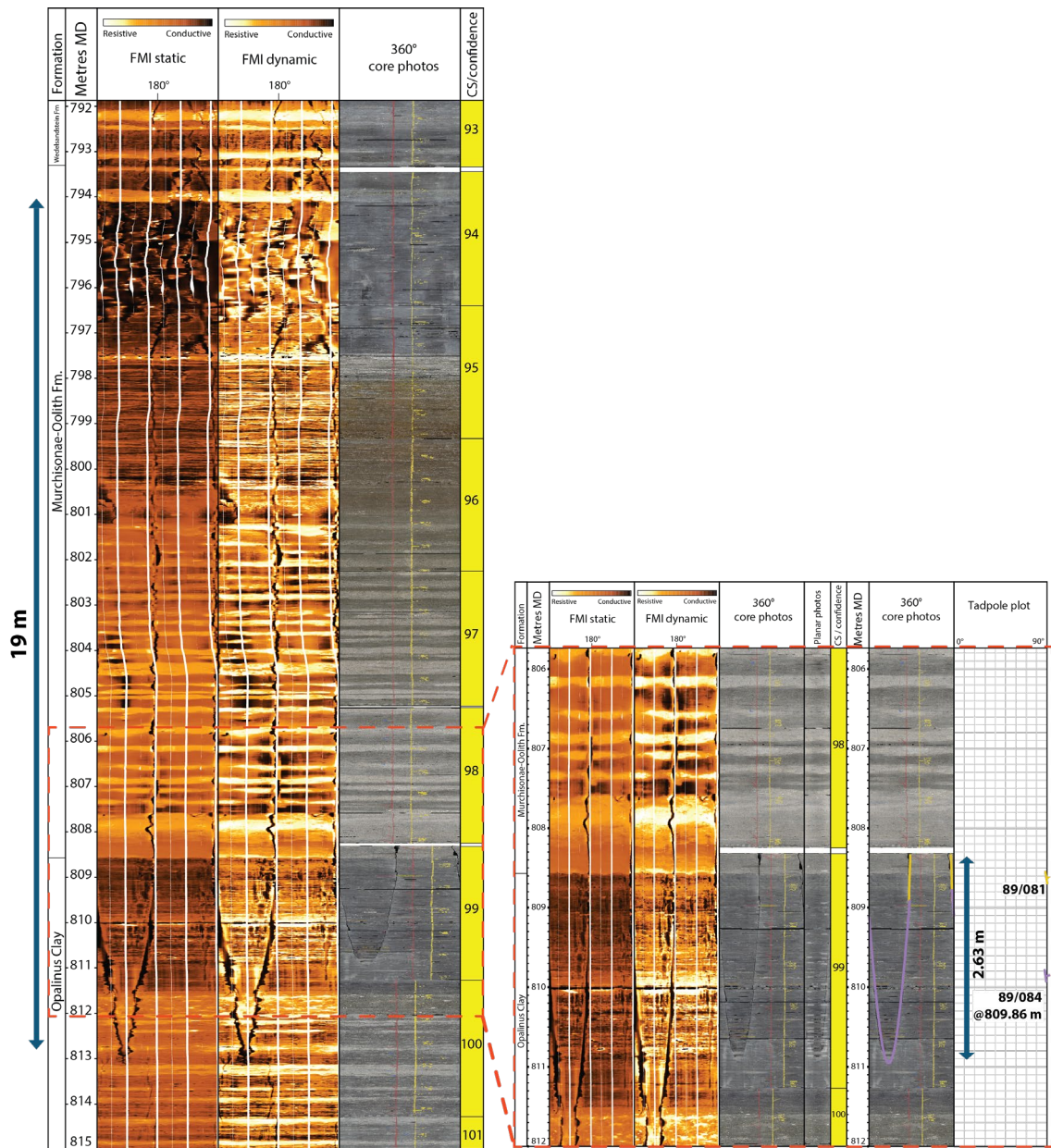


Fig. 3-26: Appearance of the vertical fracture in FMI borehole image and in the drill cores

4 Geo-statistical evaluation: results

Vector means of orientation values (dip azimuth and dip angle) of bedding planes and planar structural discontinuities were calculated for different data clusters in a stereogram projection (see Tab. 4-1). Bedding dips and structural discontinuities recorded in non-oriented cores ($n = 101$) were excluded from the following stereographic evaluation unless otherwise specified. However, they were included in the fracture density calculations (P32 curves) presented in Section 4.1.3 and in Tab. 4-1.

Tab. 4-1: Vector means of orientation for bedding planes and structural discontinuities
Azim: azimuth

	Cluster 1 (main)			Cluster 2 (subordinate)			Cluster 3 (subordinate)		
	Azim	Dip	No.	Azim	Dip	No.	Azim	Dip	No.
Bedding	125	03	524						
Fault planes	163	06	424						
Tension gashes, joints, unassigned fractures	276	78	304						
Stylolites	147	02	295	176	77	124	355	78	90

4.1 Entire cored borehole section (517.58 m to 1'306.77 m MD log depth)

A total of 3'294 individual planar and non-planar structural discontinuities were identified during the core analysis and manual dip picking of the 789.19 m of core material (including open pores, fold axes and all bedding planes). They are visualised on different scales in the structural composite plots of Appendix A and are briefly evaluated below.

4.1.1 Basic structural dip evaluation

Bedding dips, particularly of plane-parallel nature in lithologies such as claystone, marl and siltstone are considered as the best structural dip indicators. The dip variations along the current borehole are well reflected in the stereograms of Fig. 4-1, Fig. 4-2 and in the vector azimuth plot in Fig. 4-3, as well as in the structural composite plots in Appendix A.

The studied borehole section (517.58 m to 1'306.77 m MD log depth) ranging from the Late Jurassic Malm to the Permian Weitenau Formation reveals an overall subhorizontal to shallow (1° to 10°) structural dip towards the SE. The mean structural dip is 125/03 (dip azimuth/dip angle; $n = 524$, see cluster 1 in Tab. 4-1). However, local dip disturbances were observed within the Opalinus Clay from approximately 884 m to 887 m MD (log depth) and are most likely governed by soft-sediment deformation. This borehole section reveals inclined to steep (up to 43°) dip angles and E-ly dip azimuths. Further dip variations were encountered within the evaporitic Zeglingen-Fm. between approximately 1143 m to 1201 m MD. The latter are related to a tectonic deformation and faulting (see Appendix C and Fig. 4-3). Slightly steeper dip angles ($\sim 7^\circ$ to 20°) observed below approximately 1250 m MD are governed by the sand-prone character of the Dinkelberg and the Weitenau Formations (Fig. 4-3).

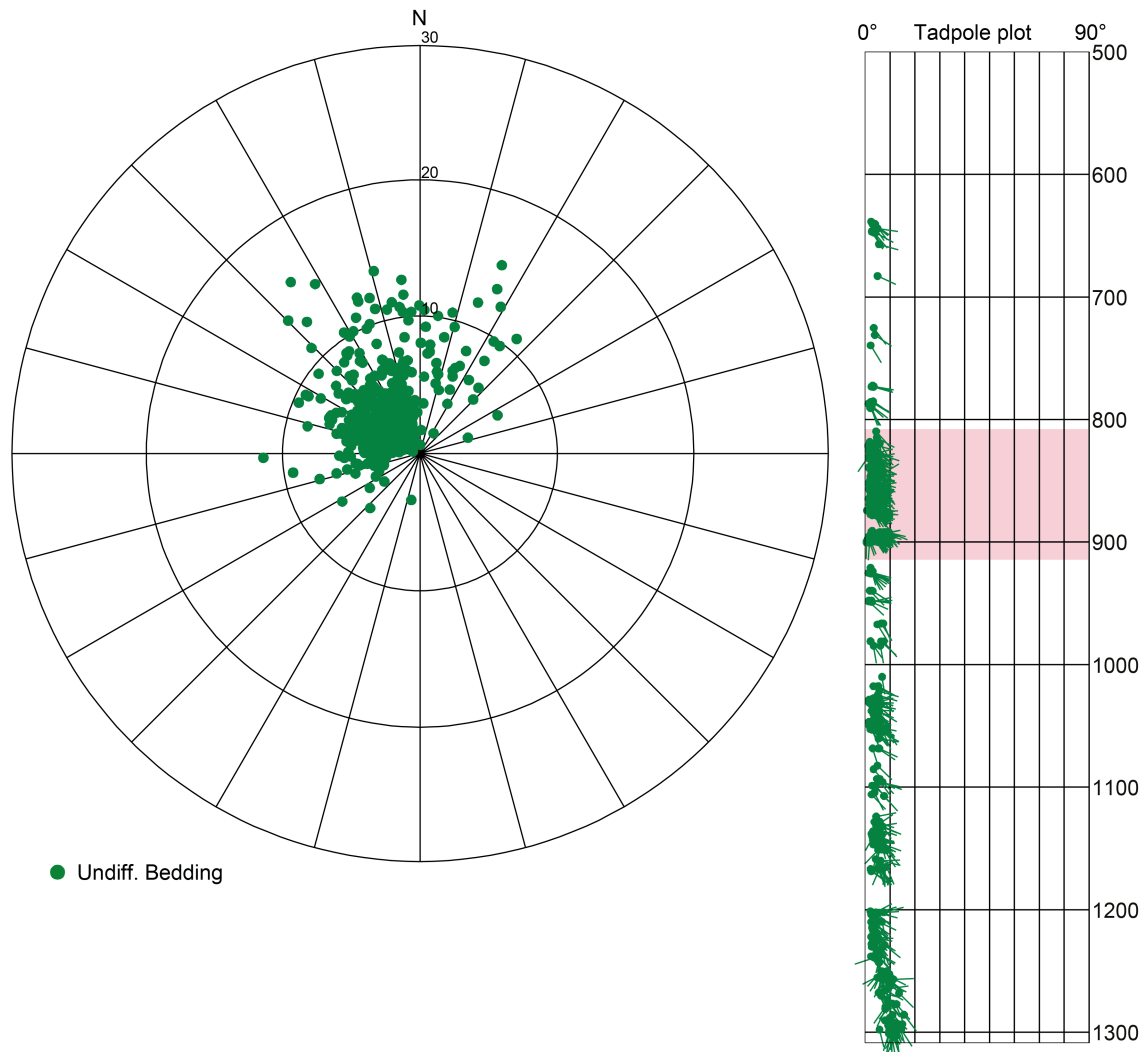


Fig. 4-1: Stereogram and depth plot for bedding planes (n = 629) in oriented cores
 Note the predominance of 0° to 10° SE dips with an overall mean of 125/03 (selected cluster of n = 524). The depth range is 517.58 m to 1'306.77 m MD (log depth). The Opalinus Clay interval is indicated by a light-red bar in the tadpole plot. The perimeter of the stereogram corresponds to a 30° dip.

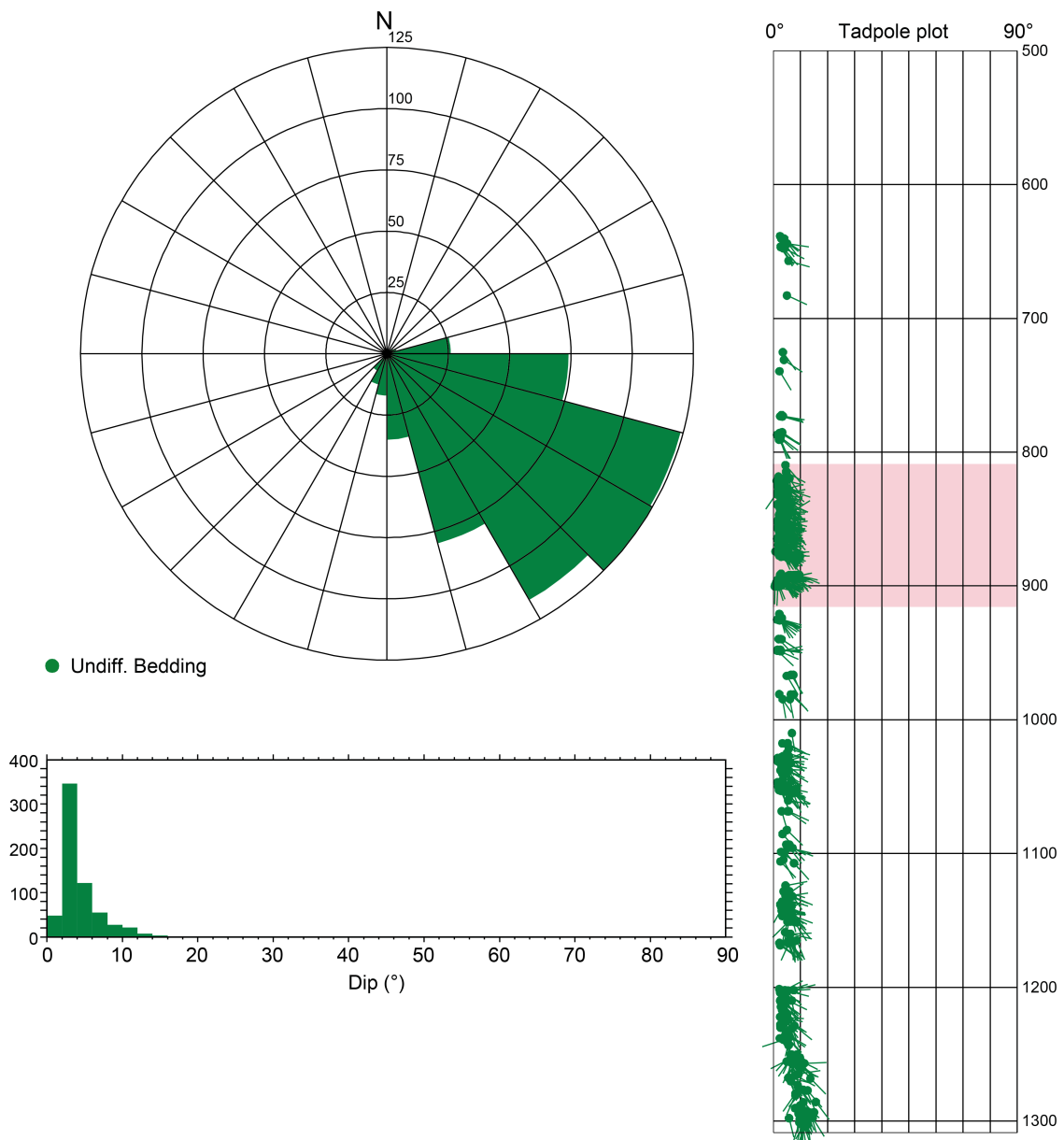


Fig. 4-2: Dip azimuth rose diagram, dip histogram and depth plot for bedding planes (n = 629) in oriented cores

Note the predominance of SE-ly dip azimuth. The depth range is 517.58 m to 1'306.77 m MD (log depth). The Opalinus Clay interval is indicated by a light-red bar in the tadpole plot.

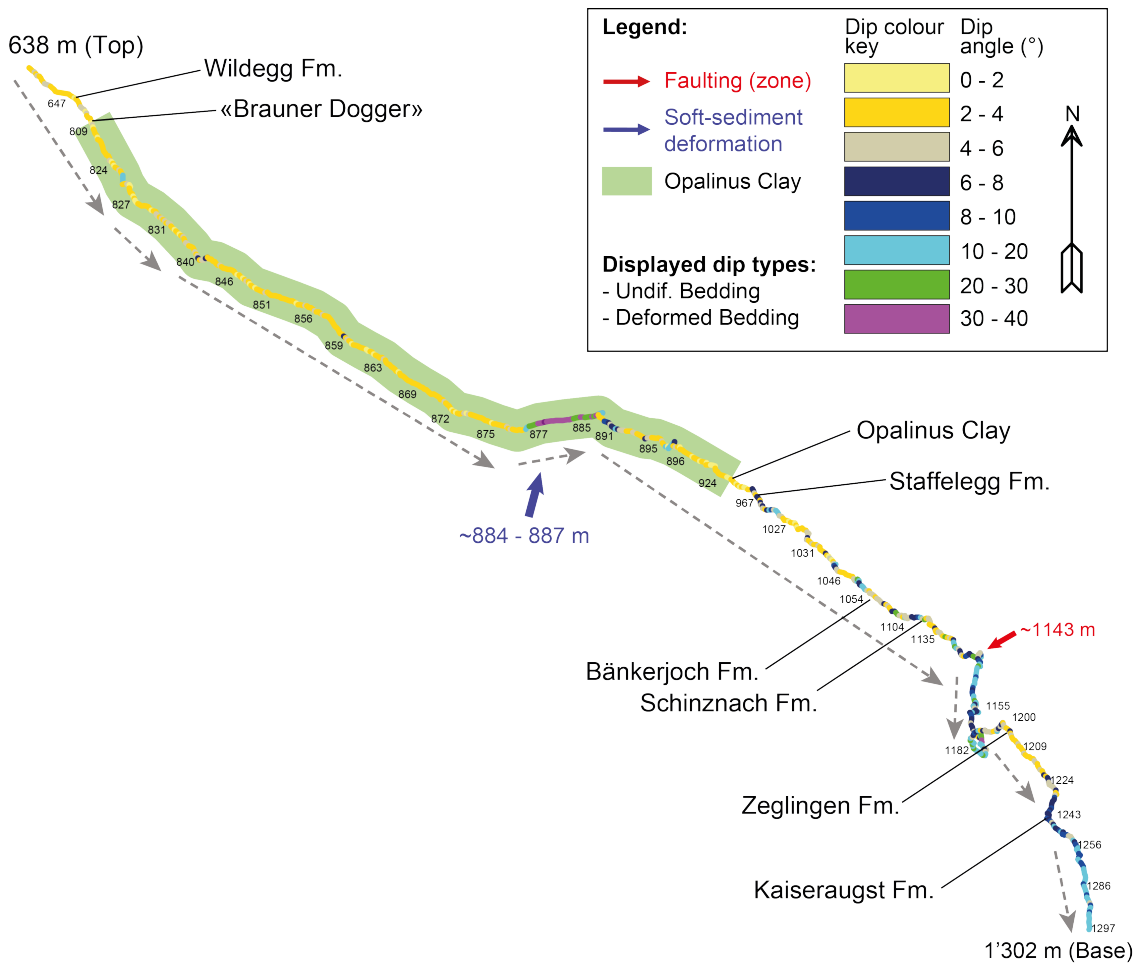


Fig. 4-3: Vector azimuth (or walkout) plot with bedding dips (n = 782) in oriented cores picked on oriented 360° core photographs

The colour-coding reflects the dip angle. The horizontal distance has no meaning and only visualises the bedding pick frequency. Grey, dashed arrows point in the direction of the overall dip azimuth. Lithostratigraphic formation boundaries (bottoms) are indicated as well as zones with possible soft-sediment (blue arrow) and tectonic (red arrow) deformation. The Opalinus Clay interval is shaded green. Bedding planes from non-oriented cores are excluded from this figure. Depths are given in metres MD (log depth).

4.1.2 Natural structural discontinuities

Fault planes

In total, 763 individual fault planes were recorded in the BAC1-1 borehole. The count includes shear bands in the halite of the Zeglingen Formation. Faults are planes of shear failure, i.e. planes with plane-parallel movement (Ebert & Decker 2019). Depending on their appearance in the drill core, they were assigned to one of three types of fault planes: (1) fault planes (n = 427, including [n = 11] shear bands), (2) mirror-like fault planes (n = 219) and (3) stylolitic fault planes (n = 117). Out of all recorded fault planes, 716 (94%) were detected in oriented cores and are included in this evaluation.

Several structurally complex intervals along the BAC1-1 borehole were interpreted as fault zones. They are commonly associated with intense fracturing and high fracture densities. The latter correspond to the different fracture density classes (FDC) defined by Ebert & Decker (2019). A total of 8 individual fault zones were defined for the entire cored interval along with their FDC in some zones (see Tab. 4-2). Additionally, 8 zones with closely spaced fault planes, mirror-like fault planes or shear bands were distinguished. Not all structural discontinuities within these zones could be recorded individually.

Fault planes are unevenly distributed along the borehole as shown in Fig. 4-4 and are discussed more in detail in Section 4.1.4. At certain depths, fault planes are absent, whereas at other depths, they occur as swarms with a large number of individual fault planes causing heavily fractured and disintegrated rock. Such fault zones and core intervals are described using the FDC classes.

The orientations of all recorded fault planes are displayed in the stereograms of Figs. 4-5 and 4-6. Faults show a scattered orientation with variable dip azimuths and dip angles ranging from horizontal to subvertical (1° to 89°). However, there is a predominance of bedding-subparallel SSE-dipping faults with an overall mean of 163/06 (n = 424; mean of selected cluster). Associated kinematic data could be defined on 520 fault planes out of 763 and are further evaluated in Section 4.1.4.

Explanation for Fig. 4-4:

In addition, a lithostratigraphic subdivision, core sections and goniometry confidence as well as fault zones associated with intense fracturing (described by FDC; see Tab. 2-2 below) are shown. For colour legend see Fig. 2-2. Stereograms with the respective number of planes are displayed for 100 m intervals, except for the topmost diagrams which cover 82.42 m thick intervals. An overview plot with the orientation of recorded structures within each lithostratigraphic formation is provided in Appendix B.

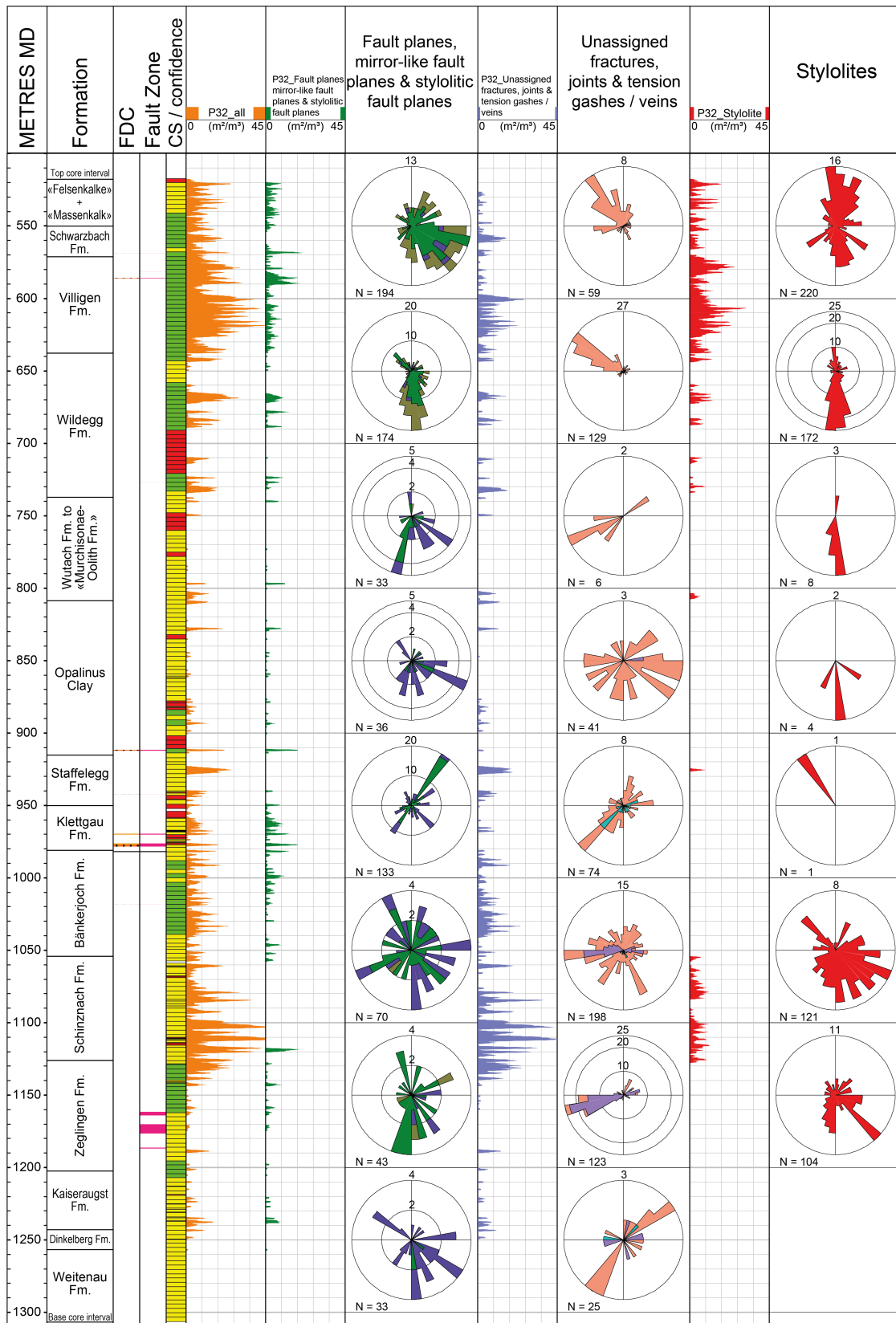


Fig. 4-4: Overview plot showing P32 densities for fractures and stylolites along the BAC1-1 borehole
 For explanations see opposite side.

Tab. 4-2: List of interpreted fault zones, salt SB (shear band) zones and the associated FDC

Fault zones				FDC
Top [m MD log depth]	Bottom [m MD log depth]	Thickness [m]	Type	Type
568.71	568.87	0.16	Fault zone	
581.66	581.7	0.04	Fault zone	
585.86	586.02	0.16	Fault zone	
726.83	726.89	0.06	Fault zone	
911.63	912.16	0.53	Fault zone	FDC 3
942.35	942.38	0.03	Fault zone	FDC 4
969.51	970.04	0.53	Fault zone	FDC 2
976.27	977.75	1.48	Fault zone	FDC 2
977.22	978.31	1.09	Fault zone	FDC 3
977.69	977.75	0.06	Fault zone	FDC 3
981.73	981.95	0.22	Fault zone	
1'018.18	1'018.26	0.08	Fault zone	
1'161.61	1'164.15	2.54	Salt SB zone	
1'170.26	1'176.65	6.39	Salt SB zone	
1'186.24	1'186.9	0.66	Salt SB zone	

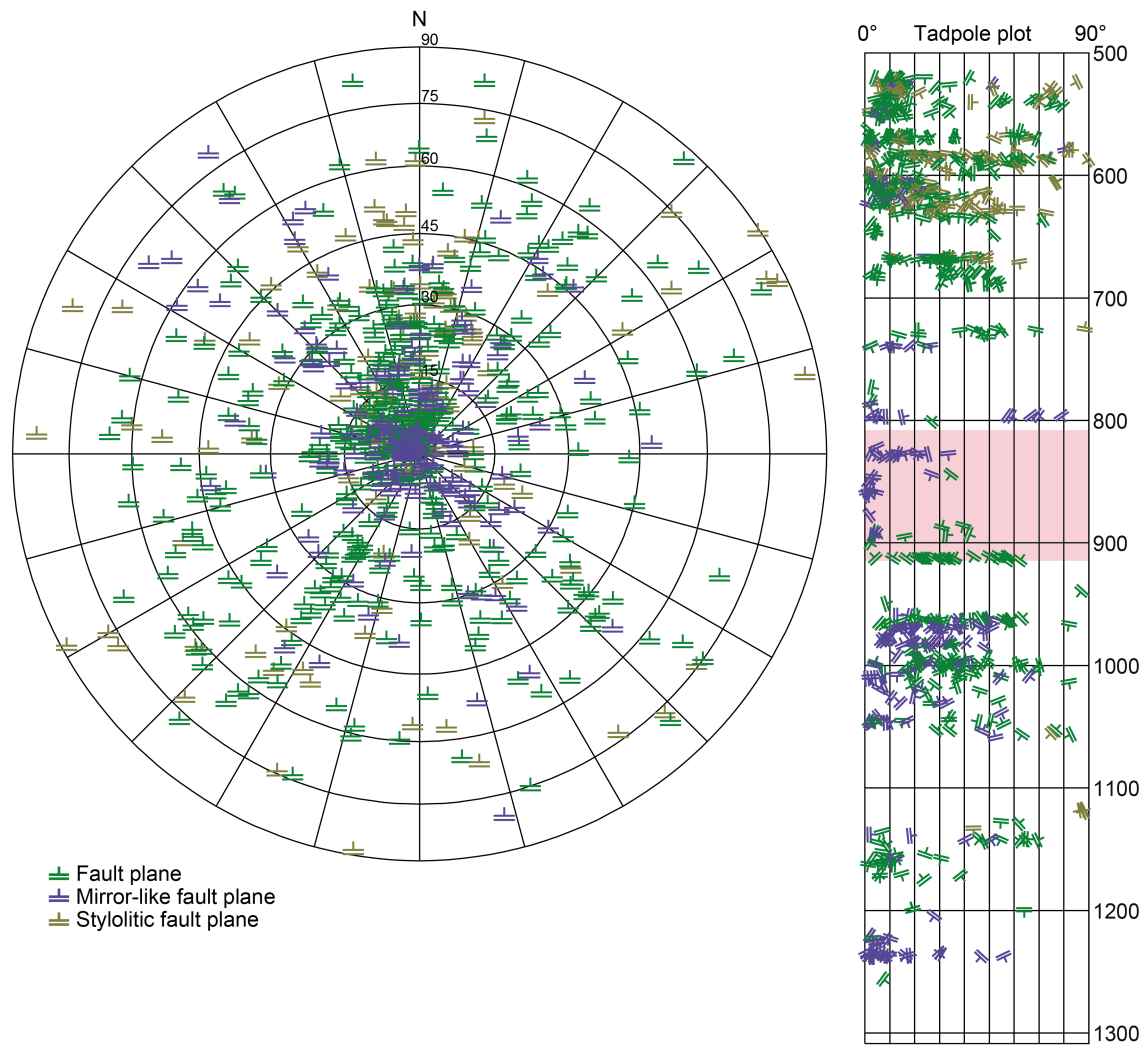


Fig. 4-5: Stereogram and depth plot of fault planes for the entire cored interval
 A total of 716 fault planes in oriented cores are plotted: fault planes (n = 413, n = 11 shear bands included), mirror-like fault planes (n = 188) and stylolitic fault planes (n = 115). The depth range is 517.58 m to 1'306.77 m MD (log depth). In the tadpole plot, the Opalinus Clay interval is indicated by a light-red bar.

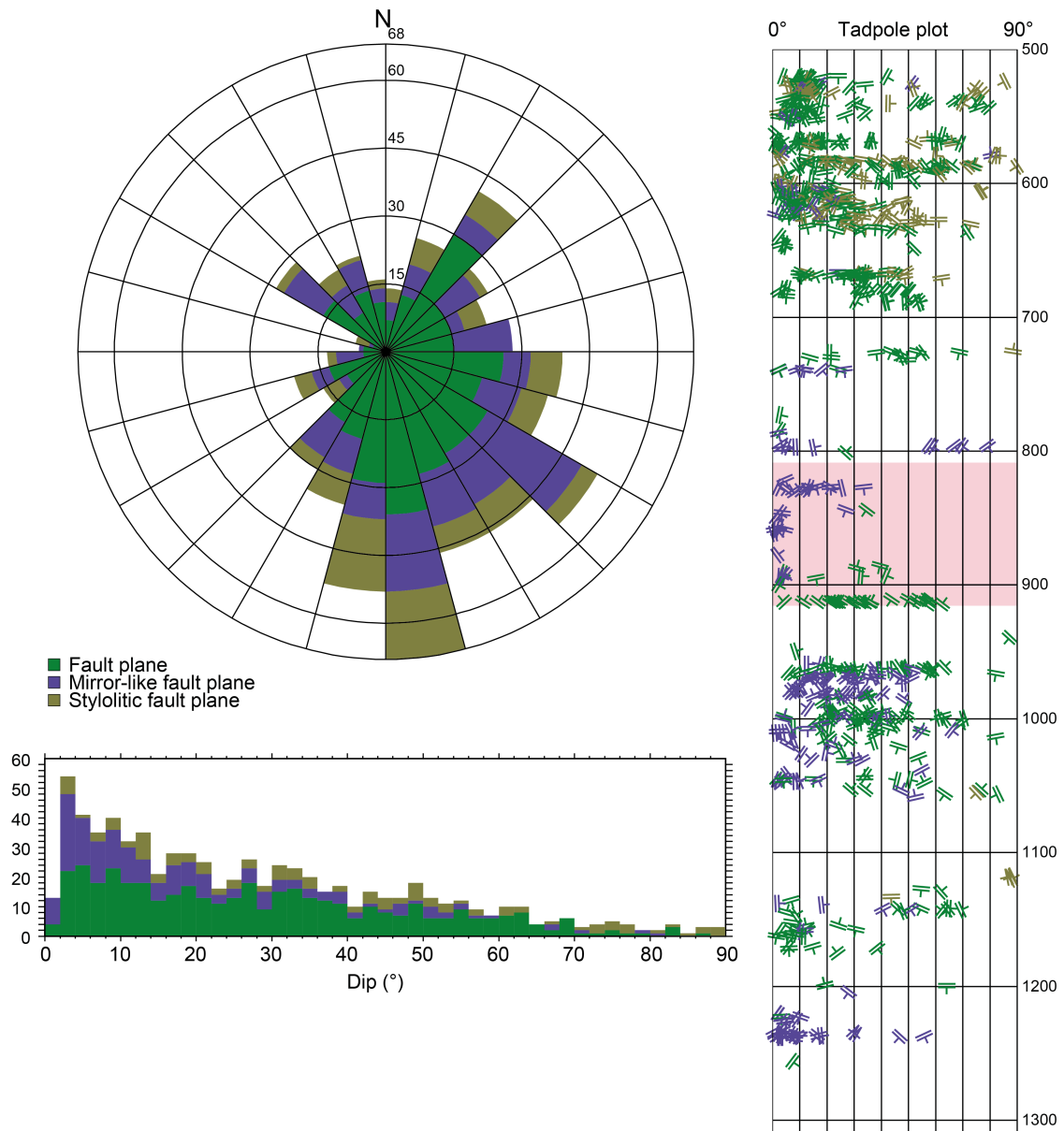


Fig. 4-6: Dip azimuth rose diagram, dip histogram and depth plot for fault planes in the entire cored interval

A total of 716 fault planes in oriented cores are plotted: fault planes (n = 413, n = 11 shear bands included), mirror-like fault planes (n = 188) and stylolitic fault planes (n = 115). The depth range is 517.58 m to 1'306.77 m MD (log depth). In the tadpole plot, the Opalinus Clay interval is indicated by a light-red bar.

Tension gashes / veins, joints and unassigned fractures

This group of structures represents extensional fractures without shear indicators and comprises tension gashes / veins ($n = 488$) and joints ($n = 150$). Fractures that could not be assigned to a specific class of structures are also included. In total, 19 tension gashes-rich zones as well as 1 zone for joints and 1 zone for unassigned fractures were identified. With a total of 673 individual fractures, they represent a smaller group of structural discontinuities than the fault planes. Out of these 673 fractures, 655 (97.3%) planes were recorded in oriented cores.

The spatial distribution of tension gashes / veins, joints and unassigned fractures along the BAC1-1 borehole is presented in Fig. 4-4 and discussed in Section 4.1.4. Compared to fault planes, they reveal a considerable orientation scatter as shown in Fig. 4-7 and Fig. 4-8. However, one orientation cluster can be distinguished (see Tab. 4-1). It represents a steeply to subvertical (75° to 90°) W-ly dipping cluster (overall mean: $276/78$; $n = 304$).

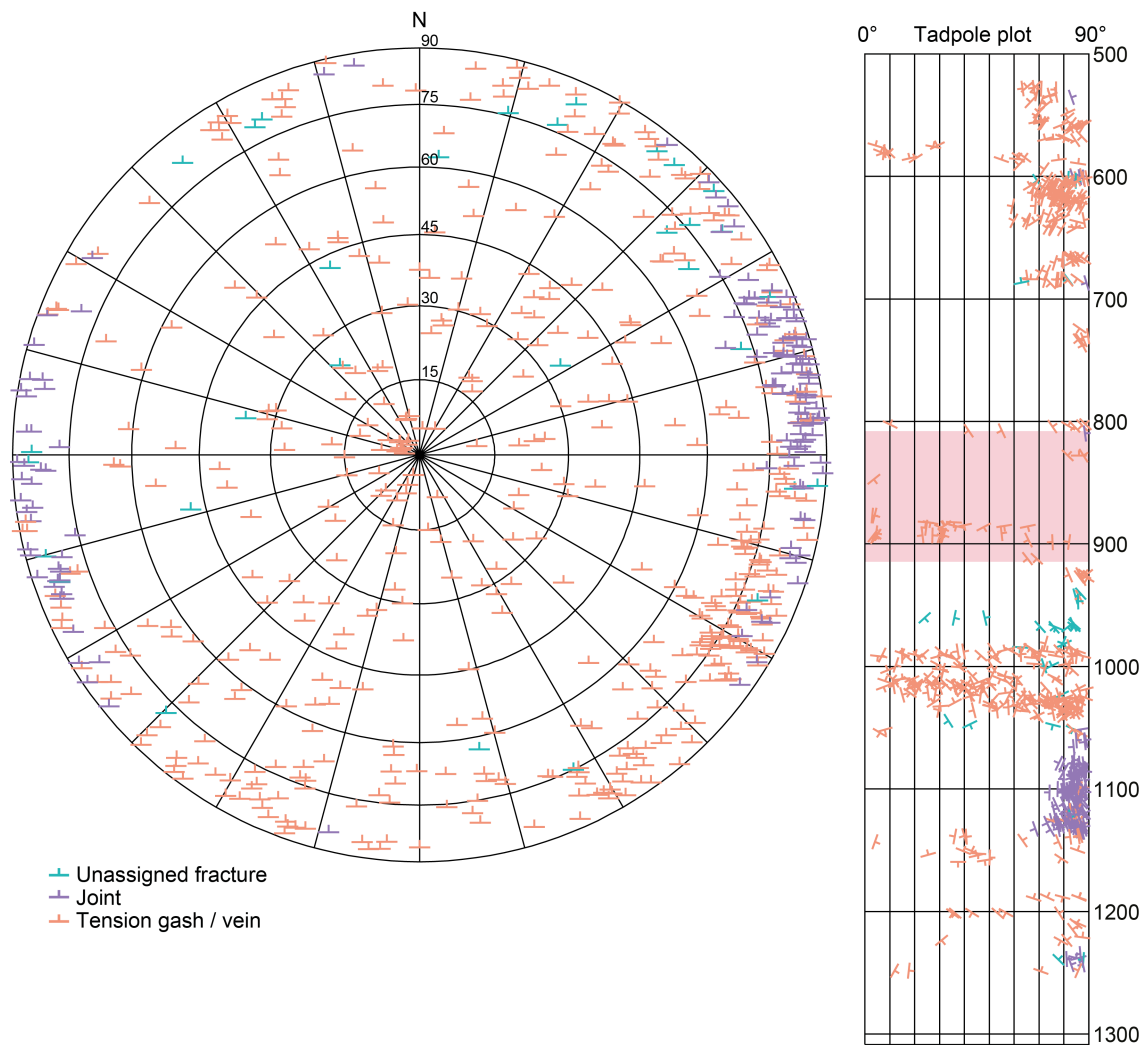


Fig. 4-7: Stereogram and depth plot for tension gashes / veins, unassigned fractures and joints in the entire cored interval

A total of 655 fractures recorded in oriented cores are displayed: tension gashes / veins (n = 478), joints (n = 146) and unassigned fractures (n = 31). The depth range is 517.58 m to 1'306.77 m MD (log depth). In the tadpole plot, the Opalinus Clay interval is indicated by a light-red bar.

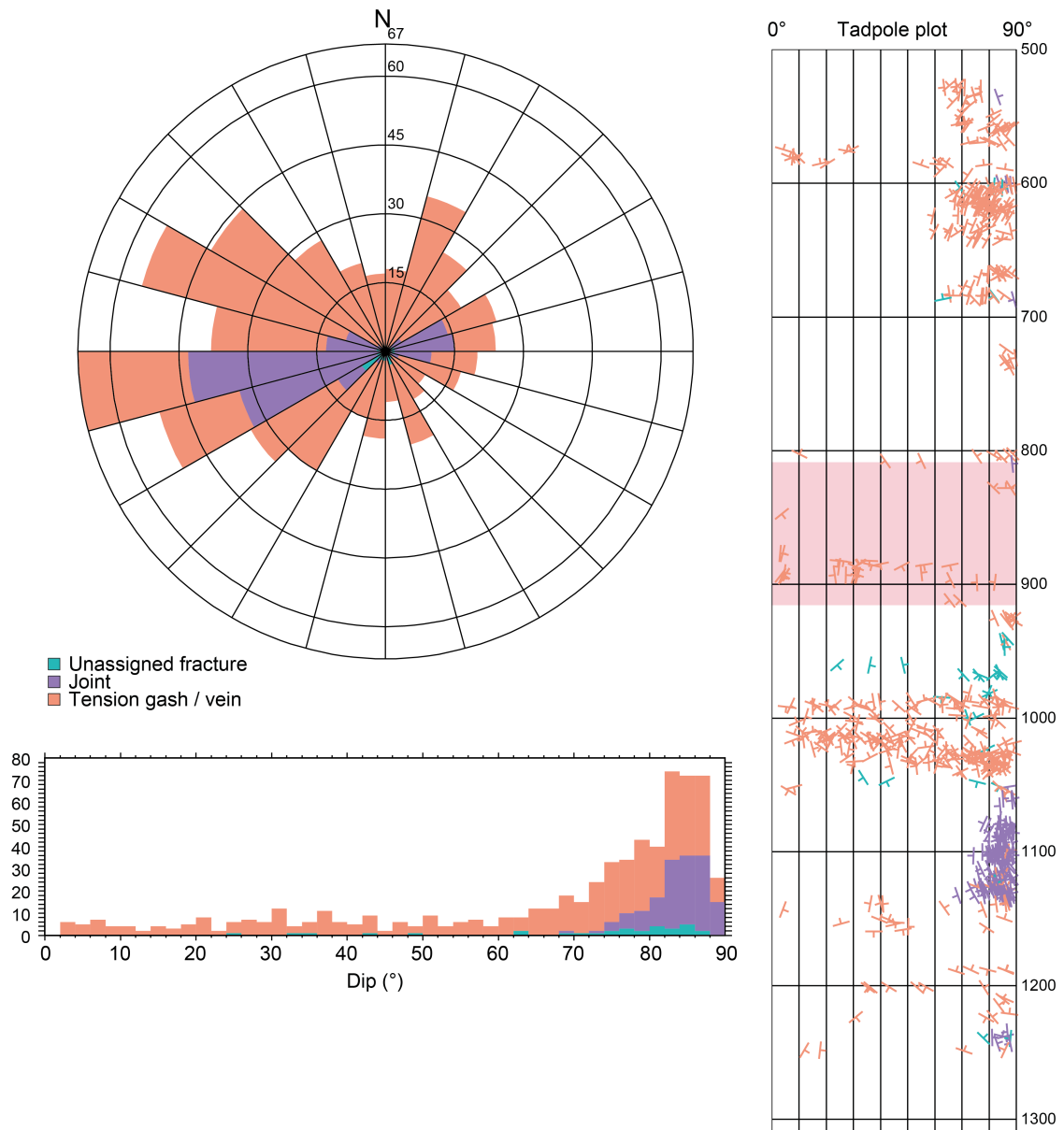


Fig. 4-8: Dip azimuth rose diagram of tension gashes / veins, unassigned fractures and joints in the entire cored interval

A total of 655 structures recorded in oriented cores are displayed: tension gashes / veins (n = 478), joints (n = 146) and unassigned fractures (n = 31). The depth range is 517.58 m to 1'306.77 m MD (log depth). In the tadpole plot, the Opalinus Clay interval is indicated by a light-red bar.

Stylolites

A total of 658 stylolites and 3 stylolite-rich zones were identified in the BAC1-1 borehole. Out of these, 630 (96%) stylolites were recorded in oriented cores. Particularly in stylolite-rich intervals such as the Malm and the Schinznach Formation (see Fig. 4-9), not all individual stylolites could be recorded. Thus, only dominant stylolites clearly observed in core photographs were recorded and categorised. Intervals with high densities of stylolites were defined as stylolitic zones (see Appendix A).

Stylolites show one well-developed and two subordinate orientation clusters (Fig. 4-9, Fig. 4-10 and Tab. 4-1): a subhorizontal to shallow (1° to 25°) SE-dipping cluster (overall mean: $147/02$; $n = 295$) and two steep to subvertical (50° to 90°) clusters with dip directions towards the N and S (overall means: $355/78$; $n = 90$ and $176/72$; $n = 124$).

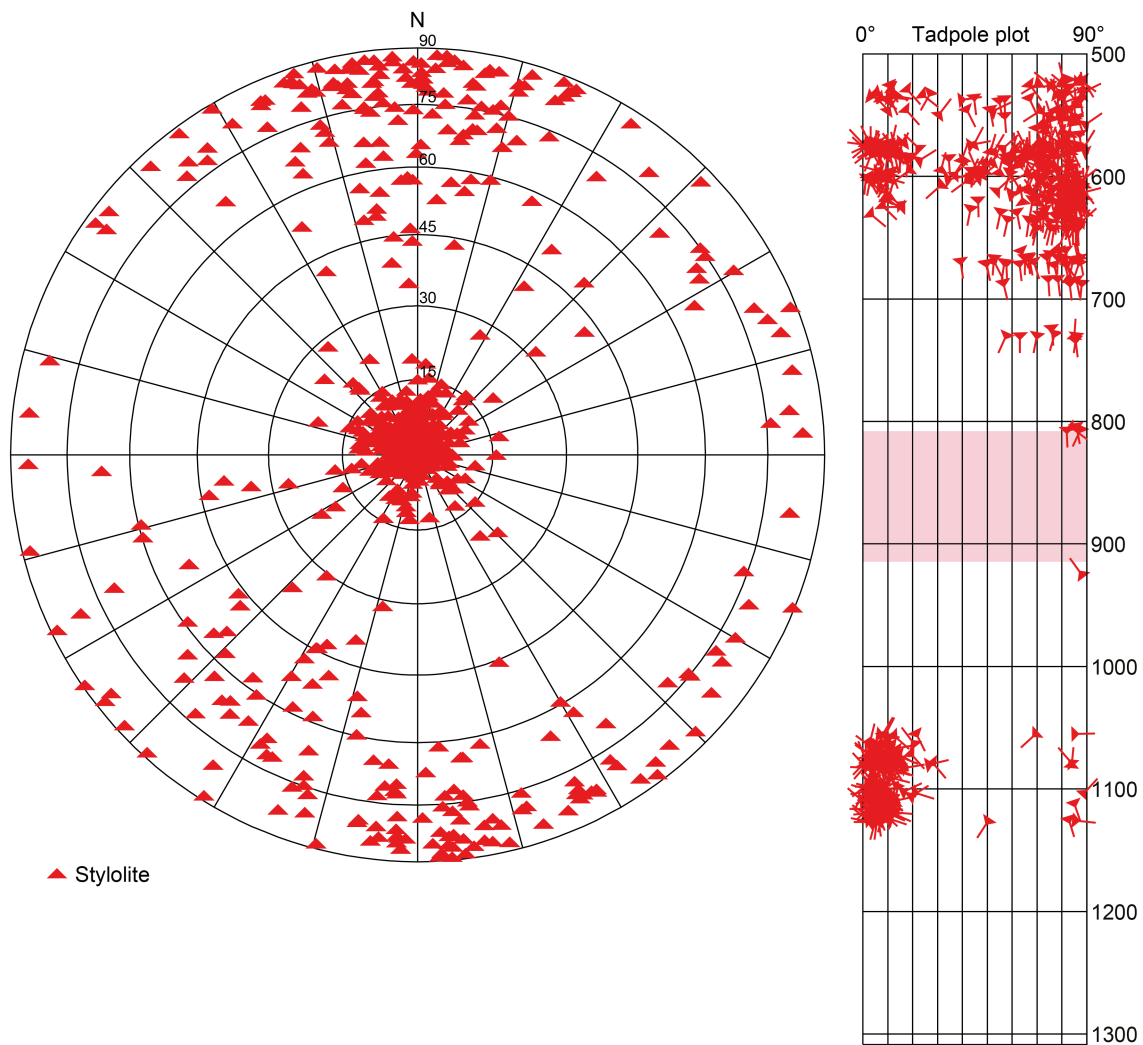


Fig. 4-9: Stereogram and depth plot for stylolites ($n = 630$) recorded in oriented cores of the BAC1-1 borehole

The depth range is 517.58 m to 1'306.77 m MD (log depth). In the tadpole plot, the Opalinus Clay interval is indicated by a light-red bar.

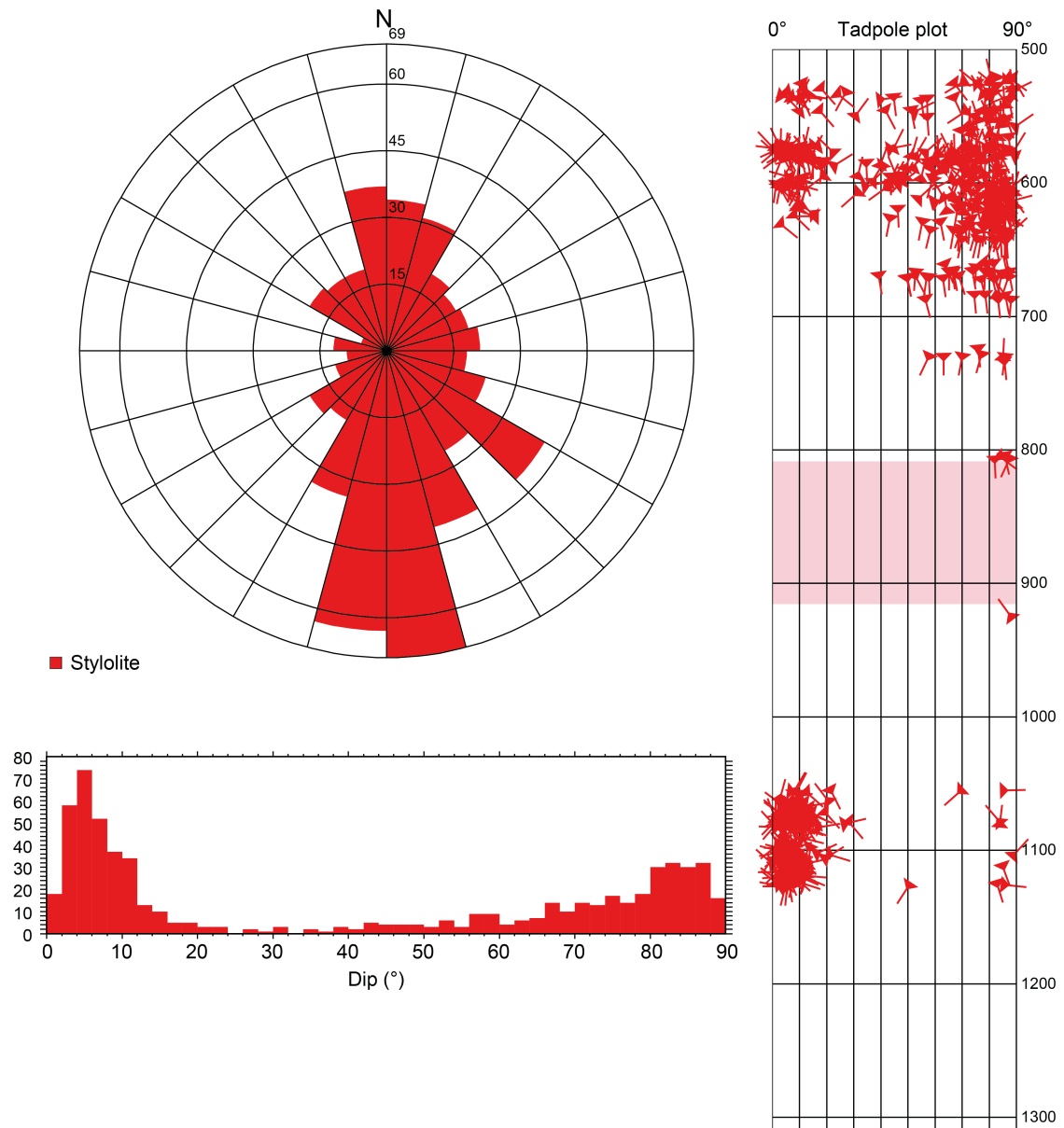


Fig. 4-10: Dip azimuth rose diagram and depth plot for stylolites (n = 630) recorded in oriented cores
 The depth range is 517.58 m to 1'306.77 m MD (log depth). In the tadpole plot, the Opalinus Clay interval is indicated by a light-red bar.

4.1.3 Fracture density (P10 and P32) and distribution

Density histograms were calculated in order to evaluate the spatial distribution of fractures and stylolites (see Fig. 4-4 and Appendix A). As mentioned above, also structural discontinuities recorded in non-oriented cores (n = 95) were considered in the fracture density calculations.

Fault planes are unevenly distributed along the cored interval. Higher fault plane counts (>10 / m) occur within the borehole intervals from 567.60 m to 586.50 m MD (log depth) within the Schwarzbach Formation, from 668.00 m to 679.00 m MD (log depth) within the Wildegg Formation, from 911.00 m to 912.50 m MD (log depth) within the Opalinus Clay, and from 969.00 m to 999.00 m MD (log depth) within the Keuper. The highest density of fault planes with up to 22 planes per metre was observed within the fault zone in the Keuper. Abundant fault planes commonly form prominent fault zones associated with intensely fractured and partly disintegrated drill cores (FDC 2-4; see Tab. 4-2 and Fig. 4-4). The average density of fault planes for the entire cored borehole section was 1.0 planes per metre.

Tension gashes / veins, joints and unassigned fractures (with a fracture count of up to 14 / m) are particularly abundant within the Bänkerjoch Formation (see Fig. 4-4 and Appendix A). The highest fracture density (with up to 14 fractures per metre) was encountered within the Bänkerjoch Formation at approximately 1'014 m MD (log depth). However, the average fracture density for the entire cored borehole section was about 0.9 fractures per metre.

Stylolites revealed an uneven distribution along the borehole and occurred predominantly within the carbonate-rich lithologies of the Malm from 517.58 m to approximately 730 m MD (log depth), and in the Schinznach Formation from approximately 1'055 m to 1'128 m MD (log depth). The highest density (with up to 13 stylolites per metre) occurred within the Villigen Formation at approximately 576 m MD (log depth) and within the Schinznach Formation at approximately 1'115 m MD (log depth). However, the average density for the whole borehole section was about 0.9 stylolites per metre.

4.1.4 Kinematic indicators

A total of 540 striations could be measured on 520 fault planes. Overall, 92% of the striations (n = 496) were collected in oriented cores. Their orientations are given in Fig. 4-11 to Fig. 4-16. There is a clear predominance of S-dipping striations. The plunge of striations varies from subhorizontal to steep (1° to 40°). However, the vast majority does not exceed 20°.

Three different shear senses were distinguished for the analysed drill cores:

- up = thrust / reverse faulting
- down = normal faulting
- dextral / sinistral = strike-slip faulting

The vast majority of shear indicators (n = 196) were identified as thrusts / reverse faults (Tab. 4-3). In contrast, the number of faults classified as normal faults (n = 44) or strike-slip faults (n = 21) is much lower (Tab. 4-3). However, for most fault planes (n = 279) the shear sense could either not be clearly identified or was not observed at all (Tab. 4-3).

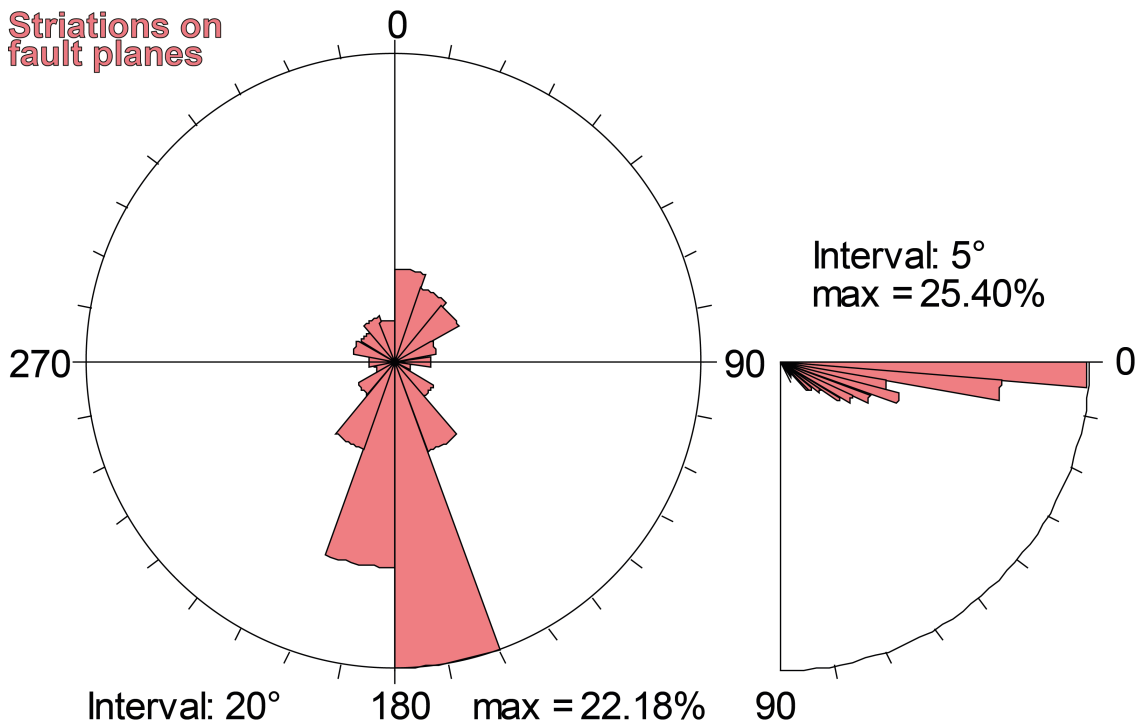


Fig. 4-11: Plunge azimuth of striations along fault planes in the entire cored interval
 This figure presents the striations (n = 496) from oriented cores of the entire cored interval from the Malm to the Permian. Left: azimuth rose diagram, right: plunge histogram. The depth range is 517.58 m to 1'306.77 m MD (log depth).

Tab. 4-3: List of all kinematic indicators in oriented and non-oriented cores

Shear sense	Number
Up	196
Down	44
Sinistral	14
Dextral	7
Unknown	279
In oriented cores	496
In non-oriented cores	44
Total measured lineations	540

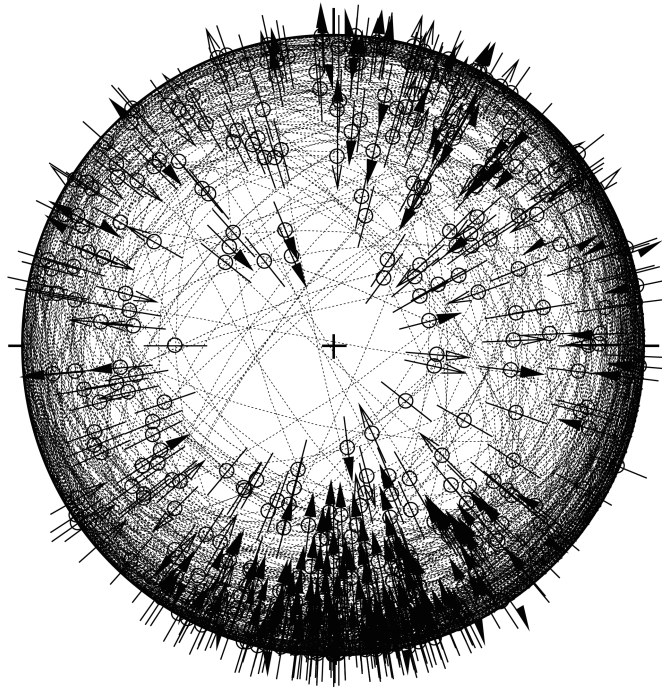


Fig. 4-12: Stereogram of striations on all oriented fault planes (including multiple lineations on a single fault plane) and associated kinematic data

Shear sense up (n = 193), down (n = 43), dextral (n = 7), sinistral (n = 14) and unknown (n = 239). The depth range is 517.58 m to 1'306.77 m MD (log depth).

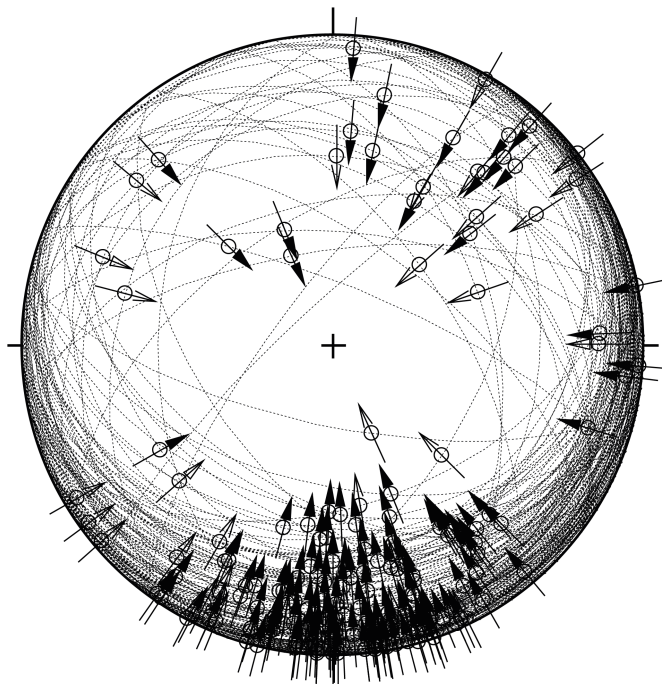


Fig. 4-13: Stereogram of all striations of oriented thrust / reverse fault planes (including multiple lineations on a single fault plane)

Shear sense up (n = 193). The depth range is 517.58 m to 1'306.77 m MD (log depth).

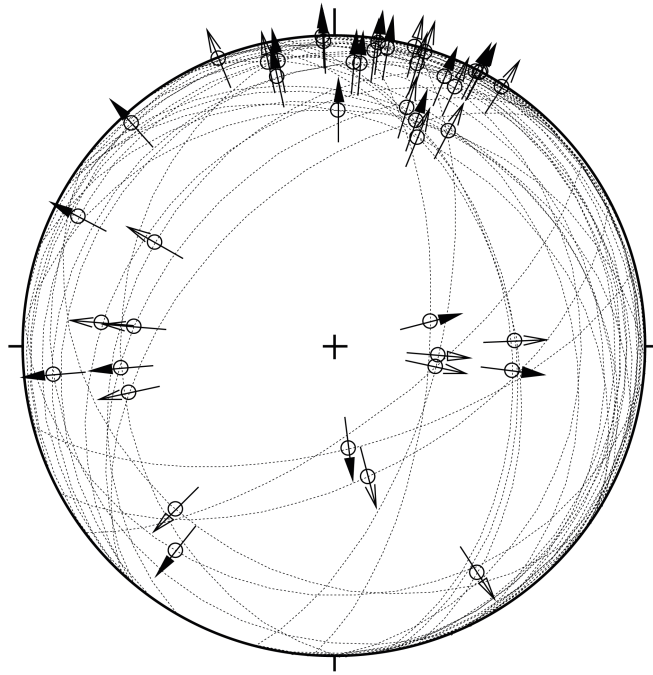


Fig. 4-14: Stereogram of striations on all oriented normal fault planes (including multiple lineations on a single fault plane)
Shear sense down ($n = 43$). The depth range is 517.58 m to 1'306.77 m MD (log depth).

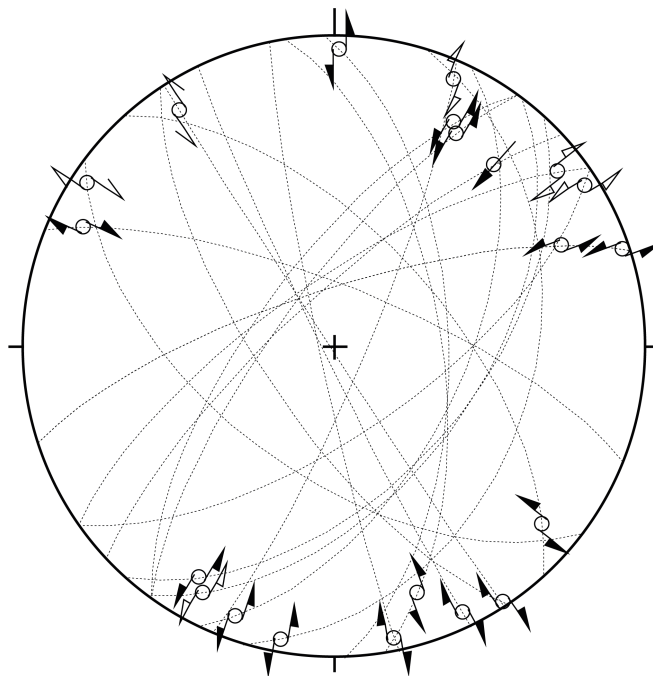


Fig. 4-15: Stereogram of striations on all oriented strike-slip fault planes (including multiple lineations on a single fault plane)
Shear sense dextral ($n = 7$) and sinistral ($n = 14$). The depth range is 517.58 m to 1'306.77 m MD (log depth).

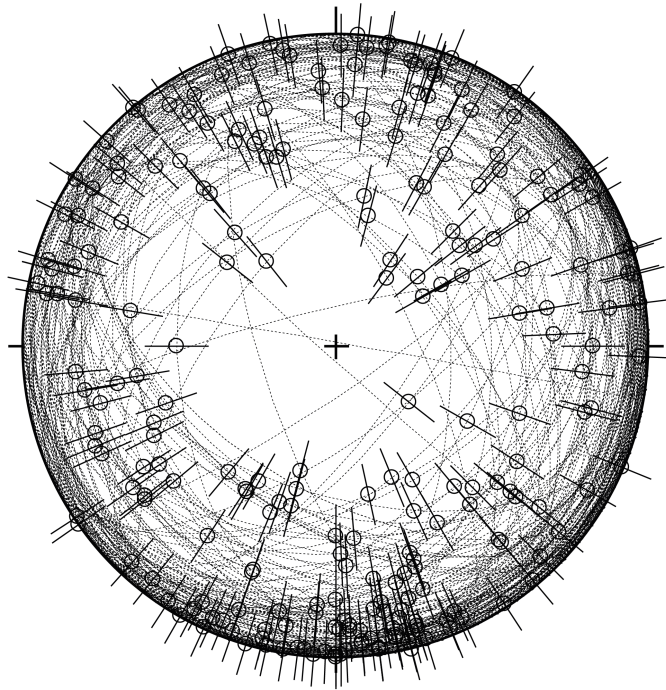


Fig. 4-16: Stereogram of striations on all oriented fault planes with unknown shear sense (including multiple lineations on a single fault plane)
Shear sense unknown (n = 239). The depth range is 517.58 m to 1'306.77 m MD (log depth).

4.2 Malm

The cored Malm covers the interval from 517.58 m to 737.32 m MD (log depth). The Malm shows a high density of all structure types. The dominant structure types are fault planes and stylolites. Further structures are tension gashes and stylolitic fault planes. Mirror-like fault planes, joints and unassigned fractures are rather rare. The structures are fairly evenly distributed over the entire Malm. However, the highest fracture density was observed within the Villigen Formation.

Fault planes and stylolitic fault planes preferably dip towards the SE in the «Felsenkalke» + «Massenkalk» and the Schwarzbach Formation. However, in the Villigen Formation and the Wildegg Formation, they preferably dip towards the S. The plunge azimuth of the striations is scattered with a preferred dip towards the S. Reverse faulting dominates, however normal faulting was also observed.

Tension gashes are mostly steeply dipping to subvertical. They preferably dip towards the NW.

Stylolites reveal either subhorizontal to shallow dip or steep to subvertical dip angles and a predominant E-W strike direction. Shallow dipping stylolites are rare or absent in the marly layers.

For the detailed stereographic evaluation, four lithostratigraphic units were defined within the Malm interval. Only the data from oriented cores are presented.

4.2.1 «Felsenkalke» + «Massenkalk»

The orientation and spatial distribution of recorded structures in the «Felsenkalke» + «Massenkalk» (517.58 m to 550.03 m MD log depth) are shown below.

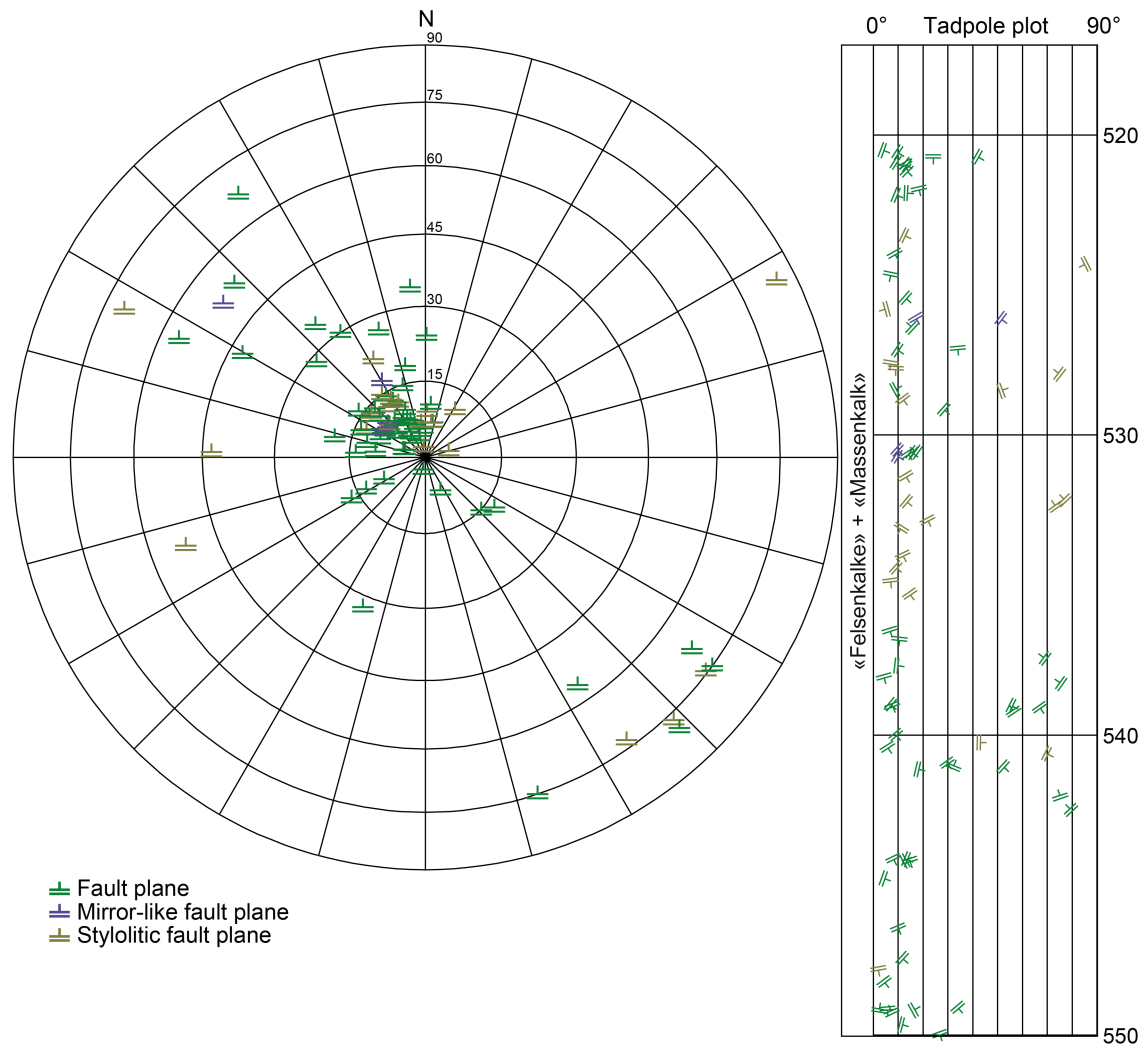


Fig. 4-17: Stereogram and depth plot of fault planes («Felsenkalke» + «Massenkalk») Fault planes (n = 56), mirror-like fault planes (n = 4) and stylolitic fault planes (n = 21).

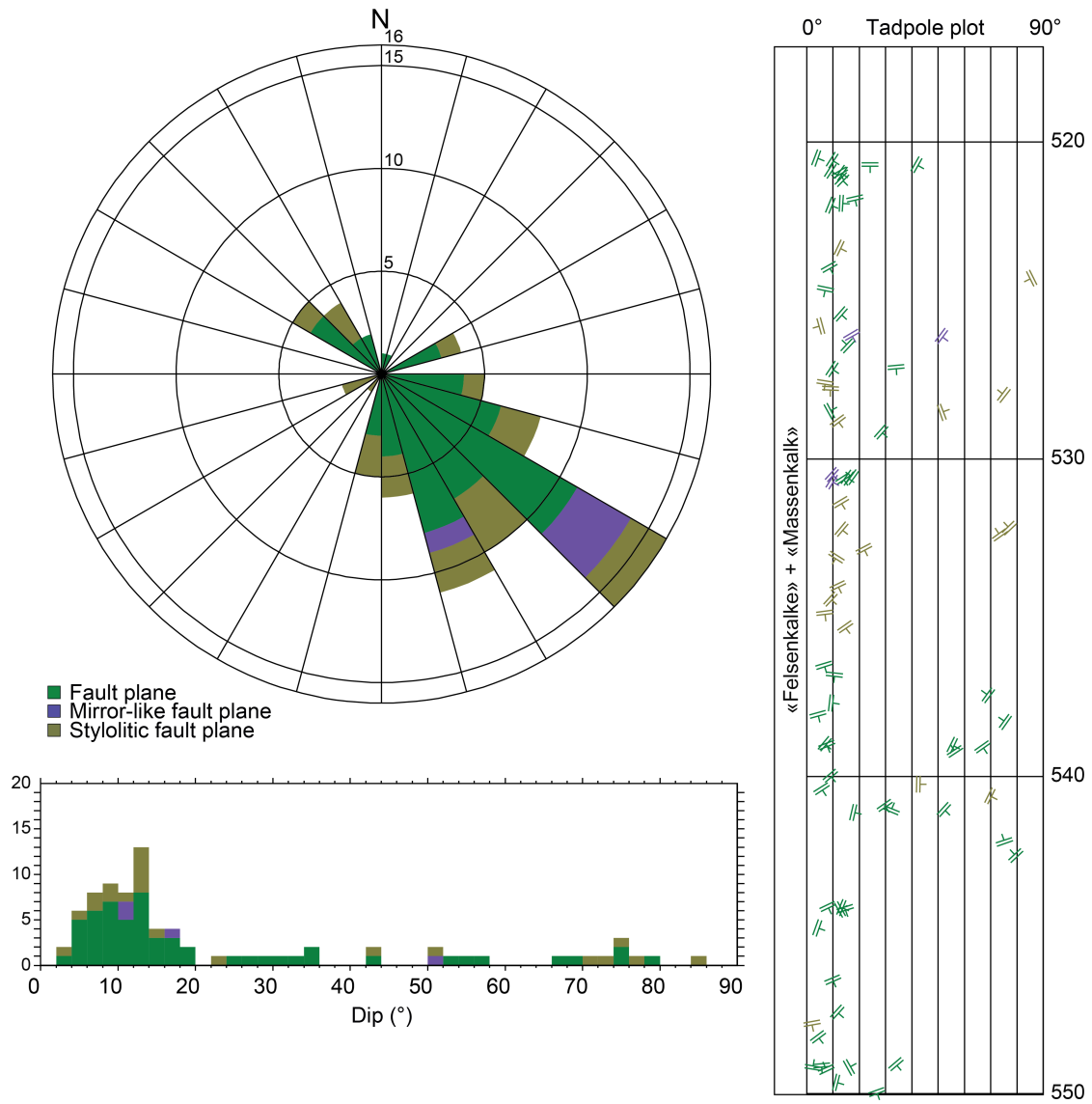


Fig. 4-18: Dip azimuth rose diagram, dip histogram and depth plot of fault planes («Felsenkalk» + «Massenkalk») Fault planes (n = 56), mirror-like fault planes (n = 4) and stylolitic fault planes (n = 21).

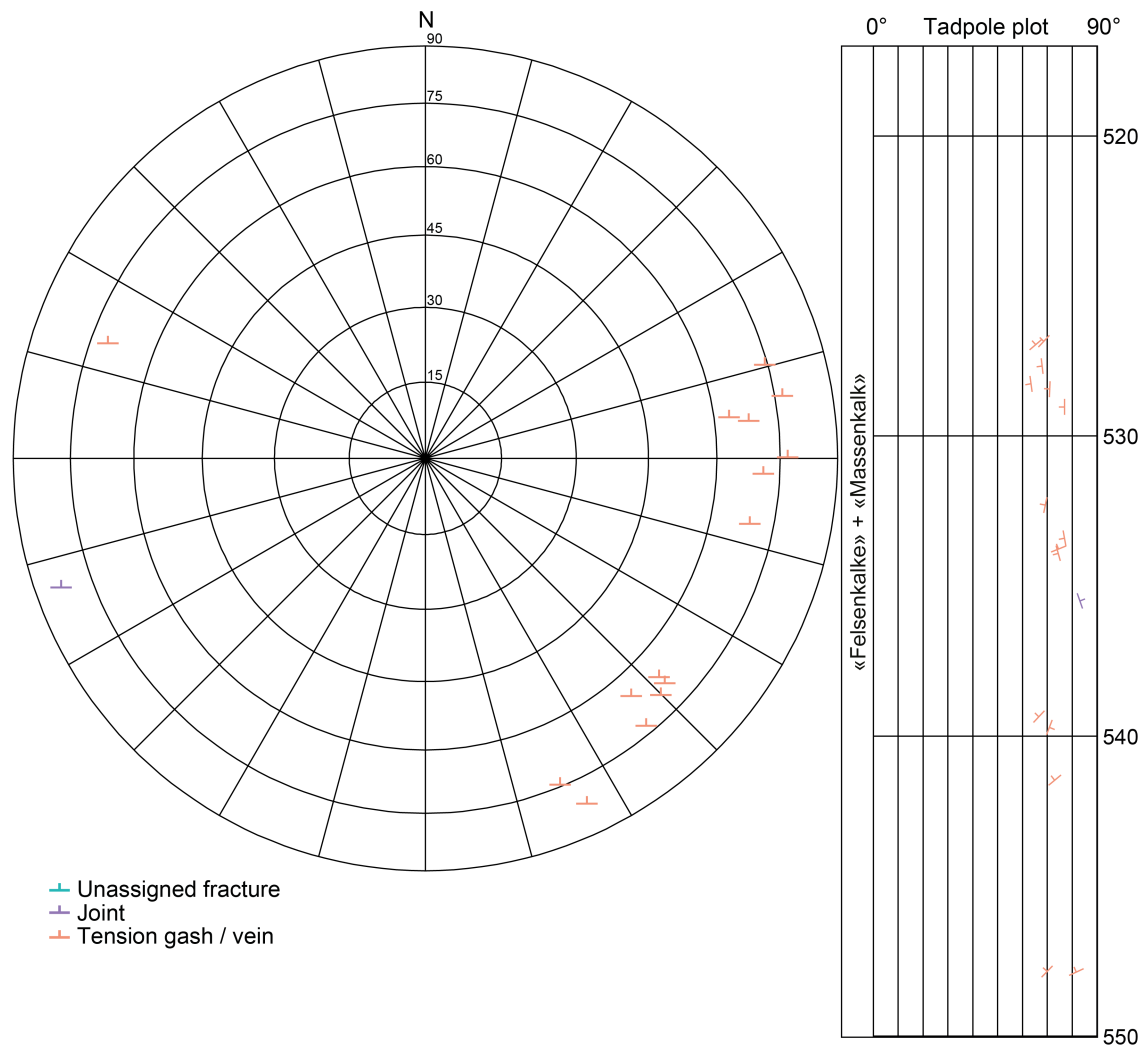


Fig. 4-19: Stereogram and depth plot of tension gashes / veins and unassigned fractures («Felsenkalke» + «Massenkalk»)

Joints (n = 1) and tension gashes / veins (n = 15); no unassigned fractures were observed (n = 0).

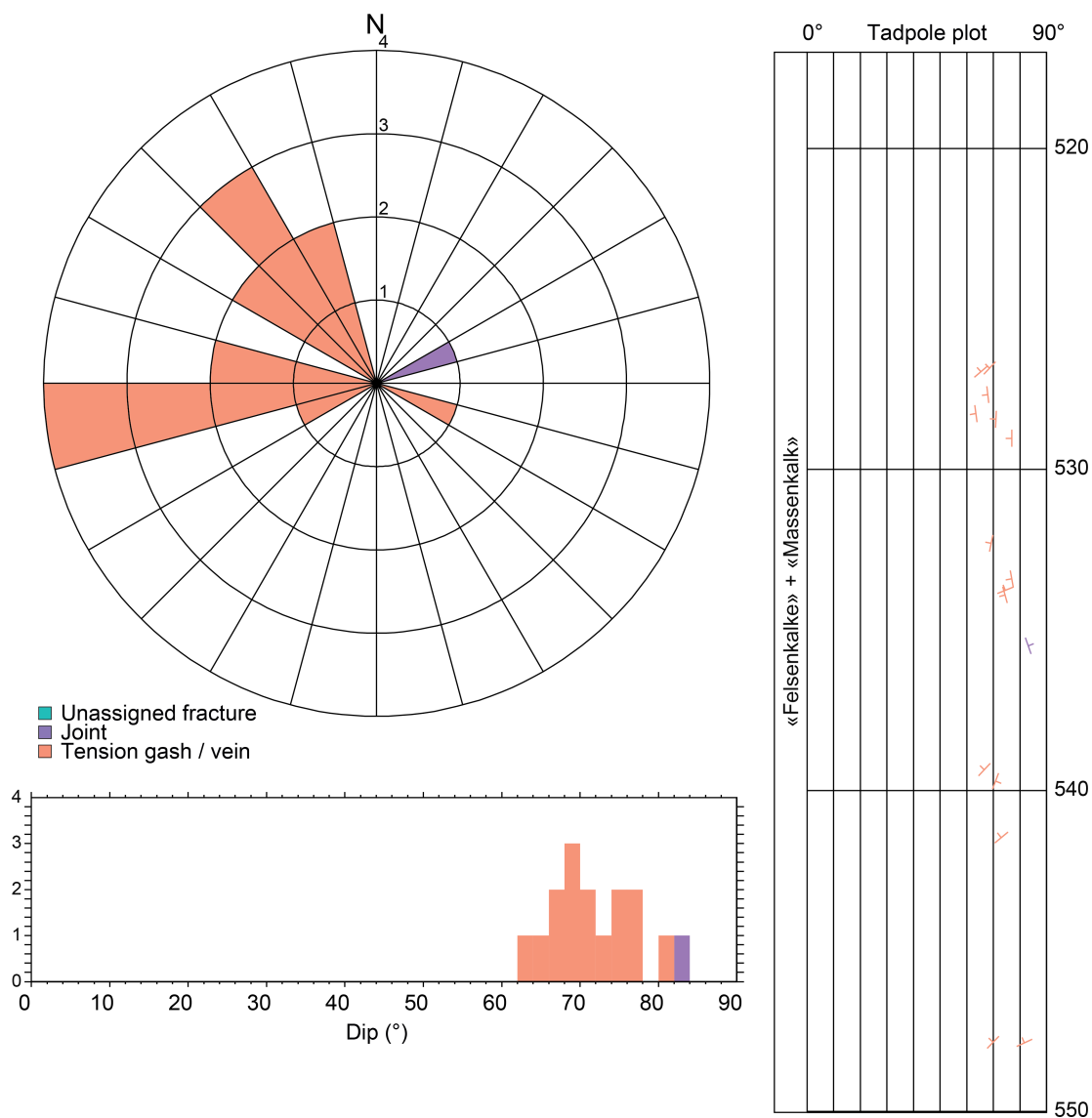


Fig. 4-20: Dip azimuth rose diagram, dip histogram and depth plot of tension gashes / veins, joints and unassigned fractures («Felsenkalke» + «Massenkalk»)

Joints (n = 1) and tension gashes / veins (n = 15); no unassigned fractures were observed (n = 0).

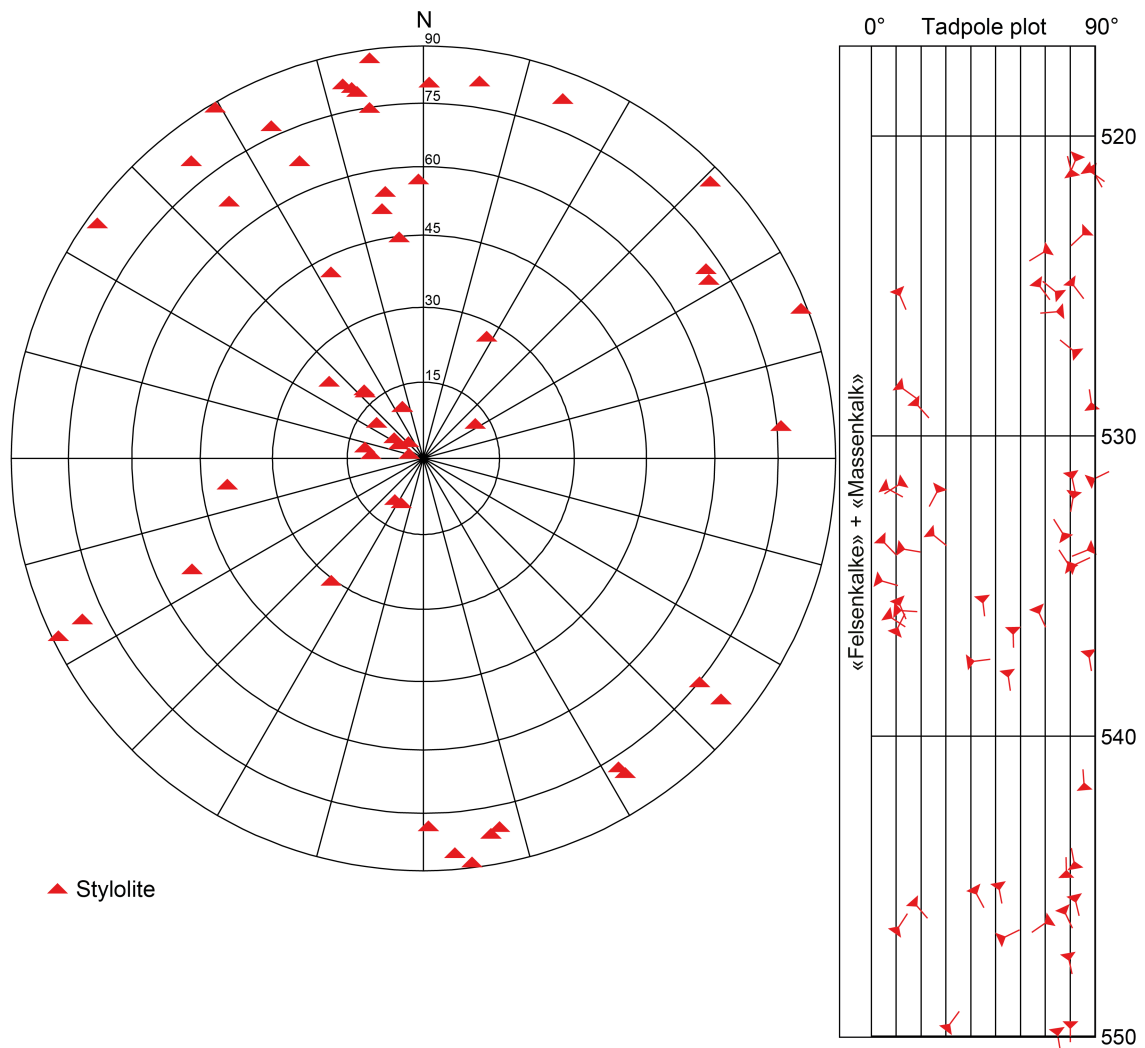


Fig. 4-21: Stereogram and depth plot of stylolites («Felsenkalke» + «Massenkalk», n = 54)

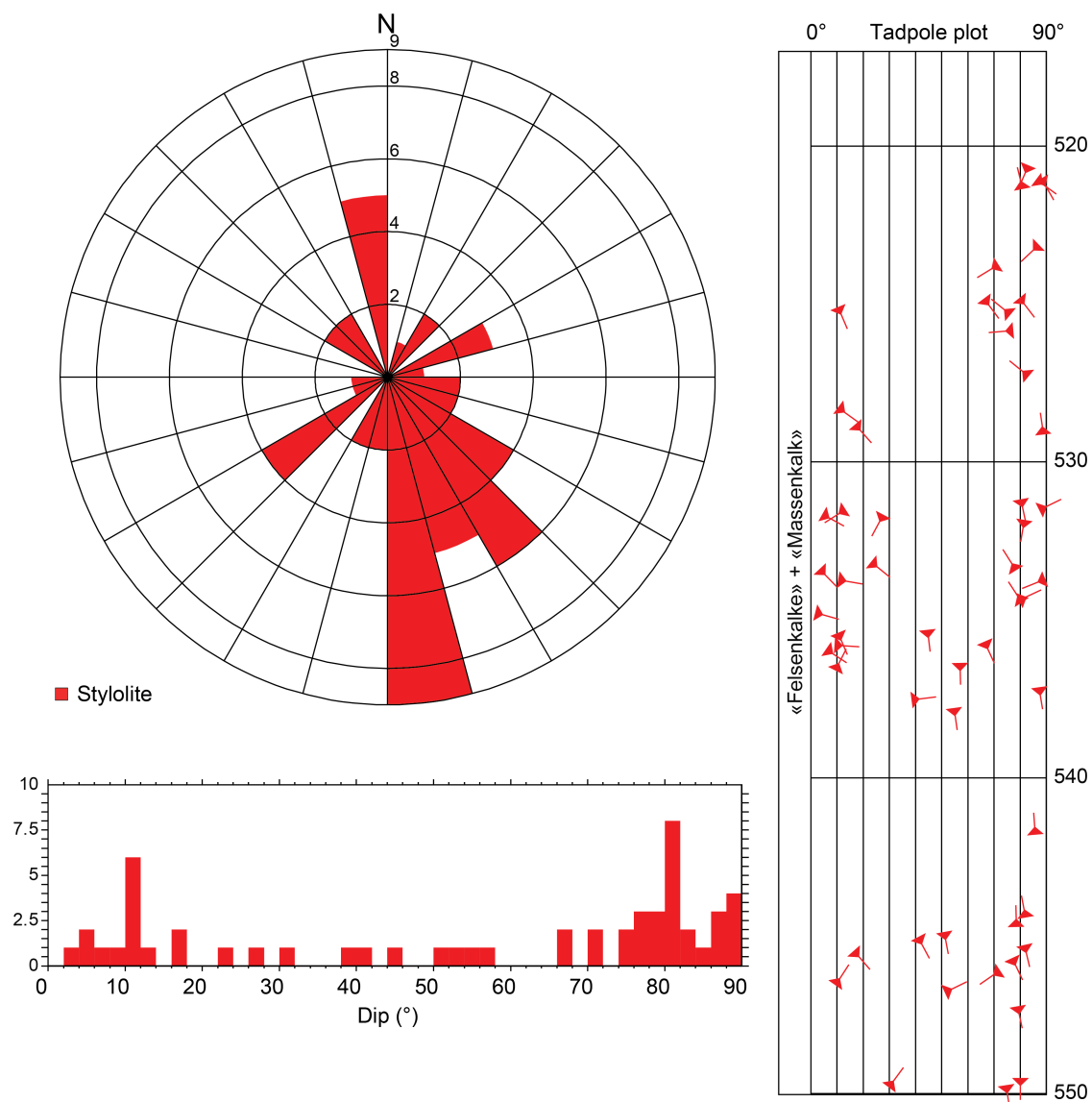


Fig. 4-22: Dip azimuth rose diagram, dip histogram and depth plot of stylolites («Felsenkalke» + «Massenkalk», n = 54)

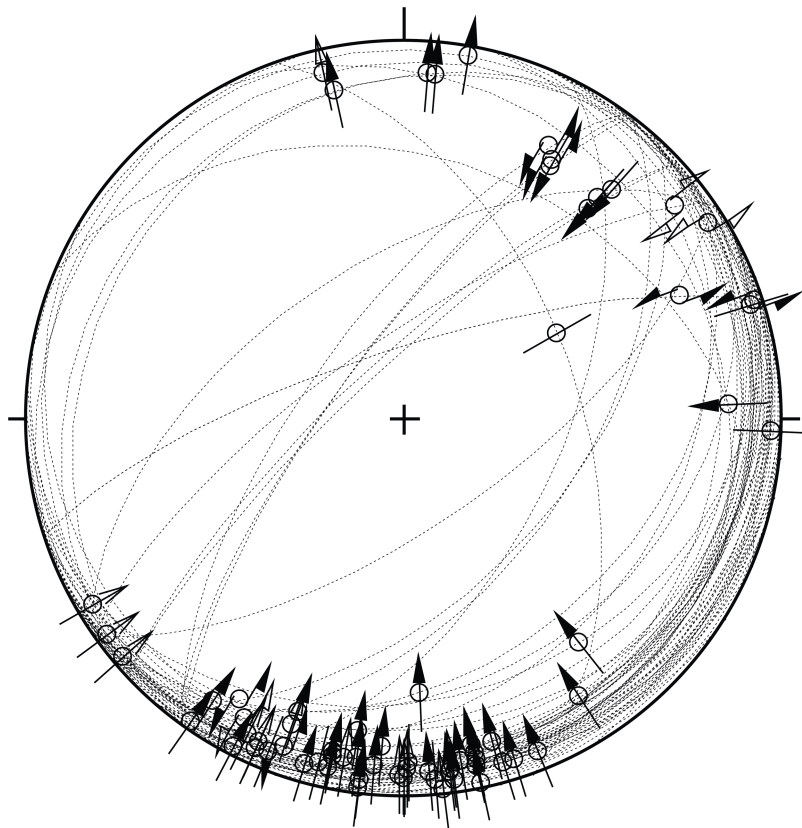


Fig. 4-23: Stereogram of striations on fault planes (including multiple lineations on a single fault plane) («Felsenkalke» + «Massenkalk», $n = 69$)

4.2.2 Schwarzbach Formation

The orientation and spatial distribution of recorded structures in the Schwarzbach Formation (550.03 m to 571.29 m MD log depth) are shown below.

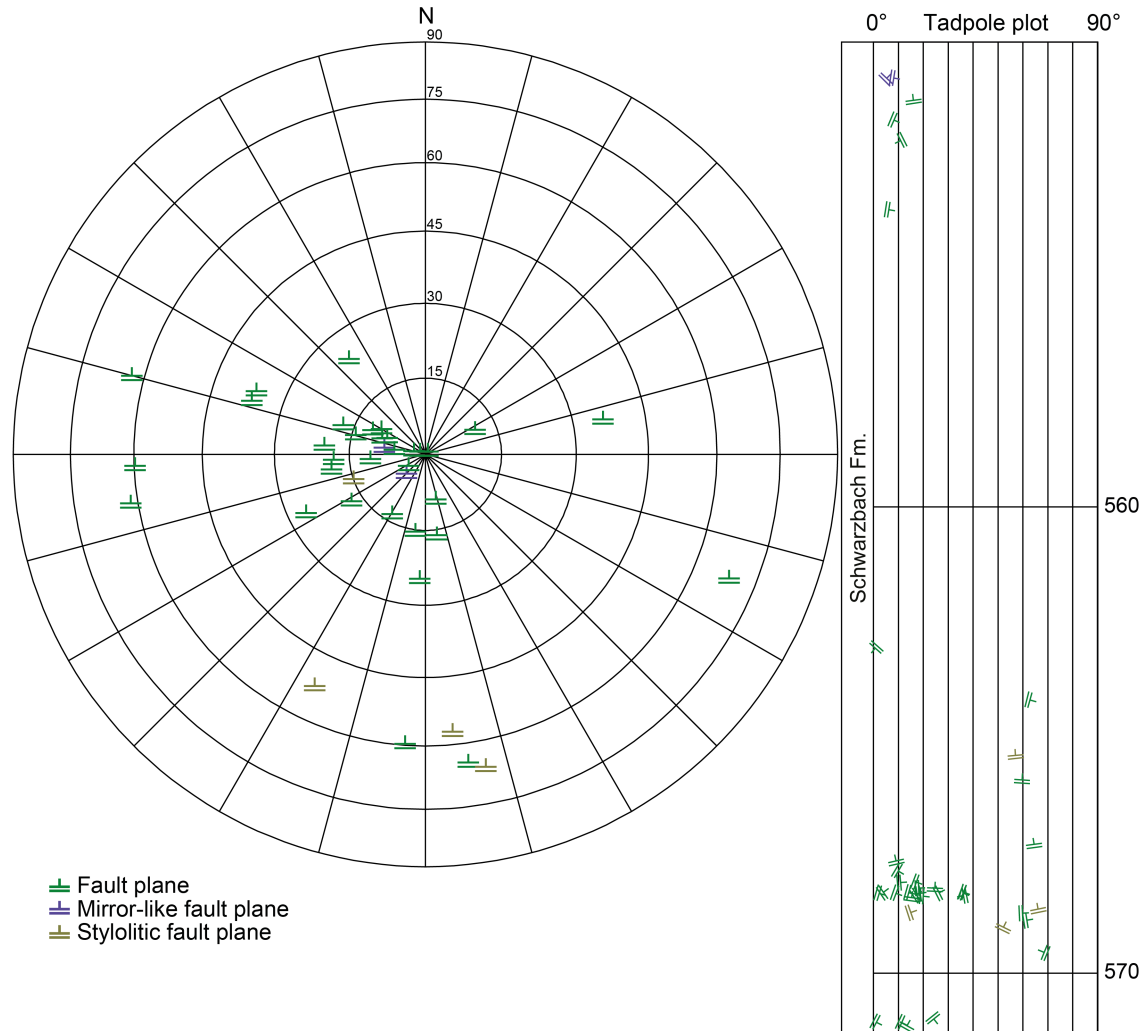


Fig. 4-24: Stereogram and depth plot of fault planes (Schwarzbach Formation)
 Fault planes (n = 33), mirror-like fault planes (n = 2) and stylolitic fault planes (n = 4).

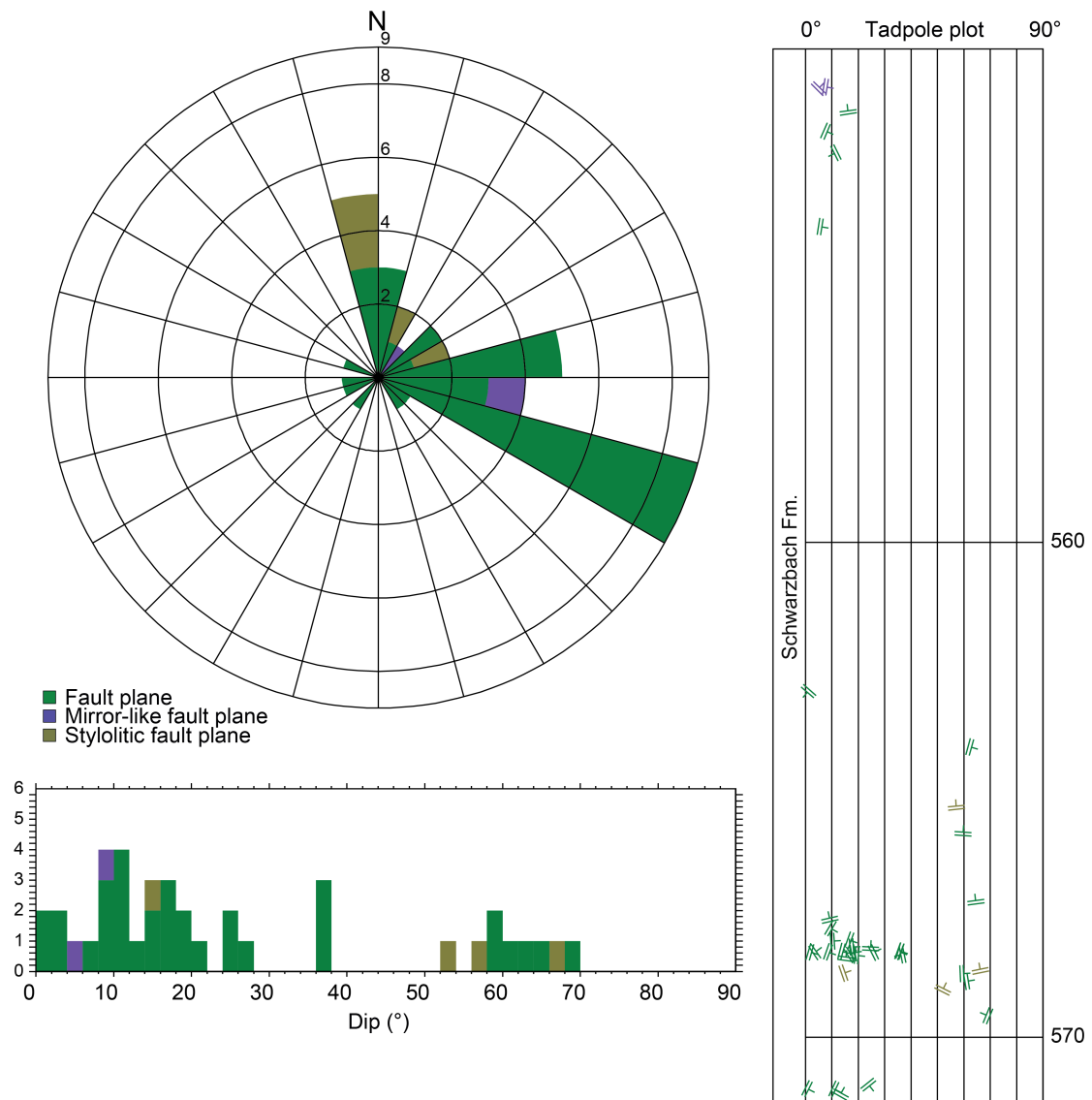


Fig. 4-25: Dip azimuth rose diagram, dip histogram and depth plot of fault planes (Schwarzbach Formation)

Fault planes (n = 33), mirror-like fault planes (n = 2) and stylolitic fault planes (n = 4).

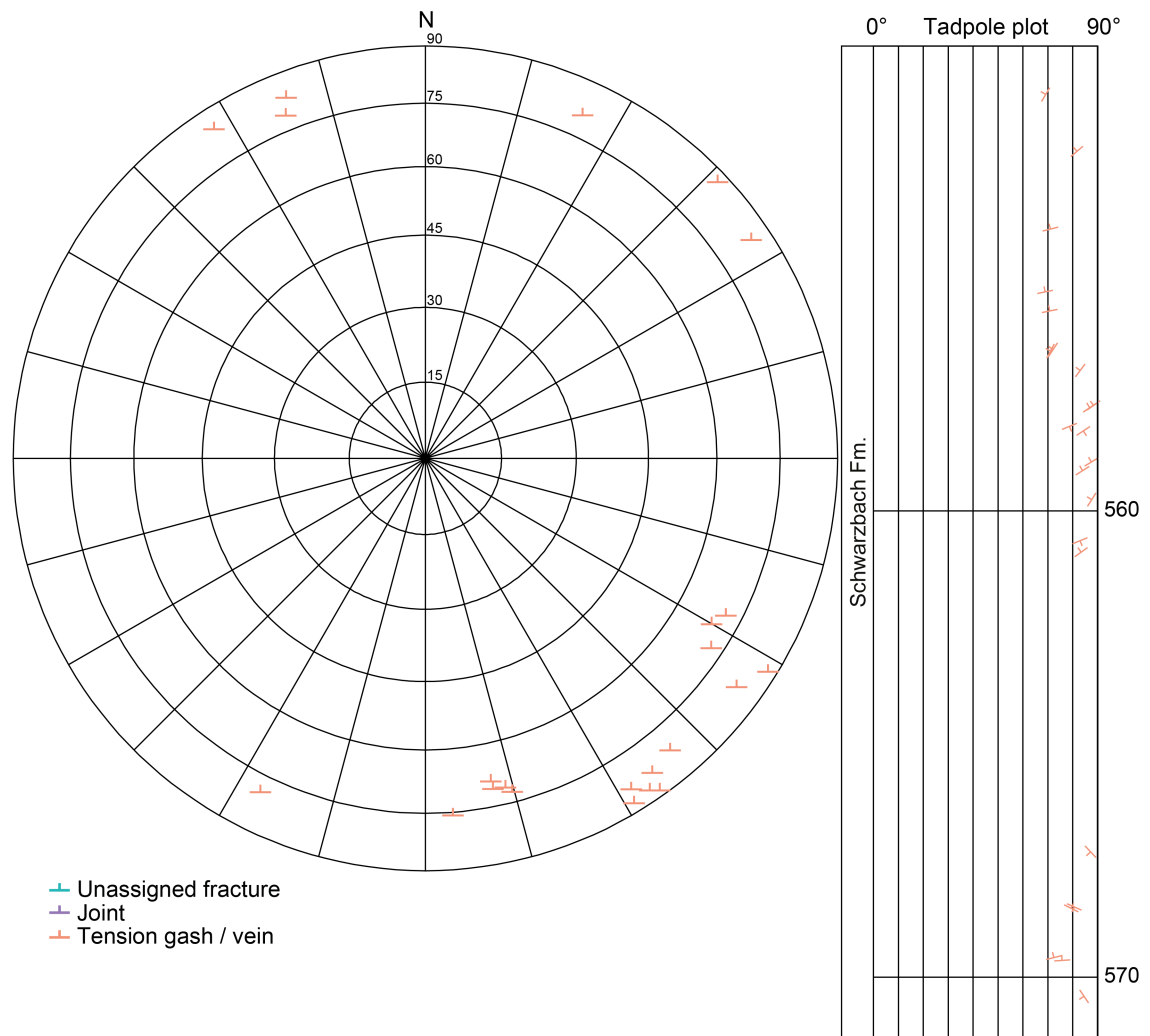


Fig. 4-26: Stereogram and depth plot of tension gashes / veins and unassigned fractures (Schwarzbach Formation)

Tension gashes / veins (n = 23); no joints or unassigned fractures were observed (n = 0).

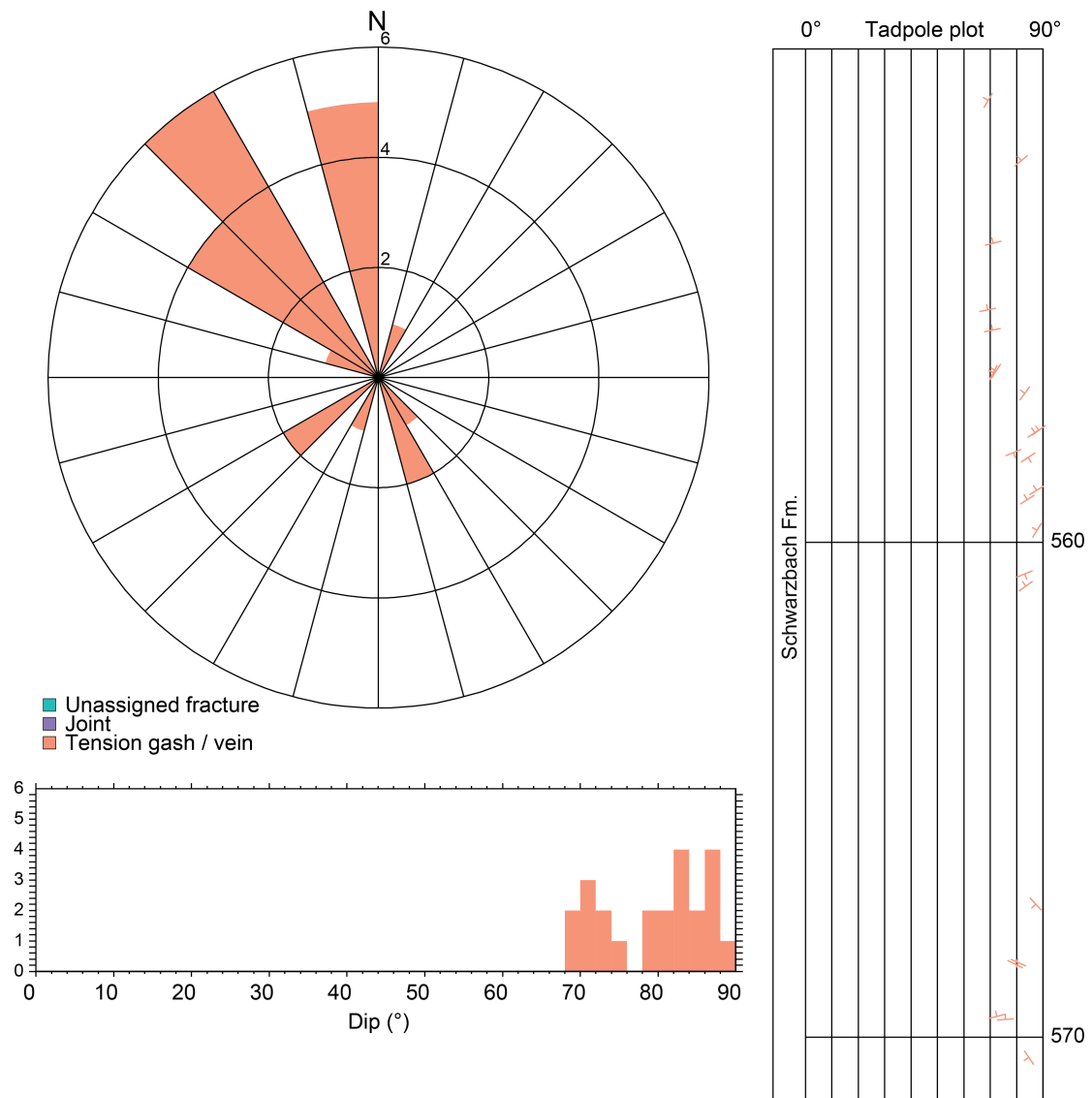


Fig. 4-27: Dip azimuth rose diagram, dip histogram and depth plot of tension gashes / veins, joints and unassigned fractures (Schwarzbach Formation)

Tension gashes / veins (n = 23); no joints or unassigned fractures were observed (n = 0).

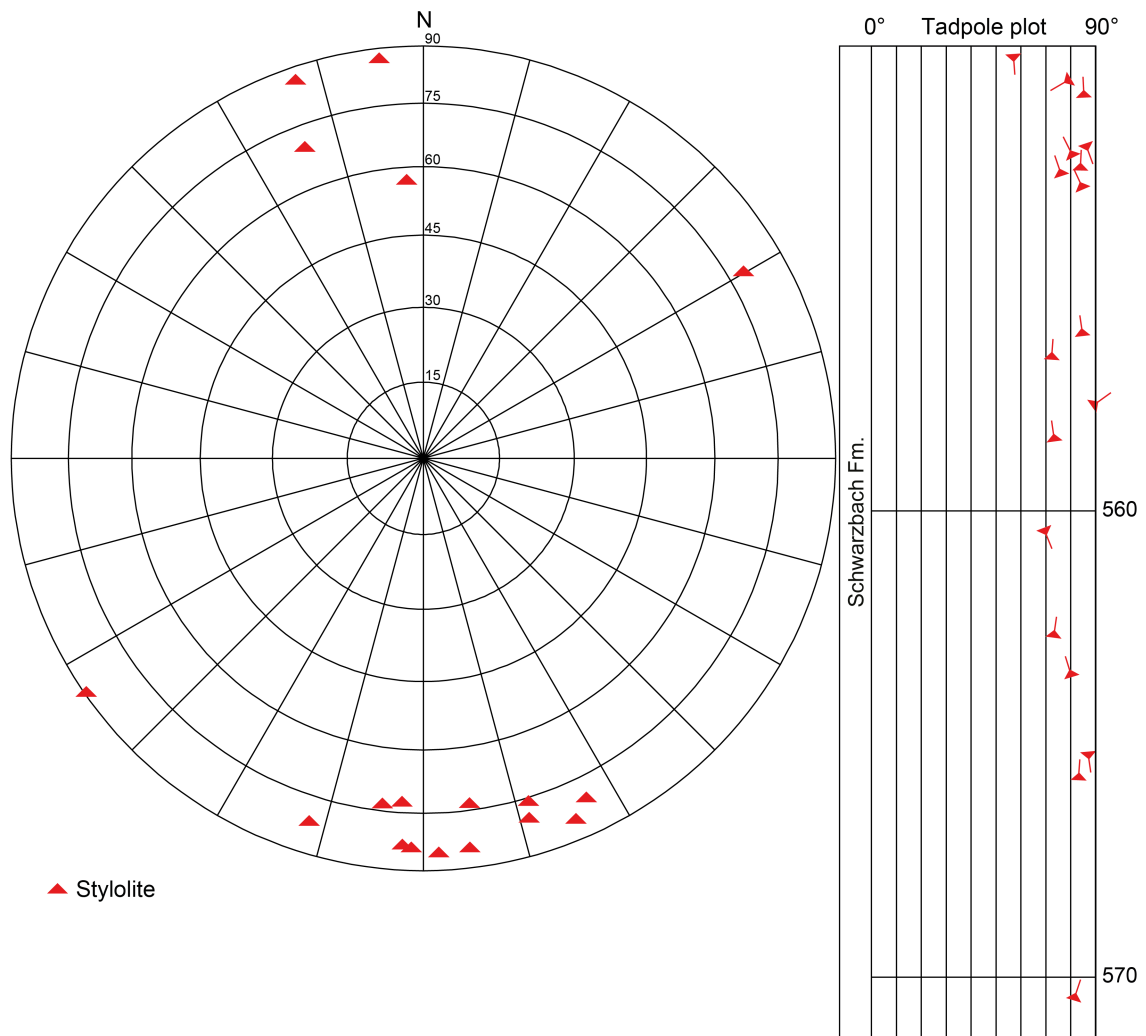


Fig. 4-28: Stereogram and depth plot of stylolites (Schwarzbach Formation, n = 18)

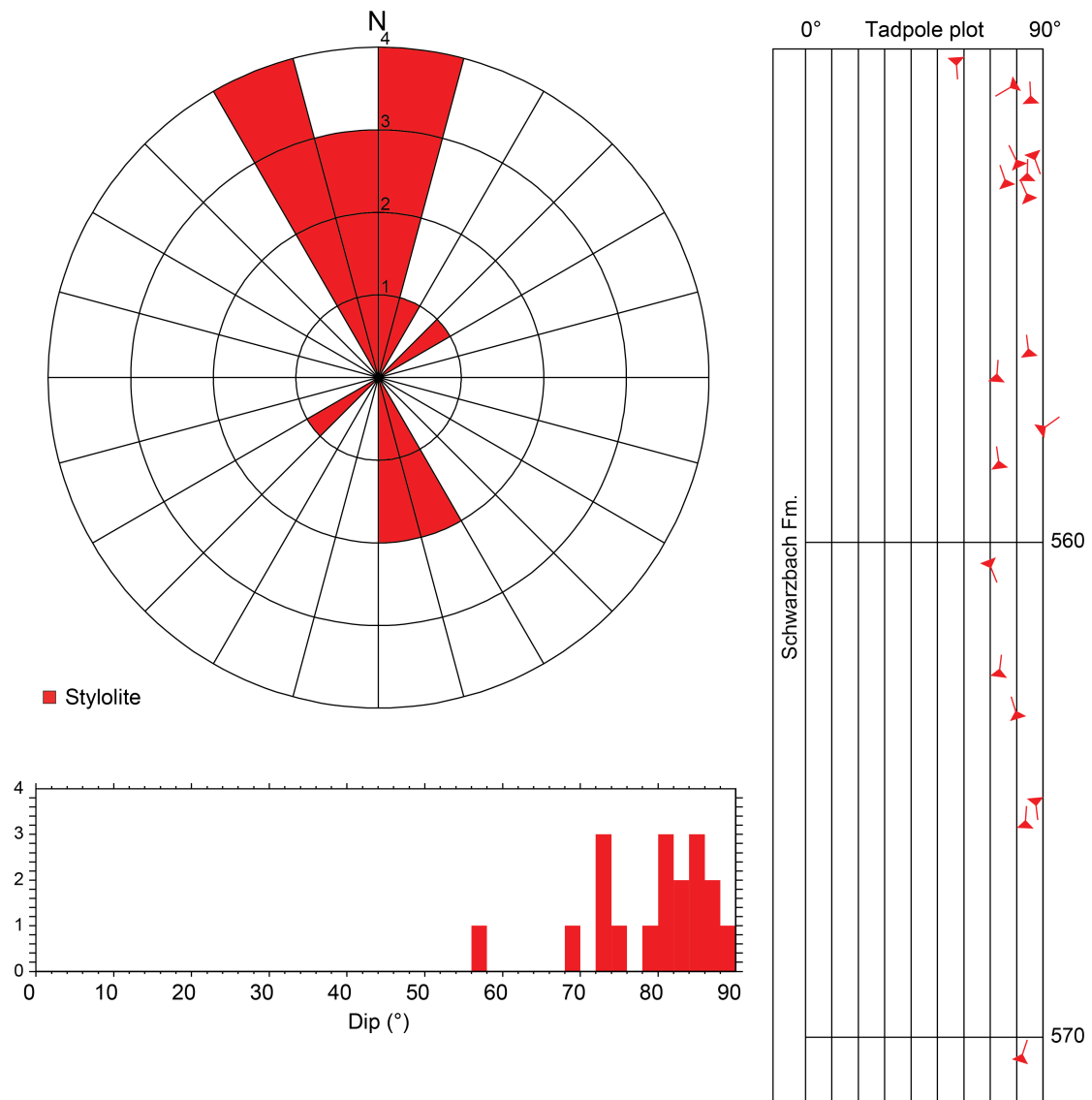


Fig. 4-29: Dip azimuth rose diagram, dip histogram and depth plot of stylolites (Schwarzbach Formation, n = 18)

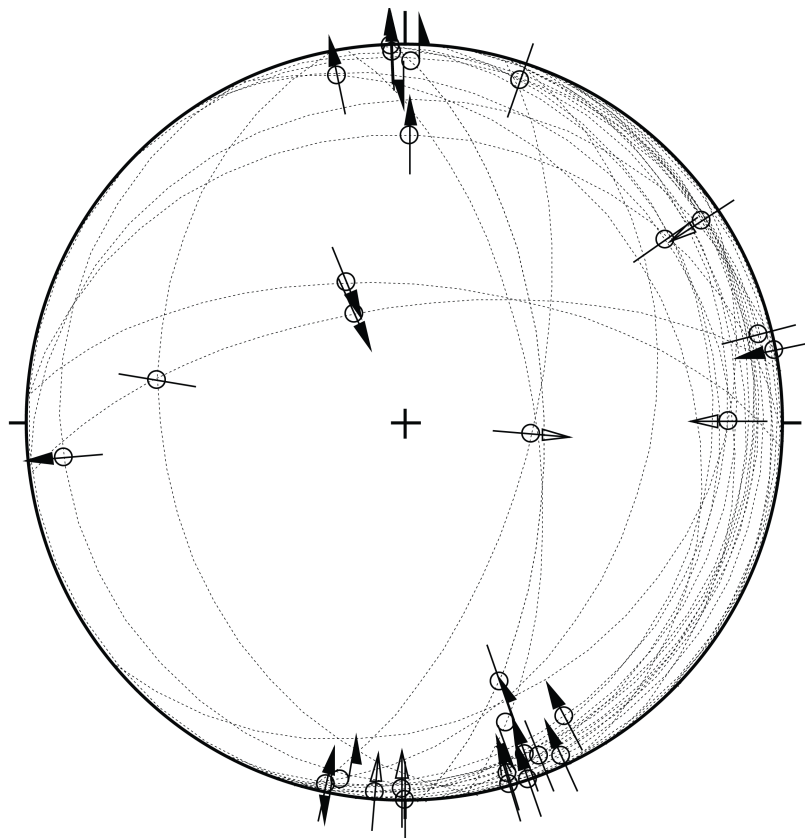


Fig. 4-30: Stereogram of striations on fault planes (including multiple lineations on a single fault plane) (Schwarzbach Formation, n = 30)

4.2.3 Villigen Formation

The orientation and spatial distribution of recorded structures in the Villigen Formation (571.29 m to 637.55 m MD log depth) are shown below.

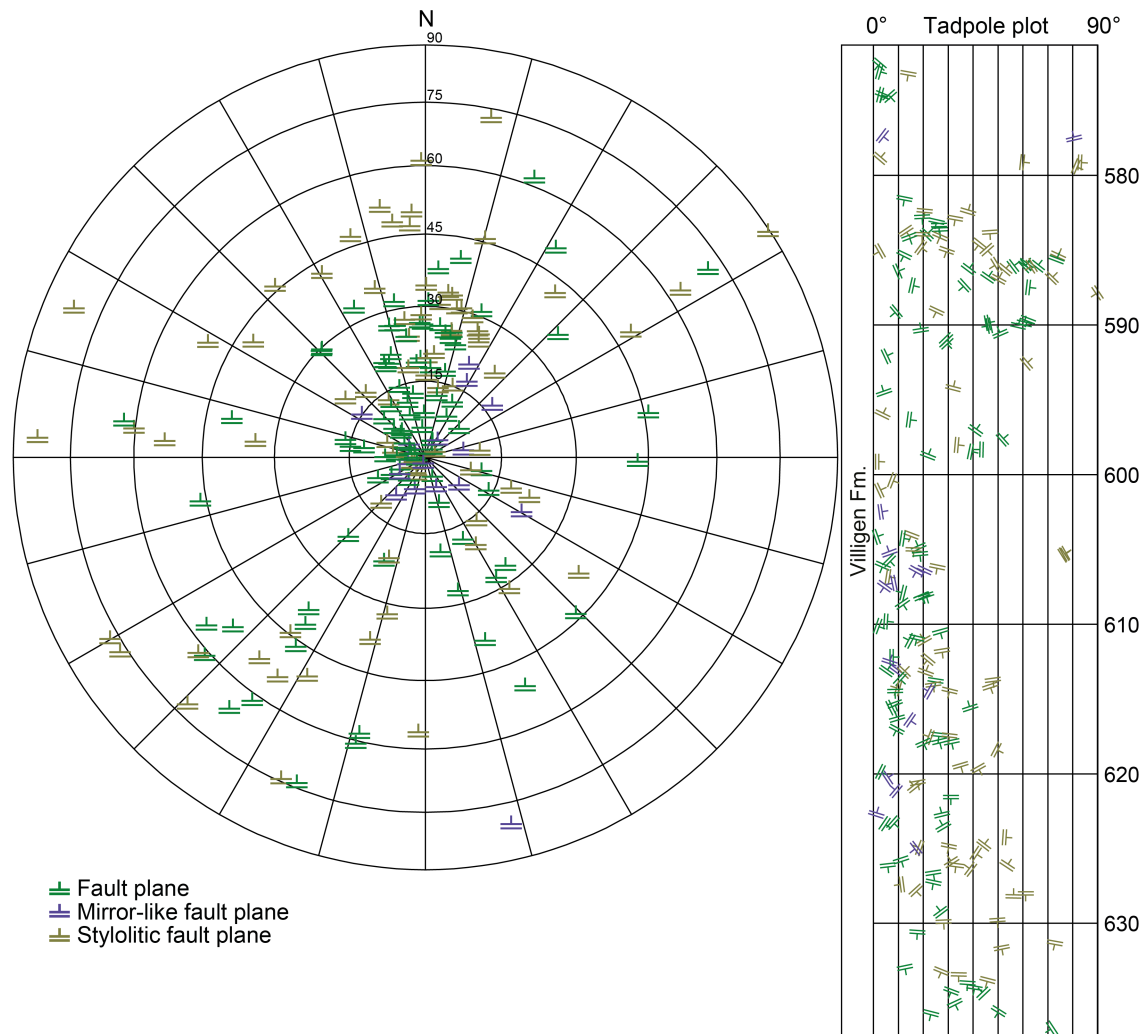


Fig. 4-31: Stereogram and depth plot of fault planes (Villigen Formation)
 Fault planes (n = 93), mirror-like fault planes (n = 16) and stylolitic fault planes (n = 75).

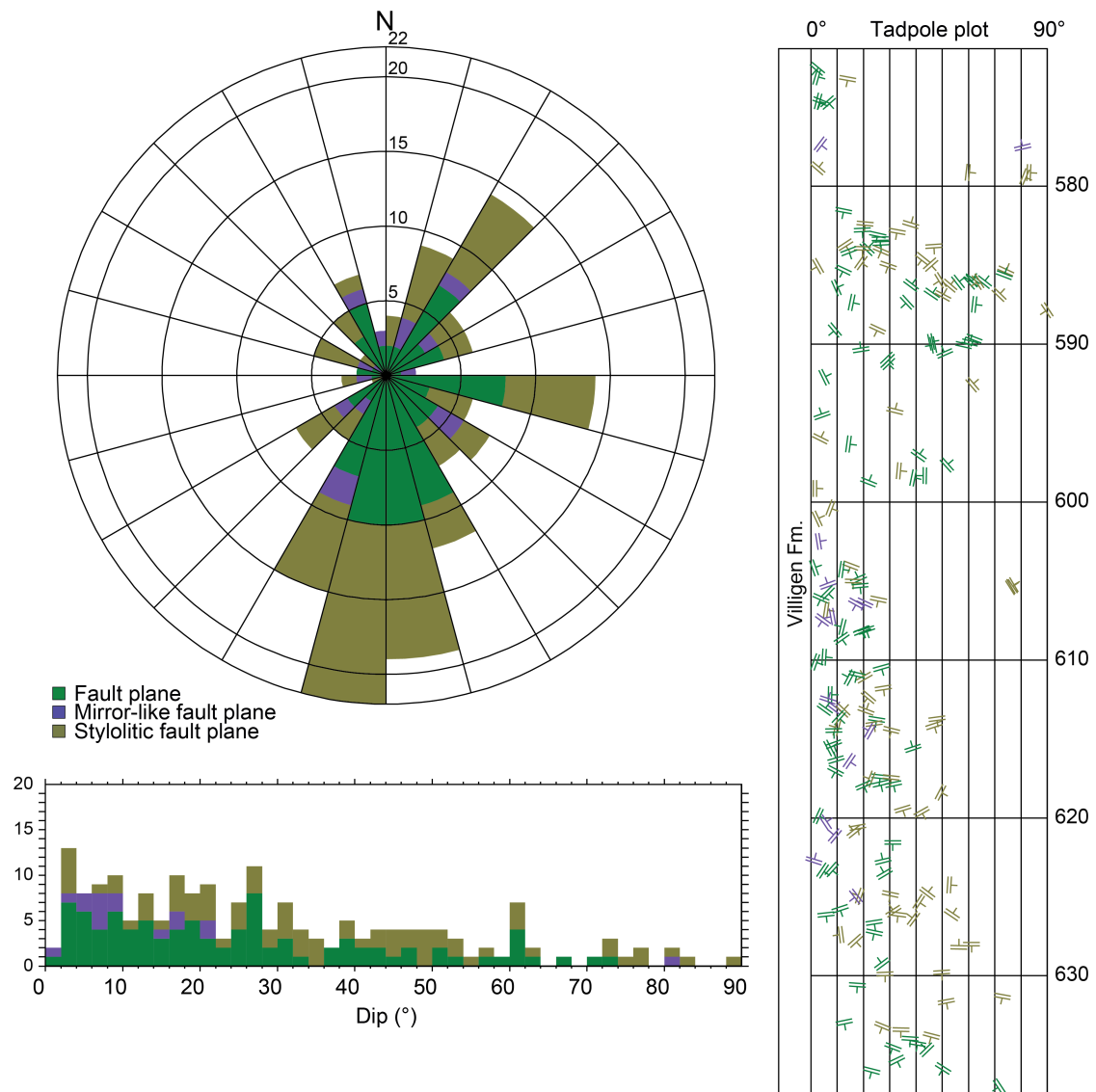


Fig. 4-32: Dip azimuth rose diagram, dip histogram and depth plot of fault planes (Villigen Formation)
 Fault planes (n = 93), mirror-like fault planes (n = 16) and stylolitic fault planes (n = 75).

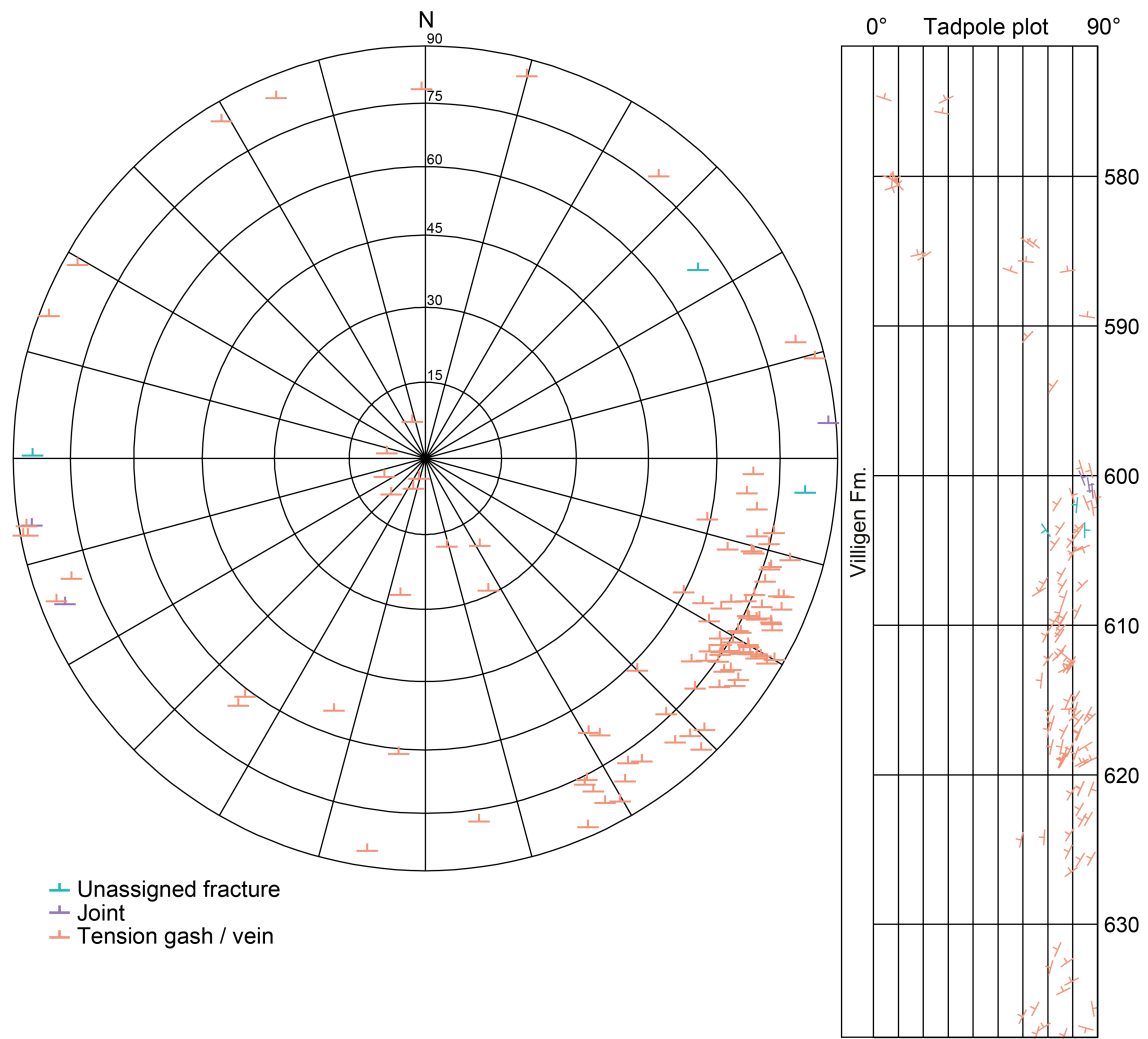


Fig. 4-33: Stereogram and depth plot of tension gashes / veins and unassigned fractures (Villigen Formation)

Unassigned fractures (n = 3), joints (n = 3) and tension gashes / veins (n = 108).

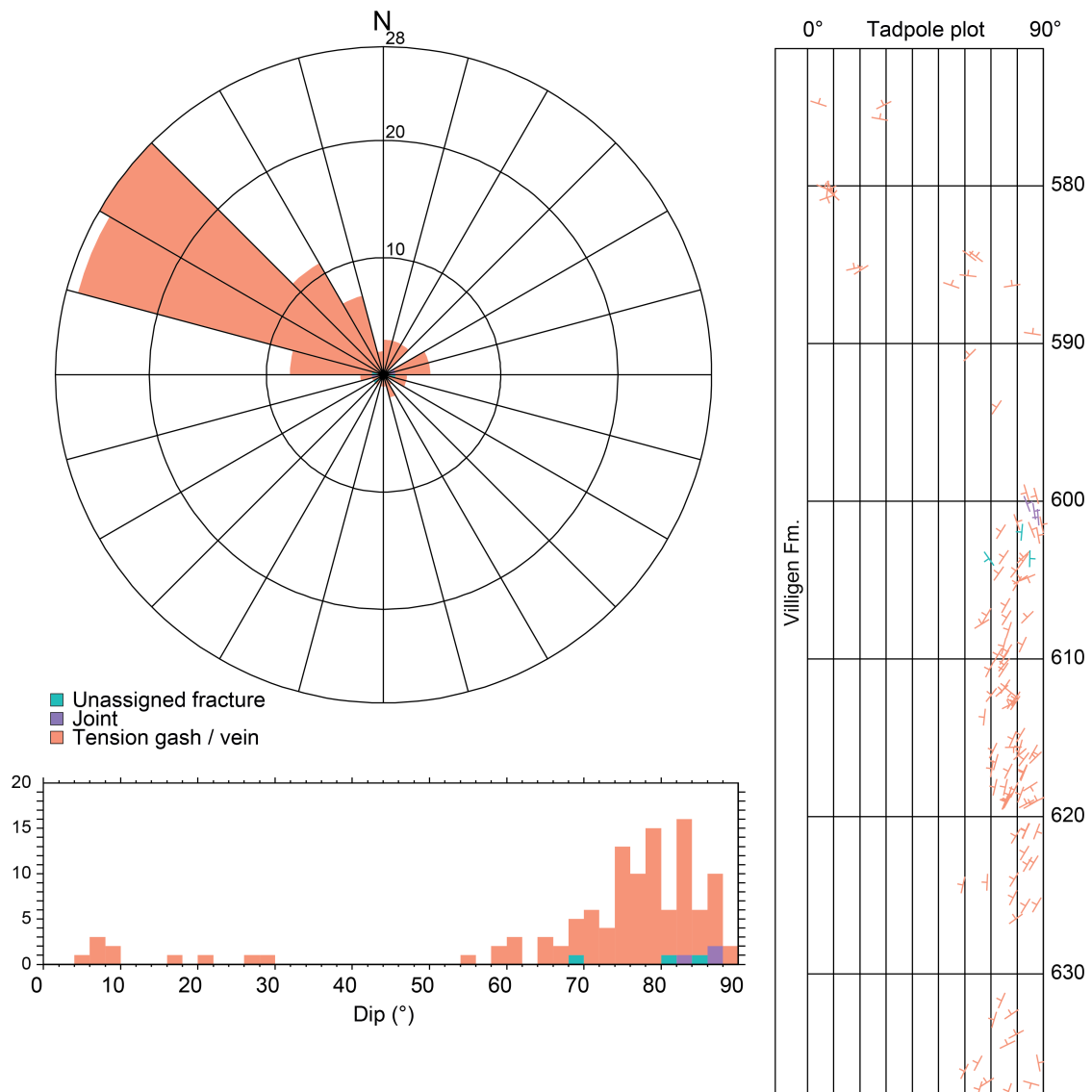


Fig. 4-34: Dip azimuth rose diagram, dip histogram and depth plot of tension gashes / veins, joints and unassigned fractures (Villigen Formation)
 Unassigned fractures (n = 3), joints (n = 3) and tension gashes / veins (n = 108).

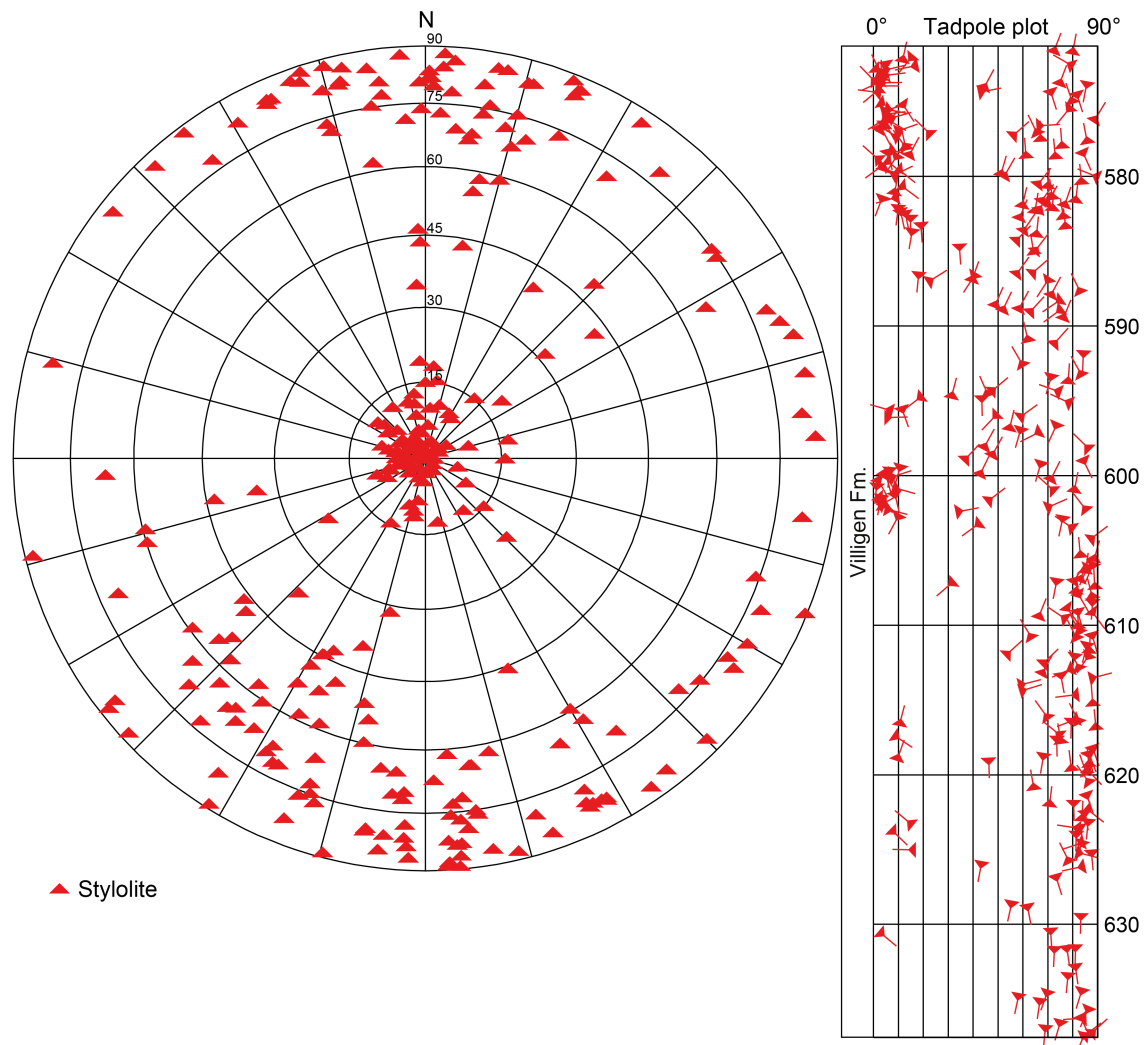


Fig. 4-35: Stereogram and depth plot of stylolites (Villigen Formation, n = 276)

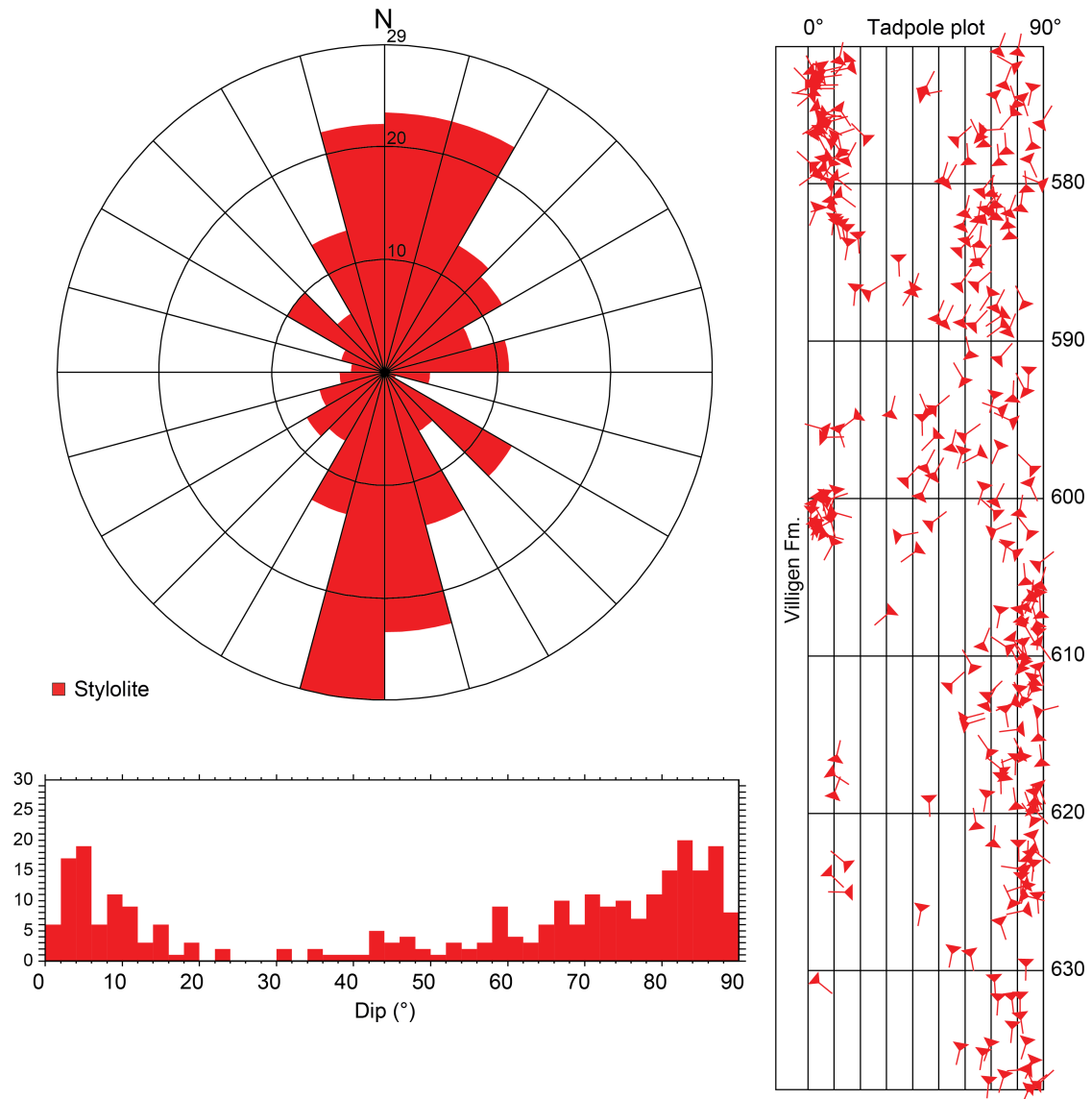


Fig. 4-36: Dip azimuth rose diagram, dip histogram and depth plot of stylolites (Villigen Formation, n = 276)

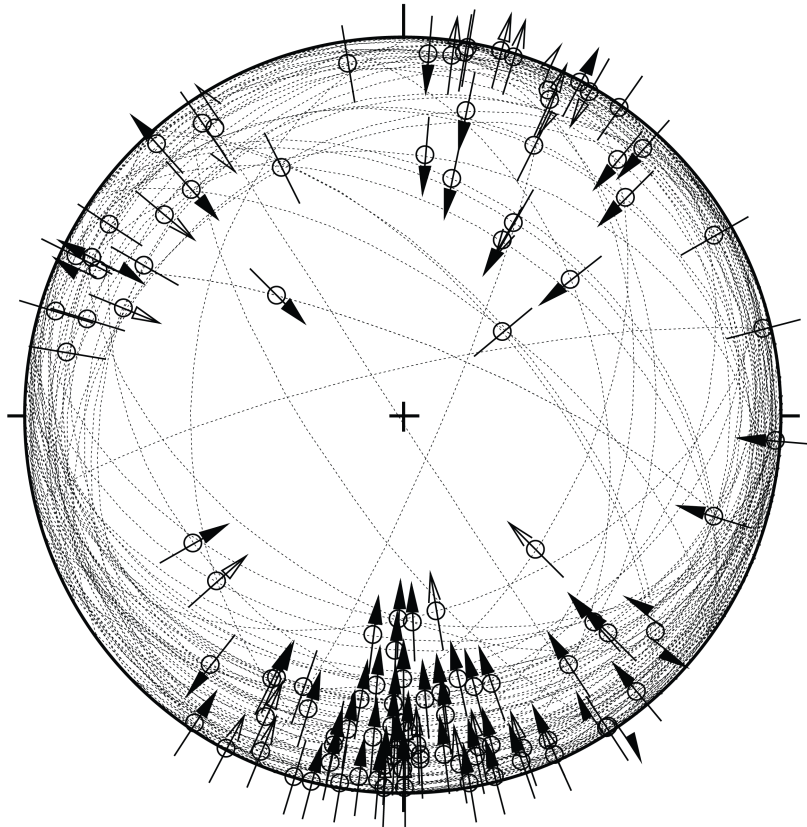


Fig. 4-37: Stereogram of striations on fault planes (including multiple lineations on a single fault plane) (Villigen Formation, $n = 112$)

4.2.4 Wildegg Formation

The orientation and spatial distribution of recorded structures in the Wildegg Formation (637.55 m to 737.32 m MD log depth) are shown below.

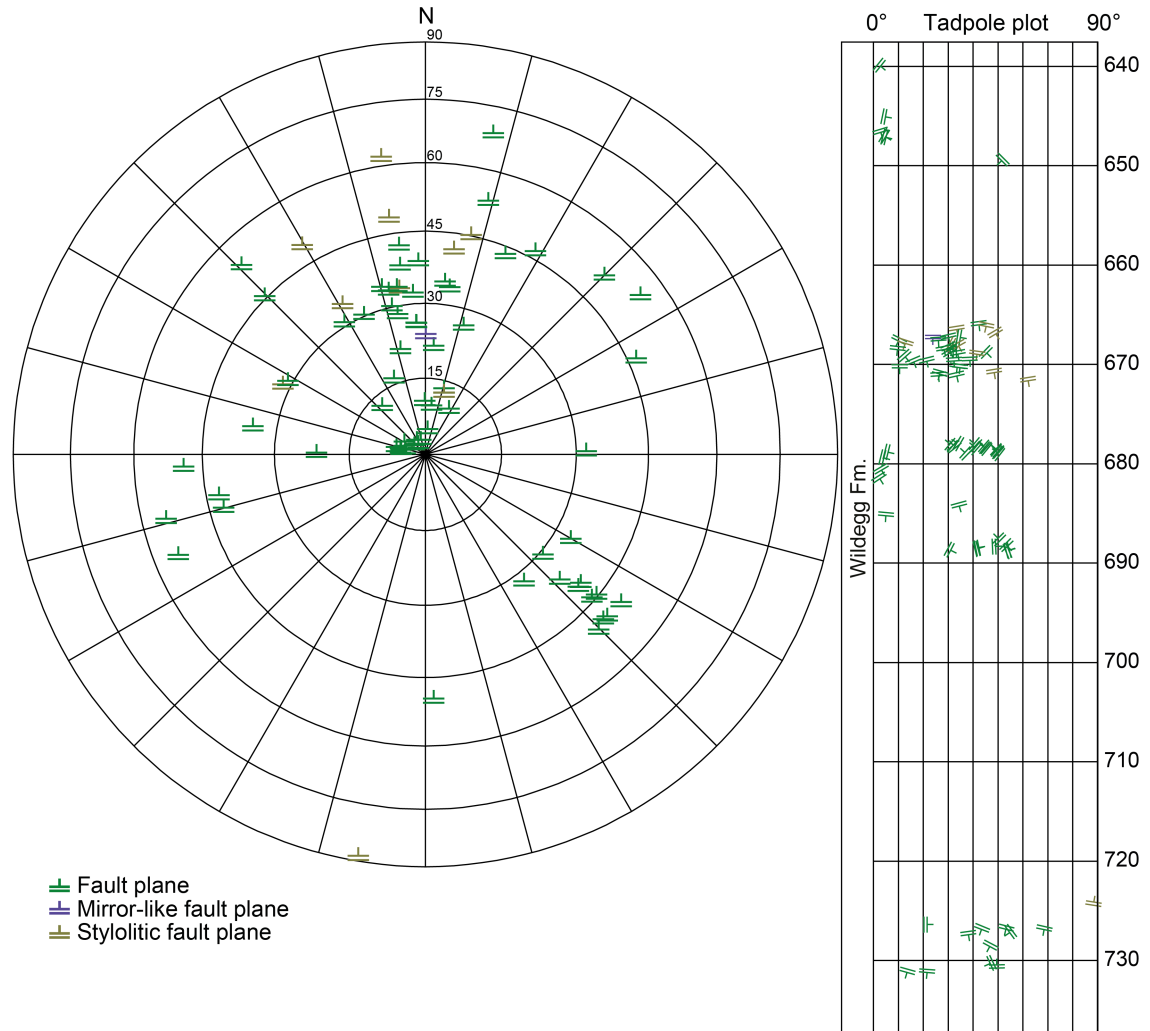


Fig. 4-38: Stereogram and depth plot of fault planes (Wildegg Formation)
 Fault planes (n = 65), mirror-like fault planes (n = 1) and stylolitic fault planes (n = 10).

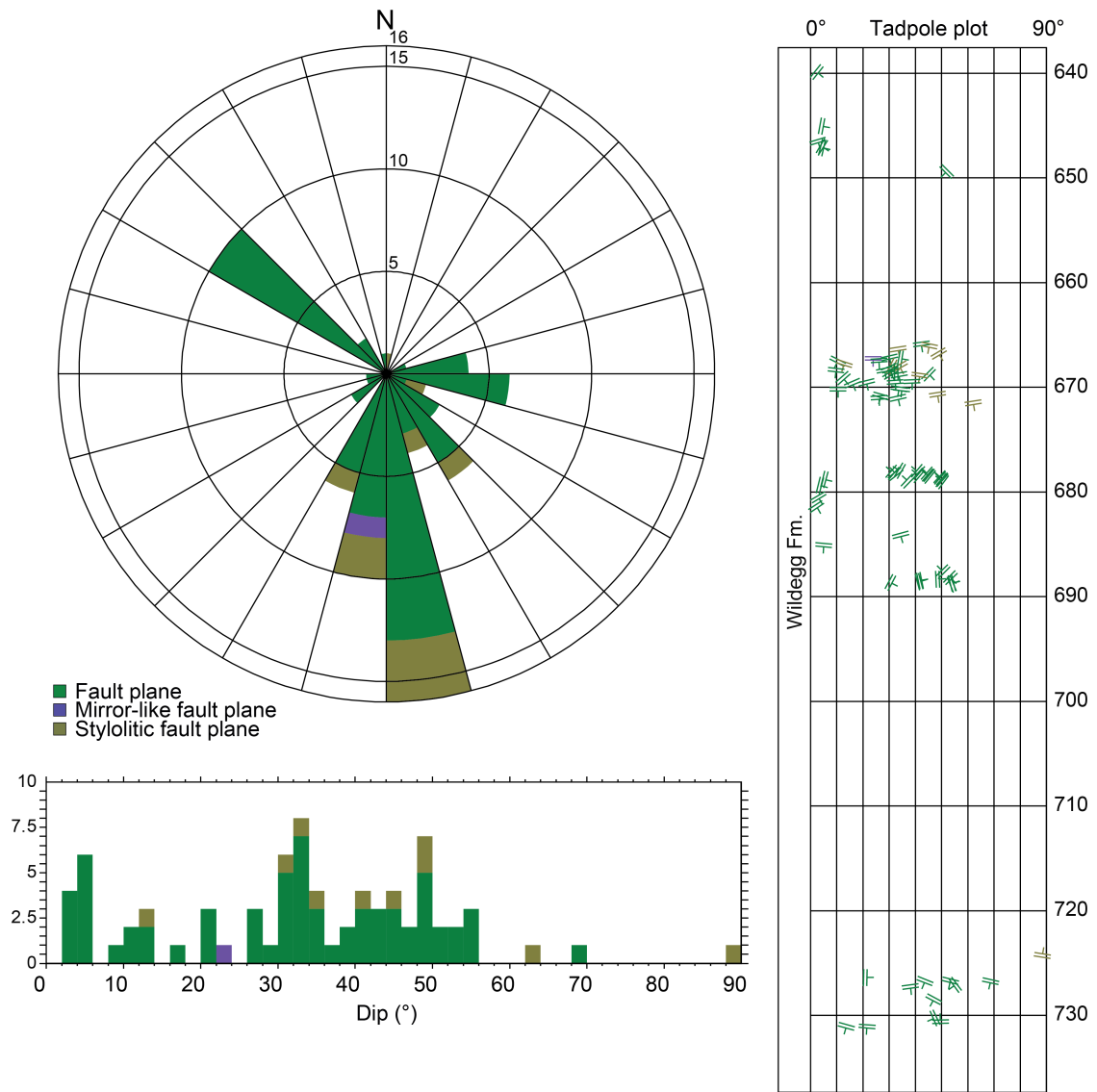


Fig. 4-39: Dip azimuth rose diagram, dip histogram and depth plot of fault planes (Wildegg Formation)

Fault planes (n = 65), mirror-like fault planes (n = 1) and stylolitic fault planes (n = 10).

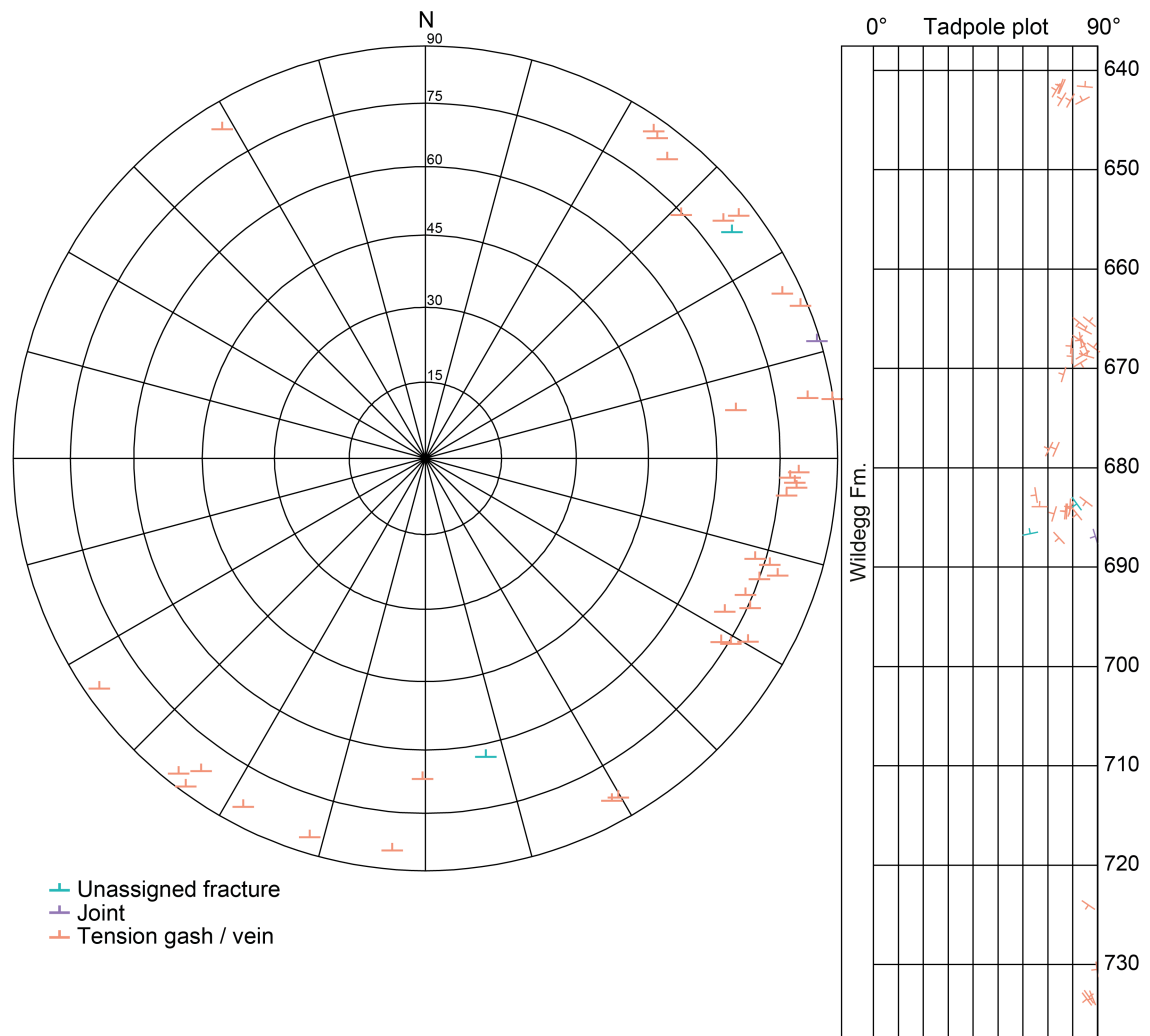


Fig. 4-40: Stereogram and depth plot of tension gashes / veins and unassigned fractures (Wildegge Formation)

Unassigned fractures (n = 2), joints (n = 1) and tension gashes / veins (n = 37).

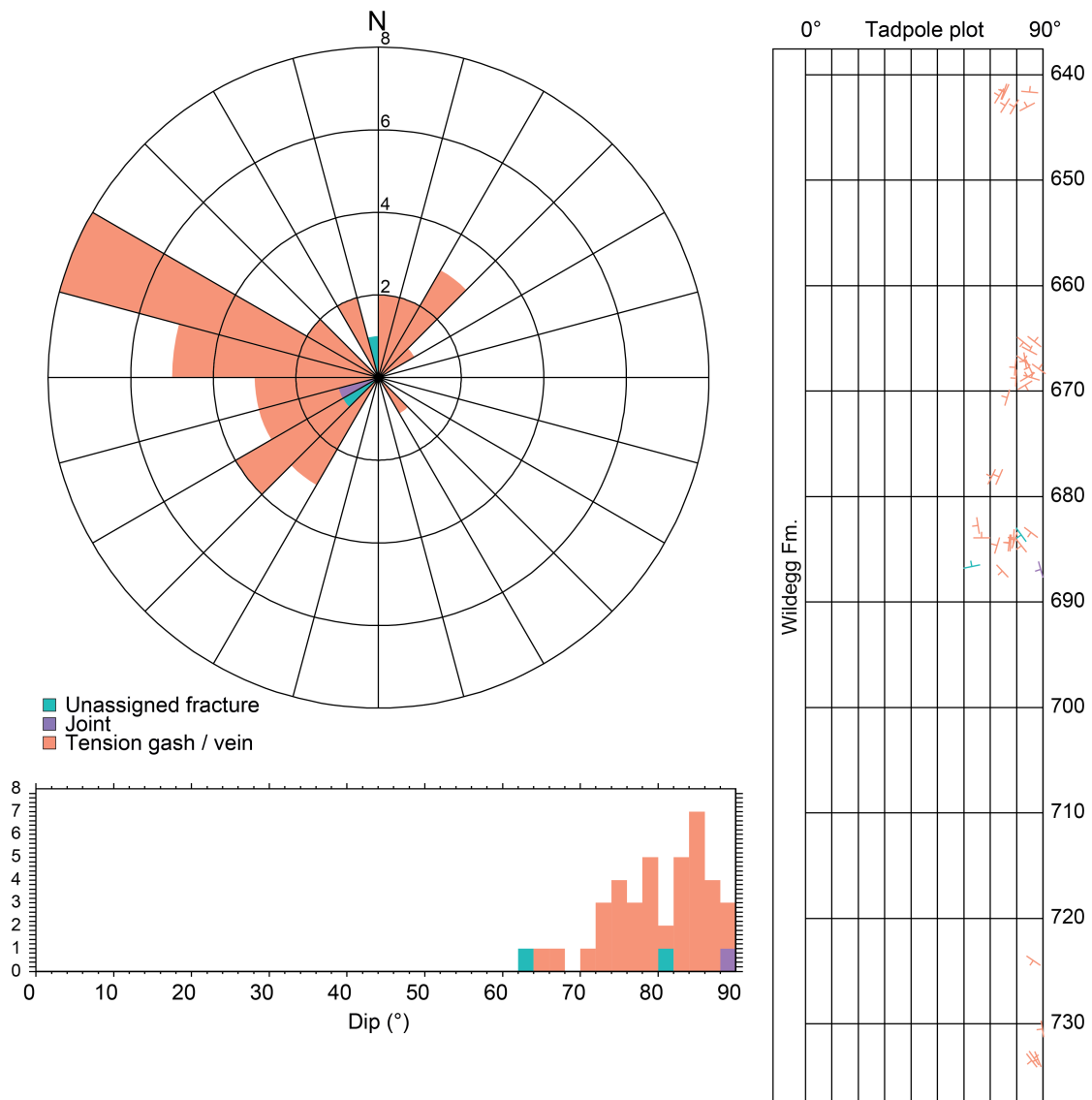


Fig. 4-41: Dip azimuth rose diagram, dip histogram and depth plot of tension gashes / veins, joints and unassigned fractures (Wildegge Formation)

Unassigned fractures (n = 2), joints (n = 1) and tension gashes / veins (n = 37).

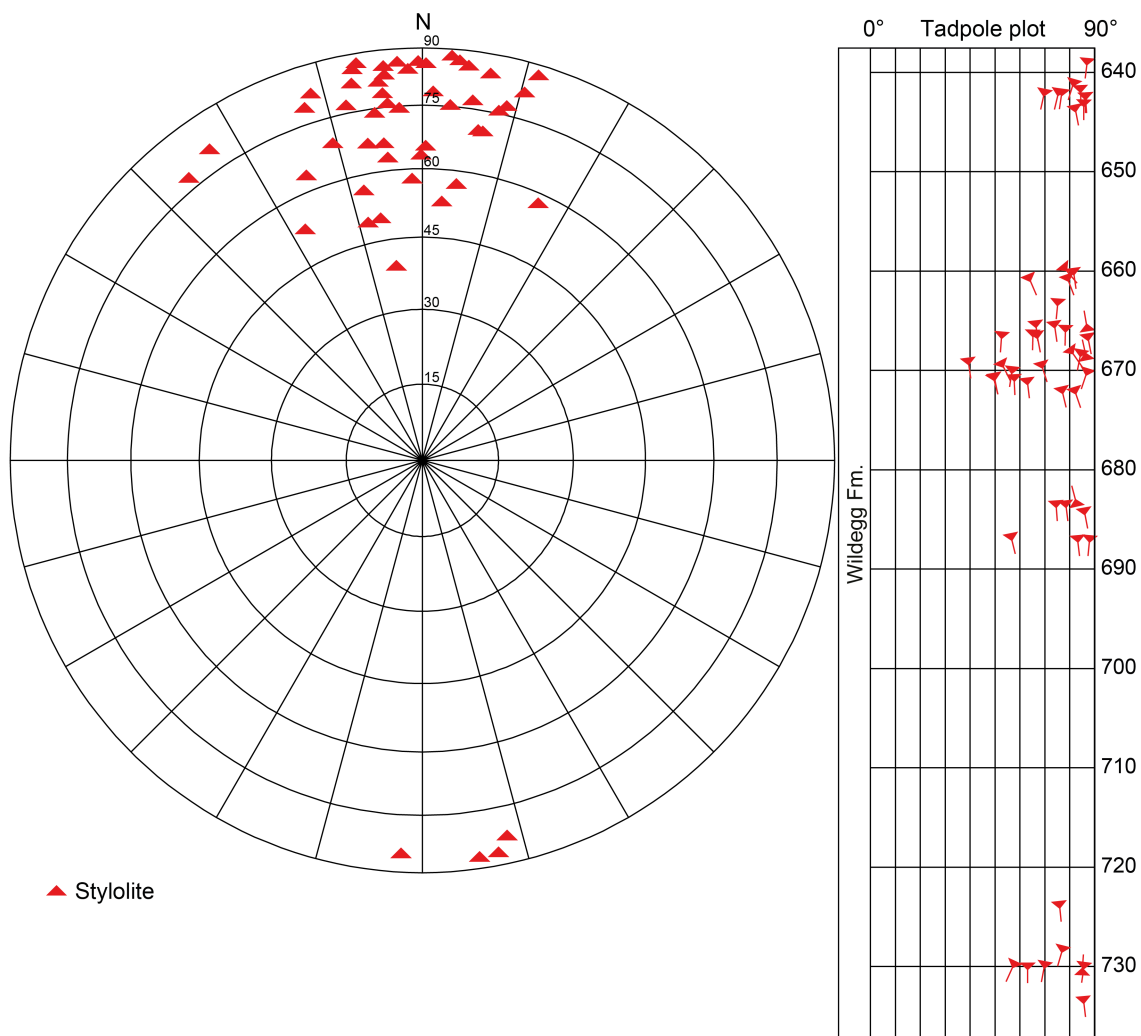


Fig. 4-42: Stereogram and depth plot of stylolites (Wildegg Formation, n = 52)

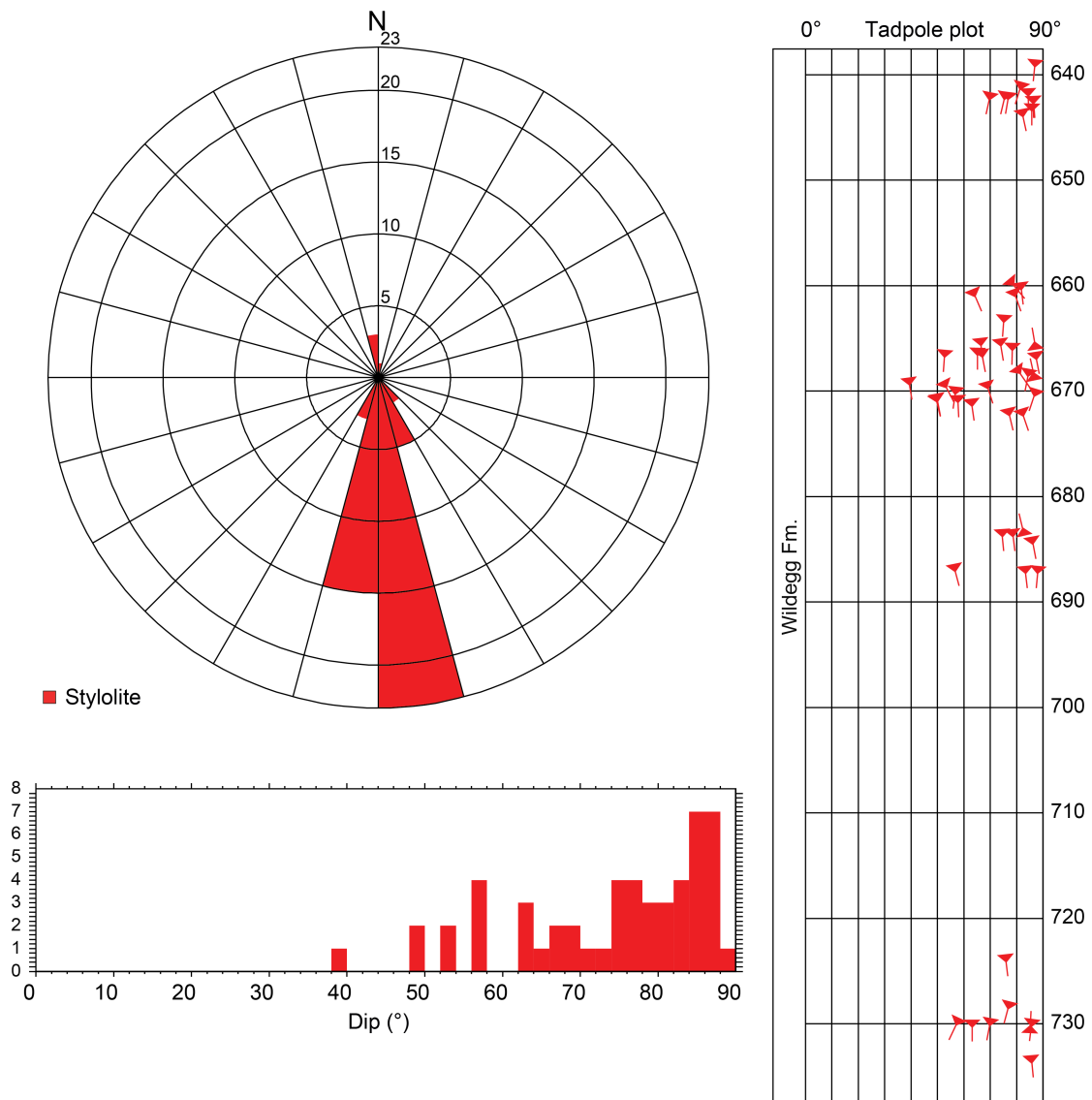


Fig. 4-43: Dip azimuth rose diagram, dip histogram and depth plot of stylolites (Wildegg Formation, n = 52)

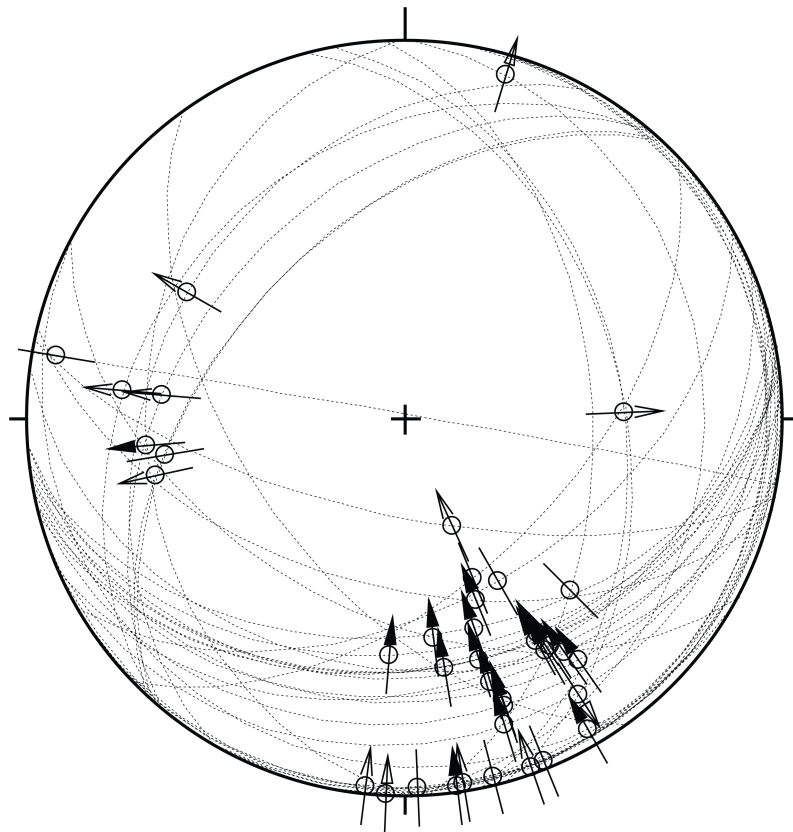


Fig. 4-44: Stereogram of striations on fault planes (including multiple lineations on a single fault plane) (Wildegge Formation, n = 39)

4.3 Dogger

For the detailed stereographic evaluation, the Dogger was subdivided into two units: the «Brauner Dogger» and the Opalinus Clay. The orientation and spatial distribution of recorded structures are shown below. Only the data from oriented cores are presented.

4.3.1 «Brauner Dogger» (Wutach Formation to «Murchisonae-Oolith Formation»)

The «Brauner Dogger» (737.32 m to 808.57 m MD log depth) is an informal lithostratigraphic unit including predominantly claystone-rich lithologies from the Wutach to the «Murchisonae-Oolith Formation». This generally shows a low density of all structure types. The main structures are mirror-like fault planes. Fault planes, tension gashes and stylolites are rare. However, a total of five thick (up to 1.13 m) zones rich in tension gashes have been observed and are concentrated between 803.55 m and 807.88 m MD (log depth). Stylolitic fault planes, joints and unassigned fractures were not observed. The mirror-like fault planes dip towards the SE. The striations dip predominantly towards the S or N. Reverse faulting dominates.

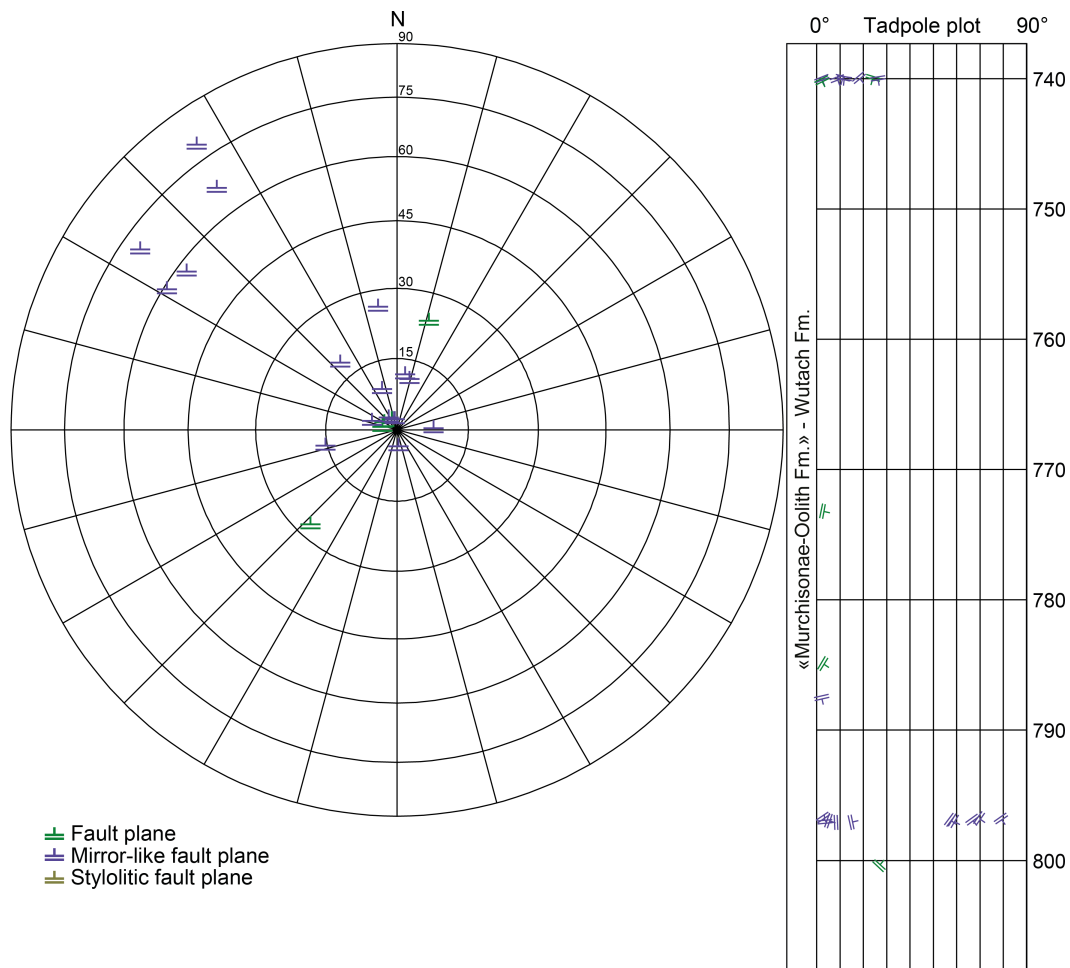


Fig. 4-45: Stereogram and depth plot of fault planes («Brauner Dogger») Fault planes (n = 5) and mirror-like fault planes (n = 17); no stylolitic fault planes were observed (n = 0).

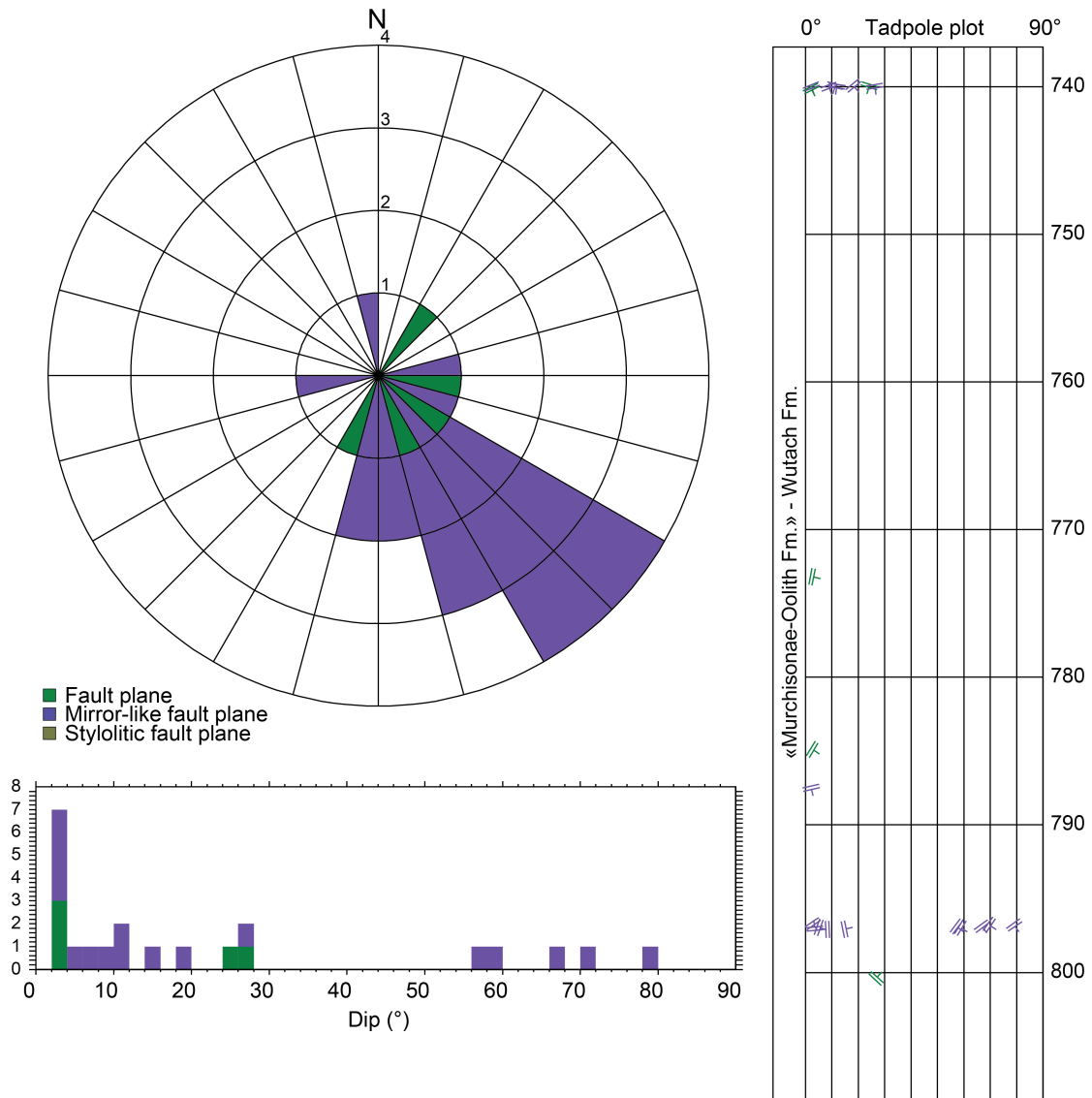


Fig. 4-46: Dip azimuth rose diagram, dip histogram and depth plot of fault planes («Brauner Dogger»)

Fault planes (n = 5) and mirror-like fault planes (n = 17); no styloitic fault planes were observed (n = 0).

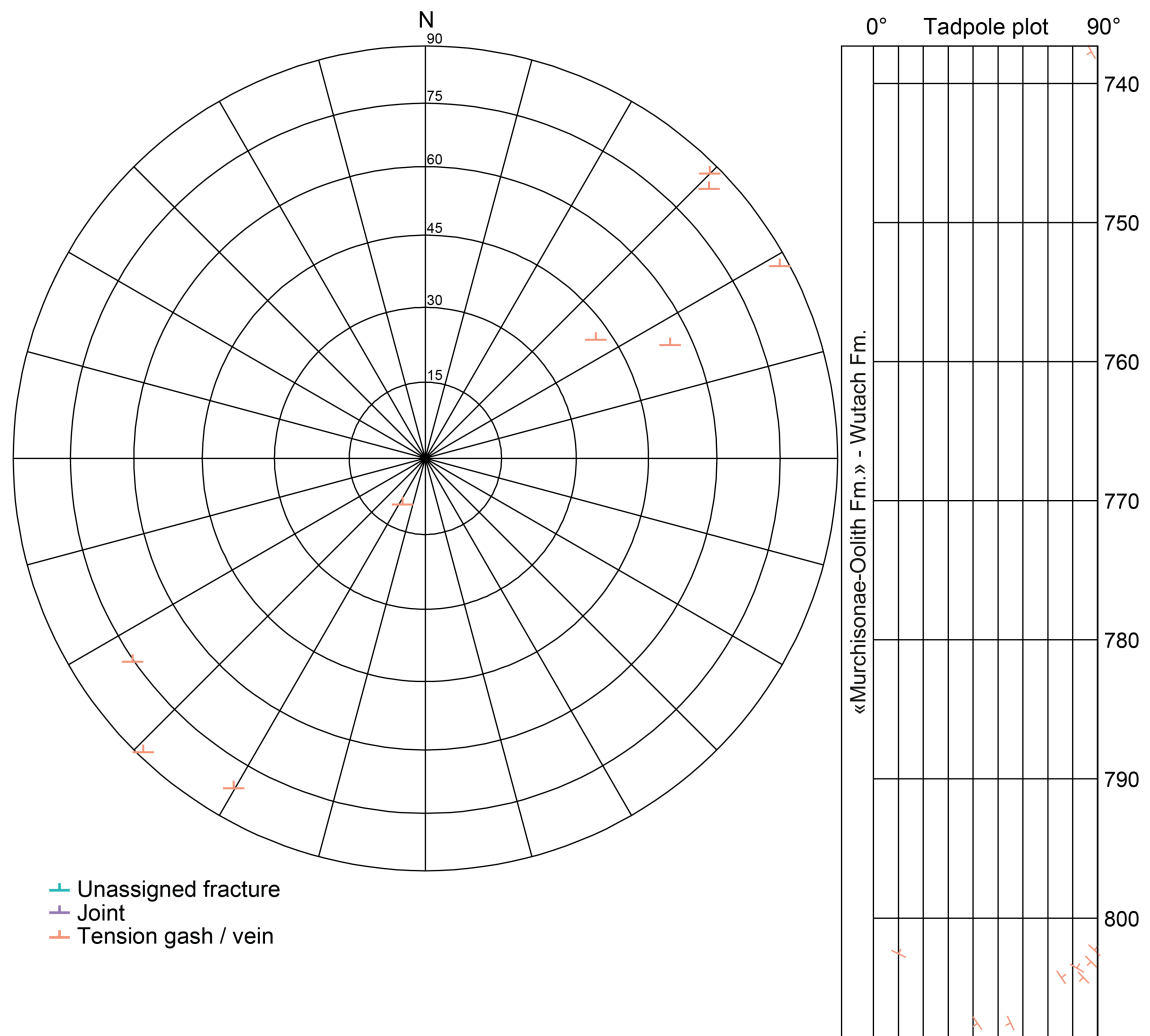


Fig. 4-47: Stereogram and depth plot of tension gashes / veins, joints and unassigned fractures («Brauner Dogger»)

Tension gashes / veins (n = 9); no unassigned fractures or joints were observed (n = 0).

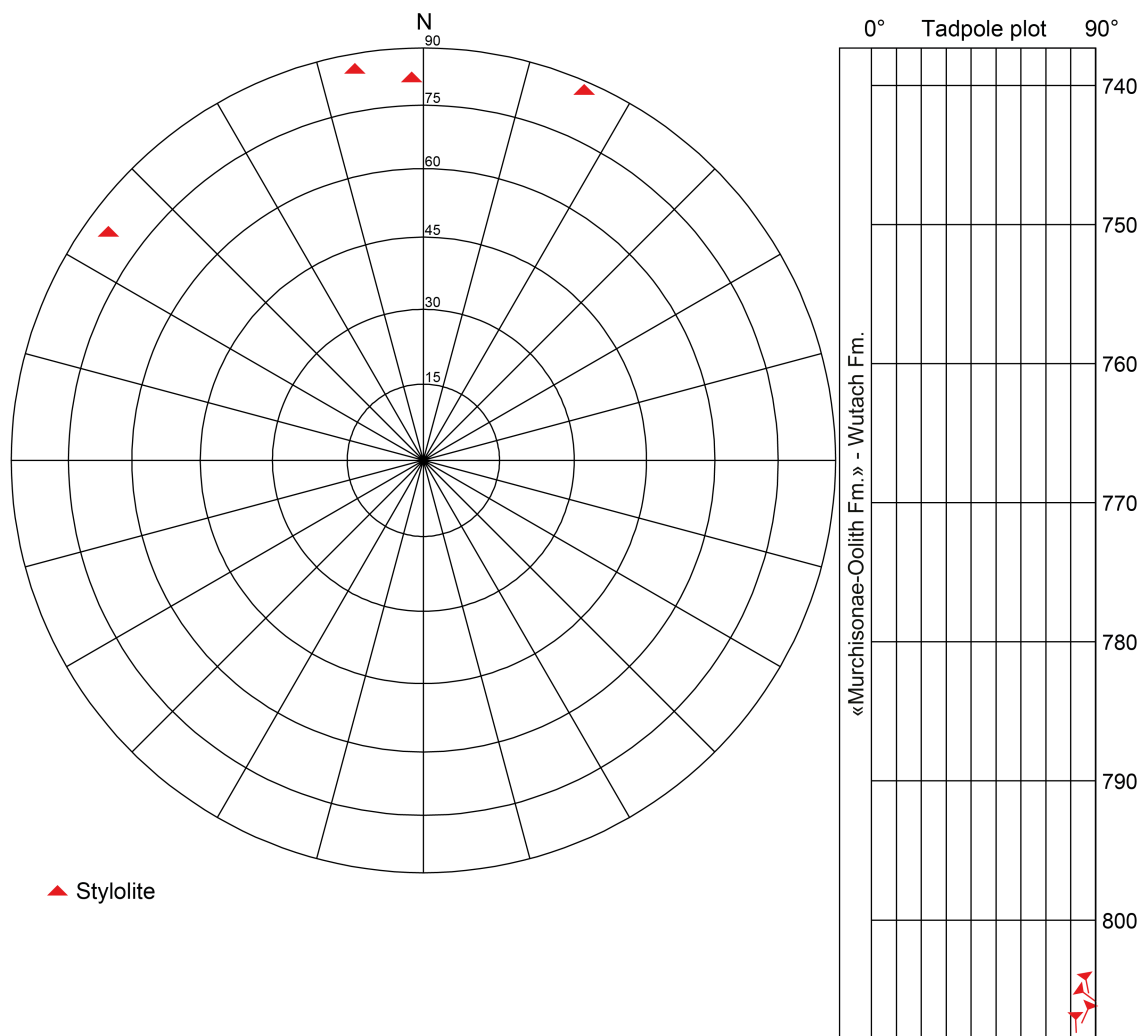


Fig. 4-48: Stereogram and depth plot of stylolites («Brauner Dogger», n = 4)

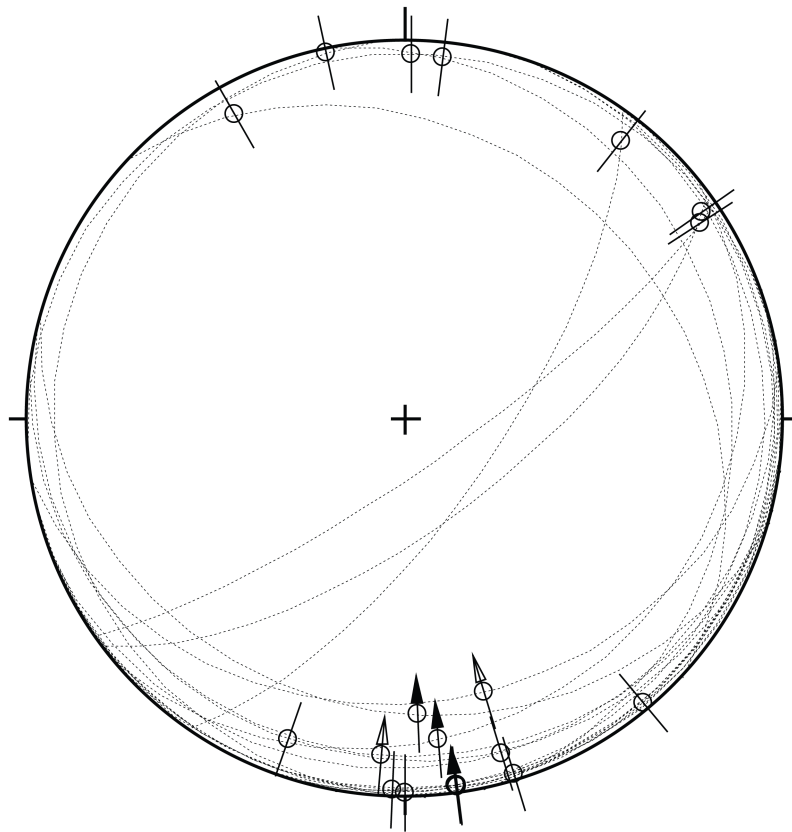


Fig. 4-49: Stereogram of striations on fault planes (including multiple lineations on a single fault plane) («Brauner Dogger», $n = 20$)

4.3.2 Opalinus Clay

The Opalinus Clay (808.57 m to 915.30 m MD log depth) reveals a low density of fault planes, mirror-like fault planes and tension gashes. Stylolitic fault planes, unassigned fractures and stylolites were not observed. Only one joint was found. The fault planes and tension gashes are often concentrated within thin zones, e.g. in the prominent 0.53 m thick fault zone between 911.53 m and 912.16 m MD (log depth). Tension gashes generally dip towards the E or S, their dip angle varies from subhorizontal to subvertical. In drill cores they often show fibrous calcite mineralisation with mineral grains oriented normal to the fracture plane.

The fault planes show shallow to steep dip angles. Most of the fault planes dip towards the NE. Reverse shear senses dominate, with striations predominantly plunging to the S. Fault planes are often characterised by synkinematic calcite fillings, which are commonly less than 1 mm thick.

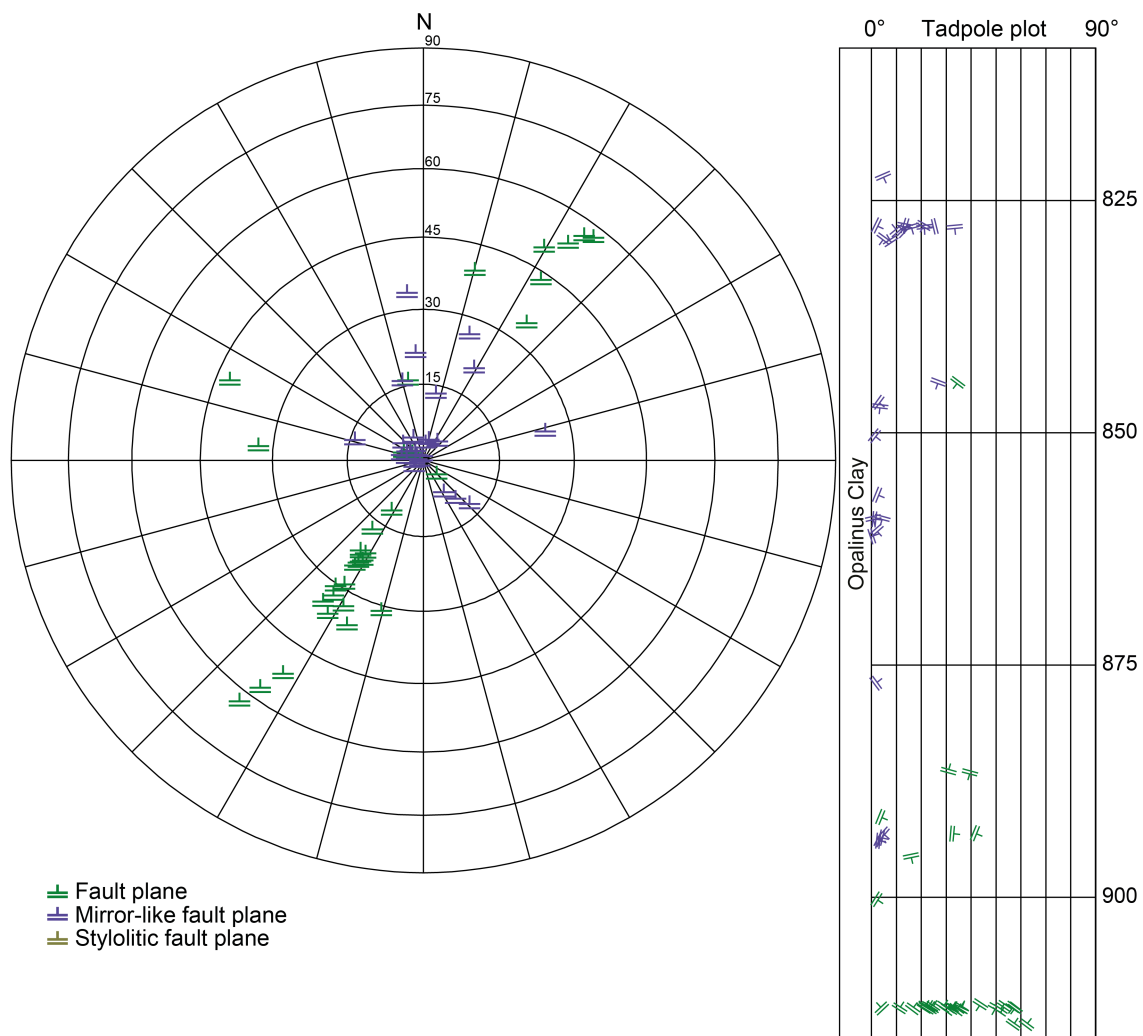


Fig. 4-50: Stereogram and depth plot of fault planes (Opalinus Clay)
 Fault planes (n = 32) and mirror-like fault planes (n = 28); no stylolitic fault planes were observed (n = 0).

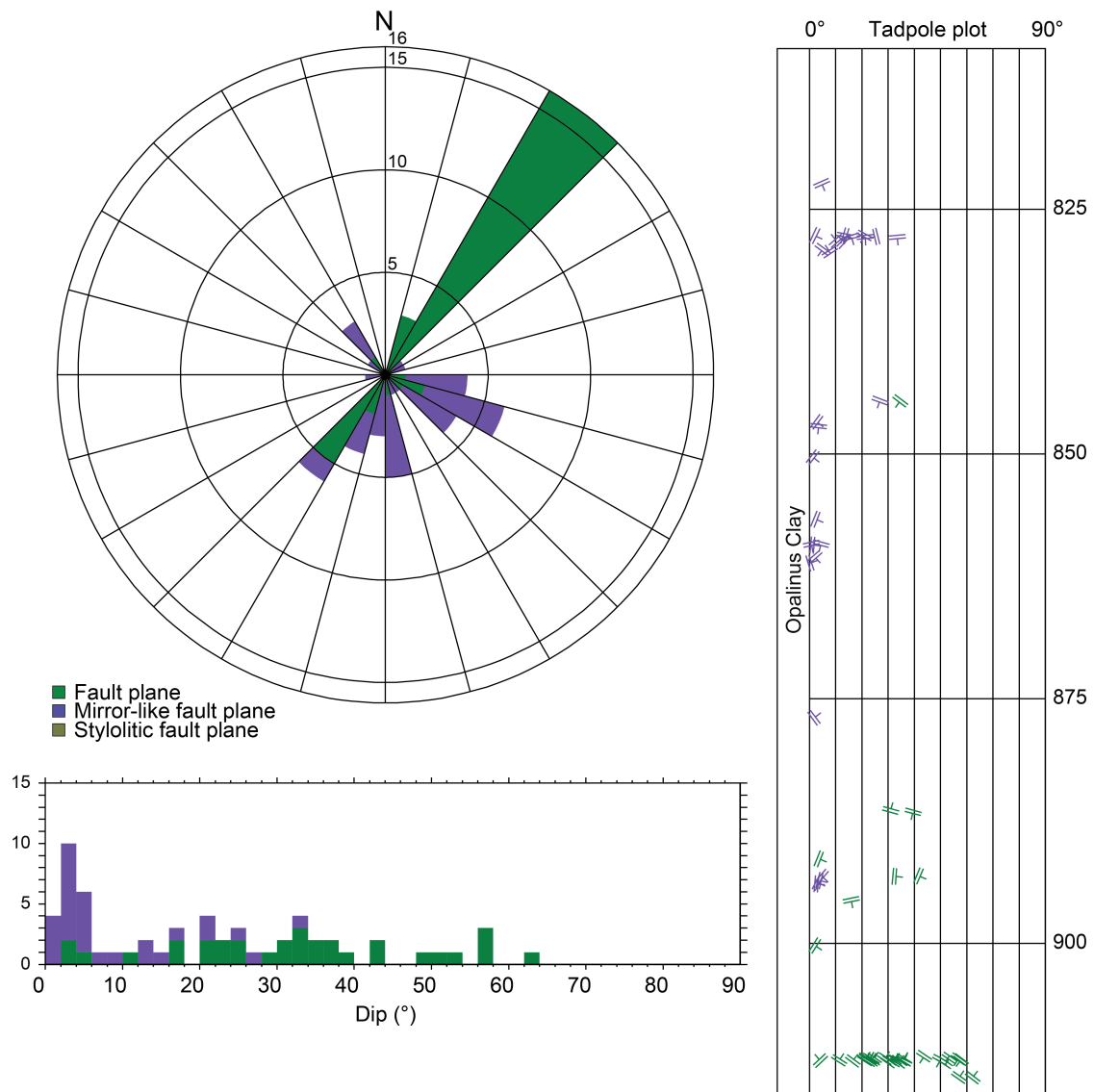


Fig. 4-51: Dip azimuth rose diagram, dip histogram and depth plot of fault planes (Opalinus Clay)

Fault planes (n = 32) and mirror-like fault planes (n = 28); no styloitic fault planes were observed (n = 0).

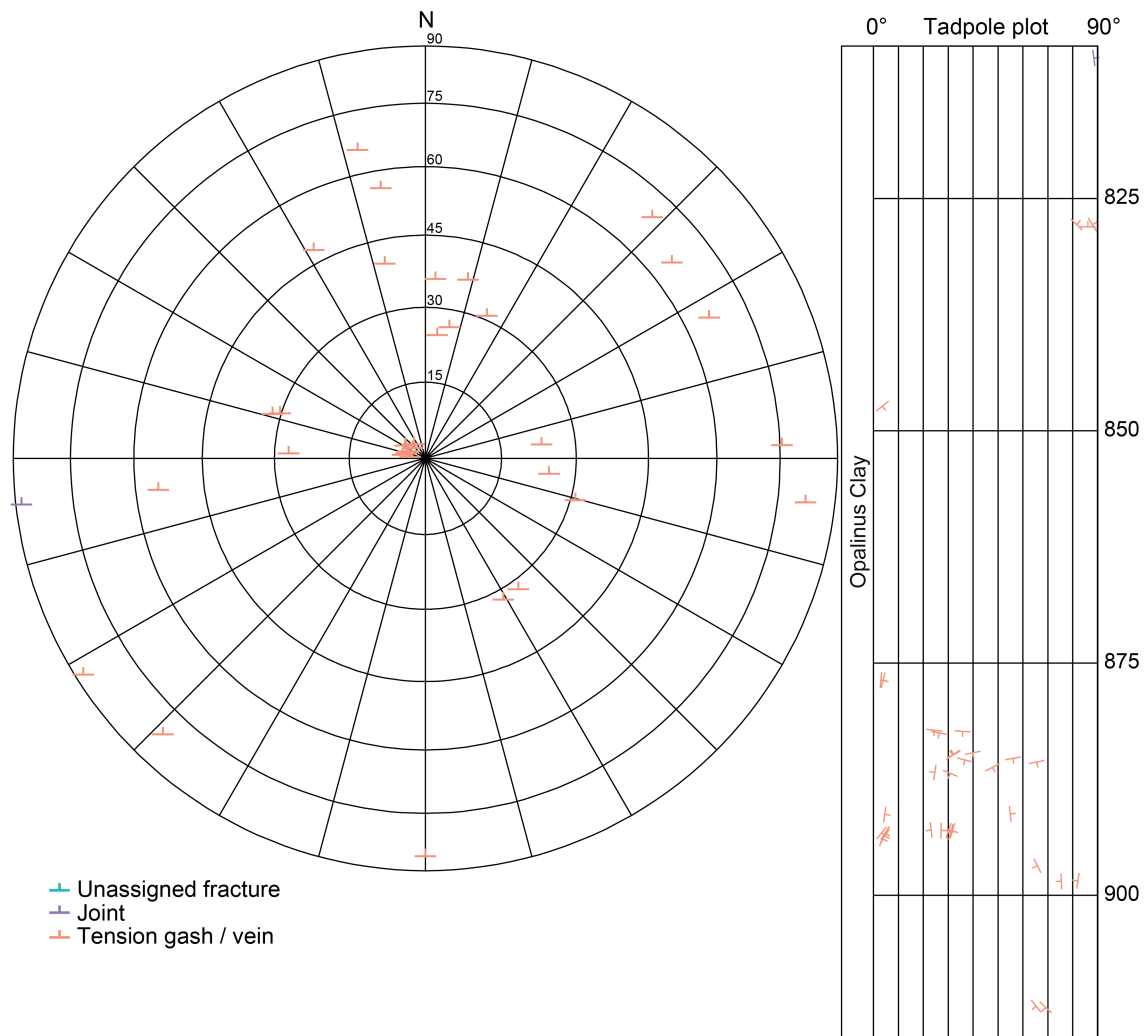


Fig. 4-52: Stereogram and depth plot of tension gashes / veins, joints and unassigned fractures (Opalinus Clay)
 Joints (n = 1) and tension gashes / veins (n = 34); no unassigned fractures were observed (n = 0).

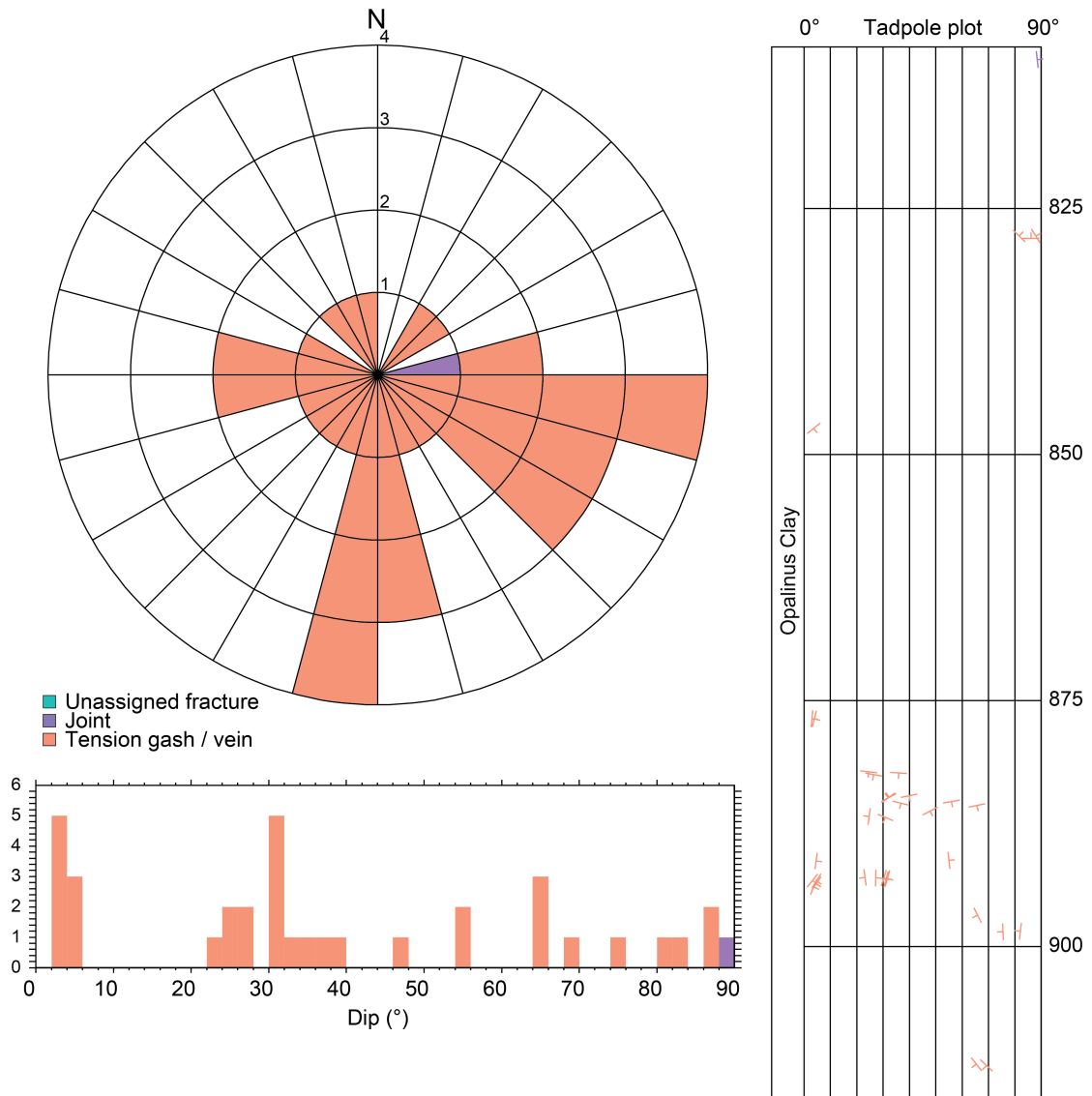


Fig. 4-53: Dip azimuth rose diagram, dip histogram and depth plot of tension gashes / veins, joints and unassigned fractures (Opalinus Clay)

Joints (n = 1) and tension gashes / veins (n = 34); no unassigned fractures were observed (n = 0).

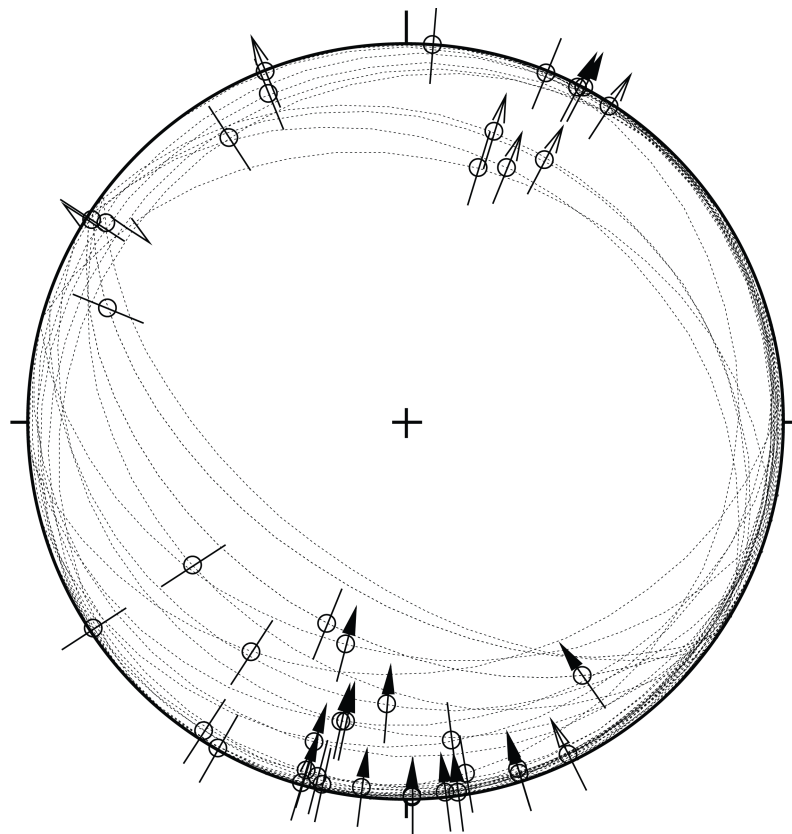


Fig. 4-54: Stereogram of striations on fault planes (including multiple lineations on a single fault plane) (Opalinus Clay, n = 41)

4.4 Lias (Staffelegg Formation)

As presented below, the Lias (915.30 m to 950.07 m MD log depth) is characterised by a low fracture density. The dominant structure types are subhorizontal, mirror-like fault planes and steeply dipping tension gashes. Note that the mirror-like fault planes are not shown in Fig. 4-55 because several core intervals are not oriented. All other fault plane types, joints, stylolites and unassigned fractures were rare or not observed. Striations plunge either towards the SE or towards the NW. Only the data from oriented cores are presented.

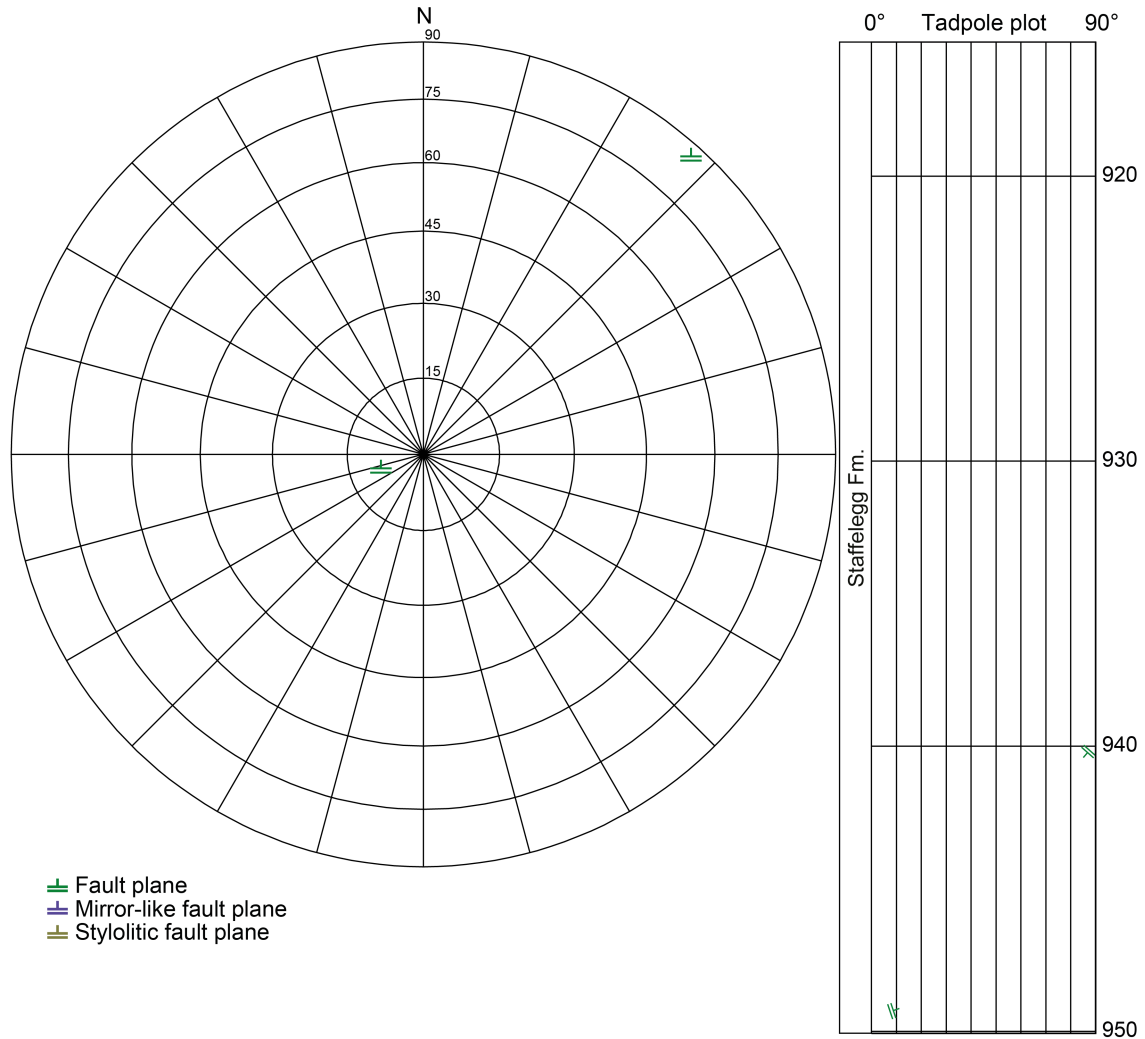


Fig. 4-55: Stereogram and depth plot of fault planes (Lias)
 Fault planes (n = 2); no mirror-like fault planes or stylolitic fault planes were observed (n = 0).

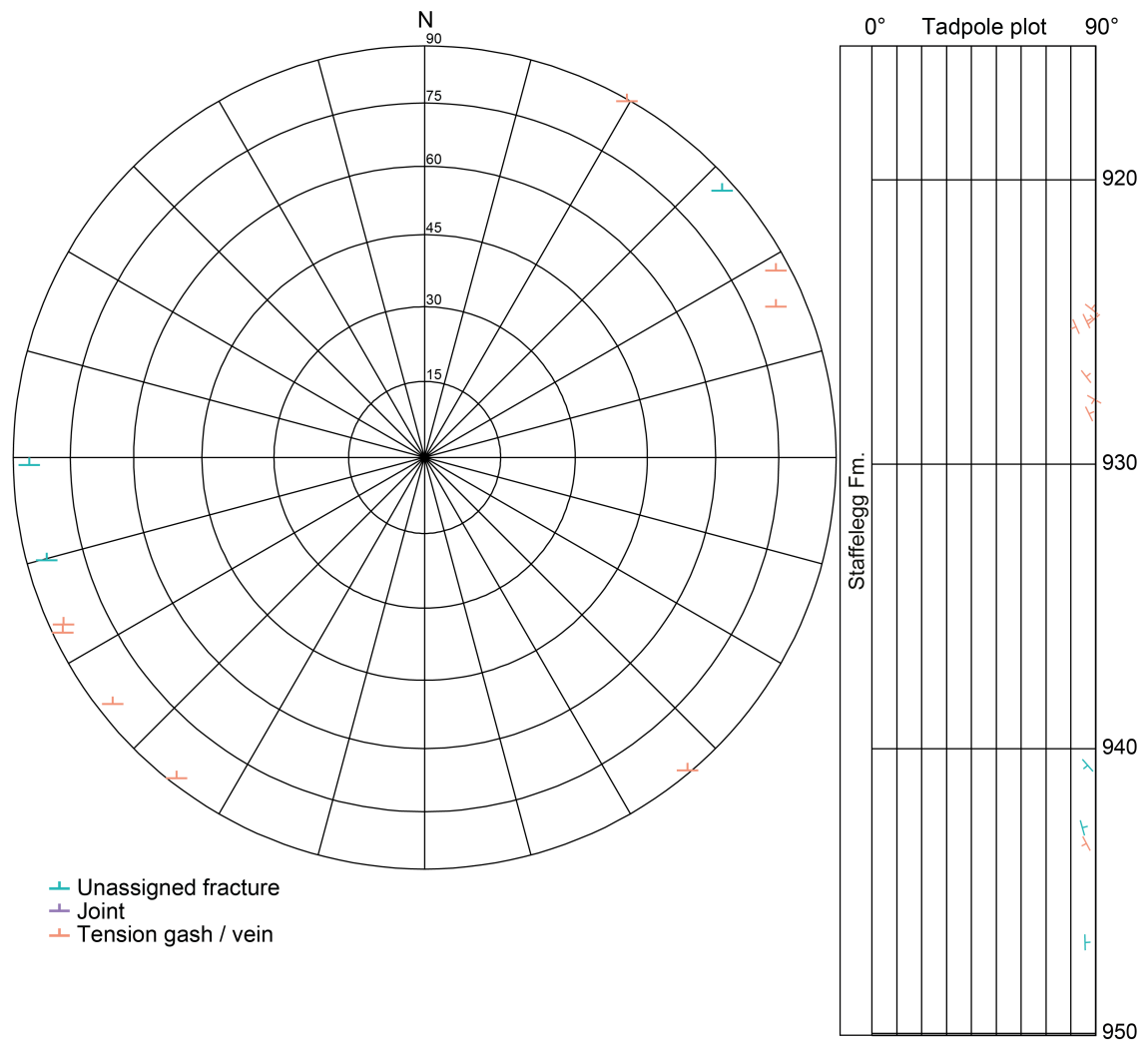


Fig. 4-56: Stereogram and depth plot of tension gashes / veins, joints and unassigned fractures (Lias)
 Unassigned fractures (n = 3) and tension gashes / veins (n = 8); no joints were observed (n = 0).

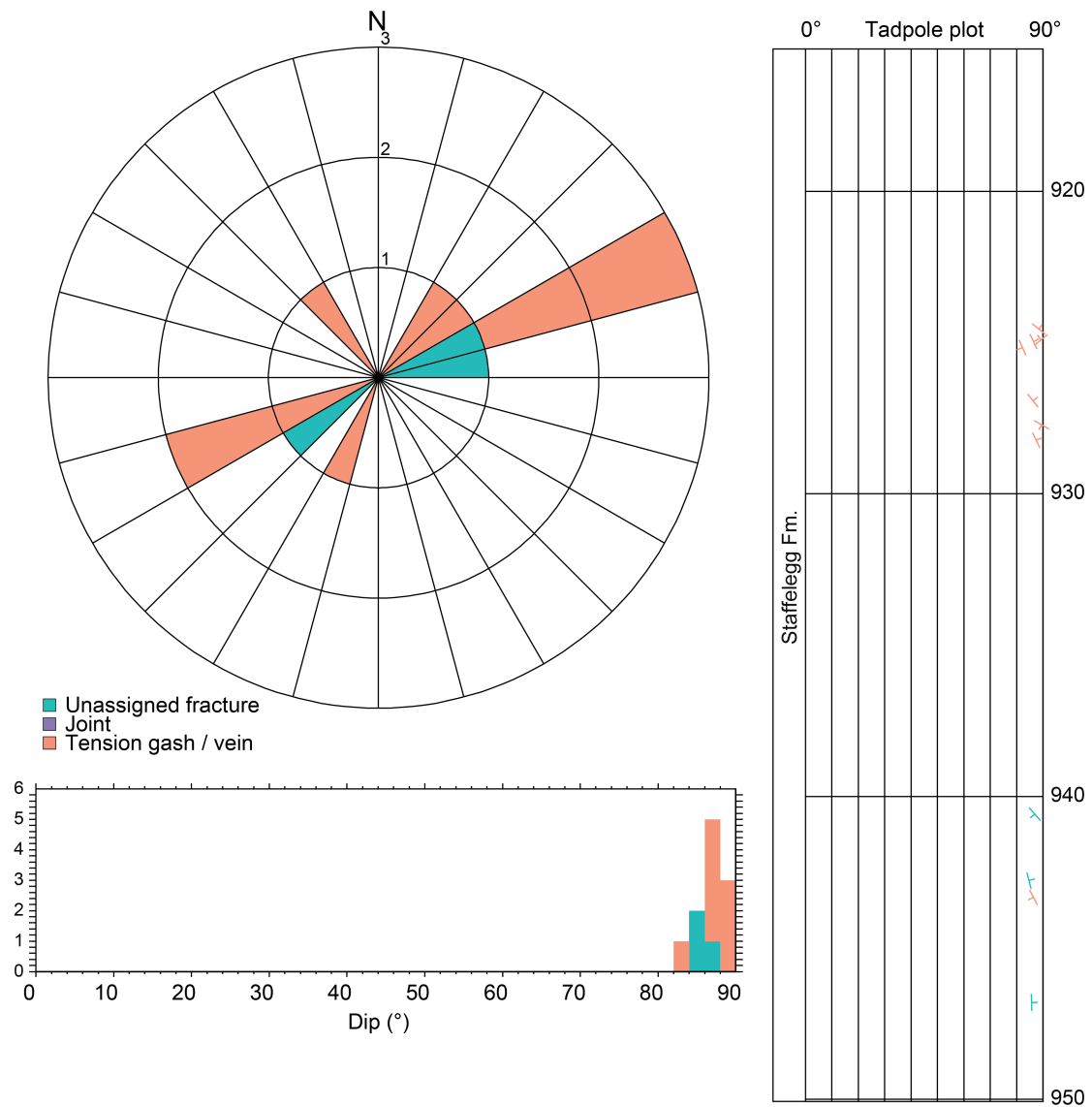


Fig. 4-57: Dip azimuth rose diagram, dip histogram and depth plot of tension gashes / veins, joints and unassigned fractures (Lias)

Unassigned fractures (n = 3) and tension gashes / veins (n = 8); no joints were observed (n = 0).

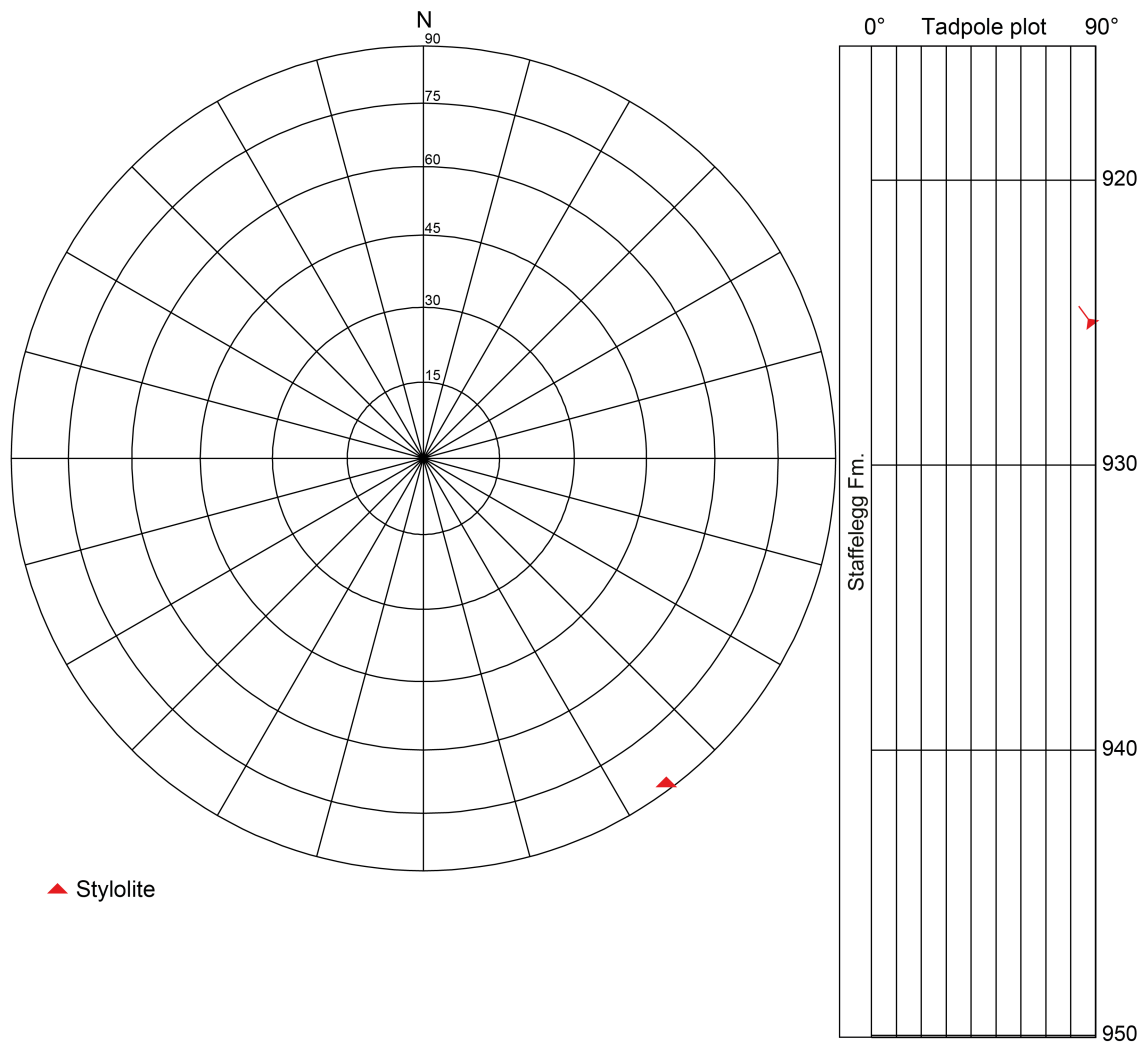


Fig. 4-58: Stereogram and depth plot of stylolites (Lias, n = 1)

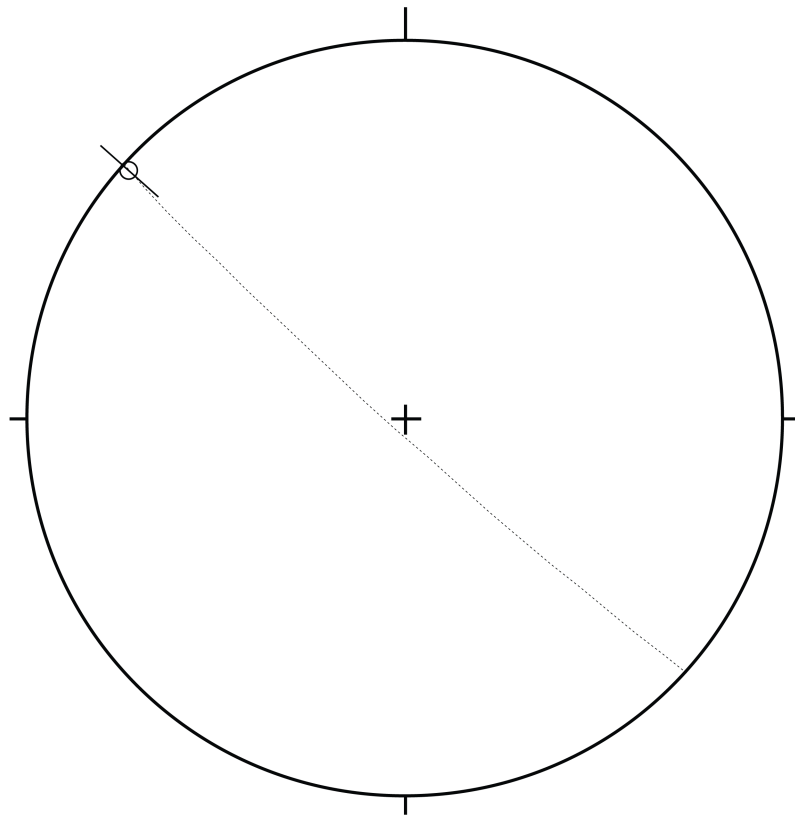


Fig. 4-59: Stereogram of striation on a single ($n = 1$) fault plane in the Lias

4.5 Keuper

The Keuper (950.07 m to 1'054.30 m MD log depth) revealed the highest average fracture density of 4.0 fractures per metre. Mirror-like fault planes, fault planes and tension gashes / veins prevail. The latter are mainly found within the Bänkerjoch Formation and show scattered orientations. Only the data from oriented cores are presented.

5.5.1 Klettgau Formation

In the Klettgau Formation (950.07 m to 981.27 m MD log depth), fault planes and mirror-like fault planes are the dominant fracture types. They are scattered throughout the interval. Note that not all structures are shown in Fig. 4-60 because several m-long core intervals could not be oriented. The fault planes show random orientations with a weak predominance of NE and SW dipping structures. The dip angles are mostly shallow to steep (10° to 60°). The striations are randomly oriented. Shear sense indicators were generally not recognised. Unassigned fractures are rare. Stylolitic fault planes, tension gashes / veins, joints and stylolites were absent.

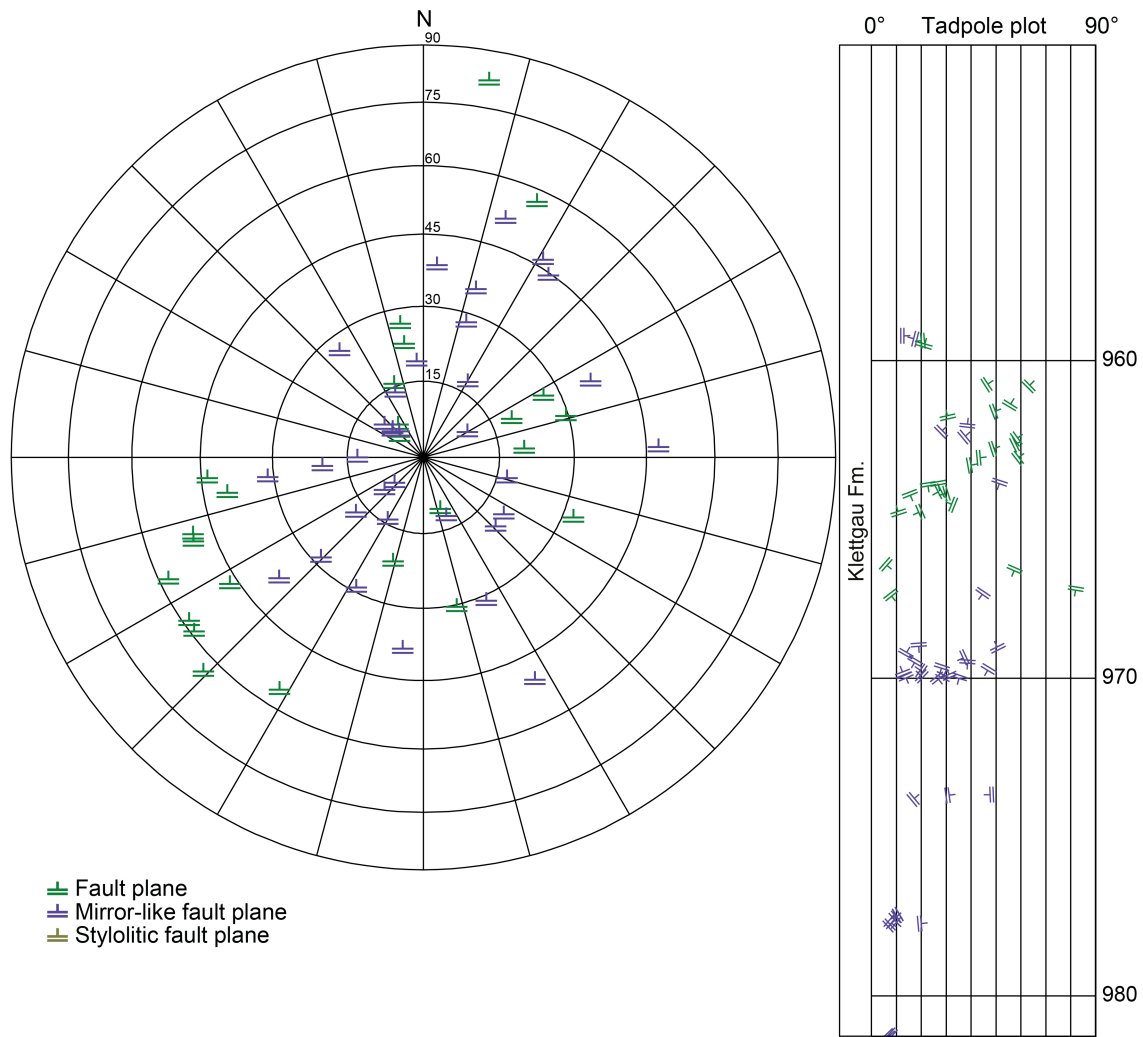


Fig. 4-60: Stereogram and depth plot of fault planes (Klettgau Formation)
Fault planes (n = 25) and mirror-like fault planes (n = 35); no stylolitic fault planes were observed (n = 0).

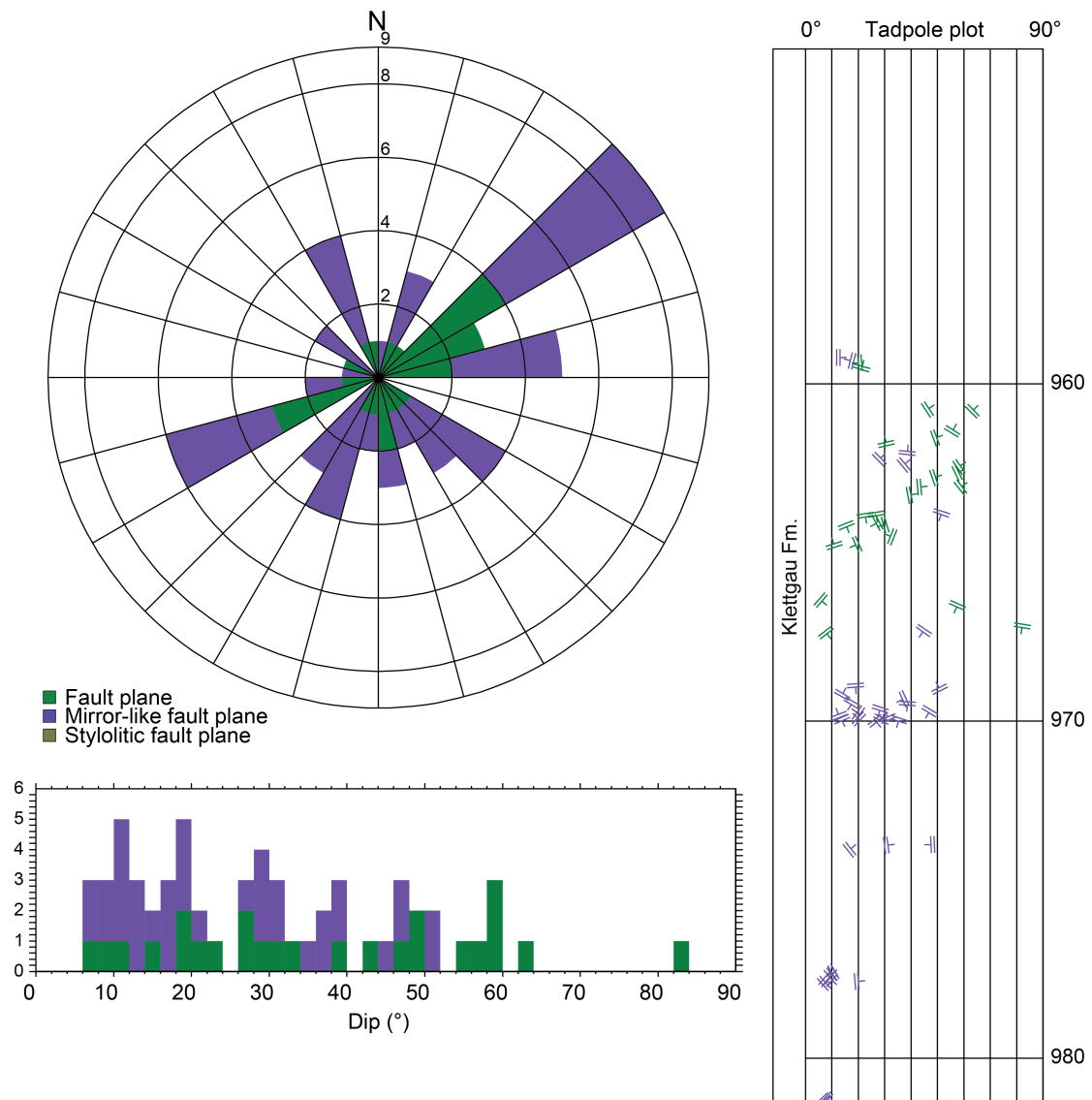


Fig. 4-61: Dip azimuth rose diagram, dip histogram and depth plot of faults (Klettgau Formation)

Fault planes (n = 25) and mirror-like fault planes (n = 35); no styloitic fault planes were observed (n = 0).

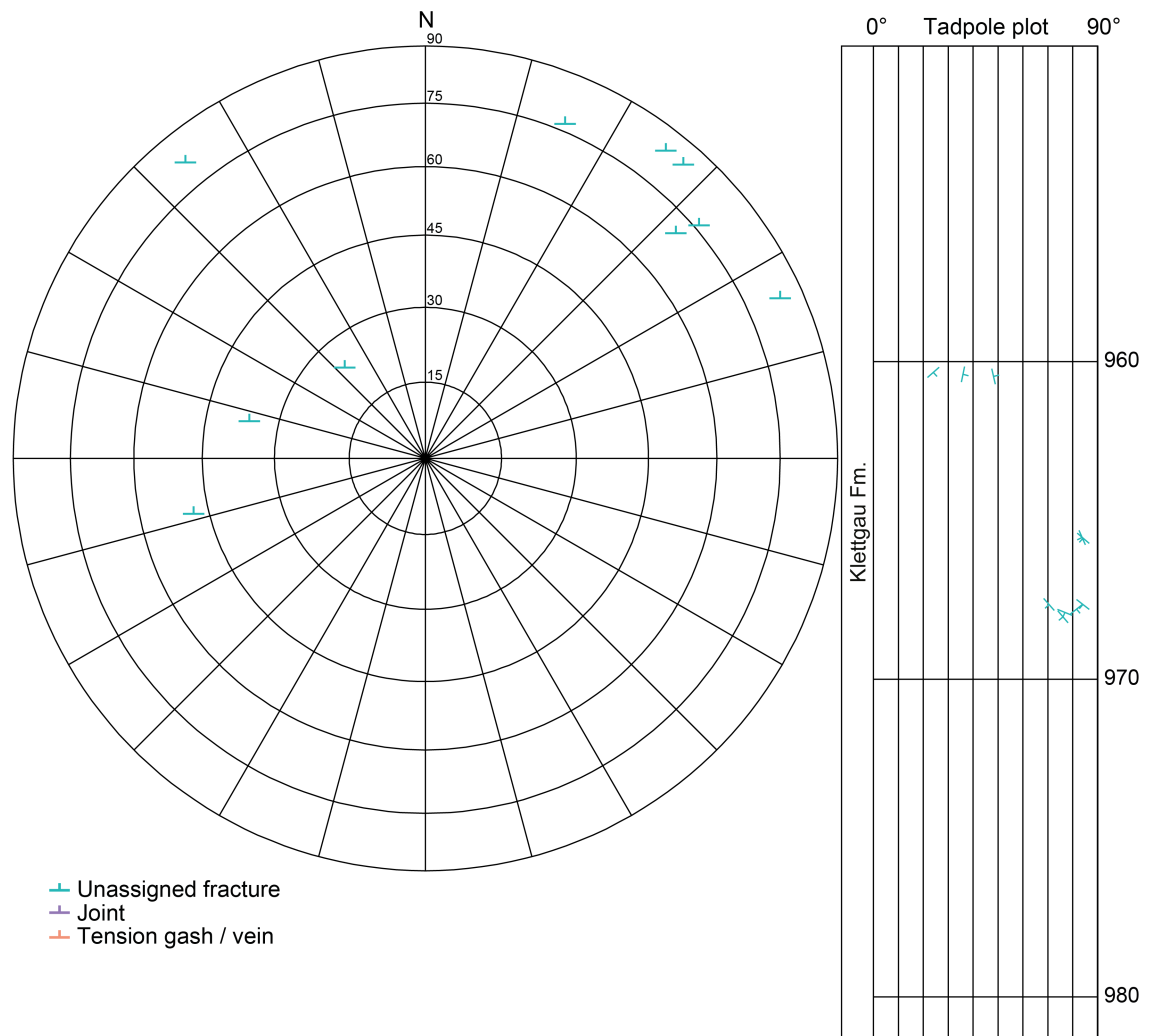


Fig. 4-62: Stereogram and depth plot of tension gashes / veins, joints and unassigned fractures (Klettgau Formation)

Unassigned fractures (n = 10); no joints or tension gashes / veins were observed (n = 0).

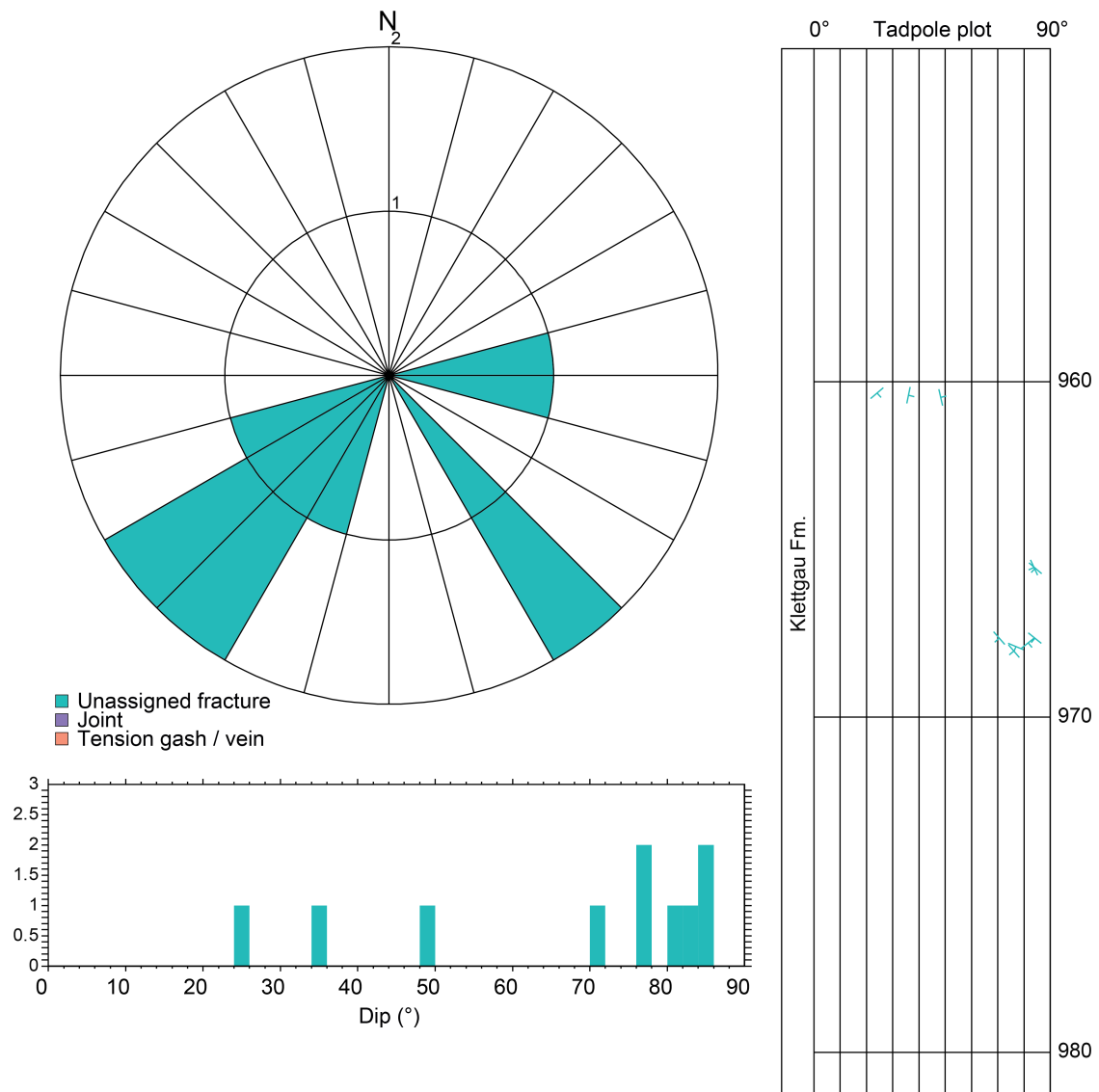


Fig. 4-63: Dip azimuth rose diagram, dip histogram and depth plot of tension gashes / veins, joints and unassigned fractures (Klettgau Formation)

Unassigned fractures (n = 10); no joints or tension gashes / veins were observed (n = 0).

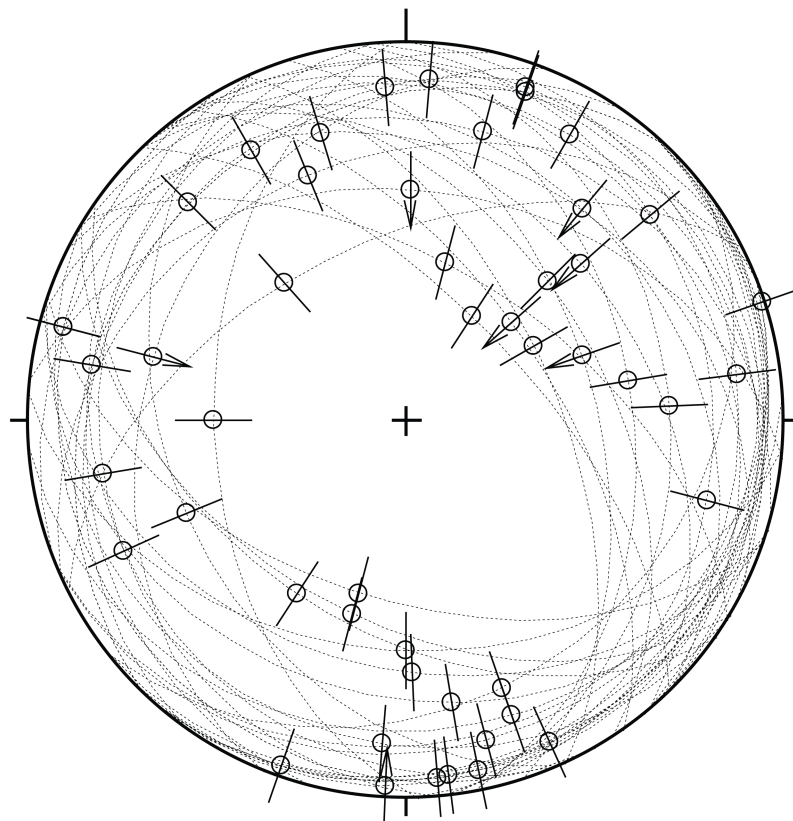


Fig. 4-64: Stereogram of striations on fault planes (including multiple lineations on a single fault plane) (Klettgau Formation, n = 50)

4.5.2 Bänkerjoch Formation

The orientation and spatial distribution of recorded structures in the Bänkerjoch Formation (981.27 m to 1'054.30 m MD log depth) are shown below. Fault planes and mirror-like fault planes are abundant and evenly distributed. They are randomly oriented with clusters dipping towards the NE, SE, SW and NW. Associated striations are also randomly oriented. Shear sense indicators were generally not recognised. Randomly oriented and evenly distributed tension gashes dominate above 1'040 m MD (log depth). Structure types other than the ones mentioned above are rare or absent within this borehole section.

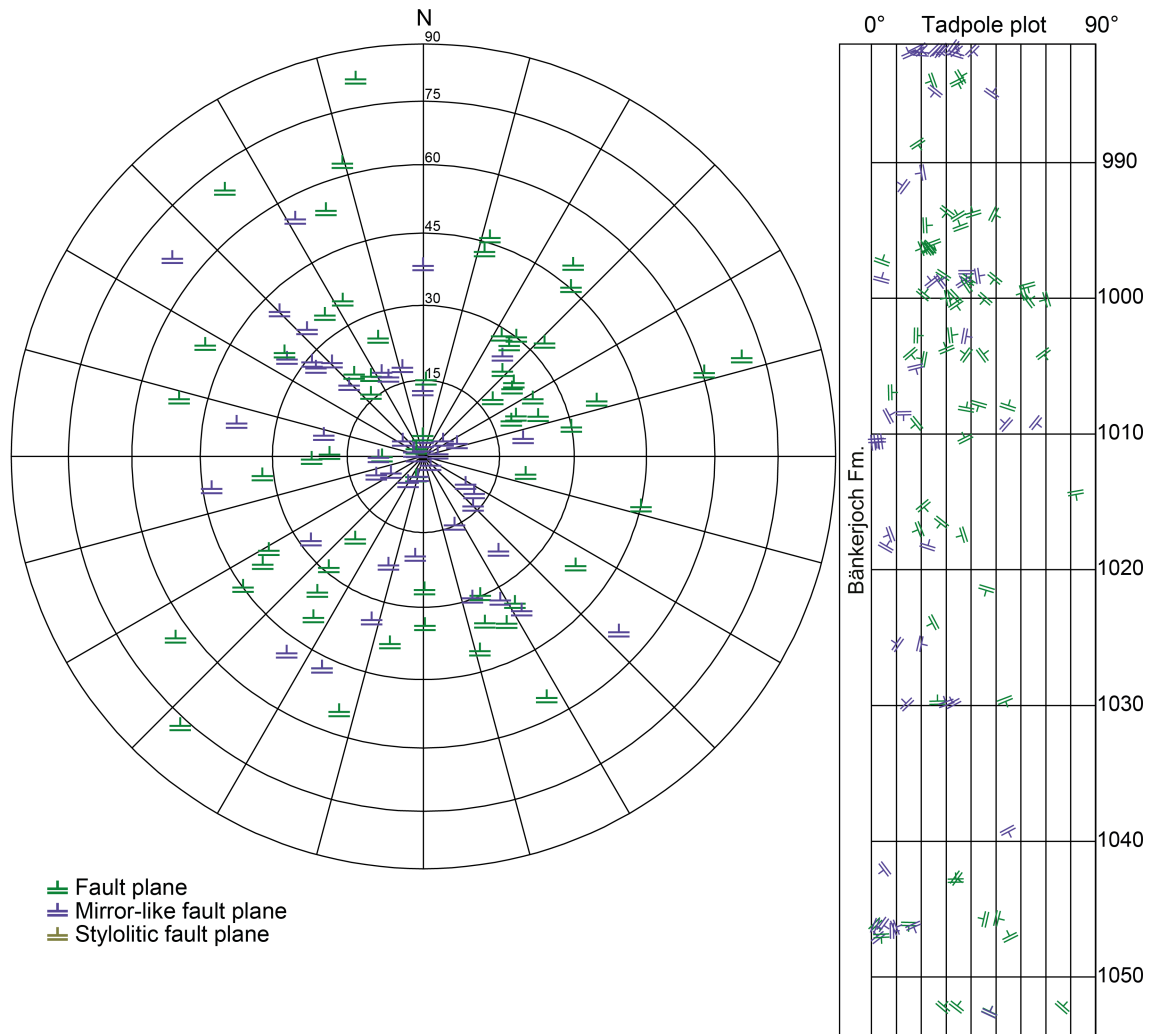


Fig. 4-65: Stereogram and depth plot of fault planes (Bänkerjoch Formation)
 Fault planes (n = 64) and mirror-like fault planes (n = 48); no stylolitic fault planes were observed (n = 0).

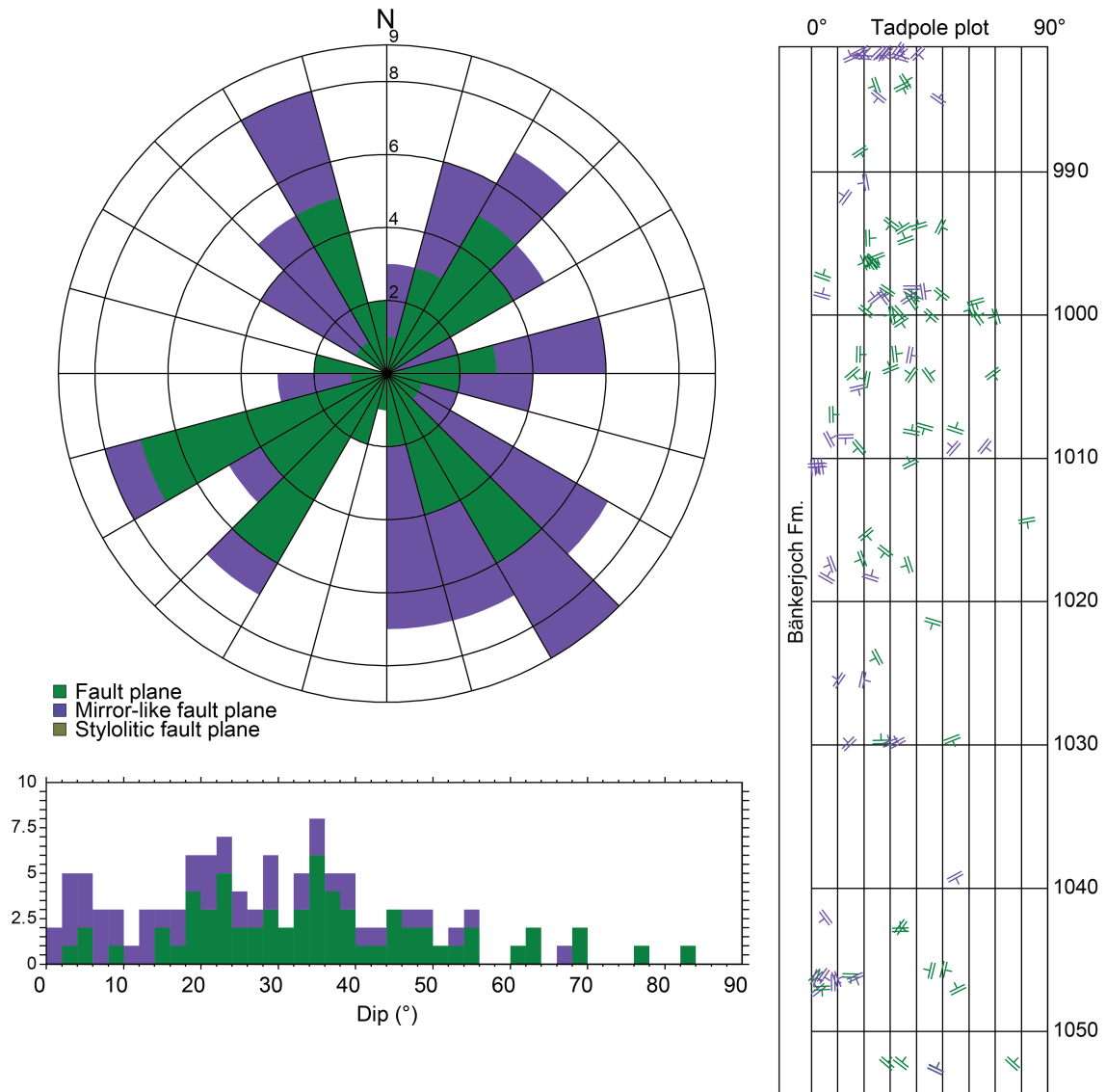


Fig. 4-66: Dip azimuth rose diagram, dip histogram and depth plot of faults (Bänkerjoch Formation)

Fault planes (n = 64) and mirror-like fault planes (n = 48); no styloitic fault planes were observed (n = 0).

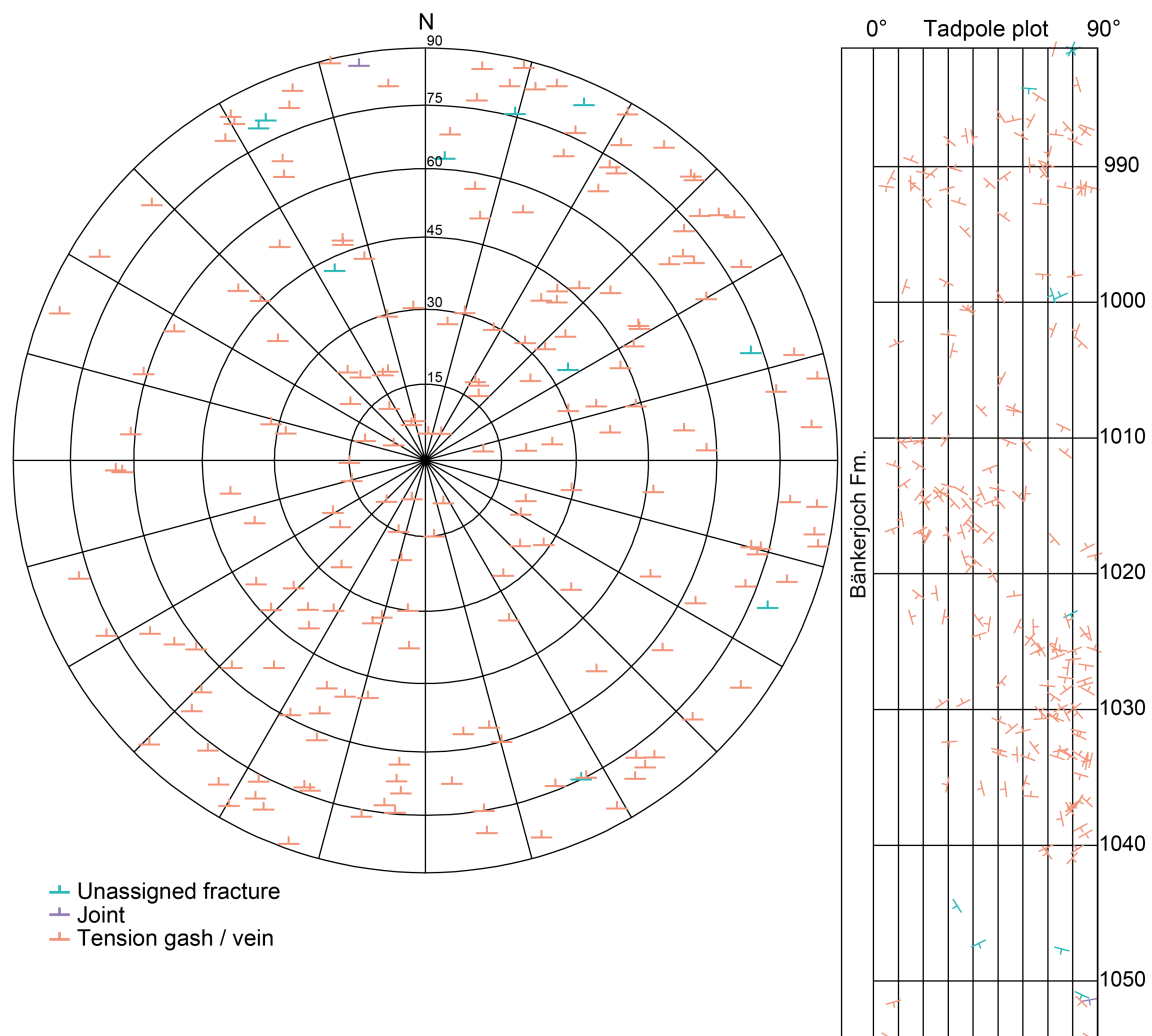


Fig. 4-67: Stereogram and depth plot of tension gashes / veins, joints and unassigned fractures (Bänkerjoch Formation)
 Unassigned fractures (n = 10), joints (n = 1) and tension gashes / veins (n = 193).

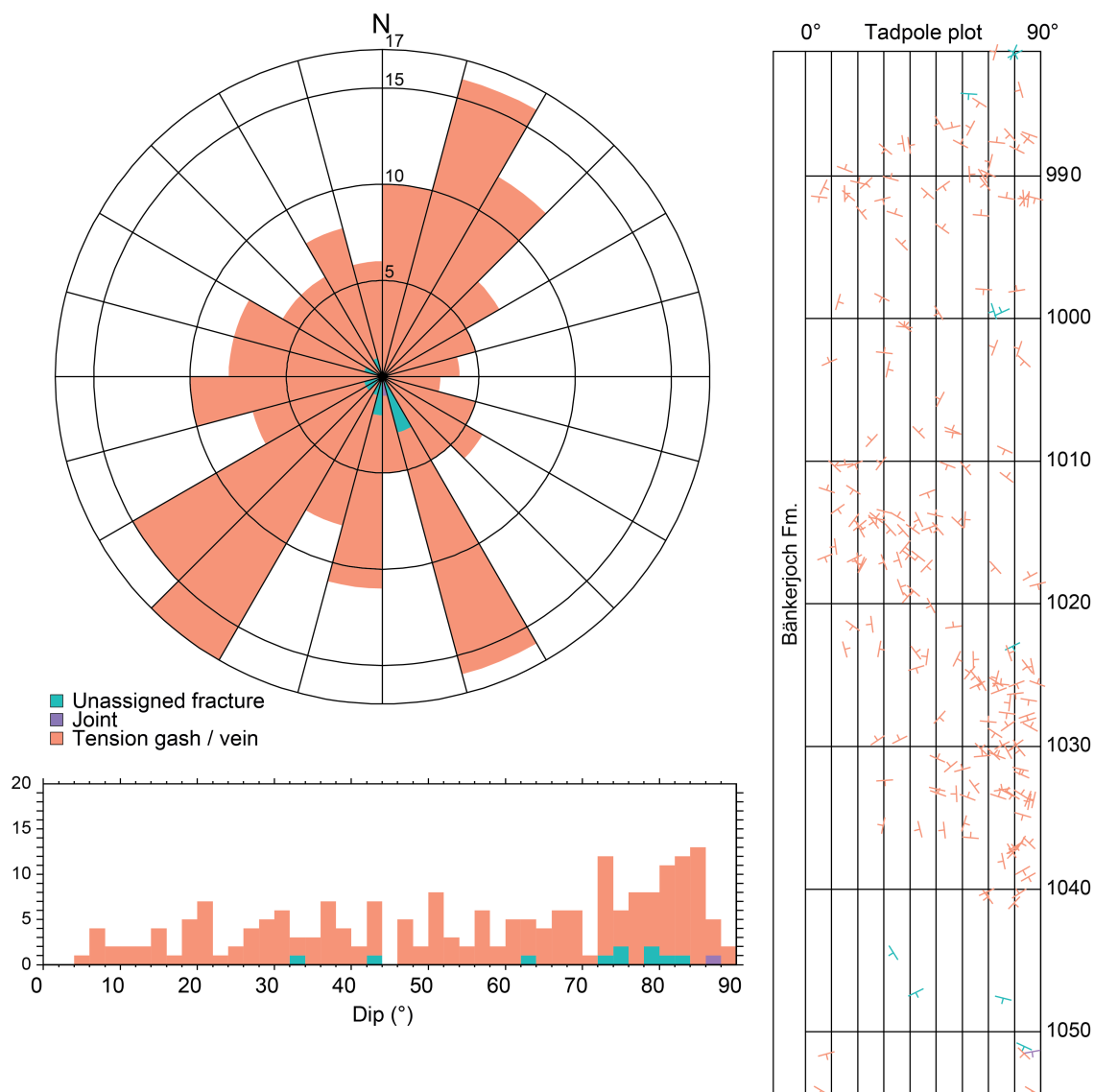


Fig. 4-68: Dip azimuth rose diagram, dip histogram and depth plot of tension gashes / veins, joints and unassigned fractures (Bänkerjoch Formation)
 Unassigned fractures (n = 10), joints (n = 1) and tension gashes / veins (n = 193).

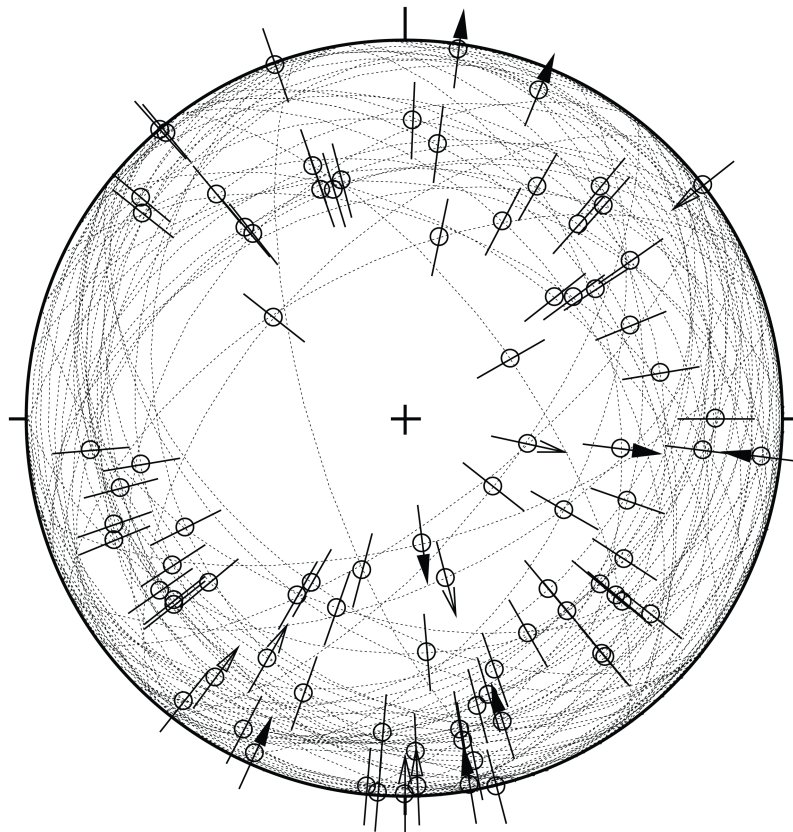


Fig. 4-69: Stereogram of striations on fault planes (including multiple lineations on a single fault plane) (Bänkerjoch Formation, $n = 88$)

4.6 Muschelkalk

The Muschelkalk (1'054.30 m to 1'243.12 m MD log depth) shows a moderate density of fault planes, joints and tension gashes. A high density of stylolites is restricted to the Schinznach Formation. In addition, abundant mm- to cm-sized open pores (vugs) were recorded. Only the data from oriented cores are presented.

4.6.1 Schinznach Formation

The orientation and spatial distribution of recorded structures in the Schinznach Formation (1'054.30 m to 1'126.20 m MD log depth) are shown below. The Schinznach Formation displays a high density of stylolites and a moderate density of joints. The stylolites are evenly distributed throughout the formation. Most stylolites have shallow to subhorizontal dip angles with preferably SE and S dip azimuths. Joints show a predominant subvertical dip angles with W dip directions. Fault planes and tension gashes are rare.

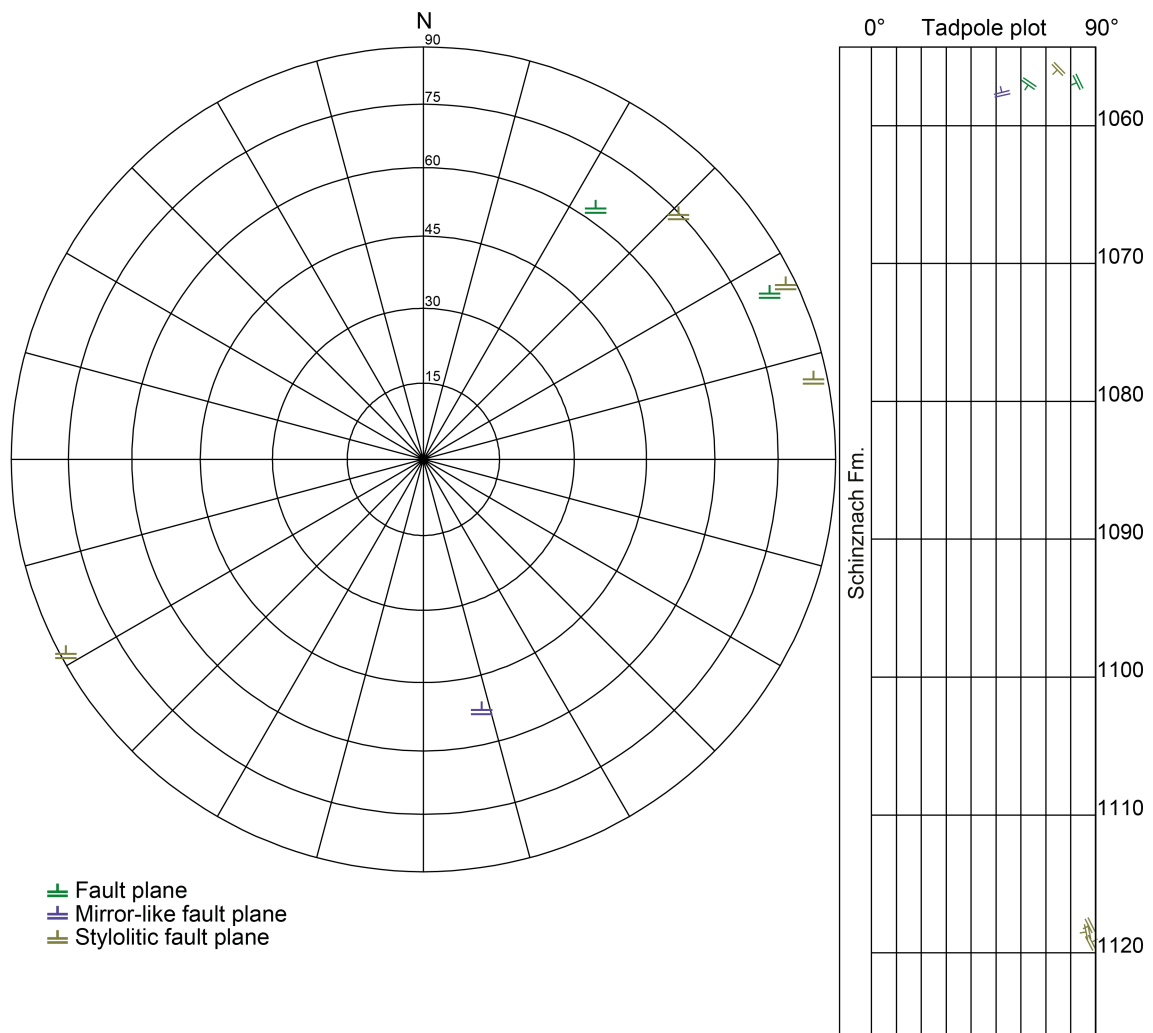


Fig. 4-70: Stereogram and depth plot of fault planes (Schinznach Formation)
 Fault planes (n = 2), mirror-like fault planes (n = 1) and stylolitic fault planes (n = 4).

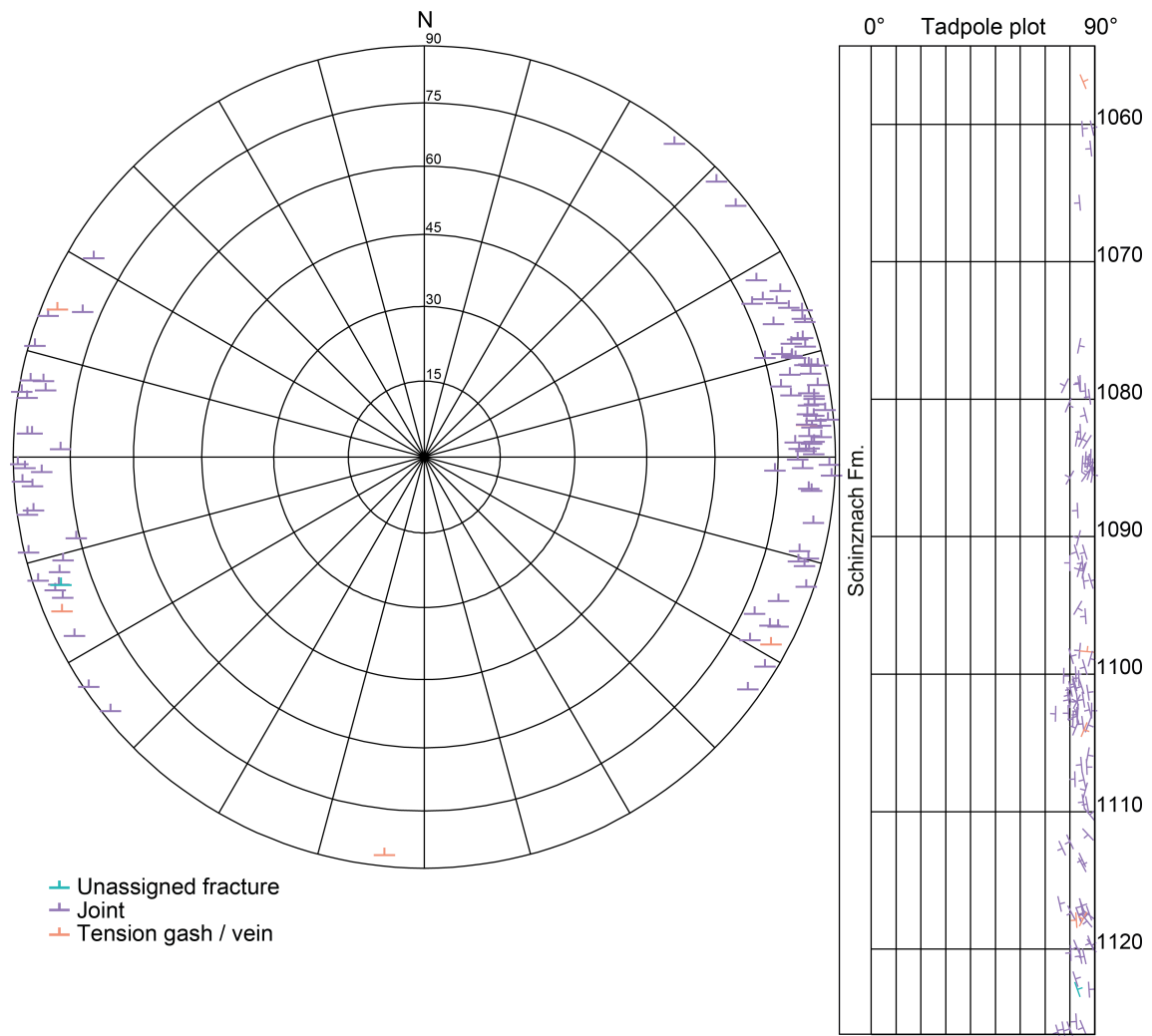


Fig. 4-71: Stereogram and depth plot of tension gashes / veins, joints and unassigned fractures (Schinznach Formation)

Unassigned fractures (n = 1), joints (n = 103) and tension gashes / veins (n = 5).

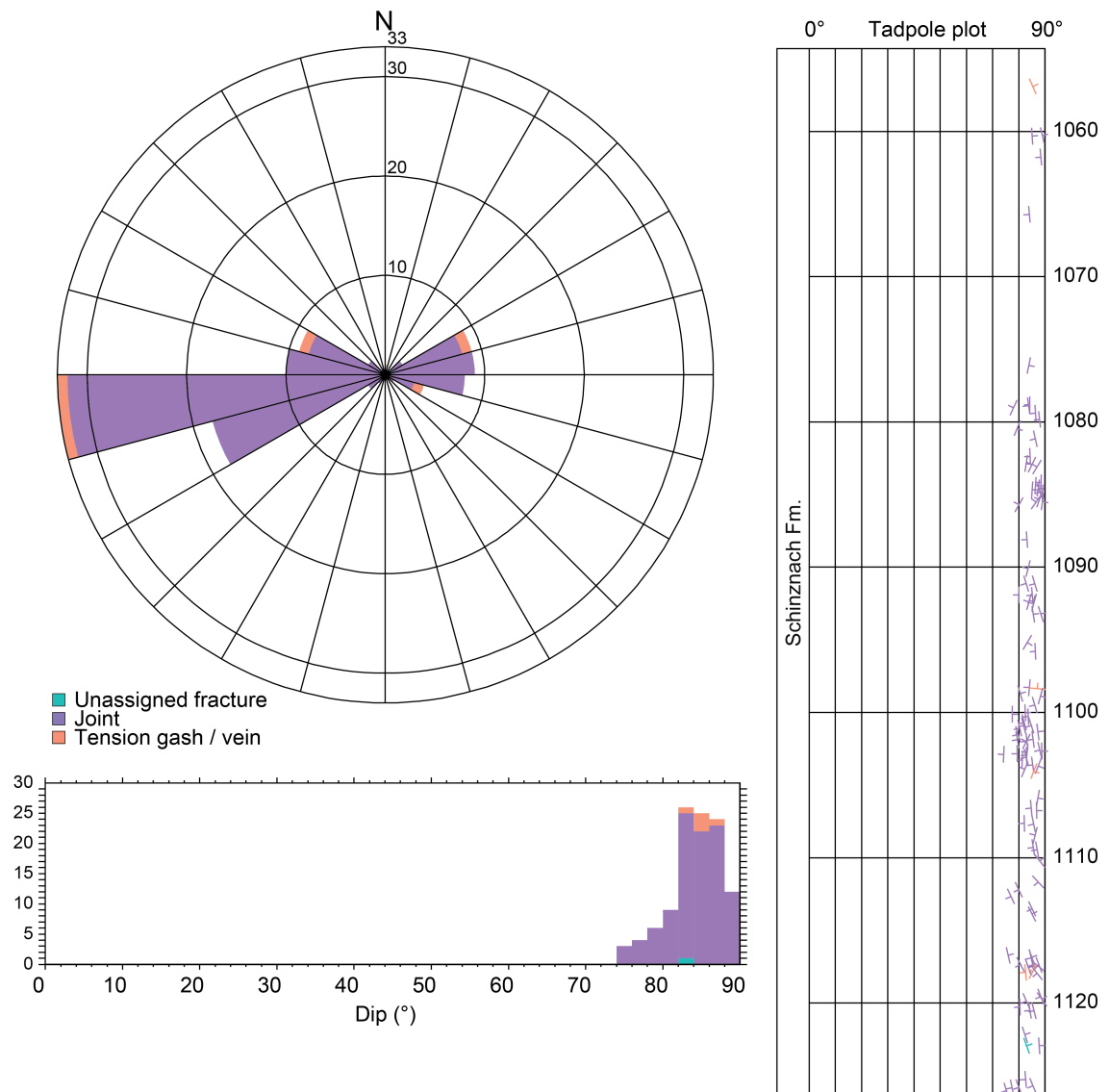


Fig. 4-72: Dip azimuth rose diagram, dip histogram and depth plot of tension gashes / veins, joints and unassigned fractures (Schinznach Formation)
 Unassigned fractures (n = 1), joints (n = 103) and tension gashes / veins (n = 5).

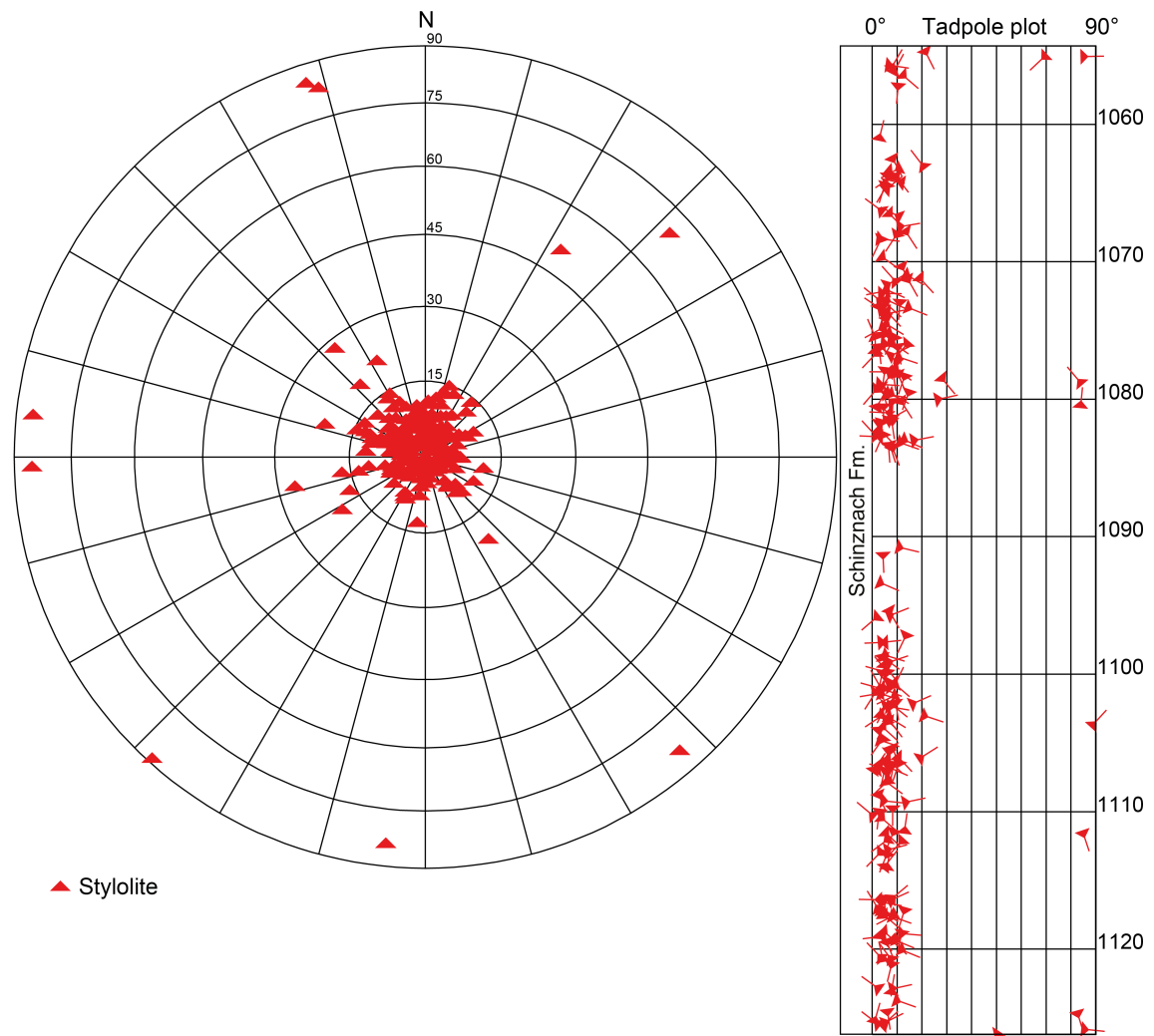


Fig. 4-73: Stereogram and depth plot of stylolites (Schinznach Formation, n = 221)

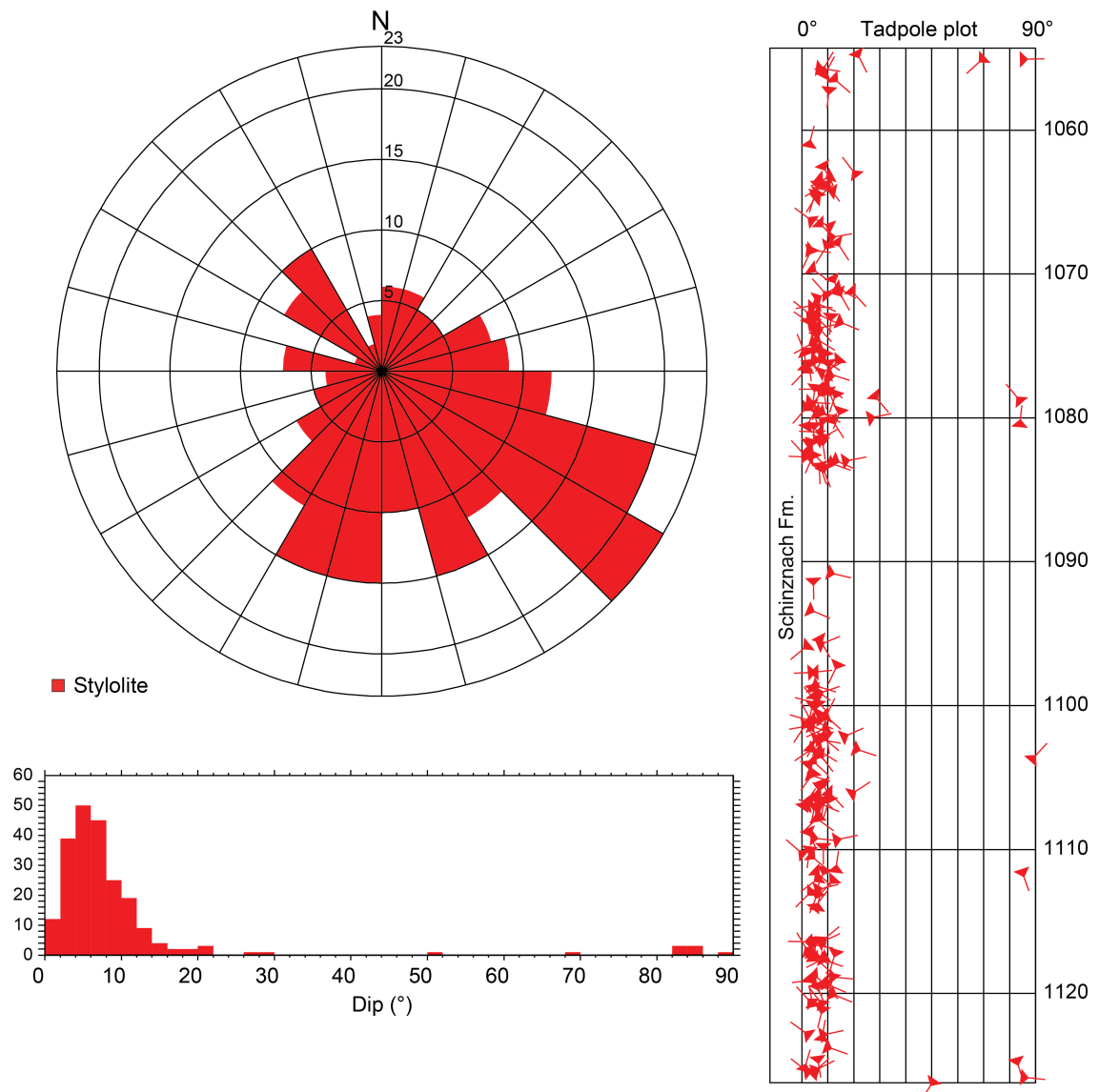


Fig. 4-74: Dip azimuth rose diagram, dip histogram and depth plot of stylolites (Schinznach Formation, n = 221)

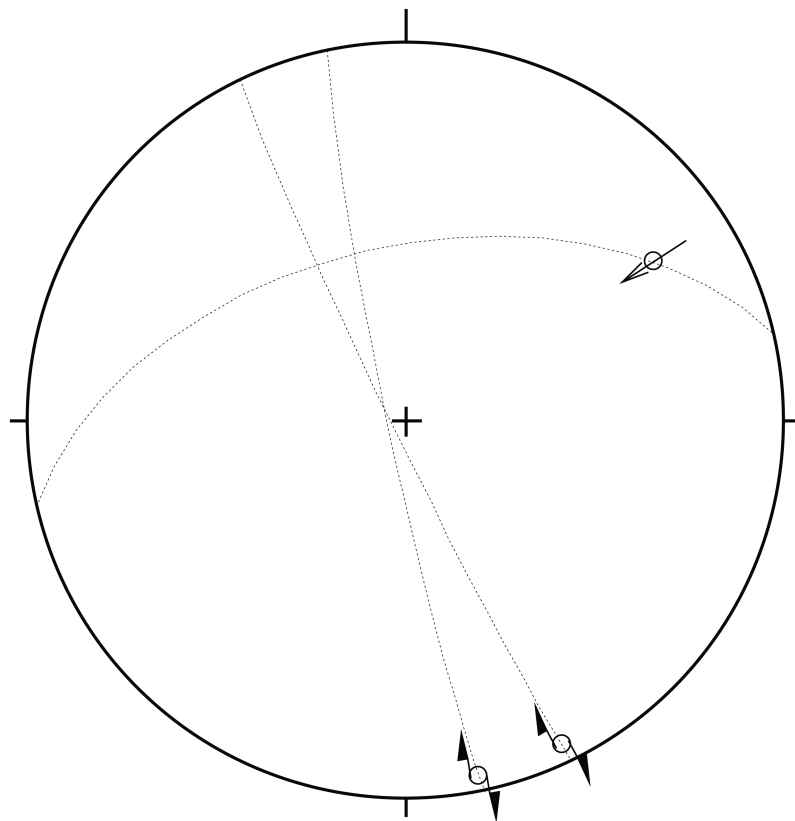


Fig. 4-75: Stereogram of striations on fault planes (including multiple lineations on a single fault plane) (Schinznach Formation, $n = 3$)

4.6.2 Zeglingen Formation

The orientation and spatial distribution of recorded structures in the Zeglingen Formation (1'126.20 m to 1'202.43 m MD log depth) are shown below. It reveals a moderate density of fault planes, joints and tension gashes. The structures are concentrated in the upper part of the formation above approximately 1'175 m MD (log depth). The shallow to steeply dipping fault planes dip preferably towards the S, while the steep to subvertical joints show a strong predominance of WSW to W dipping planes. The subvertical tension gashes dip towards the NNE or WSW to W. The plunge azimuth of the striations shows a tendency towards the N and S. Shear sense indicators are generally not observed. Stylolites, unassigned fractures and stylolitic fault planes are rare.

There are three evident shear bands characterised by dynamically recrystallised rock salt located at 1'161.61 m to 1'164.15 m MD (log depth), 1'170.26 m to 1'176.65 m MD (log depth) and 1'186.24 m to 1'186.90 m MD (log depth). The rock salt appears as fine-grained halite with elongated grains alternating with partly recrystallised layers with sigma clasts. Recrystallised salt is characterised by mm-sized elongated grains with an aspect ratio of 1:2 or 1:3. The preferred orientation of recrystallised grains and sigma clasts indicates a reverse sense of shear. The long axes of the recrystallised salt grains plunge towards the S. Undeformed halite comprises cm-sized blocky halite crystals.

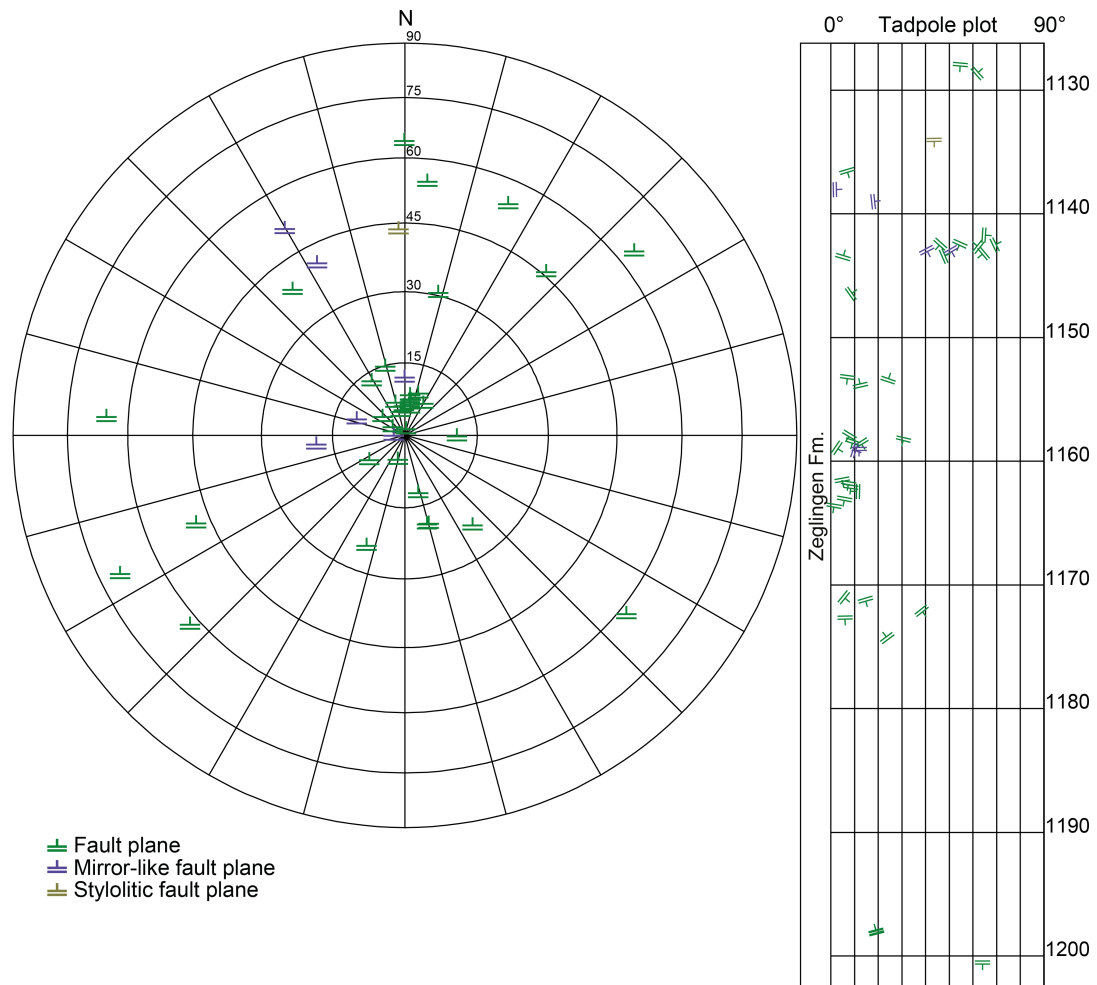


Fig. 4-76: Stereogram and depth plot of fault planes (Zeglingen Formation)
 Fault planes / shear bands (n = 34), mirror-like fault planes (n = 6) and styloitic fault planes (n = 1).

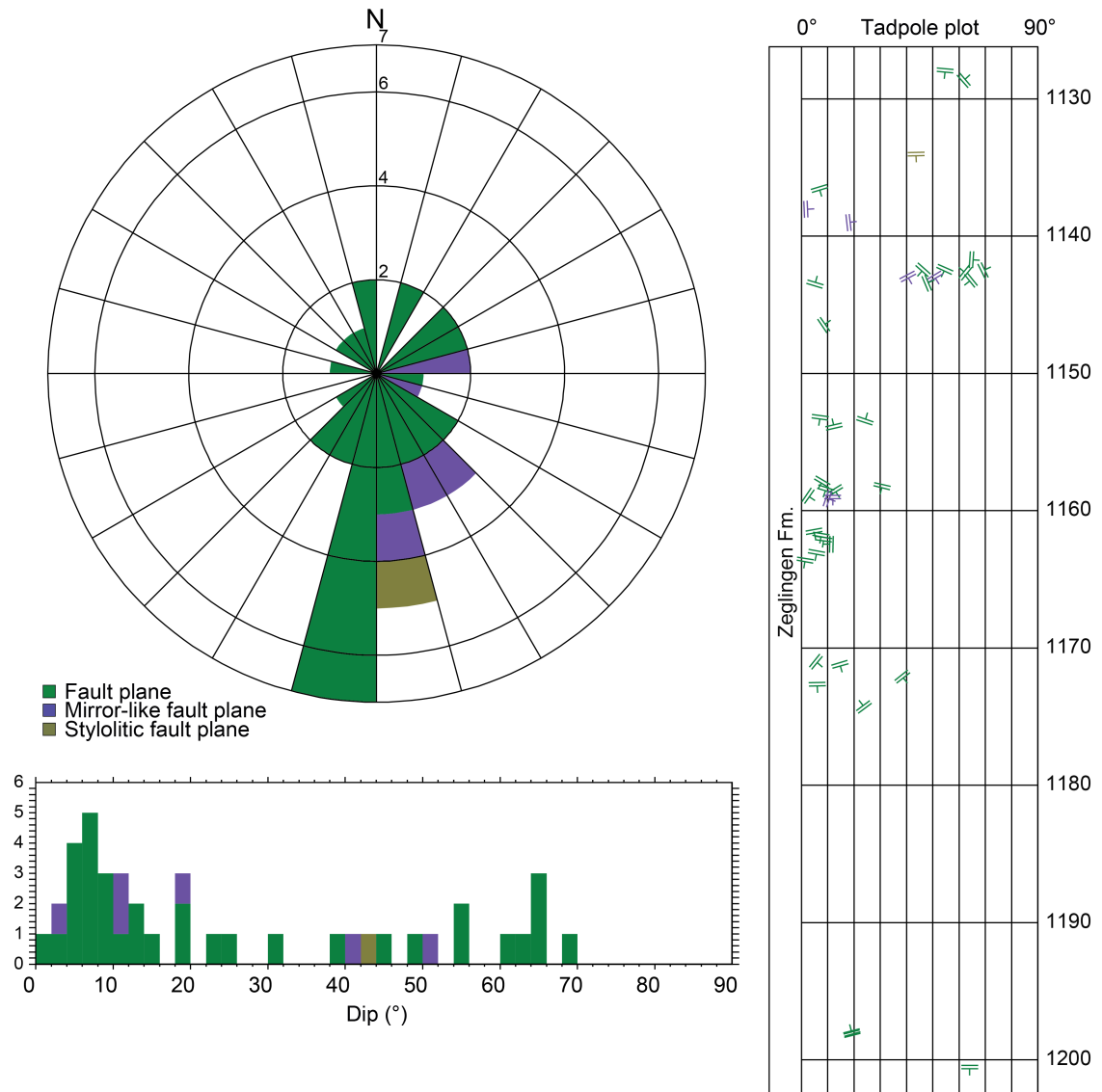


Fig. 4-77: Dip azimuth rose diagram, dip histogram and depth plot of fault planes (Zeglingen Formation)

Fault planes / shear bands (n = 34), mirror-like fault planes (n = 6) and stylotitic fault planes (n = 1).

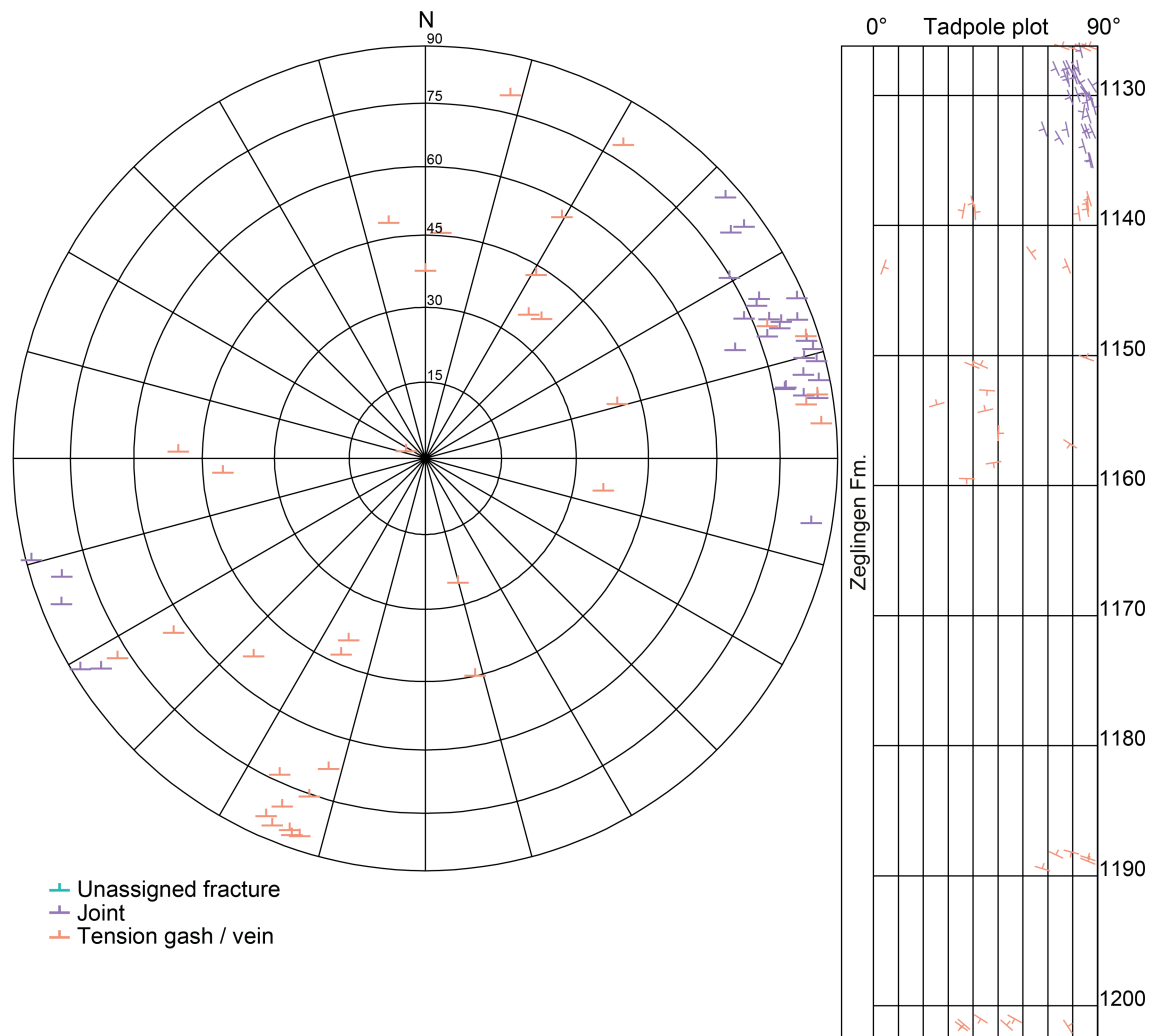


Fig. 4-78: Stereogram and depth plot of tension gashes / veins, joints and unassigned fractures (Zeglingen Formation)
 Joints (n = 30) and tension gashes / veins (n = 35); no unassigned fractures were observed (n = 0).

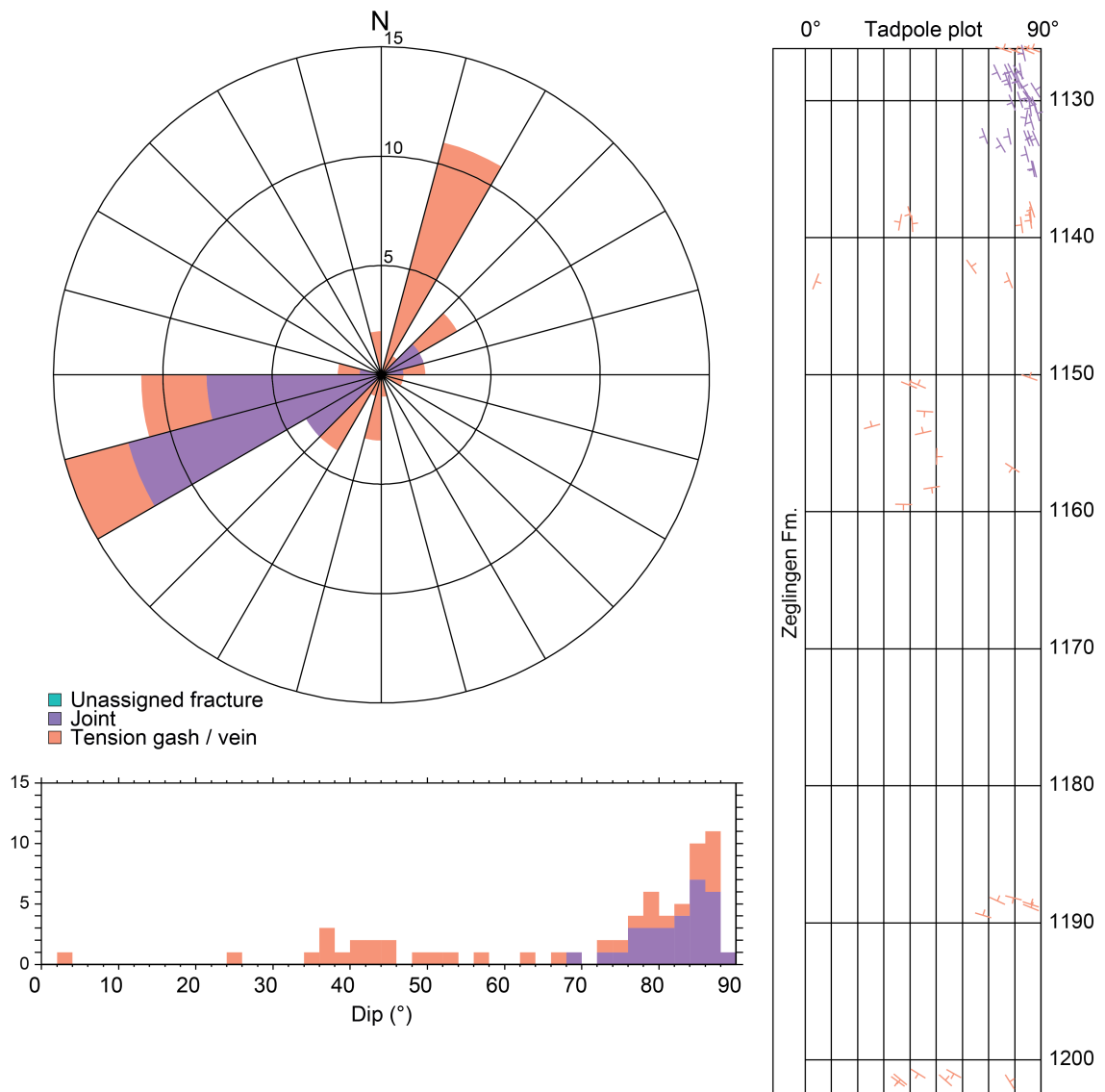


Fig. 4-79: Dip azimuth rose diagram, dip histogram and depth plot of tension gashes / veins, joints and unassigned fractures (Zeglingen Formation)

Joints (n = 30) and tension gashes / veins (n = 35); no unassigned fractures were observed (n = 0).

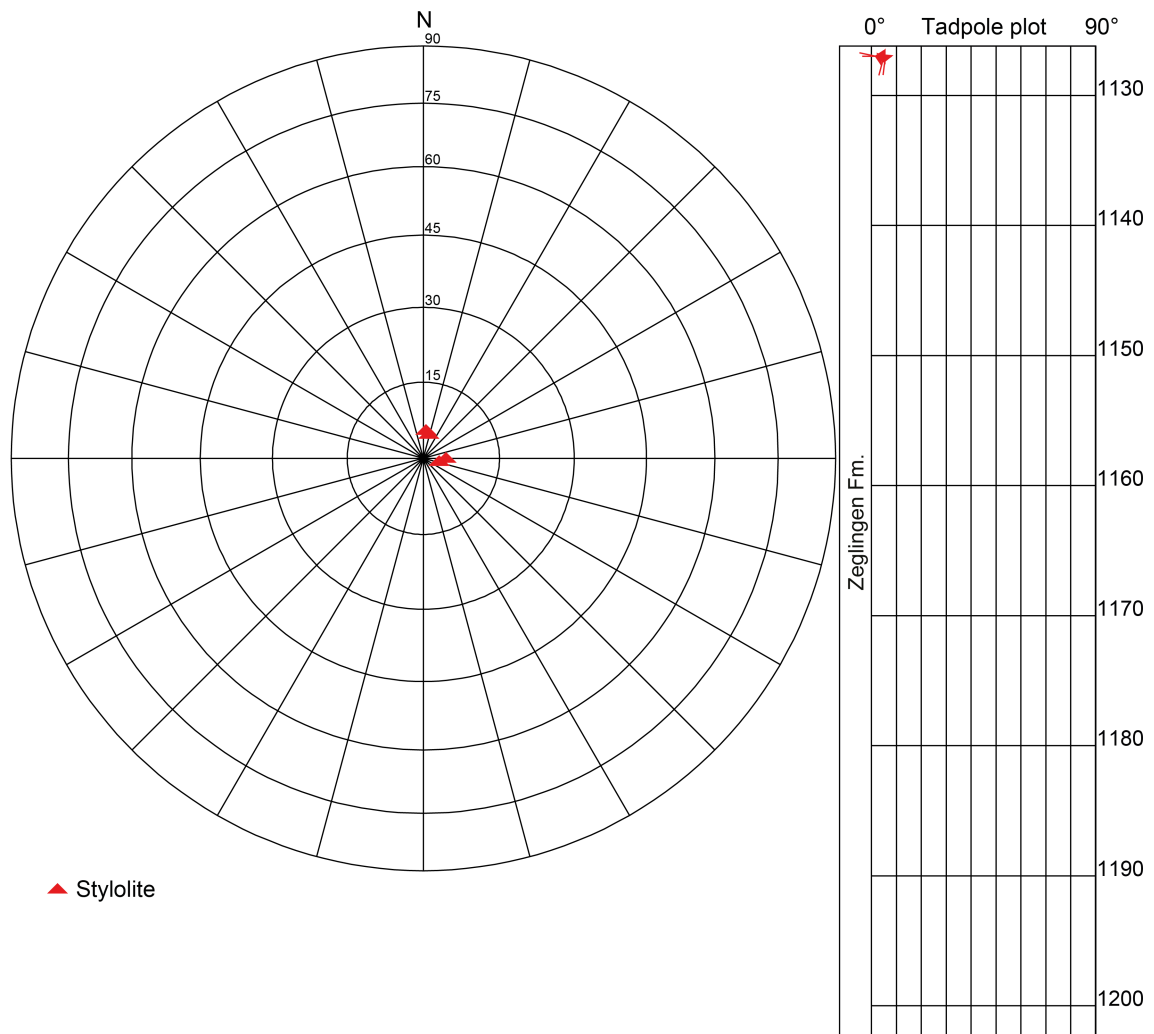


Fig. 4-80: Stereogram and depth plot of stylolites (Zeglingen Formation, n = 4)

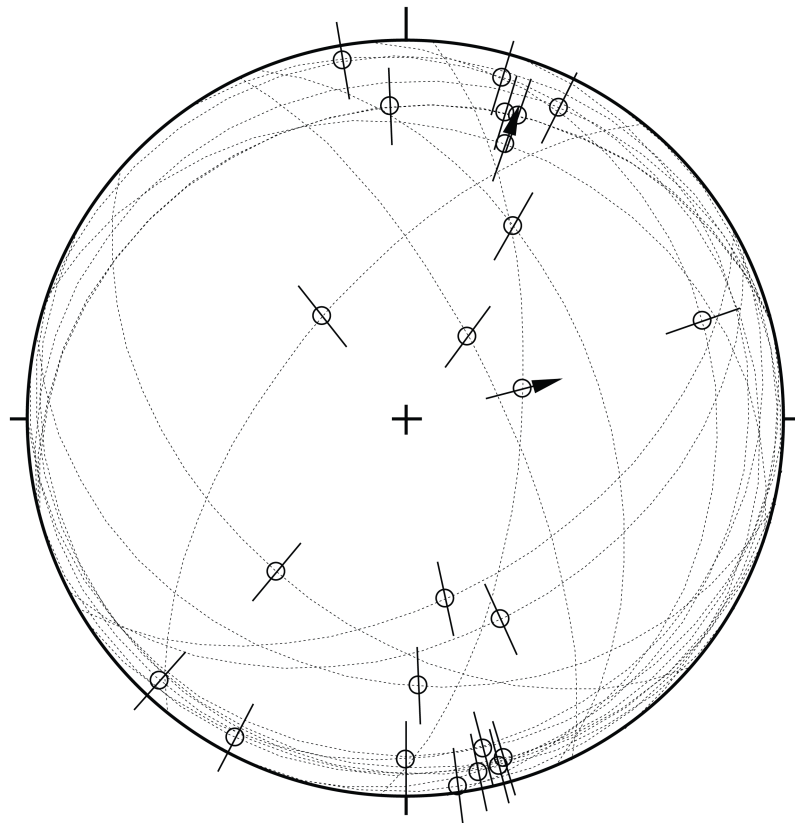


Fig. 4-81: Stereogram of striations on fault planes (including multiple lineations on a single fault plane) (Zeglingen Formation, n = 24)

4.6.3 Kaiseraugst Formation

The orientation and spatial distribution of recorded structures in the Kaiseraugst Formation (1'202.43 m to 1'243.12 m MD log depth) are shown below. The overall fracture density is low. The dominant structures are mirror-like fault planes dipping gently towards the S and SE. The plunge azimuths of the striations are randomly oriented. Shear senses could generally not be defined. All other structure types are rare or absent.

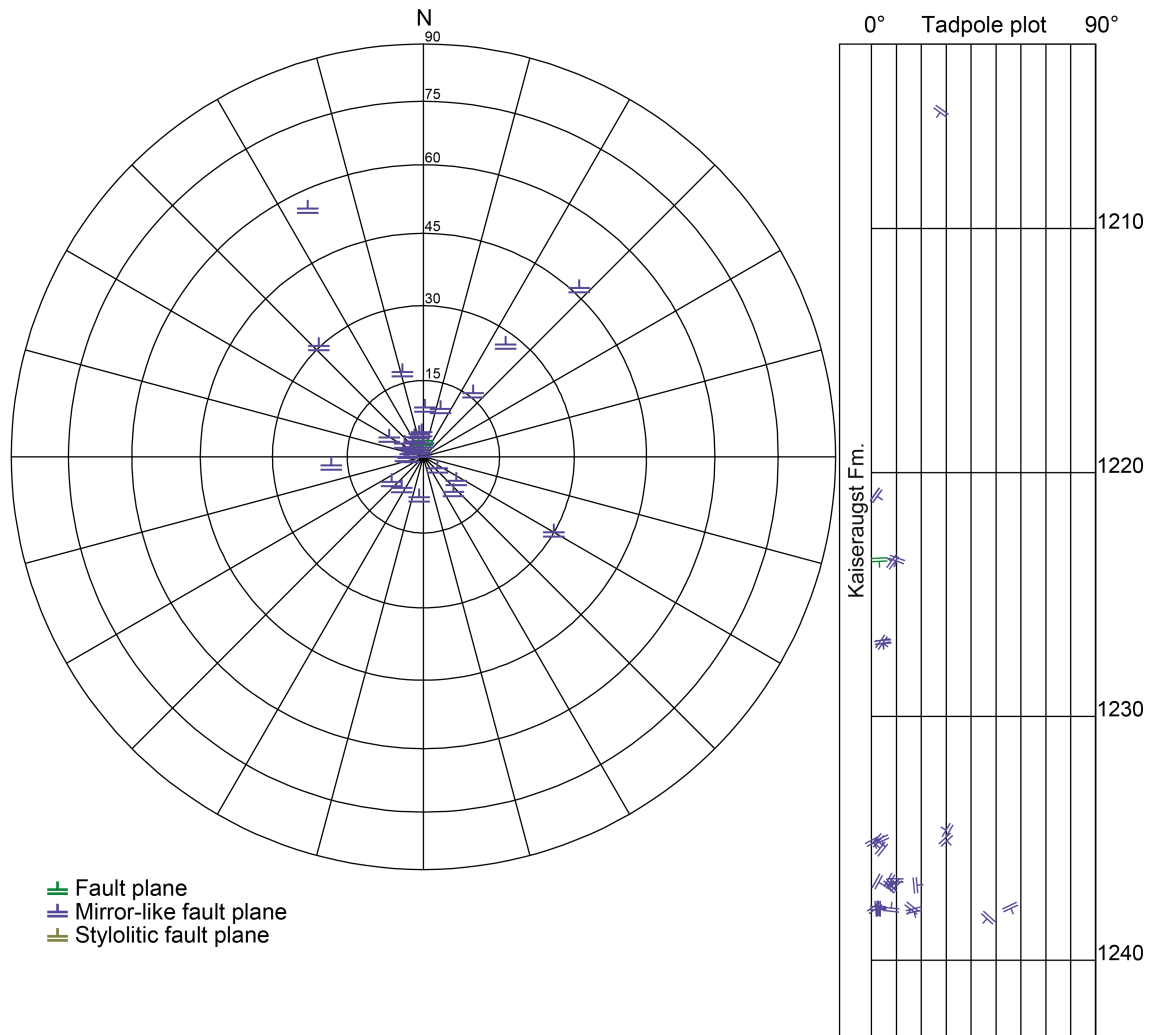


Fig. 4-82: Stereogram and depth plot of fault planes (Kaiseraugst Formation)
 Fault planes (n = 1) and mirror-like fault planes (n = 30); no stylolitic fault planes were observed (n = 0).

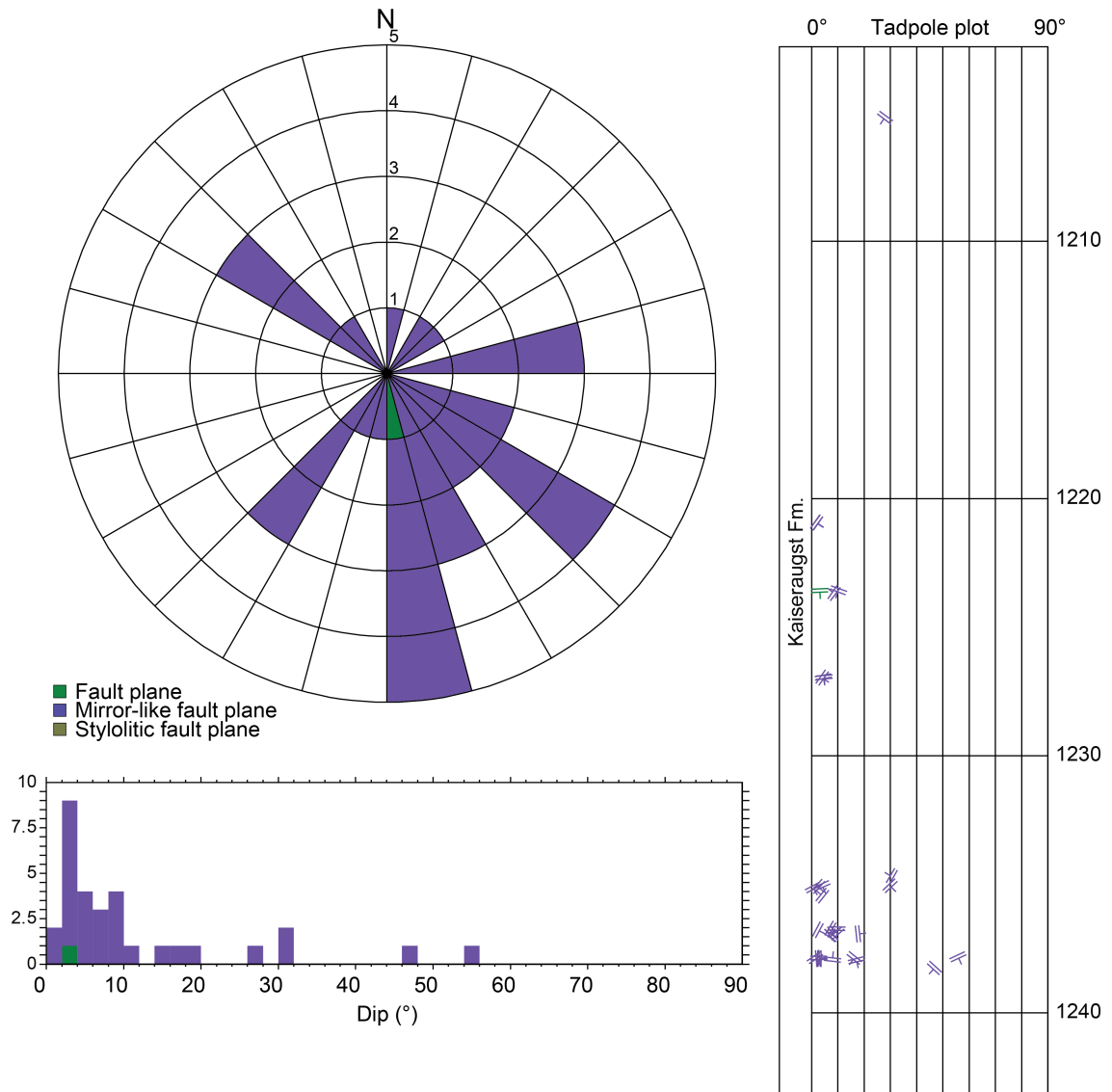


Fig. 4-83: Dip azimuth rose diagram, dip histogram and depth plot of fault planes (Kaiseraugst Formation)

Fault planes (n = 1) and mirror-like fault planes (n = 30); no stylolitic fault planes were observed (n = 0).

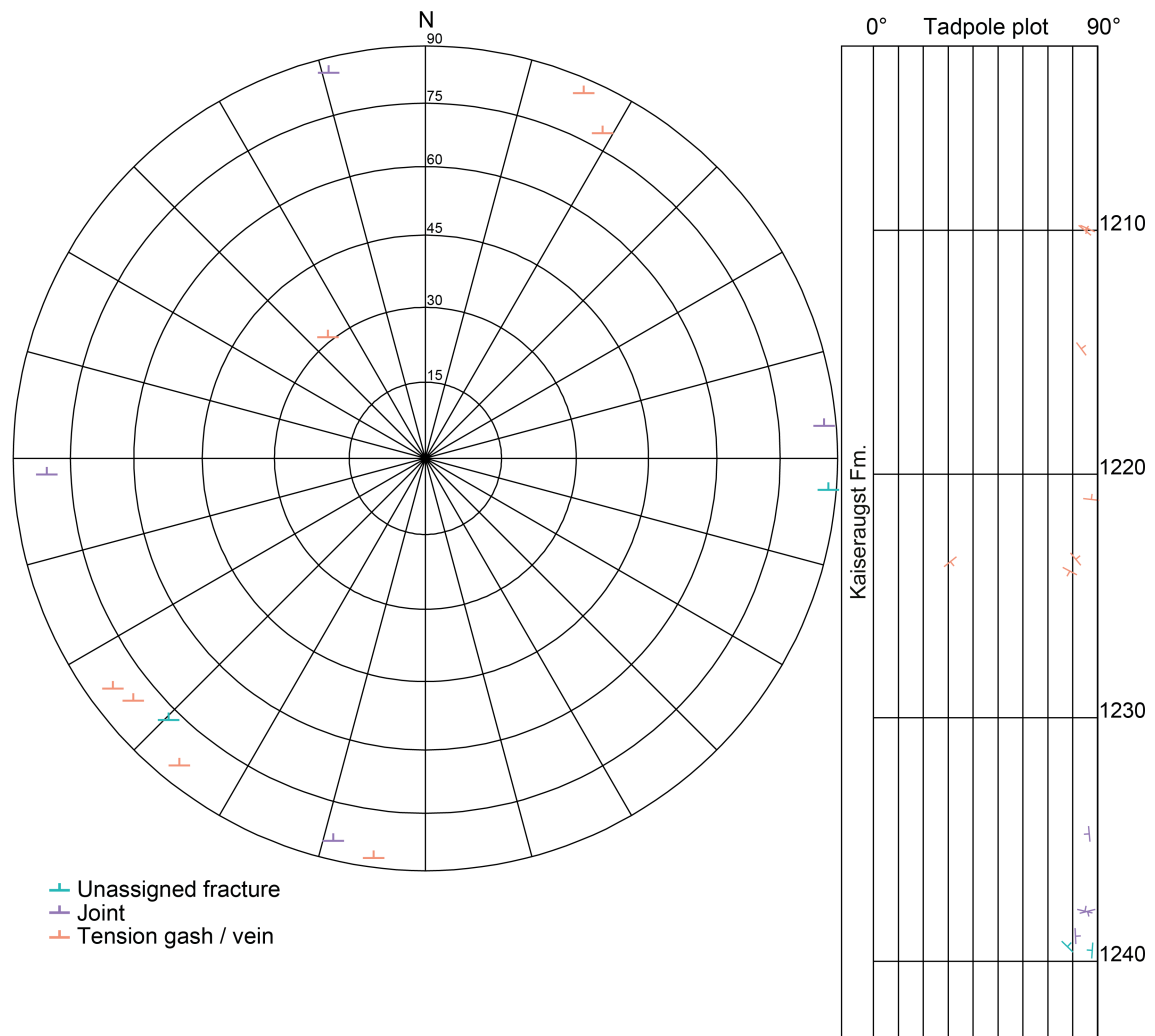


Fig. 4-84: Stereogram and depth plot of tension gashes / veins, joints and unassigned fractures (Kaiseraugst Formation)

Unassigned fractures (n = 2), joints (n = 4) and tension gashes / veins (n = 7).

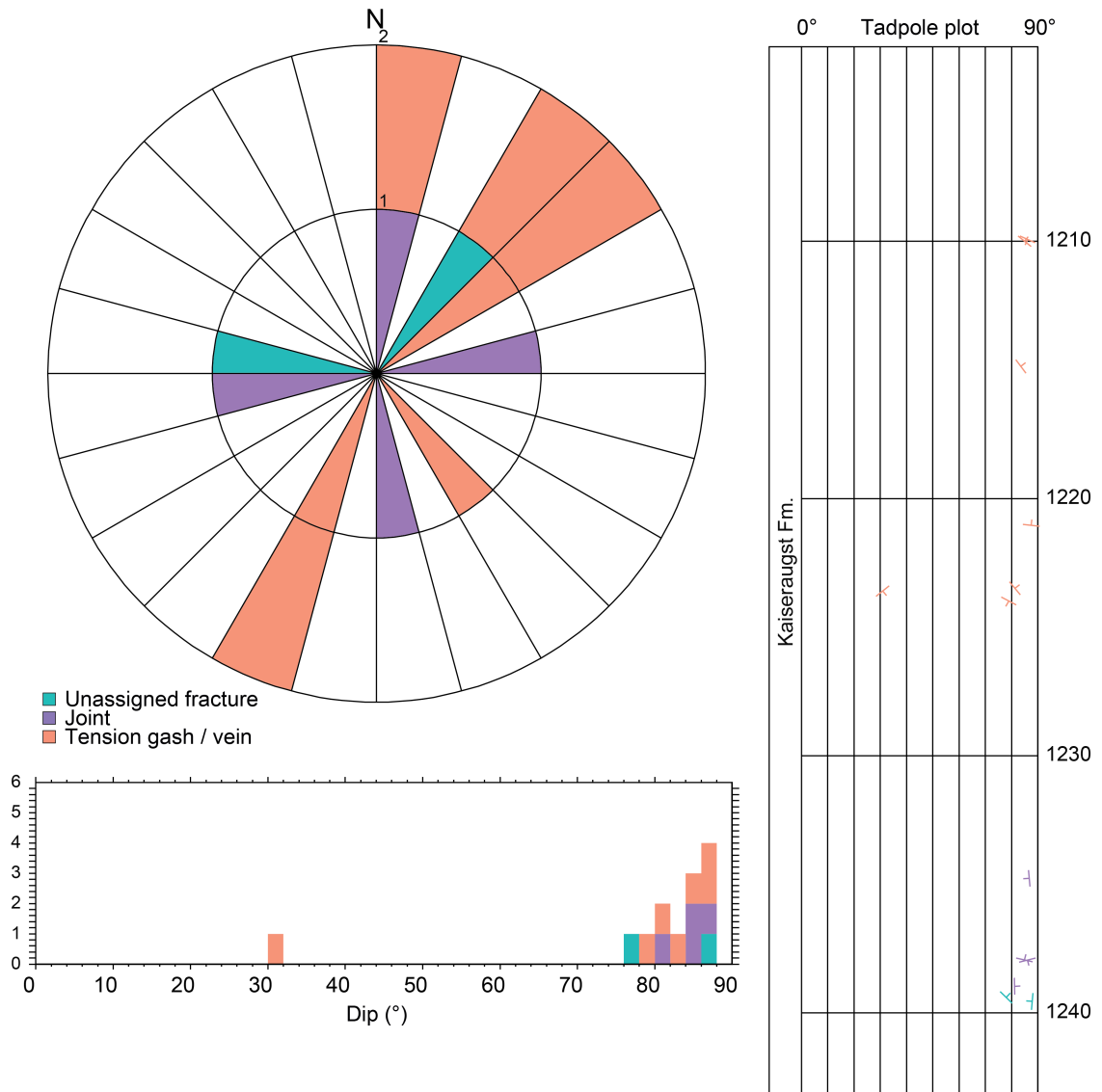


Fig. 4-85: Dip azimuth rose diagram, dip histogram and depth plot of tension gashes / veins, joints and unassigned fractures (Kaiseraugst Formation)
 Unassigned fractures (n = 2), joints (n = 4) and tension gashes / veins (n = 7).

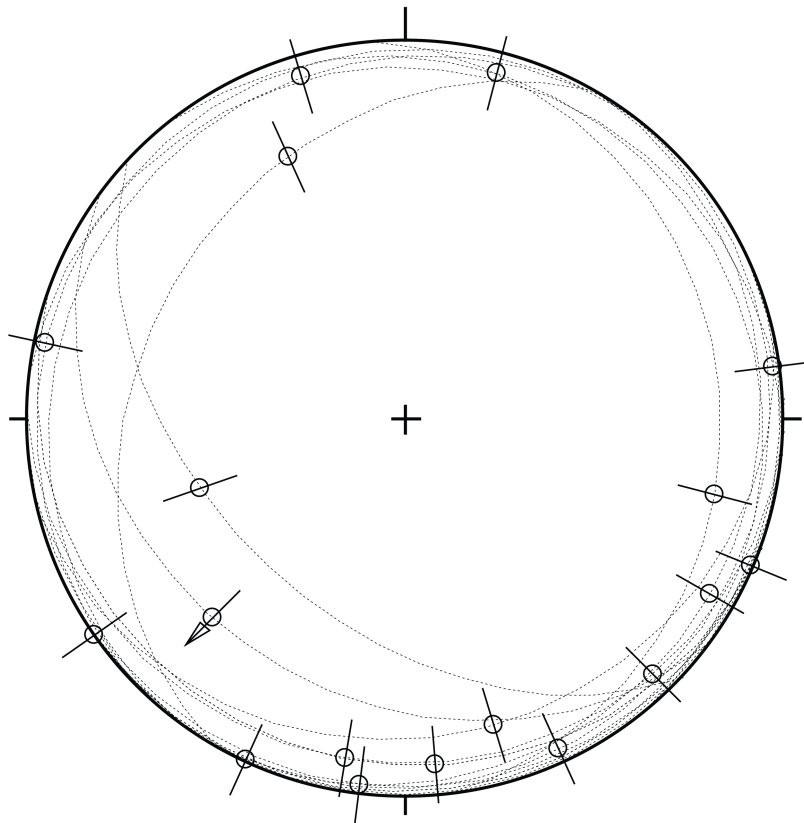


Fig. 4-86: Stereogram of striations on fault planes (including multiple lineations on a single fault plane) (Kaiseraugst Formation, $n = 18$)

4.7 Dinkelberg and Weitenau Formations

The orientation and spatial distribution of recorded structures in the Dinkelberg and the Weitenau Formations (1'243.12 m to 1'306.77 m MD log depth; base of cored section) are shown below. These formations are characterised by a very low number of structures. Stylolites, stylolitic fault planes, mirror-like fault planes and unassigned fractures are absent.

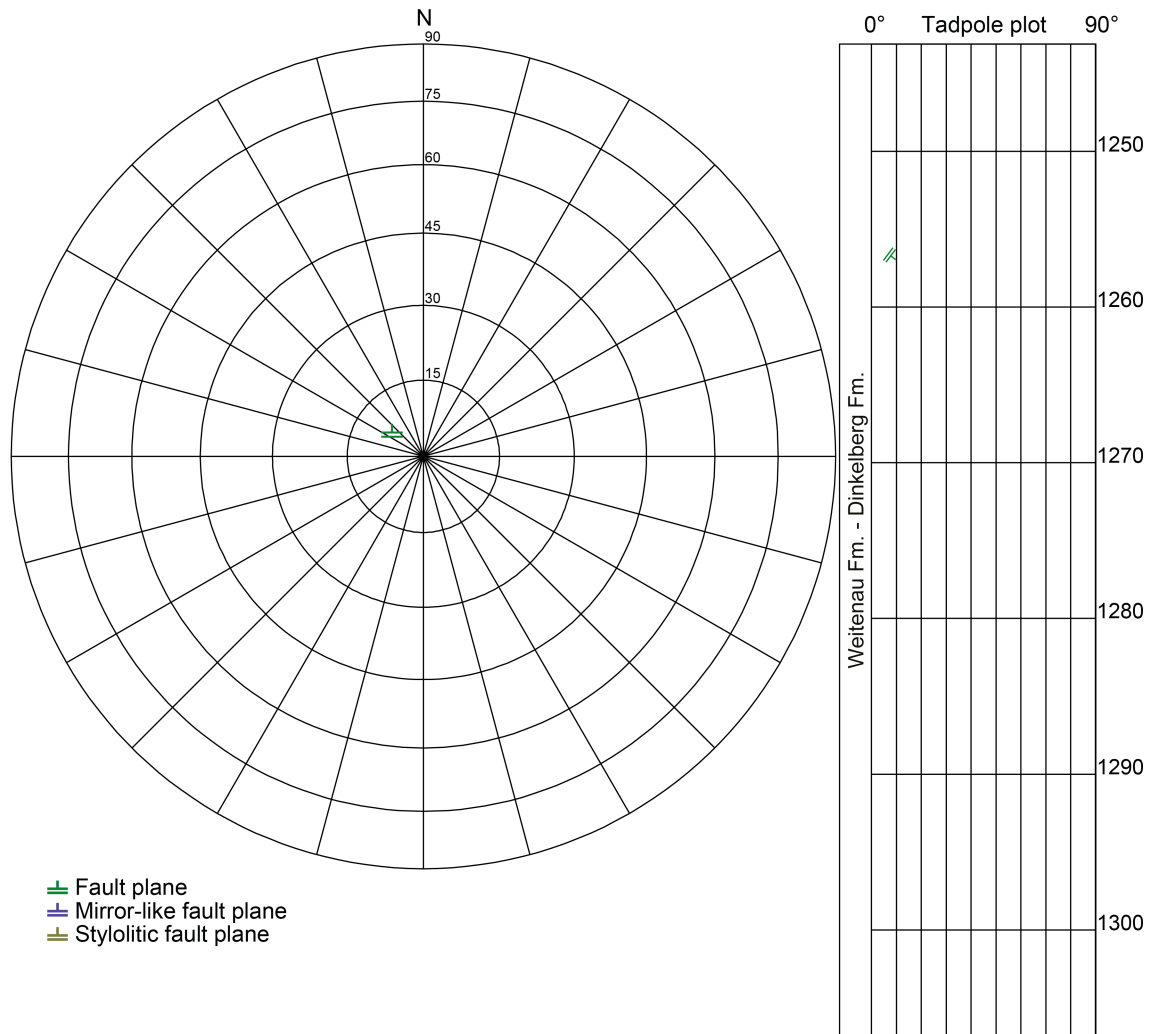


Fig. 4-87: Stereogram and depth plot of fault planes (Dinkelberg Formation and Weitenau Formation)

Fault planes (n = 1); no mirror-like fault planes or stylolitic fault planes were observed (n = 0).

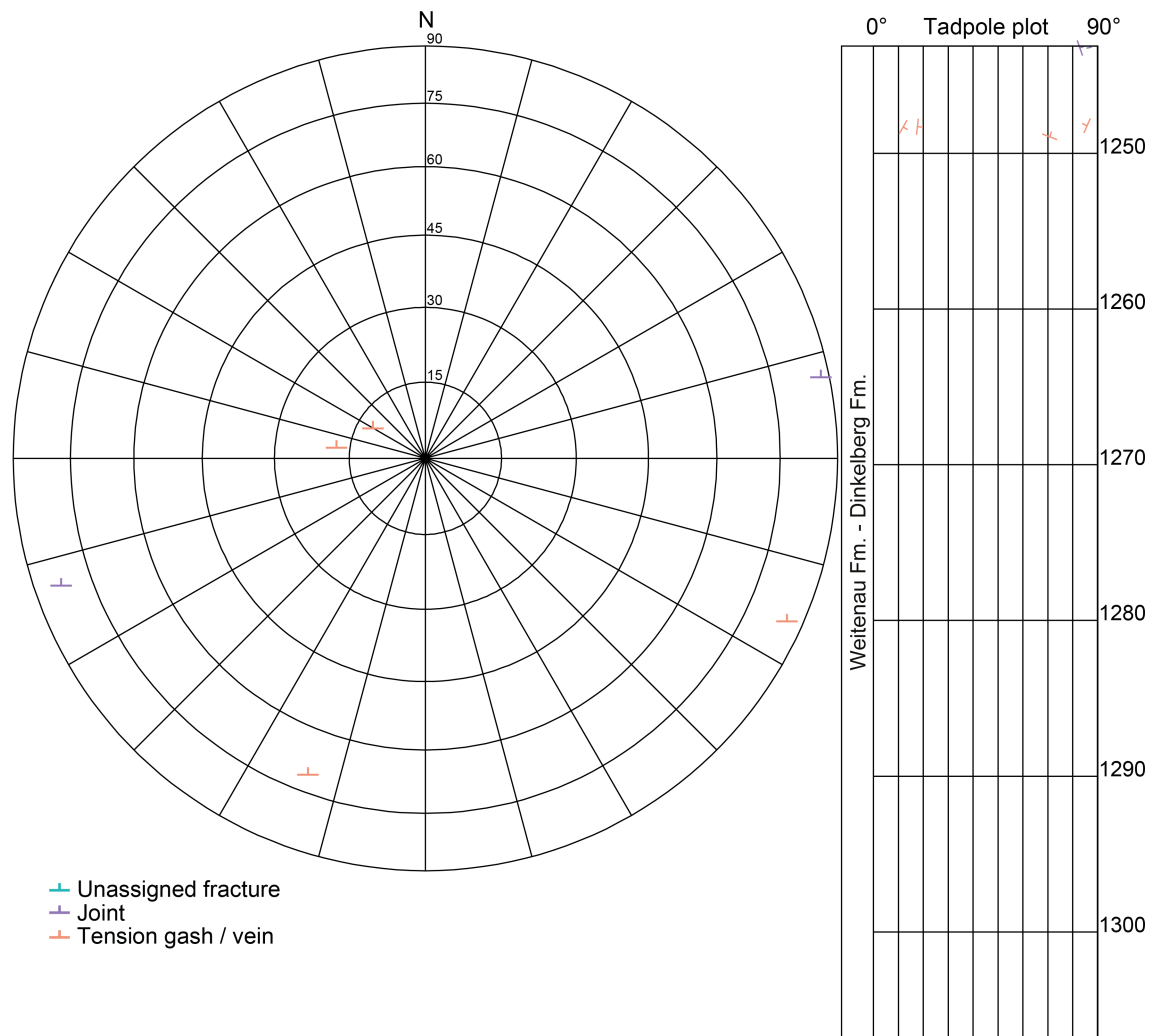


Fig. 4-88: Stereogram and depth plot of tension gashes / veins, joints and unassigned fractures (Dinkelberg Formation and Weitenau Formation)
 Joints (n = 2) and tension gashes / veins (n = 4); no unassigned fractures were observed (n = 0).

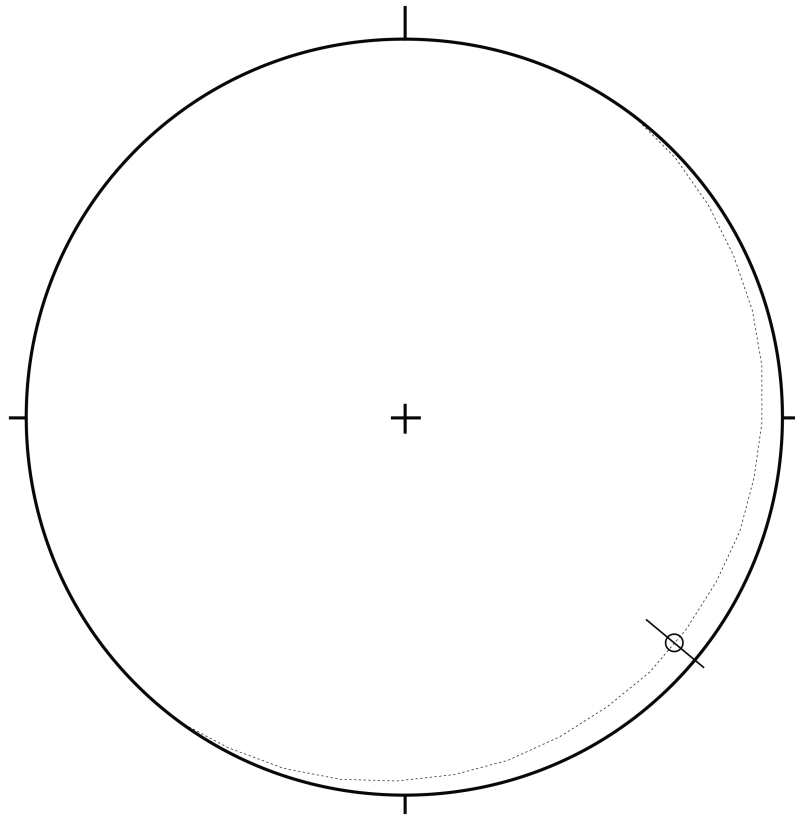


Fig. 4-89: Stereogram of striation on a single fault plane within the Dinkelberg and Weitenau Formations ($n = 1$)

5 Main structural findings

Among the relevant geological features within the studied cored section from 517.58 m to 1'306.77 m MD (log depth) presented in Chapter 2 and Chapter 4, one prominent deformation zone within the Opalinus Clay and three partly open structures deserve a more detailed examination.

5.1 Deformation zone in the Opalinus Clay between 911.63 m and 912.16 m MD (log depth)

A distinct deformation zone was found in the Opalinus Clay from 911.63 m to 912.16 m MD (log depth). This 0.53 m-thick zone is characterised by numerous fault planes and tension gashes forming a prominent fault zone with a fracture density equivalent to FDC 3 (Fig. 5-1). This fault zone reveals a well-defined NW-SE strike (Fig. 5-2) having a mean orientation of 215/53 (n = 24). Structural dip can neither be defined on the FMI nor on 360° core images from 901.45 m to 920.34 m MD (log depth). However, above and below a horizontal to shallow (1° – 5°) SE structural dip prevails.

A total of 22 fault planes and 2 tension gashes / veins were determined on the 360° core images. The vast majority of fault planes are mineralised with 0.5 mm to 1.0 mm thick synkinematic calcite with well-developed striations. Most of the fault planes terminate on three main fault planes showing up to 4 mm thick mineralisation. Those three fault planes reveal one or two striations and are thus summarised in Tab. 5-1 and shown in Fig. 5-3. Some fault planes terminating on the three main faults show a normal sense of shear. Most striations on these fault planes dip towards the NNE or NW (Fig. 5-3).

Tab. 5-1: Orientation of the three main fault planes and associated striations and shear senses

mMD (log depth)	FP orientation	Lin1/ shear sense	Lin2 / shear sense
911.67	213/43	202/38 (unknown)	142/23 (up/ reverse)
911.85	214/53	285/12 (unknown)	118/02 (unknown)
912.03	217/57	298/02 (dextral)	

The two observed 10 mm thick tension gashes dip steeply towards the SW, parallel to the main fault planes and are mineralised with calcite. It is possible, that the tension gashes represent in fact mineralised fault planes with an extend larger than the core diameter and thus not distinguishable on the scale of observation.

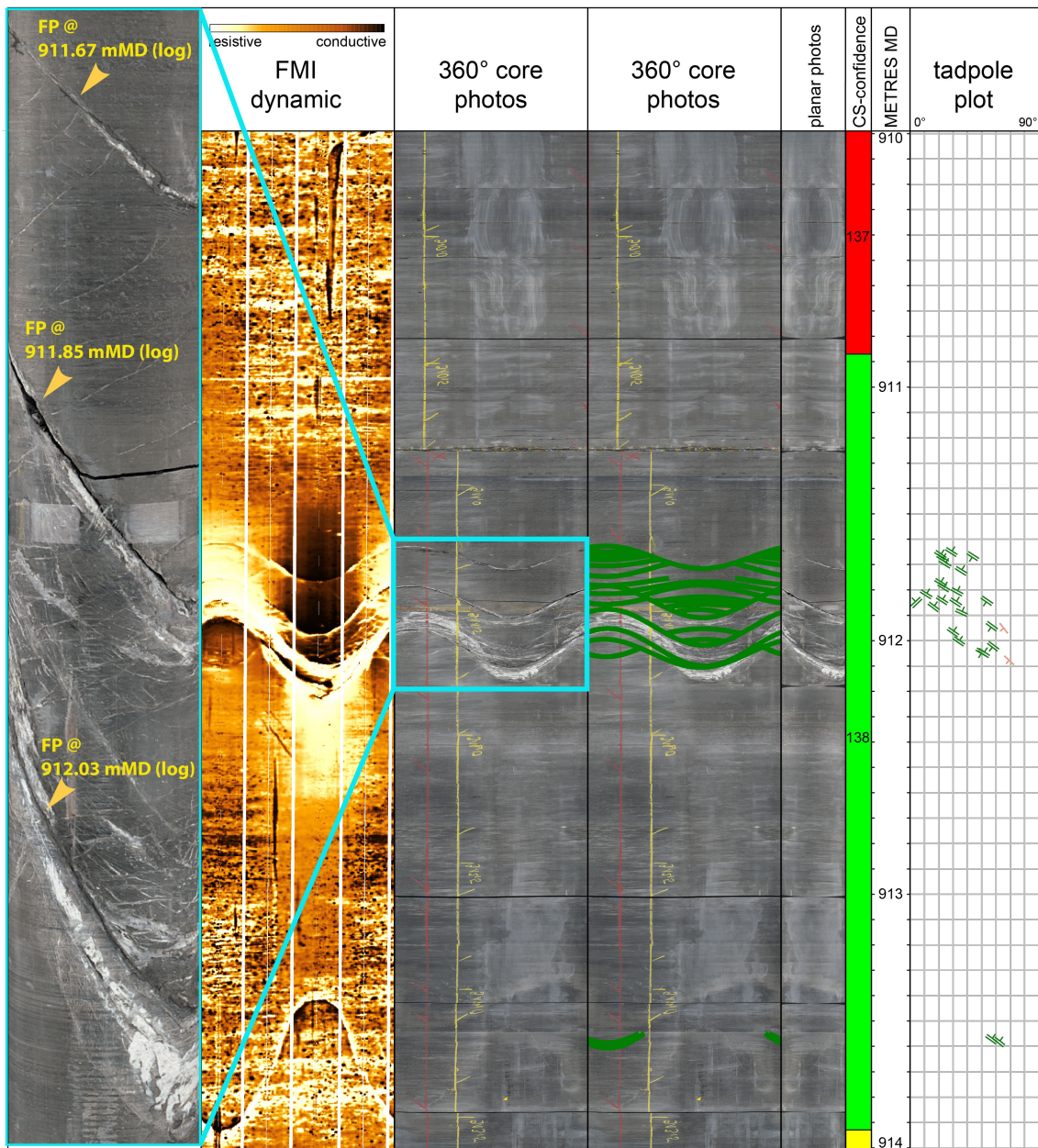


Fig. 5-1: Overview plot of the Opalinus Clay from 910.00 m to 914.00 m MD (log depth)
 Note the distinct fault zone from 911.63 m to 912.16 m MD (log depth) with the three main fault planes highlighted on the planar core photo on the left. Their orientations and associated striations are given in Tab. 5-1.

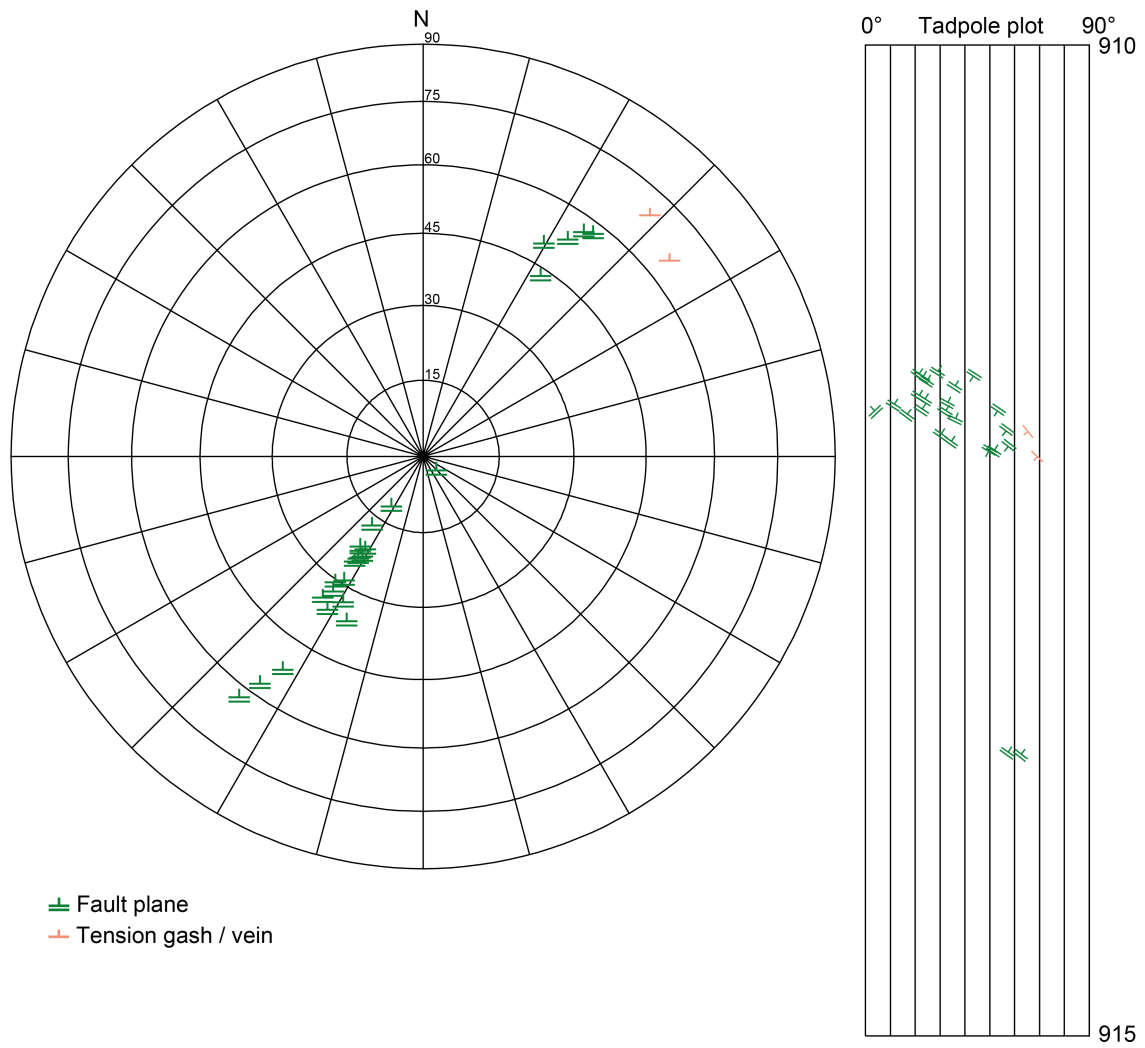


Fig. 5-2: Stereogram and depth plot of structures from 910.00 m to 915.00 m MD (log depth)
Fault planes (n = 22) and tension gashes / veins (n = 2).

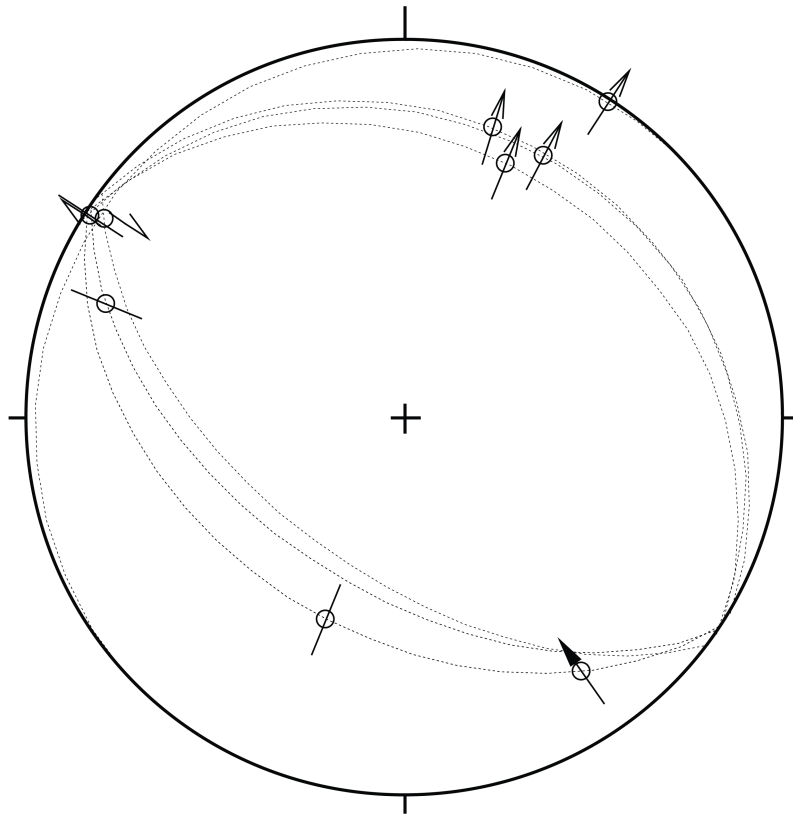


Fig. 5-3: Stereogram of striations on fault planes from 910.00 m to 915.00 m MD (log depth)

5.2 Fractures in the Staffelegg Formation at 940.58 m, 941.62 m and 942.78 m MD (log depth)

These three structures were defined as unassigned fractures and reach up to 1.6 m in length (Fig. 5-4). They are subvertical and dip towards either the NE or the SE and are partly open along their traces, however not exceeding 2 mm of opening width. The fracture planes are overgrown with druse-like minerals and show high fracture plane roughness. No mud losses were documented.

5.3 Joint in the Schinznach Formation at 1'060.82 m MD (log depth)

This particular structure was defined as a joint (Fig. 5-5) and not as centreline fracture (C-DIF) for the following reasons: (a) no plumose structures were found on the fracture plane, (b) there are few additional parallel fracture planes running in and out of the main fracture plane, (c) part of the fracture shows no cohesion loss, and (d) the bottom of the joint runs into another 30 cm long joint (orientated 086/85) running out of the core, which is atypical for a C-DIF. The latter structure can be followed downdip into the next core section (#188). On the other hand, it reveals some characteristics being typically for a C-DIF: (a) the fracture shows low roughness and (b) it splits the core in half and (c) starts at the top of the core section (although at a transition from a clay-rich layer to a dolomite). Note that this core section is the first one of drilling section III. Parts of the fracture are filled with drilling mud, which acts like a glue. The fracture appears conductive on the FMI image. No obvious mud losses were documented at this depth interval.



Fig. 5-4: Partly open fractures within the Staffegg Formation from 940.30 m to 943.10 m MD (log depth)

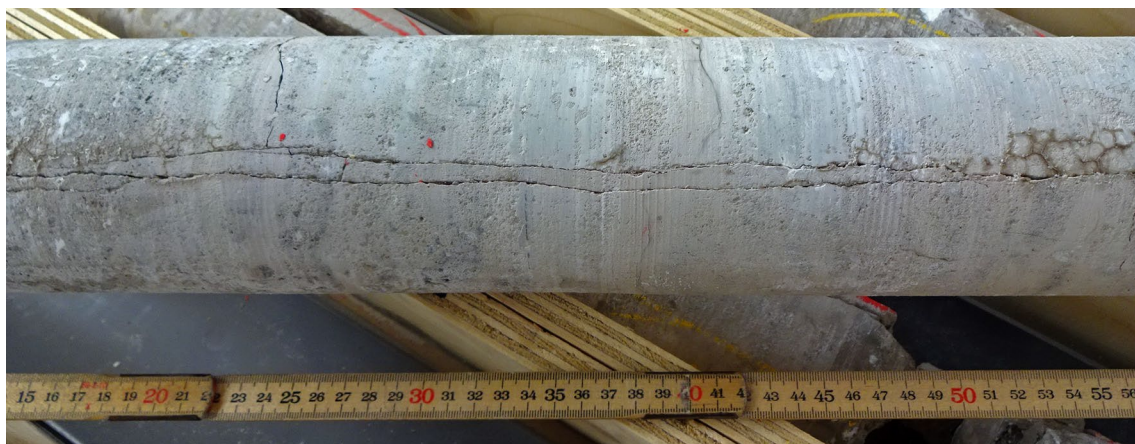


Fig. 5-5: Joint within the Schinznach Formation from 1'059.15 m to 1'059.55 m MD (log depth)

5.4 Joints in the Schinznach Formation from 1'099.40 m to 1'103.98 m MD (log depth)

In the cored interval below 1'100 m MD (core depth), continued drilling mud losses were detected. The interval from 1'099.40 m to 1'103.98 m MD (log depth) is characterised by abundant subvertical joints appearing electrically conductive on both, the UBI and FMI borehole images (Fig. 5-6). As shown in Fig. 5-7 they strike N-S and dip towards either the E (mean orientation of 088/84; n = 20) or the W (mean orientation of 265/82; n = 5). Some joints terminate on subhorizontal stylolites and therefore only reach lengths of a few cm to a maximum of 93 cm. In drill cores, half of the joints are broken. On the scale of observation, they appear to be closed, however many chunks and cavities were observed at the core rim and on broken core pieces, which may indicate some openings on sub-mm to-mm range. The latter may in indeed caused the observed mud losses. The roughness of the joint planes is moderate. Examples are shown in Fig. 5-8.

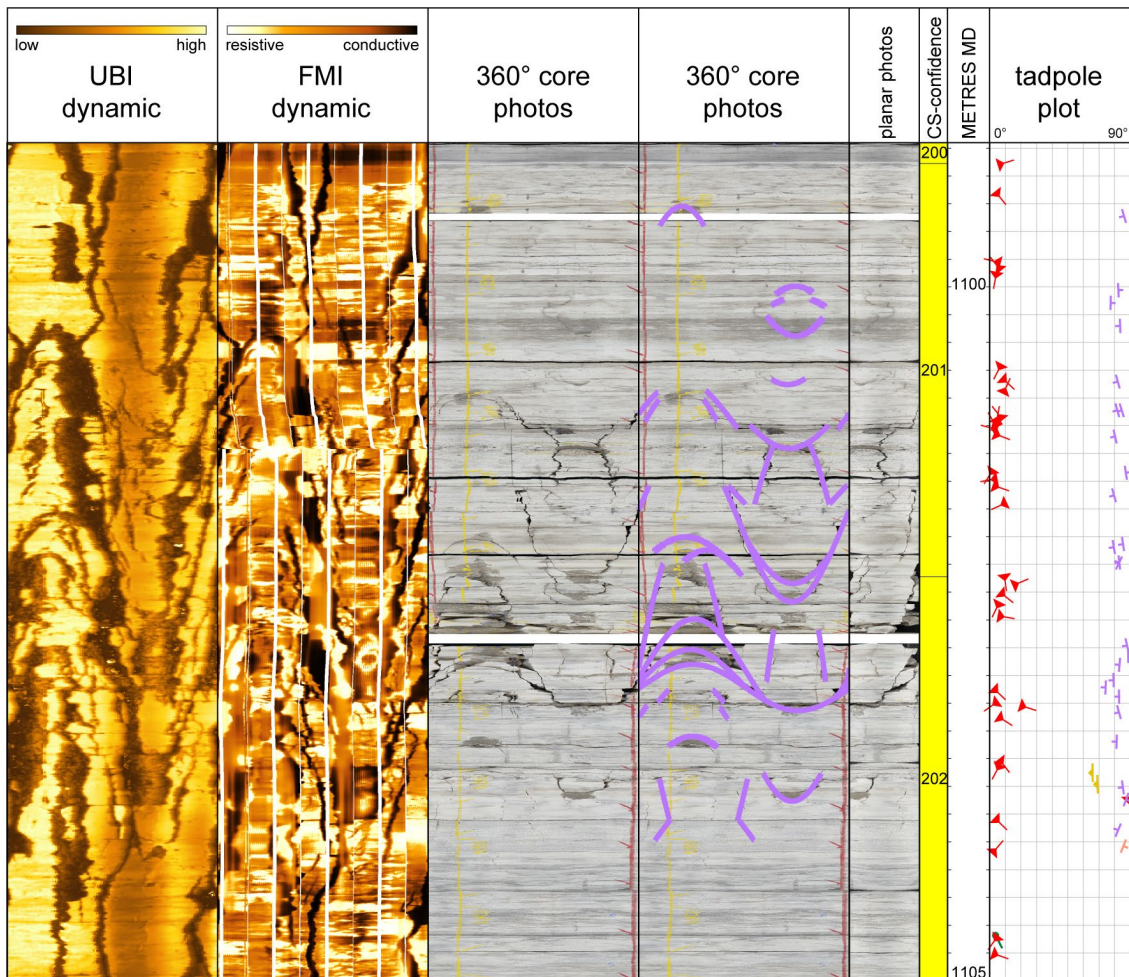


Fig. 5-6: Overview plot of the joints in the Schinznach Formation (interval from 1'099.00 m to 1'105.00 m MD log depth)
 For a better overview, only the joints are shown on the 360° core photos.

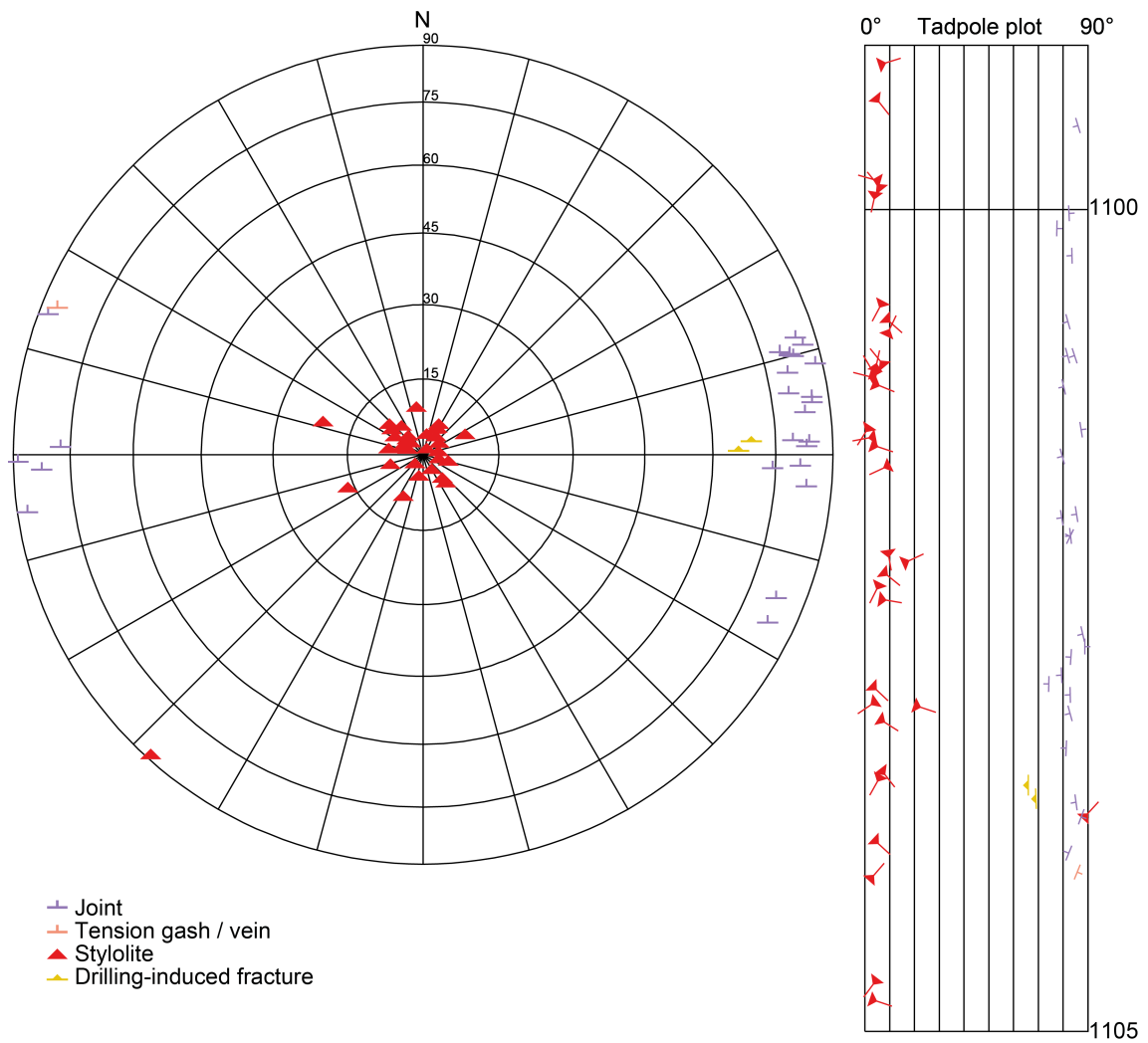


Fig. 5-7: Stereogram and depth plot of structures within the interval 1'099.00 m to 1'105.00 m MD (log depth)
 Joints (n = 25), tension gashes / veins (n = 1), stylolites (n = 33) and drilling-induced fractures (n = 2).

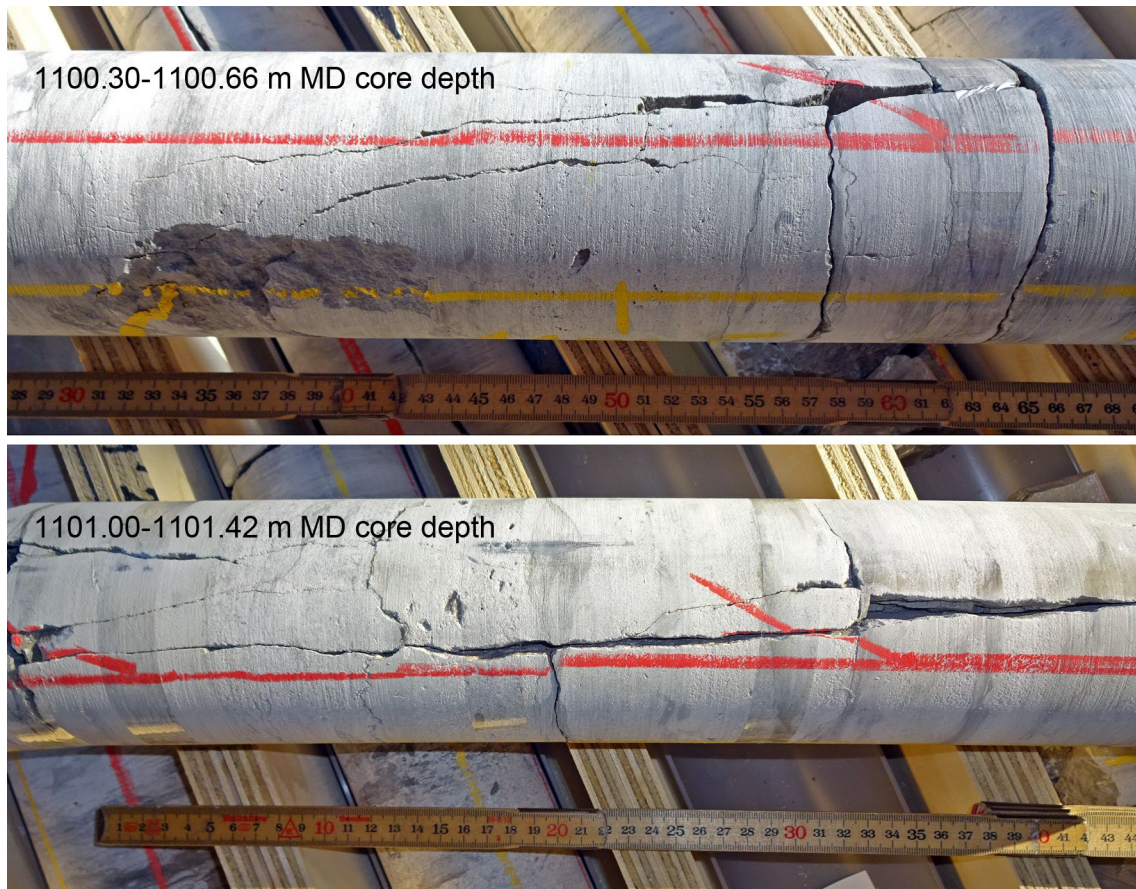


Fig. 5-8: Examples of joints in the Schinznach Formation

6 References

- Barton, N. (1976): The shear strength of rock and rock joints. *Int. J. Rock. Mech. Min. Sci. & Geomech. Abstr.* 13/9, 255-279.
- Barton, N. & Choubey, V. (1977): The shear strength of rock joints in theory and practice. *Rock mechanics* 10/1-2, 1-54.
- Bauer, H., Schröckenfuchs, T. & Decker, K. (2016): Hydrogeological properties of fault zones in a karstified carbonate aquifer (Northern Calcareous Alps, Austria). *Hydrogeology Journal* 24, 1147-1170.
- Ebert, A. & Decker, K. (2019): Structural Analysis Manual. Nagra Arbeitsbericht NAB 19-12.
- Hancock, P.L. (1985): Brittle microtectonics: principles and practice. *J. Structural Geology* 7/3-4, 437-457.
- Isler, A., Pasquier, F. & Huber, M. (1984): Geologische Karte der zentralen Nordschweiz 1:100'000. Herausgegeben von der Nagra und der Schweiz. Geol. Komm.
- Nagra (2002): Projekt Opalinuston: Synthese der geowissenschaftlichen Untersuchungs-ergebnisse: Entsorgungsnachweis für abgebrannte Brennelemente, verglaste hochaktive sowie langlebige mittelaktive Abfälle. Nagra Technical Report NTB 02-03.
- Nagra (2008): Vorschlag geologischer Standortgebiete für das SMA- und das HAA-Lager – Geologische Grundlagen. Nagra Technical Report NTB 08-04.
- Nagra (2014): SGT Etappe 2: Vorschlag weiter zu untersuchender geologischer Standortgebiete mit zugehörigen Standortarealen für die Oberflächenanlage – Geologische Grundlagen. Dossier II – Sedimentologische und tektonische Verhältnisse. Nagra Technical Report NTB 14-02.
- Nagra (2018): Preliminary horizon and structure mapping of the Nagra 3D seismics NL-16 (Nördlich Lägern) in time domain. Nagra Arbeitsbericht NAB 18-35.
- Nagra (2020): Gesuch um Erteilung einer Bewilligung für erdwissenschaftliche Untersuchungen im Standortgebiet Nördlich Lägern (NL) – Sondierbohrungen Bachs-1. Nagra Sondiergesuch NSG 20-01.
- Passchier, C.W. & Trouw, R.A.J. (1996): *Microtectonics*. Springer, 289 pp.
- Peacock, D.C.P., Nixon, C.W., Rotevatn, A. & Sanderson, D.J. (2016): Glossary of faults and other fracture networks. *J. Structural Geology* 92, 12-29.
- Pietsch, J. & Jordan, P. (2014): Digitales Höhenmodell Basis Quartär der Nordschweiz – Version 2013 (SGT E2) und ausgewählte Auswertungen. Nagra Arbeitsbericht NAB 14-02.